MORPHOLOGICAL AND MECHANICAL PROPERTIES OF DISPERSION-CAST AND EXTRUDED NAFION® MEMBRANES SUBJECTED TO THERMAL AND CHEMICAL TREATMENTS

Shawn James Osborn

Dissertation submitted to the faculty of the Virginia Polytechnic Institute and State University in partial fulfillment of the requirements for the degree of

DOCTOR OF PHILOSOPHY
in
Macromolecular Science and Engineering

Robert B. Moore, chairman
David A. Dillard
Michael W. Ellis
Kenneth A. Mauritz
James E. McGrath

March 16, 2009
Blacksburg, Virginia

Keywords: perfluorosulfonate ionomers, Nafion®, morphology, proton exchange membrane, glass transition temperature, crystallinity, annealing, chemical degradation, Fenton's Test

ABSTRACT

MORPHOLOGICAL AND MECHANICAL PROPERTIES OF DISPERSION-CAST AND EXTRUDED NAFION® MEMBRANES SUBJECTED TO THERMAL AND CHEMICAL TREATMENTS

Shawn James Osborn

The focus of this research project was to investigate morphological and mechanical properties of both extruded and dispersion-cast Nafion® membranes. The project can be divided into three primary objectives; obtaining a fundamental understanding of the glass transition temperature of Nafion®, determining the effect of thermal annealing treatments on the morphology and mechanical properties of dispersion-cast Nafion®, and examination of dispersion-cast Nafion® subjected to an ex-situ, Fenton's chemical degradation test. Nafion®, a perfluorosulfonate ionomer, is considered a commercially successful semi-crystalline ionomer with primary applications in chlor-alkali cells and proton exchange membrane fuel cells.

With the aid of dynamic mechanical analysis (DMA) and dielectric spectroscopy (DS), we were able to provide definitive evidence for a genuine glass transition in Nafion®. DMA of Nafion® samples that were partially neutralized with tetrabutylammonium counterions showed a strong compositional dependence suggesting that the β-relaxations of H^+-form Nafion® and the neutralized ionomers have the same molecular origin with respect to backbone segmental motions. Building upon our previous studies of the molecular and morphological origins of the dynamic mechanical relaxations of Nafion® neutralized with a series of organic ions, the glass transition

temperature of H^+-form Nafion® is now confirmed to be the weak β-relaxation centered at -20 °C. Dielectric spectra also showed this transition from the perspective of dipole relaxation. The signature of cooperative long range segmental motions in dielectric spectra was seen here, as with other polymers, mainly through the excellent agreement of the β-relaxation time-temperature dependence with the Vogel-Fulcher-Tammann equation.

We have also discovered that new dispersion-cast H^+-form Nafion® membranes are susceptible to disintegration/dissolution when subjected to boiling methanol. In this work, we have achieved significant decreases in the percent solubility of H^+-form Nafion® by either thermally annealing above 175 °C or solution-processing at 180 °C using a high boiling point solvent. Small Angle X-ray Scattering (SAXS) displayed a change in the morphology of H^+-form membranes with increasing annealing temperature by a shift in the crystalline scattering peak ($q \approx 0.05$ $Å^{-1}$) to lower q values. Counterion exchange of Nafion® from H^+ to Na^+-form had no influence on the membrane's susceptibility to disintegration in boiling methanol. In order to achieve mechanical stability in boiling methanol, Na^+-form membranes had to be annealed at 275 °C for at least fifteen minutes. The SAXS data of annealed Na^+-form membranes showed a dramatic decrease in crystalline order with annealing temperature, ultimately leading to the disappearance of the crystalline scattering peak after fifteen minutes at 275 °C. The onset of methanol stability with the melting of Nafion® crystallites suggests that chain entanglement is an important parameter in obtaining solvent stability.

With respect to chemical stability, we performed studies aimed at examining the effects of Fenton's Reagent on the resistance to radical attack of new generation,

dispersion-cast Nafion®. Changes in the ^{19}F solid-state NMR spectra of dispersion-cast Nafion® before and after chemical degradation via Fenton's Reagent predicts a rather random attack by ·OH and ·OOH radicals. Several membranes were also thermally annealed between 100-250 °C in an attempt to correlate crystallinity with chemical degradation kinetics of Nafion® via Fenton's Reagent. The results indicate that the effect of counterion exchange into the Na^+-form was minimal, but the degree of thermal degradation had a tremendous effect on the fluoride release rate and chemical degradation kinetics. By exchanging the membranes into the Na^+-form, thermal degradation was avoided, allowing us to study the role of crystallinity as a function of fluoride release. Ultimately, Nafion® crystallinity was deemed an important factor in deterring peroxide radical attack. As the percent crystallinity decreased with annealing temperature, the fluoride concentration in the resulting Fenton's media increased accordingly, indicating that the amorphous regions of the polymer are more susceptible to chemical degradation via peroxide radical attack.

ACKNOWLEDGEMENTS

I would like to thank my graduate research advisor, Dr. Robert B. Moore, for his guidance, support, and friendship throughout my graduate career at both The University of Southern Mississippi (USM) and Virginia Tech (VT). I would also like to thank the Moore Research Group of the past (Alan Phillips, Peyton Hopson, Kirt Page, Bret Calhoun, Greg Gemeinhardt, Angels Domenech) and the present (Angela Baldree, Jong Keun Park, Gilles Divoux, Sonya Benson) for their assistance and support throughout my research. I also acknowledge Brady Pitts, Brooks Abel, and Robert Bourne as undergraduate researchers at USM who contributed to some of the work contained in this dissertation.

I greatly appreciate the guidance provided by my committee at USM during the majority of my doctoral work. My USM committee consisted of Drs. William Jarrett, Kenneth Mauritz, Sergei Nazarenko, and Marek Urban. I would also like to extend a special thanks to the following staff members at USM for their invaluable assistance throughout my graduate career, Jim Bridges, Steve Selph, and Laura Fosselman.

I also appreciate the guidance of my committee members at VT for their inspirational thoughts and ideas during the conclusion of my graduate career. My VT committee consists of Drs. David Dillard, Michael Ellis, Kenneth Mauritz from USM, and James E. McGrath.

I would also like to thank E.I. DuPont de Nemours, Inc. for both funding and provision of the materials for which the majority of my research was conducted. Funding was also provided by DuPont Fuel Cells and DOE Office of Energy Efficiency and Renewable Energy; contract # DE-FC36-03GO13100 and DE-FG36-06GO86065.

In general, I express my gratitude to the researchers at the Advanced Photon Source (Argonne National Laboratories) for the opportunity to visit and utilize the synchrotron X-ray source for data collection towards my dissertation.

Finally, I would like to thank my parents Raymond and Kathleen Osborn and brothers Brian, James, and Chad for their support and encouragement. Above all I would like to thank my fiancée, Angela Baldree, who has not only been an emotional supporter but also an academic one as well. Her thoughtfulness and generosity are only surpassed by her genuine ability to bring out the best in whoever she comes across.

TABLE OF CONTENTS

LIST OF FIGURES

LIST OF TABLES

LIST OF EQUATIONS

CHAPTER 1

PERFLUOROSULFONATE IONOMERS

Introduction

Perfluorosulfonate ionomers (PFSI's) have become a commercially successful class of semicrystalline ionomers. PFSI's are copolymers containing runs of tetrafluoroethylene and generally less than 15 mole percent of randomly incorporated pendant perfluorovinyl ether side chains terminated with sulfonic acid moieties. The structures of three commercially available PFSI's are shown in Figure 1.1. The first PFSI shown, 1.1a, was developed by DuPont in the 1960's under the trade name Nafion®.[1] Nafion® has been the most widely studied perfluorosulfonate ionomer and is currently the benchmark material for use in chlor-alkali cells[2] and fuel cells.[3] Dow Chemical introduced a perfluorinated ionomer[4, 5], 1.1b, with a much shorter side chain than Nafion®. This ionomer, bearing the two carbon side chain, is now a product of Solvey Solexis and is termed the Hyflon Ion.[6] 3M has recently introduced a perfluorinated ionomer, 1.1c, with an intermediate side chain length between Dupont and Solvey's perfluorinated ionomers.[7, 8]

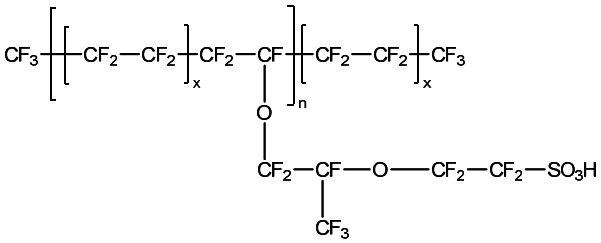

1.1a) Nafion®

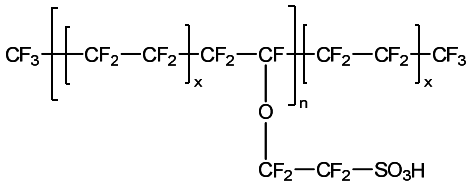

1.1b) Hyflon Ion

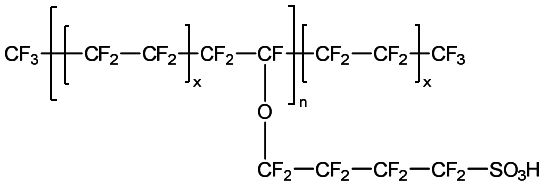

1.1c) 3M Ionomer

Figure 1.1. Structure of a) Dupont's Nafion® b) Solvey's Hyflon Ion, originally developed by Dow and c) 3M's current ionomer

The major difference between all three types of PFSI's shown in Figure 1.1 is the length and complexity of the pendent side chains containing the sulfonate moieties. All three polymers are capable of forming "teflon-like" crystallites based on the molar ratio of perfluorovinyl ether side chains to polytetrafluoroethylene backbone units (*n*/*x* in Figure 1.1a-c). The extent of branching is displayed in terms of equivalent weight (EW), which is defined as the grams of polymer per equivalent of sulfonic acid.[9] The equivalent weight can be determined by acid-base titration, analysis of atomic sulfur, and Fourier transform infrared spectroscopy.[10] Determination of EW for Nafion®, Hyflon Ion, and 3M Ionomer are shown below in Equations 1-1 through 1-3, respectively.

$$\mathrm{EW} = 100x + 443 \qquad \textbf{Eq. 1-1}$$

$$\mathrm{EW} = 100x + 277 \qquad \textbf{Eq. 1-2}$$

$$\mathrm{EW} = 100x + 377 \qquad \textbf{Eq. 1-3}$$

The most common EW for Nafion® reported in the literature is 1100 g/mol SO_3^-.[3] Based on a complete random copolymerization, an EW of 1100 would yield an *x* value of approximately 6.57, or twelve to fourteen CF_2 units in the backbone, capable of crystallization. Because of the smaller side chains of both the Hyflon Ion and 3M Ionomer, their EW's will be lower when directly compared to an 1100EW Nafion® membrane. Based on Equations 1-1 through 1-3, an 1100EW membrane of Nafion® would be similar in ionic content to a 935 EW Hyflon Ion and a 1035 EW 3M Ionomer. Ghielmi and coworkers, have recently verified that a Nafion® membrane of 1100 EW is equivalent to a 925 EW Hyflon Ion membrane based on water uptake analysis.[11]

History of Perfluorosulfonate Ionomers

As previously mentioned, the PFSI Nafion® was created in the 1960's by Connolly and coworkers for E. I. du Pont de Nemours and Company.[1] Nafion® was initially used as a separator membrane in the chlor-alkali cell industry but was quickly adapted as a proton exchange membrane in a hydrogen/oxygen fuel cell for portable energy use in NASA's space shuttle program.[12] Some of the earliest studies of Nafion® focused on examining mechanical analysis,[13-15] dielectric spectroscopy,[14] solid-state nuclear magnetic resonance,[16] ion transport,[17] and proton conductivity.[18] Due to Nafion's® large success in the chlor-alkali and fuel cell industries, the bulk of this review will be centered on the various processing procedures, morphologies, and membrane applications of this unique PFSI membrane.

In the early 1980's, Dow Corporation began filing a series of patents on the synthesis of a perfluorosulfonic acid film directly related to DuPont's ionomer Nafion® but with a shorter side-chain.[4, 5, 19-23] The earliest characterization literature reported on

the Dow ionomer was by Tant et al., where dynamic mechanical analysis (DMA), differential scanning calorimetry (DSC), and wide angle X-ray diffraction (WAXD) were employed to examine the physical properties and crystallinity of the short-side-chain ionomer.[24, 25] The most significant results from Tant and coworkers were the increased crystallinity at a given equivalent weight of the Dow polymer when compared to Nafion® as well as an increase in the temperature at which thermo-mechanical transitions occur. Extrapolation of the WAXD and DSC data at various equivalent weights of the precursor of both polymers showed a loss of crystallinity below 700 EW for the Dow polymer compared to 965 EW for Nafion®.[25] Conversion of the precursor into the ionomer or salt form showed a disappearance of crystallinity for an 800 EW Dow ionomer membrane due to ionic association between the sulfonate moieties.[25] The disappearance of crystallinity in the Dow ionomer was also verified by Moore et al, where WAXD and DSC were utilized to study the morphology and crystallinity of the ionomer in the Na^+ salt form.[26] Using a wider range of equivalent weights, Moore and coworkers showed that the extent of crystallinity increases with equivalent weight, similar to Nafion®. Higher crystallinity for the Dow ionomer resulted because the shorter side chains were less disruptive to the crystallization of the polytetrafluoroethylene backbone segments. Moore et al. were also the first to show evidence of ionic aggregation in the Dow polymer by observing the small angle x-ray scattering (SAXS) "ionomer peak" at q = 0.15 $Å^{-1}$.[26] A decrease in the intensity of the ionomer peak with increasing equivalent weight was attributed to a decrease in water content. As the water content decreases, the electron density contrast between the ionic domains and the fluorocarbon matrix diminishes, resulting in lower intensity. Similar SAXS results for the ionomer peak in

Nafion® were shown by Gierke et al.[27] Using DSC, Moore and coworkers showed that the crystalline melting temperatures for the Dow ionomer were similar throughout a wide range of equivalent weights. Due to this observation, Moore et al. proposed that the Dow ionomer contained more of a block copolymer structure as opposed to a true random copolymer.

Since the early works of both Tant and Moore, more recent publications have involved the hydrogen diffusion and solubility,[28] impedance spectroscopy,[29] transportation of alkenes via silver neutralization,[30] and atomic force microscopy[31] of the Dow ionomer. Tsou and coworkers examined the hydrogen diffusion and solubility of the Dow ionomer in both the sulfonic and carboxylic acid forms.[28] They concluded that the diffusion and solubility of hydrogen occurred throughout interfacial areas between the aqueous and fluorocarbon phases, and the hydrogen solubility increased with decreasing equivalent weight. The dramatic increase in hydrogen solubility was attributed to the disappearance of crystallinity below 900 EW along with the increase in the available interfacial area due to the higher extent of intrusion of the fluorocarbon phase into the aqueous phase. Hill et al. used atomic force microscopy to study the dewetting properties of the Dow ionomer at various annealing temperatures and counterions. A thin film of the ionomer was self-assembled onto a silicon wafer and annealed at 180 °C for 254 hours, then 17 hours at 260 °C, and finally an additional 243 hours at 340 °C. The authors showed that the short-side-chain ionomer exhibited a unique stability and no visible dewetting occurred throughout the tortuous annealing process. They concluded that the thermal perturbations were not strong enough to cause the ionomer films to break up or dewet due to the dominant ionic forces present in the membrane.

Gebel and Moore continued the morphological characterization of the short-side-chain Dow ionomer by incorporating SAXS and small angle neutron scattering (SANS) to determine the structure of the ionomer at various equivalent weights and water contents.[32] The authors noticed a significant shift in the SAXS ionomer peak to smaller q values with increasing ionic and water content. A Porod representation (I q^4 vs q^2) of the SAXS data was conducted in order to determine the Porod limit, defined by the asymptotic behavior of the scattering at large q values. The Porod representation of the data indicated the existence of a sharp polymer-solvent interface, confirming that the structure is dominated by interfacial phenomena. Based on both the SAXS and SANS profiles, a local order model was chosen to best represent the morphology of the Dow ionomer. The local order model is based on the hypothesis that each ionic aggregate is spherical and surrounded by four aggregates in a tetrahedral coordination at a well-defined distance, while the overall ionic domains are considered to be randomly distributed.[33]

Even though the Dow polymer had demonstrated superior performance in a hydrogen/oxygen fuel cell,[34] the industrial development of the ionomer was abandoned for unknown reasons. A possible reason for the lack in advancement of the Dow polymer was the complex synthesis of the base functional monomer.[35] Solvey Solexis has recently developed a more simple route for the synthesis of the short-side-chain sulfonylfuoridevinylether monomer and has taken advantage of a proprietary microemulsion polymerization process in order to develop the ionomer on an industrial scale.[6] Solvey Solexis has named the short-side-chain ionomer Hyflon Ion and has published various articles involving the mechanical, thermal, and chemical properties of

the ionomer.[11, 35-39] Arcella and coworkers examined the shorter synthetic route to producing Hyflon Ion as well as the mechanical and fuel cell properties of the ionomer.[35, 36] The authors mention that a completely amorphous membrane is produced when the sulfonylfuoridevinylether content is greater than 20%. As the molar content of sulfonylfuoridevinylether increases from 10% to 30% the glass transition temperature (T_g) of the polymer decreases from 50 °C to 5 °C, which is much higher than the Tg of 1100 EW semicrystalline Nafion® ($T_g \approx$ -20 °C).[40] It is important to realize that the lower equivalent weight ionomers have T_g's below room temperature, so they exhibit rubber like behavior at fuel cell operating temperatures. Besides having a higher glass transition temperature, the Hyflon Ion also exhibits a DMA α-relaxation temperature of 160 °C compared to 110 °C for Nafion®.[11, 35, 36] The high-temperature α-relaxation was found to be due to the onset of long-range mobility of the ionomer main chains and side chains via a thermally activated destabilization of the electrostatic interactions, yielding a *dynamic* network involving significant ion-hopping processes.[40, 41] Arcella and coworkers conclude that the higher α-relaxation temperature will allow for higher fuel cell operating temperatures, which will reduce the complexity of the system as well as decrease the amount of carbon monoxide poisoning of the platinum catalyst.[35]

Based on DMA, DSC, water uptake, and fuel cell data, Solvey Solexis believes that a Hyflon Ion of 850 EW exhibits the optimum balance of properties for fuel cell performance.[11, 36] Ghielmi and coworkers show that the 850 EW Hyflon Ion exhibits excellent proton conductivity while still retaining crystallinity, when the Nafion® ionomer has poor mechanical properties at such low equivalent weights due to the lack of crystallinity.[11] The 850 EW Hyflon Ion also exhibits a higher current density during fuel

cell performance when compared to 1100 EW Nafion® of equal thickness. More recently, Merlo et al., from Solvey Solexis, have shown that the 850 EW Hyflon Ion displayed limited performance degradation after 5000 hours of operation in a hydrogen/oxygen fuel cell at 75 °C and a constant potential of 0.6 V.[38] Merlo et al. also note that the performance degradation occurs in the diffusion part of the polarization curve, referring to a loss in hydrophobicity of the gas diffusion layers as opposed to membrane or electrode performance. A proton conductivity study of the 850 EW Hyflon Ion versus an 1100 EW Nafion® membrane between 0 and -40 °C showed overall higher proton conductivity for the Hyflon Ion, due to the greater ionic content in the ionomer.[38]

The chemical degradation of the Hyflon Ion via the Fenton's test and fuel cell performance was conducted by Merlo et al.[38, 39] Four different fuel cell operation conditions were chosen in order to study the effects of cell temperature (70 °C or 90 °C) and humidity (50 or 100%) on the performance degradation of the Hyflon Ion. Hydrogen crossover in the fuel cell was monitored in order to determine the extent of membrane degradation. A decrease in humidification from 100 to 50% had the largest impact on hydrogen crossover while the change in operating temperature had little influence on the membrane performance. A chemically stable "S"-grade of the Hyflon Ion was also examined in the fuel cell and exhibited superior performance with regards to hydrogen crossover at both lower humidity and higher temperatures. The Fenton's test (involving chemical attack via peroxide radicals) was conducted on the Hyflon Ion, "S"-grade Hyflon Ion and Nafion® membranes.[38, 39] The Fenton's test revealed a significant decrease in fluoride emission from the chemically stable "S"-grade of the Hyflon Ion when compared to Nafion® and standard Hyflon Ion. The fluoride emission of the

chemically stable Hyflon Ion was relatively consistent over a range of 30 hours in the Fenton's solution. The authors concluded that the 850 EW "S"-grade Hyflon Ion maximizes the resistance to chemical attack and minimizes hydrogen crossover in order to maximize fuel cell performance.

The most recent PFSI being studied for proton exchange membrane applications is the intermediate pendent sidechain length, 3M Ionomer. Literature publications for the 3M Ionomer are scarce due to the novelty of the membrane in the academic realm. Hamrock and Yandrasits have recently published a review on proton exchange membranes for fuel cell applications and included discussion of the synthesis as well as proton conductivity results for various equivalent weights of the 3M Ionomer.[42] The synthesis of the 3M Ionomer is discussed in the U.S. patent by Guerra where electrochemical fluorination is used in the preparation of the perfluoro-4-(fluorosulfonyl)butoxyvinyl ether side chain monomer.[7] Membranes with equivalent weights as low as 730 were synthesized and determined to be stable in boiling water for several hours. The proton conductivity values of 730-980 EW 3M Ionomers were determined between 80-120 °C while maintaining an 80 °C dewpoint. The proton conductivity results showed that lower EW membranes produced higher conductivity values regardless of temperature or humidity. An overall decrease in conductivity was noticed as the temperature increased due to the sharp decline in the relative humidity from 100-25%.[42] The proton conductivity results, along with DMA and fuel cell performance, were also published by Emery et al. at 3M Corporation.[43] DMA was performed using 1000 EW ionomers of both Nafion®, as the control, and 3M Ionomer. The DMA results indicated that the α-relaxation of the 3M Ionomer occurs around

125 °C, which is approximately 25 °C higher than the α-relaxation of 1000 EW Nafion®. The authors correlate a higher α-relaxation with the notion that the ionomer will allow for higher fuel cell operating temperatures and deter the effects of creep or membrane deformation over the lifetime of the fuel cell. Emery et al. also showed an 18-fold increase in fuel cell lifetime of both 800 and 1000 EW 3M Ionomers compared to 1100 EW Nafion®. The 3M Ionomers also provided higher conductivity, lower cell resistance, and increased performance at lower humidity than the Nafion® controls.[43]

Meng and coworkers, in collaboration with 3M, examined the effect of introducing heteropolyacids (HPAs) into a 1000 EW ionomer membrane to improve high temperature fuel cell performance.[44-46] A 3M Ionomer doped with five wt% 12-phosphotungstic acid showed a dramatic increase in proton diffusion under dry conditions and elevated temperatures (80-130 °C) using pulse field gradient spin echo nuclear magnetic resonance spectroscopy. Under fully hydrated conditions, the addition of HPAs had minimal impact on the diffusion of protons between 20-130 °C. The authors also acknowledge that due to the weak interactions of the HPA molecule with the sulfonate moiety in the 3M Ionomer, a technique must be employed to immobilize the HPA molecule to prevent dissolution during fuel cell operation.[44] More recently, Haugen et al. have shown the effects of incorporating various HPAs at 10 and 20 wt% into a 1000 EW 3M PFSI.[45, 46] A vast array of HPAs was examined, but the authors concluded that α-$H_3P_2W_{18}O_{62}$, $H_6P_2W_{21}O_{71}$, and $H_4SiW_{12}O_{40}$ had the greatest impact on combating chemical degradation and maintaining higher open circuit voltages in an operating fuel cell between 85 and 100 °C.

The effects of hydration and chemical degradation (via Fenton's Reagent) of the 3M Ionomer versus Nafion® were studied using SAXS, tensile, percent weight loss, and overall fluoride ion release.[47, 48] Yandrasits et al. showed using SAXS that the crystalline peak around q = 0.05 Å^{-1} for the 1000 EW 3M Ionomer shifts to lower q values and increases in intensity as the sample is heated from 80-180 °C.[47] They also showed that the ionomer peak of the hydrated 3M Ionomer increased in intensity and shifted to lower q values at 100% humidity and 80 °C. Aieta and coworkers examined the effects of chemical degradation on the crystallinity and mechanical properties of Nafion® and the 3M Ionomer of unknown equivalent weights.[48] The chemical degradation via the Fenton's Test showed equivalent weight loss and fluoride release for both of the ionomer membranes after ten weeks. Using SAXS, the crystallinity of both membranes was determined as a function of degradation time, with minimal changes in crystallinity after ten weeks. The authors concluded that the crystalline regions of the membranes are not affected by chemical degradation and that the mechanical properties of the ionomers remain stable over the entire period of peroxide radical attack.

Membrane Applications

Various small applications of PFSI's have involved chemical separation schemes[49] and organic syntheses,[10] while the primary applications have been in chlor-alkali cells[2] and proton exchange membrane fuel cells.[3, 10] PFSI's have excellent chemical, mechanical, and thermal stability, which makes them ideal for use in chlor-alkali cells. Chlor-alkali cells consist of two chambers, containing either the catholyte (concentrated NaOH) or the anolyte (aqueous NaCl), which are separated by the PFSI membrane. During the electrochemical process, a current is applied to a platinum

electrode in the anolyte solution which converts the NaCl into Na^+ ions and Cl_2 gas. The Na^+ ions then permeate through the PFSI membrane where they combine with OH^- ions from the catholyte reaction to produce NaOH and H_2 gas.[50] PFSI membranes are outstanding separators for use in chlor-alkali cells since they are permeable to cations while hindering the passage of anions throughout the electrochemical process.

The application of greatest interest for PFSI's is the proton exchange membrane fuel cell (PEMFC). As with chlor-alkali cells, PEMFC's rely on the stability and selective ion transport of PFSI's to serve as separator membranes between an anode and cathode. The main two types of PEMFC's used for portable and transportation power are the hydrogen/oxygen (H_2/O_2) and direct methanol fuel cells (DMFC). The purpose of both types of fuel cells is to convert chemical energy into electrical energy.[51] A schematic of a general PEMFC is seen in Figure 1.2, where chemical energy is generated by continuously feeding fuel (hydrogen or methanol) to the anode and oxygen to the cathode.

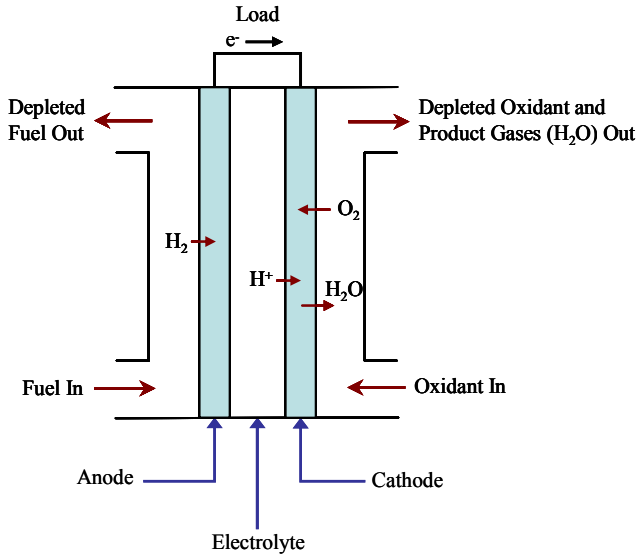

Figure 1.2. Proton Exchange Membrane Fuel Cell

At the anode, hydrogen is oxidized to produce protons and electrons at the platinum catalyst surface. The protons then permeate through the proton exchange membrane, typically a PFSI, while the electrons are forced into a circuit, creating the electrical output of the cell. At the cathode, oxygen is reduced at a platinum catalyst and the electrons from the outside circuits react with the protons resulting in the production of water and heat. In the case of an H_2/O_2 fuel cell, the electrochemical reactions taking place at the anode, cathode, and overall cell are shown below in Equations 1-4 through 1-6.[52]

Anode: $H_2 \rightarrow 2H^+ + 2e^-$ **Eq. 1-4**

Cathode: $½\ O_2 + 2H^+ + 2e^- \rightarrow H_2O$ **Eq. 1-5**

Cell Reaction: $H_2 + ½\ O_2 \rightarrow H_2O$ **Eq. 1-6**

In contrast to the H_2/O_2 fuel cell the direct methanol fuel cell uses the electrochemical reaction of methanol and water with platinum at the anode to produce carbon dioxide, protons and electrons as shown in Equation 1-7. The protons then migrate through the proton exchange membrane to the cathode and react with oxygen to produce water as shown in Equation 2-8 along with the overall cell reaction in Equation 1-9.[53, 54]

Anode: $CH_3OH + H_2O \rightarrow CO_2 + 6H^+ + 6e^-$ **Eq. 1-7**

Cathode: $3/2O_2 + 6H^+ + 6e^- \rightarrow 3H_2O$ **Eq. 1-8**

Cell Reaction: $CH_3OH + 3/2O_2 + H_2O \rightarrow CO_2 + 3H_2O$ **Eq. 1-9**

The main advantage of a DMFC versus the H_2/O_2 fuel cell is the ability to produce electrical energy from methanol without intermediate thermal steps, avoiding the need for a reformer to produce hydrogen gas. Another advantage of the DMFC is the

ease of use of liquid fuel, which can be distributed through the current petroleum infrastructure. Some disadvantages of the DMFC when compared to the H_2/O_2 fuel cell are much lower power densities, poor anode electro-oxidation, and high methanol crossover through the proton exchange membrane.[53]

The performance of a PEMFC is typically measured by the voltage as a function of current density (mA/cm^2). The theoretical potential of a PEMFC using a hydrogen/oxygen system at atmospheric conditions is 1.23 Volts.[52, 55] Due to various performance losses (activation polarization, ohmic, and mass transport effects), the actual potential of an hydrogen/oxygen PEMFC is much lower than 1.23 Volts depending on the desired pressure and temperature used during operation.[53] An increase in PEMFC performance may be possible with a fundamental understanding of the morphology of PFSI membranes as well as the ability to manipulate the morphology in order to increase desired mechanical or transport properties.

PFSI Processing Procedures

PFSI's are generally produced through the free radical copolymerization of tetrafluoroethylene and a perfluorovinyl ether comonomer.[56] After polymerization, copolymers of tetrafluoroethylene and fluorinated vinyl ethers can be melt processed or extruded in the sulfonyl fluoride form ($-SO_2F$), precursor to Nafion®. Extrusion of the precursor causes microstructural orientation in the machine direction, which can be seen using SAXS, and is attributed to the clustered morphology of the material.[3] Small polytetrafluoroethylene-like crystals have also been shown to exist in the precursor material, depending on the equivalent weight or comonomer ratio used during synthesis.[27] In order to obtain the ionomer form of the membrane, a hydrolysis procedure

must be implemented to convert the pendent sulfonyl fluoride $–SO_2F$ moiety into a sulfonate group $–SO_3^-$. Hydrolysis of the sulfonyl fluoride form is traditionally carried out using a solution of 15 wt% KOH, 35 wt% dimethylsulfoxide (DMSO) and 50 wt% deionized water at 80 °C for 30 min or more depending on membrane or pellet thickness.[3, 10] The final ($-SO_3H$) form is achieved by soaking the film or pellet in a sufficiently concentrated aqueous acid solution. Gierke and coworkers have shown that a Nafion® precursor of 1800 EW exhibits a decrease in the percent crystallinity after hydrolysis but verifies that the ionic interactions are not sufficient enough to render the polymer totally amorphous.[27] The microstructural orientation in the machine direction of the Nafion® precursor can still be seen in the hydrolyzed polymer via SAXS and can affect the swelling and electrical conductance properties of the ionomer due to the anisotropy present in the membrane.[3]

Once hydrolyzed, Nafion® exhibits strong coulombic interactions between the ion pairs ($-SO_3H$ moieties), which yield ionic aggregates and form a multifunctional electrostatic network.[13, 57] The existence of ionic aggregates in an electrostatic network and small polytetrafluoroethylene-like crystals serve as barriers to processing the ionomer through compression molding or extrusion.[27] The ionomer form of Nafion® can be melt processed by eliminating the crystallinity and weakening the electrostatic network between ionic aggregates, allowing for the onset of long range chain mobility. Cable and Moore manipulated both the crystalline domains and the electrostatic network in determining the right parameters to obtain melt-processable Nafion®.[58] The authors chose to counterion exchange Nafion® using bulky tetrabutylammonium (TBA^+) counterions, which had been shown to reduce the extent of electrostatic crosslinking in

sulfonated polystyrene ionomers by forming weak ion pair dipoles.[59] Cable and Moore also eliminated the polytetrafluoroethylene crystallites by performing a "steam-stripping" technique. "Steam-stripping" involved evaporating TBA^+-form Nafion® solutions in boiling deionized water and due to the hydrophobic nature of the TBA^+ counterion, the ionomer precipitated on top of the boiling water. The authors then melt-processed the amorphous TBA^+-form powder at 190 °C and 200 psi to a thickness of approximately 200 μm, obtaining a pliable membrane.[58] WAXD was used to verify the elimination of crystallinity in the "steam-stripped" TBA^+-form Nafion® powder as well as the reintroduction of crystallinity upon melt-processing. The WAXD profiles of as-received (AR) Na^+ and TBA^+-form Nafion® as well as melt-processed (MP) and "steam-stripped" (SS) Nafion® powder are shown in Figure 1.3.

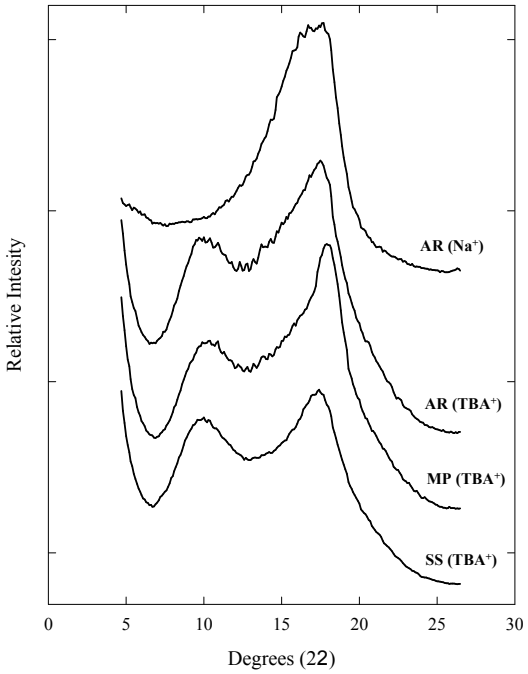

Figure 1.3. Wide-angle X-ray diffraction curves for as-received (AR), Na^+-form Nafion®, as-received TBA^+-form Nafion®, melt-processed (MP) TBA^+-form Nafion®, and "steam-stripped" (SS) TBA^+-form Nafion® powder. (Reprinted with permission from ref[58] *Journal of Membrane Science*, **75**, 7 (1992). Copyright 1992, Elsevier.)

In agreement with previous WAXD analysis of Nafion®, a crystalline reflection at 18°, 2θ, superimposed as a shoulder on a broad amorphous halo, can been seen for all Nafion® samples except the "steam-stripped" TBA^+-form Nafion® powder. The data in Figure 1.3 verifies that the "steam-stripping" method renders the ionomer totally amorphous.[58] In contrast to the "steam-stripped" powder sample, the melt-processed (MP) TBA^+-form Nafion® displays a prominent crystalline reflection at 18°, 2θ. The authors also note that the MP TBA^+ sample is insoluble in all solvents below 200 °C, while the SS TBA^+ sample is soluble in polar organic solvents at room temperature.[58]

Melt flow analysis was performed on SS and AR TBA^+-form Nafion® to determine if crystallinity or ionic aggregation was the limiting factor in melt-processing Nafion®. The melt flow analysis showed over one order of magnitude increase in the melt flow characteristics of the SS TBA^+-form sample when compared to the AR TBA^+-form Nafion®. Since the AR film was semicrystalline, the melt flow data verified that eliminating crystallinity is crucial in obtaining a true melt-processable ionomer membrane. Attempts were also made to index the melt flow properties of amorphous Na^+-form Nafion® but the material showed no evidence of flow owing to the high thermal stability of the strong dipole-dipole interactions present within sodium form ionic aggregates.

The dynamic mechanical properties of the MP TBA^+-form Nafion® were compared to the as-received state of Nafion® in the H^+, Na^+, and TBA^+ counterion forms, as shown in Figure 1.4.

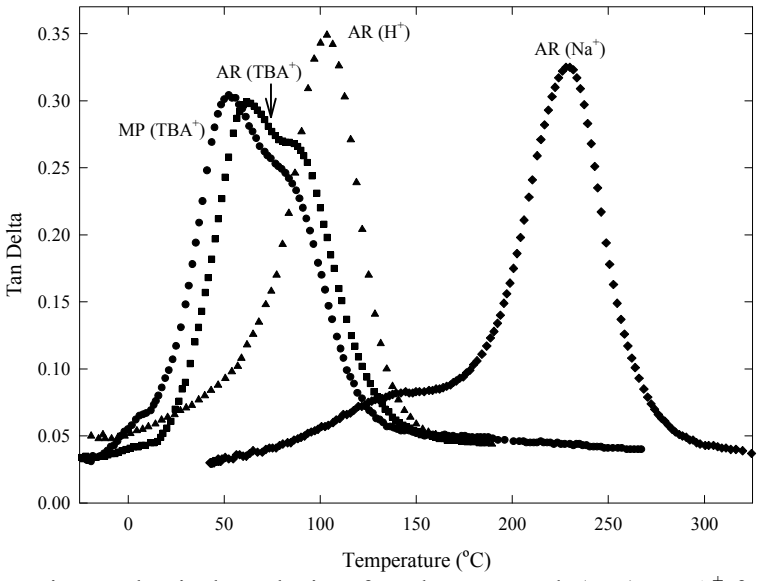

Figure 1.4. Dynamic mechanical analysis of melt-processed (MP) TBA^+-form Nafion®, as-received (AR) TBA^+-form Nafion®, AR H^+-form Nafion®, and AR Na^+-form Nafion®. (Reprinted with permission from ref[58] *Journal of Membrane Science*, **75**, 7 (1992). Copyright 1992, Elsevier.)

Figure 1.4 shows a dramatic decrease in the α-relaxation temperature upon neutralization of Nafion® using the bulky TBA^+ counterions. The large hydrophobic counterions weaken the electrostatic network and act as internal plasticizers to lower the α-relaxation temperature below that of the as-received acid form (H^+) of the ionomer. The authors also point out that even though the MP TBA^+-form sample has slightly lower relaxation temperatures than the AR TBA^+-form sample, the overall morphology is recaptured during the melt-processing procedure.

An alternative method to melt-processing Nafion® is to create a Nafion® solution and cast membranes of various thicknesses. In the early 1980's, two publications by Grot[60] and Martin[61] detailed a procedure for dissolving Nafion® membranes in water/alcohol mixtures at elevated temperatures and pressures. Martin et al. developed a procedure for the dissolution of Nafion® based on the solvent swelling studies of Yeo and coworkers on 1100 and 1200 EW Nafion®.[62] Yeo had pointed out that Nafion®

dissolution would not be possible unless the temperature was high enough to eliminate or melt the crystalline regions within the PFSI membranes. Martin et al. then proceeded to demonstrate the dissolution of Nafion® in mixed alcohol-water solvent systems under high temperature and pressure, swelling the membrane to high degrees and melting the small polytetrafluoroethylene crystallites.[61]

Based on the dissolution procedure of Grot and Martin, Aldebert and coworkers examined the nature and structure of Nafion® solutions in water and ethanol using small angle neutron scattering.[63] The Nafion® solutions were found to be heterogeneous and had one single scattering maximum attributed to the interference between nanometer-size scattering objects distributed homogeneously throughout the total volume of the sample. A separation distance between the nanometer-sized scattering objects was defined as, *d*, and varied systematically with the volume fraction of the ionomer, Φ_v. Due to the linear behavior between the separation distance and the volume fraction of ionomer, the authors concluded that the particles were exhibiting electrostatic repulsion similar to that observed for a colloidal suspension of charged particles. The authors also assumed that the solutions of Nafion® in both water and ethanol consisted of a dispersion of rodlike particles due to the slope of log *d* versus log Φ_v being greater than 0.33 but less than 0.5.[63, 64] The rodlike particles were suggested to have a compact cylinder structure with the solvent-polymer contact at the surface of the charged micelle as opposed to a more open coil model. The authors proposed that the polytetrafluoroethylene crystallites present in Nafion® were found in the center of the rodlike particles and oriented along the rod axis.[64] The overall result was later shown that Nafion® "solutions" were in fact a dispersion of colloidal particles composed of aggregated chains.[65]

Even though Nafion® solutions have been used for a variety of applications, it has been assumed that the morphologies, physical properties, and chemical characteristics of the cast membranes are identical to the as-received films. Based on various casting procedures Moore and Martin discovered that cast Nafion® is drastically different from as-received Nafion®.[66, 67] Membranes cast at room temperature from ethanol/water Nafion® dispersions were classified as recast films due to their brittleness, presence of mud cracks, and solubility in various polar organic solvents at room temperature. In contrast, the as-received Nafion® membranes were tough, pliable, and insoluble in virtually all solvents at temperatures below 200 °C. Moore and Martin then developed a "solution-processing" procedure to reconstitute the desired mechanical properties of as-received Nafion® from recast Nafion®.[66, 67] Solution-processing, shown schematically in Figure 1.5, involves adding a high boiling point solvent to the alcohol-water system to disrupt the colloidal particles.

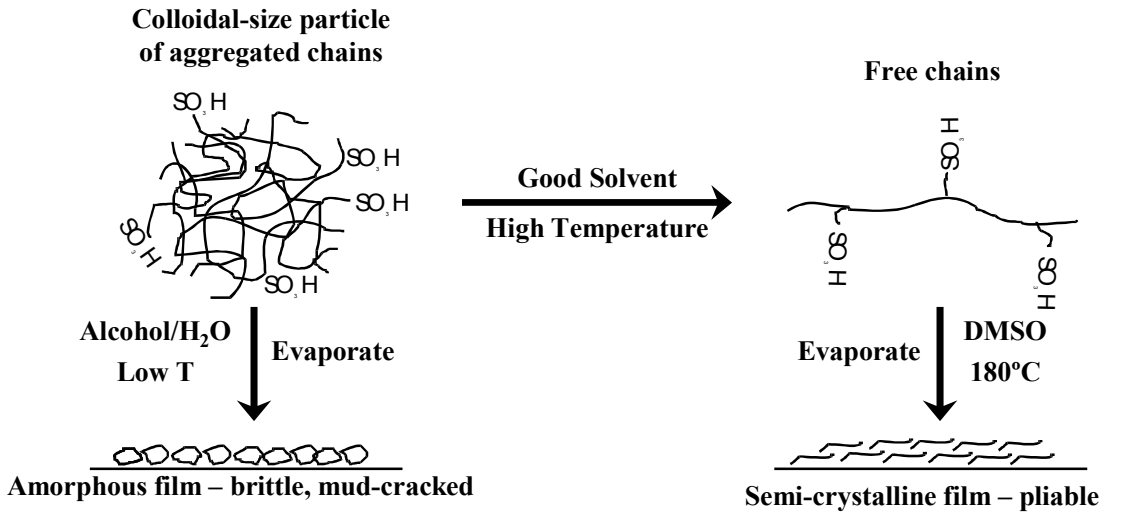

Figure 1.5. Solution processing procedure developed by Moore and Martin for perfluorosulfonate ionomers.

The membrane is then cast from solvents such as dimethylsulfoxide and dimethylformamide at an elevated temperature. Combination of the elevated casting

temperature and the plasticizing effect of the solvent provide the chain mobility necessary to facilitate macromolecular organization of the Nafion® chains in solution, thereby producing mechanically stable membranes.

Moore and Martin also documented the percent solubility of solution processed membranes by determining the percent weight loss after sonicating the films in a 50:50 ethanol/water mixture for one hour. Membranes with solubility below 5% were considered satisfactory in terms of mechanical properties in comparison to the as-received membranes. The authors concluded that the percent solubility of the Nafion® membranes was critically dependant on the solvent evaporation temperature. Membranes with less than 5% solubility were obtained by solution-processing in dimethylsulfoxide (DMSO) at 170 °C, ethylene glycol (EG) at 185 °C, or *N,N'* dimethylformamide (DMF) at 130 °C.[67]

Using SAXS and WAXD, Moore and Martin also discovered that the as-received and solution-processed membranes were semicrystalline, while the recast films were virtually amorphous.[67] The SAXS profiles of the as-received and solution-processed films displayed a distinct ionomer peak at q = 1.2 nm^{-1}, due to the presence of ionic clusters, and a prominent low angle maximum at q = 0.5 nm^{-1} attributed to the crystalline domains in the ionomer. On the other hand, the SAXS profile of the recast Nafion® only displayed the ionomer peak, confirming that the crystallinity was absent during casting. The enhancement in crystallinity and physical properties of the solution-processed films was attributed to the ability of the ionomer chains to reorganize from the colloidal aggregate state in solution to a more entangled network in the solid film.

PFSI Morphology

The morphology of PFSI's, particularly Nafion®, is characterized by the polar perfluoroether side-chains containing the ionic, sulfonate groups which organize into aggregates, thus leading to a nanophase-separated morphology where the ionic domains are distributed throughout the non-polar polytetrafluoroethylene (PTFE) matrix.[9, 27] In addition, the runs of tetrafluoroethylene are of sufficient length to facilitate organization into crystalline domains having unit cell dimensions virtually identical to that of pure PTFE.[68] The degree of crystallinity in PFSI's is generally less than ca. 10-wt% in 1100 equivalent weight Nafion® and has been shown to vary with equivalent weight.[27] The complex, phase-separated morphology, consisting of crystalline and ionic domains, of PFSI's has been the focus of several investigations.[9, 17, 27, 69-76]

An historical morphological model widely referenced for PFSI's is the cluster-network model first proposed by Gierke et al.[9, 27] Using SAXS and WAXD, Gierke and coworkers compared the morphological features of Nafion®, having a range of equivalent weights, in the unhydrolyzed sulfonyl fluoride precursor form, the hydrolyzed sulfonic acid form, and the neutralized metal sulfonate form. With the hydrolyzed form of Nafion®, a SAXS peak was observed at ~1.6°, 2θ. By using Bragg's Law, an interparticle spacing of 3-5 nm was calculated, which is characteristic of a system containing ionic clusters within a semicrystalline matrix. The ionomer peak was also shown to increase in intensity and shift to lower angles with various equivalent weights and increased hydration at specific equivalent weights. Based on the SAXS and WAXD observations, Gierke and coworkers concluded that the water-swollen morphology of

Nafion® was best described by a model of ionic clusters that were approximately spherical in shape with an inverted miclellar structure, as shown in Figure 1.6.

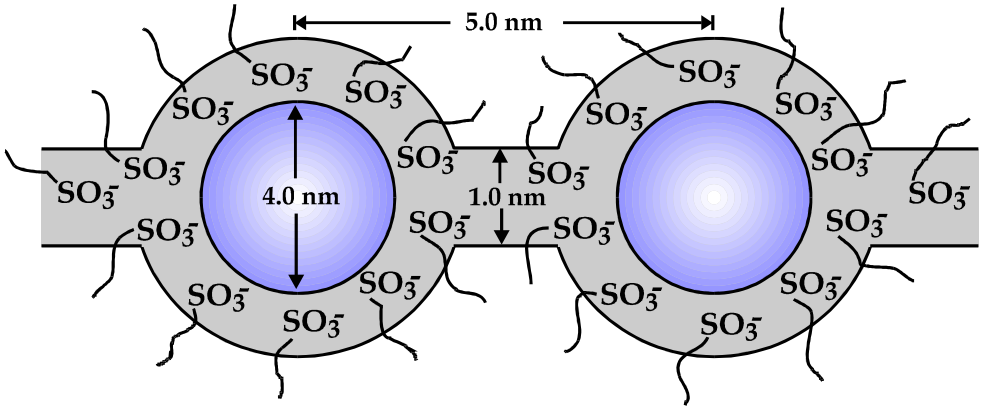

Figure 1.6. Cluster-network model for the morphology of hydrated Nafion®. (Reprinted with permission from ref[9] *Journal of Membrane Science*, **13**, 307 (1983). Copyright 1983, Elsevier.)

Cluster dimensions calculated from this simplified geometry were consistent with other experimental observations yet the observed spatial order of aggregates was not paracrystalline. Narrow (1 nm), ionic-lined channels connecting the aggregates were proposed to reconcile the permselective transport properties of solvent swollen Nafion®. The channels create a connected network of aggregates giving rise to percolation pathways through the membrane, however no direct evidence has confirmed the existence of channels within the membrane. The cluster-network model was, however, the first to offer an interparticle origin for the SAXS maximum in Nafion®.

As Hsu and Gierke were contemplating the cluster-network model, Roche and coworkers were using SAXS and small angle neutron scattering (SANS) to study the morphology of Nafion® in the acid and neutralized forms throughout a range of water contents.[69, 70] In the as-received state, Nafion® was found to have three contrast regions (three-phase system) consisting of a crystalline phase, ionic cluster phase, and an inhomogeneous matrix phase. By quenching the Na^+-form ionomer from 330 °C, the

membrane was rendered amorphous due to the disappearance of the SANS peak centered at q = 0.035 Å^{-1}.[69] By eliminating the crystallinity present in the ionomer, the number of phases were reduced, allowing for a decrease in the contrast regions available for scattering. Based on the lamellar periodicity of polytetrafluoroethylene crystals, (1000 Å), and the fact that random copolymers would exhibit an average distance of 15 Å between side groups, Roche et al. concluded that either a nonrandom distribution of side chains exists in some portion of the material or somehow included in the crystalline matrix of the ionomer.[69]

Along with eliminating the crystallinity present in Na^+-form Nafion®, Roche and coworkers examined SANS profiles using contrast matching with various mixtures of H_2O and D_2O.[70] A detailed analysis of the scattering features of the water swollen ionic domains was conducted by varying the content of H_2O and D_2O. In agreement with a simple, two-phase system, consisting of a hydrophobic and hydrophilic phase, the normalized scattering intensities of the water swollen membranes varied linearly with relative fractions of H_2O and D_2O. This observation indicated that both the zeroth-order scattering at low q values and the ionomer peak arise from the same scattering length density differences and could be attributed to the same morphological features. To account for the large dimensions portrayed by the zeroth-order scattering, an inhomogeneous distribution of clusters within the fluorocarbon matrix was proposed.

In agreement with the work by Gierke et al., Roche and coworkers also found that the ionomer peak increased in intensity and shifted to lower angles with increasing water content. The majority of water molecules in the swollen ionomer were phase separated with sharp phase boundaries, as determined by a Porod analysis of the SAXS data over a

wide range of scattering angles.[70] As opposed to Gierke's cluster-network model, Roche et al. attributed the origin of the ionomer peak in SAXS to an intraparticle scattering, for which the maximum corresponded to characteristic distances between structural elements inside the ionic particles. Despite the consistency of Roche's model with that of other proposed morphologies for PFSI's, a detailed quantitative analysis was still necessary.

Yeager and Steck[17] proposed a three region model for Nafion® based on various counterion selectivity and diffusion studies[77-80] as well as spectroscopic analysis of large bulky Ru(2,2'-bipyridine)$_3^{2+}$ counterions by Lee and Meisel[81] and the study of infrared bands of absorbed water in Na^+-form Nafion by Falk et al.[82] A depiction of the three region model can be seen below in Figure 1.7, where the letters A, B, and C represent each specific region.

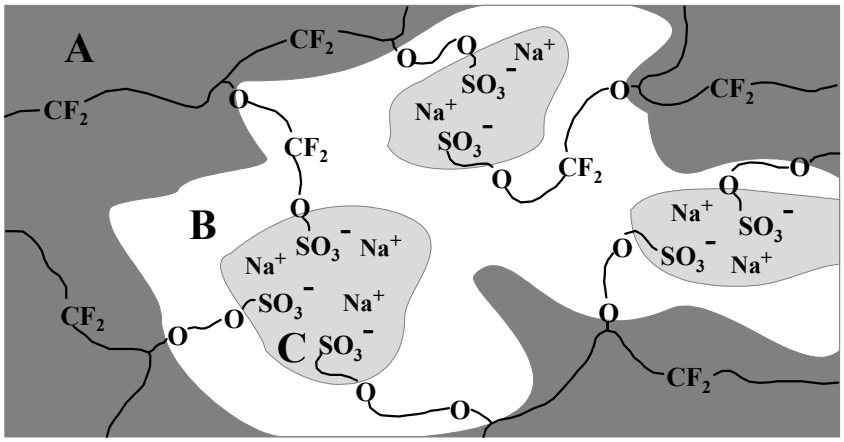

Figure 1.7. Three region model for Nafion® proposed by Yeager. (Reprinted with permission from ref[17] *J. Electrochem. Soc.*, **128**, 1880 (1981). Copyright 1981, The Electrochemical Society.)

Region A mainly consists of the polytetrafluoroethylene backbone of Nafion®, which would include any crystallinity present in the ionomer film. Region B is considered the amorphous region of the ionomer, consisting of the perfluoroether pendant side chain material, some lone ion pairs not incorporated into the ionic aggregates, and a small

amount of residual water. Region C consists of a highly polar region of ionic aggregates containing the majority of the sulfonates, counterions, and absorbed water.

Yeager et al. note that the relative proportions of counterions in regions B and C depend on their size, charge density, and hydration energy. Based on the work of Lee and Meisel, Yeager and Steck place counterions of low charge density such as Ru(2,2'-bipyridine)$_3^{2+}$ or Cs^+ in region B, while counterions of larger charge density and hydration energy are found in the more aqueous ionic domains of region C. Region B has been described as providing a continuous diffusion pathway for water between the ionic aggregates, while region C is responsible for the scattering seen from the ionomer peak in x-ray and neutron studies. The authors note that the three region model accurately depicts the differences in diffusion coefficients between Na^+ and Cs^+ counterions based on cesium's larger mean-free path in diffusing through the polymer matrix.

During the same time period as Yeager and Steck's three region model, Fujimura et al. were performing SAXS and WAXD on Nafion® ranging in equivalent weights from 1100-1500 and in the H^+, Na^+, and Cs^+ counterion forms. In agreement with previous scattering studies of Nafion®, the scattering maximum at $s \approx 0.07$ nm^{-1}, $s = ((2\sin\theta)/\lambda)$, was associated with the crystalline domain and the scattering maximum at $s \approx 0.3$ nm^{-1} was associated to the ionic domains.[68] In agreement with Gierke[27] et al., the low angle maximum also increased with increasing equivalent weight. A detailed analysis of the WAXD data for Nafion® showed an increase in the degree of crystallinity from 12-22% when varying the equivalent weight from 1100-1500, respectively. Based on the quantitative correlation of the SAXS and WAXD analysis and the scattering behavior of

uniaxially oriented Nafion®, the origin of the low angle scattering maximum was attributed to an average spacing between crystalline lamellar platelets.[68]

In a subsequent paper by Fujimura et al. the authors evaluated various models for the origin of the SAXS ionomer peak.[83] The characteristic dimensions of the ionic clusters associated with the ionomer peak at $s \approx 0.3$ nm^{-1} were evaluated for 1100 EW Nafion® in the H^+ and Cs^+ forms before and after swelling with water. With increasing water content, the cluster dimensions were shown to increase due to a shift in the scattering maximum to lower s values. Furthermore, the microscopic degree of swelling was found to be much greater than the macroscopic degree of swelling.[83] Based on these observations the ionomer morphology of Nafion® was determined to coincide with an intraparticle core-shell model similar to that proposed by McKnight[84] and coworkers[85] rather than an interparticle, two-phase, hard sphere model proposed by Cooper et al.[86] The core-shell model was portrayed as having an ion-rich core surrounded by an ion-poor shell that was comprised of mainly the perfluorocarbon chains.[83] The core-shell particles were dispersed in a matrix of fluorocarbon chains containing nonclustered ions and multiplets, so the ionomer scattering maximum was attributed to the short-range order distance within the core-shell particles.

With the aid of computer simulation, Fujimura et al. attempted to quantitatively distinguish between the two morphological models by analyzing the SAXS data.[83] For both the core-shell model and the two-phase hard sphere model, quantitative expressions for the variations in the scattering profiles with water uptake were derived from standard scattering theories and fit to the experimental data. Unfortunately, the analysis was

inconclusive due to the adequate fit of both models to the experimental data along with variations in water uptake and deformation.

The core-shell model morphology for Nafion® has recently been discounted based on SANS analysis of water swollen Nafion® performed by Gebel and Lambard.[87] Gebel and Lambard showed that the theoretical core-shell model fit poorly to the experimental SANS data between 0.3 and 2.0 nm^{-1}, and had unrealistic fits of the dimensional and contrast values extracted from the best fit profiles. Furthermore, the existence of isolated ion pairs constituting the matrix in the core-shell model was noted to be highly questionable in swollen membranes and confirmed to be improbable by electron-spin resonance measurements.[88]

Several years after the initial morphological models for Nafion®, Litt proposed a model based on a reevaluation of the SAXS analysis during swelling and deswelling experiments.[71] Litt's Lamellar model, Figure 1.8, is based on the theory that longer crystallizable regions in the ionomer will chain fold to an average lamellar thickness.

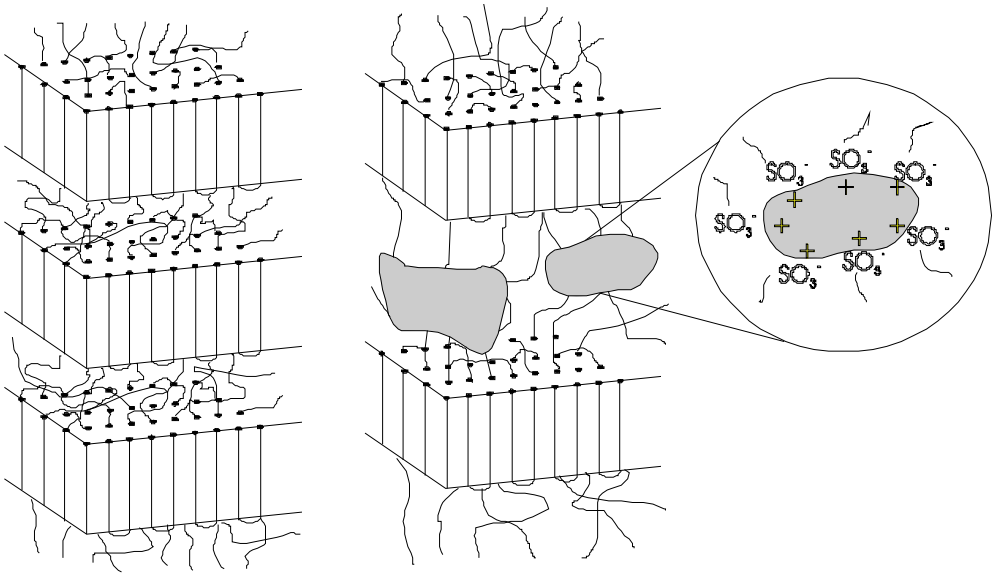

Figure 1.8. Proposed lamellar model for Nafion®

Once the lamellae have stacked on top of each other, they form a "micelle" where the surface is lined with the ionic groups and the interior is composed of the noncrystalline tie chains. Upon hydration, the amorphous region swells, pushing the micelles further apart and yielding a shift in the ionomer peak as observed with SAXS. The expansion is ultimately restricted by the tie molecules, which connect the micelle domains. An equilibrium swelling can occur due to the ability of the tie molecules to uncoil during hydration and exert a retractile force to maintain lowered conformational entropy. Though the lamellar model was in good agreement with SAXS data presented by Gierke,[27] it failed to adequately explain differing shifts in the scattering behaviors of the ionic domains and the lamellar long spacing with water content.[32]

A variation of the lamellar model was proposed by Haubold et al., in which the basic structure was projected to be a "sandwich" geometry, shown in Figure 1.9.

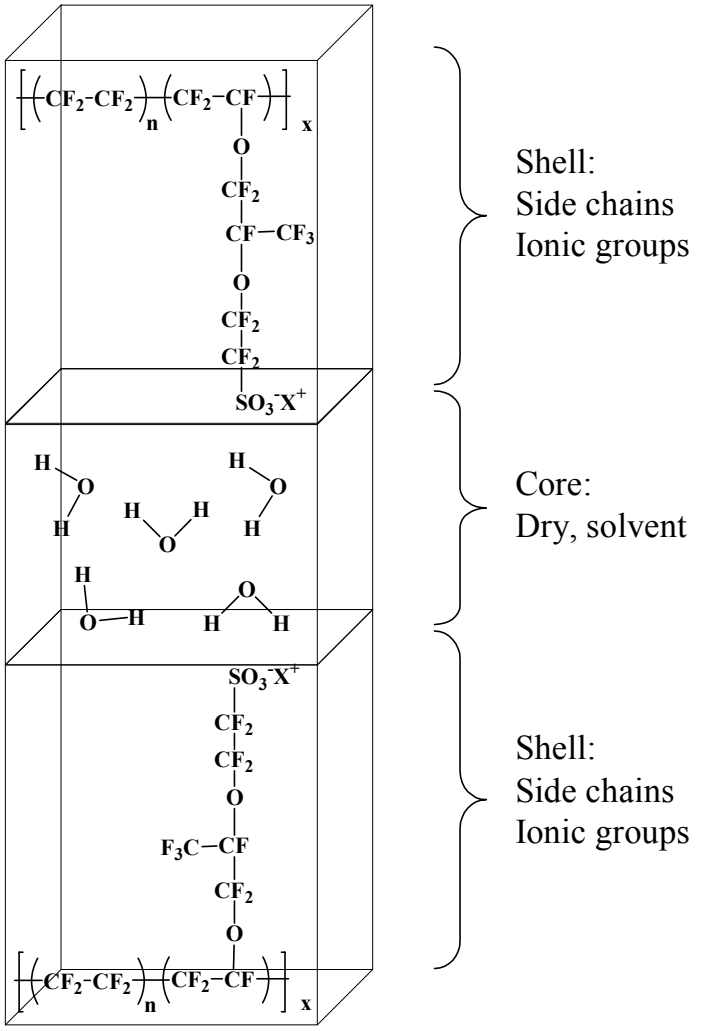

Figure 1.9. "Sandwich" Model proposed by Haubold and coworkers. (Reprinted with permission from ref[72] *Electrochimica Acta*, **46**, 1559 (2001). Copyright 2001, Elsevier.)

The outer layers of the sandwich (the "shell") is composed of side chains including the sulfonic acid functionalities whereas the inner portion (the "core") contains the swelling solvent. To provide percolation pathways through which proton conduction may occur, the structural elements are arranged in a linear fashion such that the solvent containing cores form a continuous pathway. By fitting the structure factor for a rectangular parallelepiped to the Sandwich Model, the authors extracted dimensions such as core thickness, combined shell thickness and lateral dimensions of the parallelepiped. Examining changes in fit parameters with solvent exchange from water to methanol

showed that increasing methanol content caused the spacing between neighboring shell layers to decrease while shell thickness increased, implying a conformational and/or packing change in the side chains and main chains. The authors suggested, however, that increasing methanol content leaves the side chains unaffected making geometrical understanding of the changes in layer thickness difficult.

Gebel et al. have proposed a model for the morphology of Nafion® based on the colloidal structure of rod-like particles with the ionic groups at the polymer-solvent interface.[32, 65, 73, 87] The "structural evolution" model stems from various SAXS, SANS, and ultra-small angle x-ray scattering (USAXS) data on swollen Nafion® membranes and is shown in Figure 1.10.

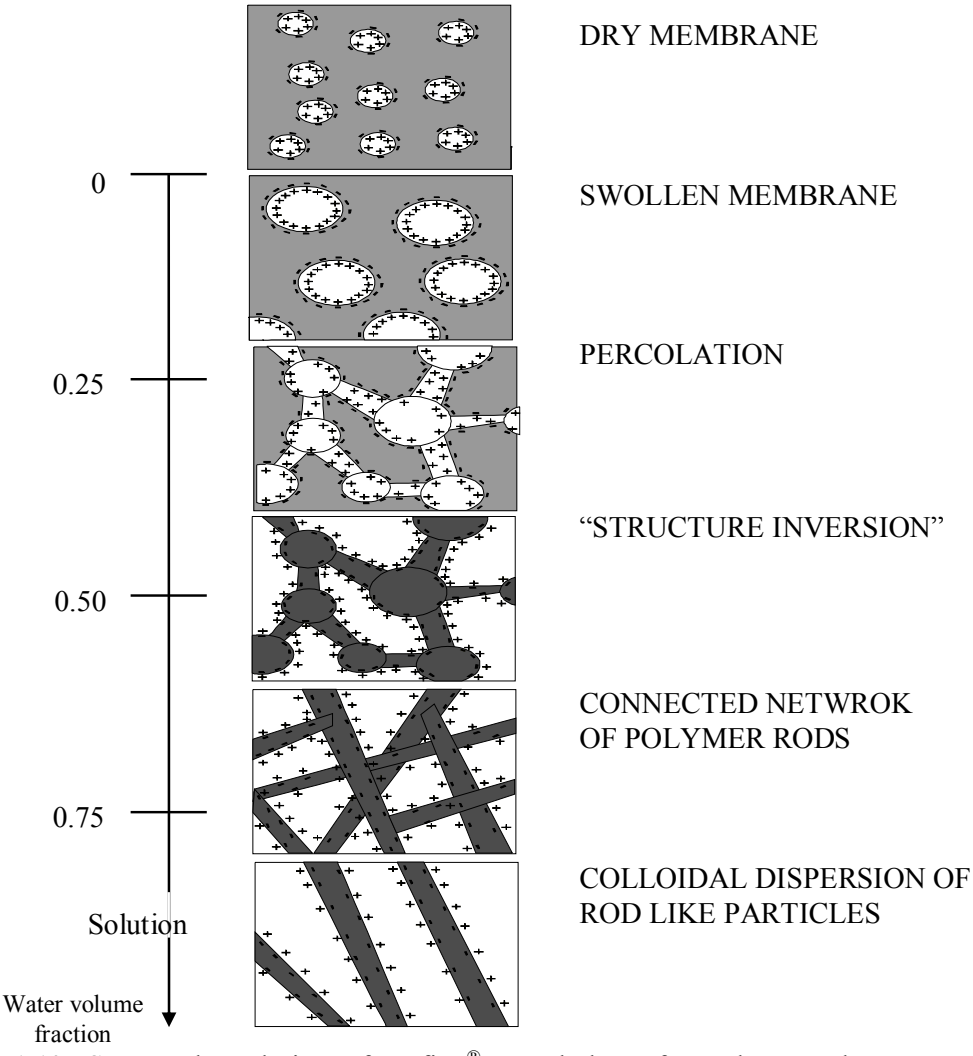

Figure 1.10. Structural evolution of Nafion® morphology from dry membrane to solution, proposed by Gebel. (Reprinted with permission from ref[73] *Polymer*, **41**, 5829 (2000). Copyright 2000, Elsevier.)

In the dry state, the membrane contains isolated, spherical ionic aggregates with diameters of ~1.5 nm and an average interaggregate separation of ~2.7 nm. Water absorption causes the aggregates to swell, encasing pools of water with ionic functionalities segregated to the polymer-water interface minimizing interfacial energy. As water content approaches 0.5 volume fraction, structural reorganization occurs in order to maintain a constant surface area. In this range of water content, percolation pathways develop in the membrane formed by connecting cylinders of water between the

swollen, spherical aggregates. At water volume fractions above 0.5, an inversion occurs such that the structure appears as a network of interconnected rods dispersed in water. Finally, as dissolution of the membrane occurs, the rod-like structures separate yielding a colloidal dispersion of isolated rods. While this model offers a reasonable mechanism for morphological evolution, no thermodynamic evidence exists for the phase inversion nor are there drastic changes to the scattering profiles making the inversion difficult to rationalize.

Based on Gierke's cluster-network model, Rollet et al. used a contrast matching method of SANS to probe the phase behavior of hydrated Nafion® exchanged with tetramethylammonium ($N(CH_3)_4^+$) counterions.[89, 90] Due to the excellent neutron scattering of tetramethylammonium counterions, a third source of contrast was introduced to examine the morphology at the interface between the water and polymer domains. By varying the composition of D_2O/H_2O in the exchanged membranes, Rollet et al. noticed a variation in the intensity as a function of q, indicating that the tetramethylammonium counterions were condensed in a thin layer with the sulfonate groups at the interface between the hydrophobic polymer domains and the solvent.[90] By assuming spherical aggregates and recognizing no structural changes occurring via water replacement with D_2O, the scattered intensity due to the structure factor was eliminated by dividing the various H_2O/D_2O SANS profiles by the profile for Nafion® in pure water. After normalization, the profiles exhibited a minimum at q = 1.5 nm^{-1}, which shifted to smaller q-values as the composition of D_2O decreased. Based on the form factor of spherical core-shell particles, a geometry of "polymer core surrounded by a counterion shell" was chosen based on the simulation of the model with the experimental data.

Therefore, based on the analysis, the authors concluded that the morphology of Nafion® was best described as polymer aggregates surrounded by water.[90]

In conjunction with Rollet et al., Rubatat and coworkers[74, 75, 91, 92] proposed a morphology of Nafion® dominated by rod-like aggregates with organization on length scales ranging from nanometers to microns, as shown in Figure 1.11.

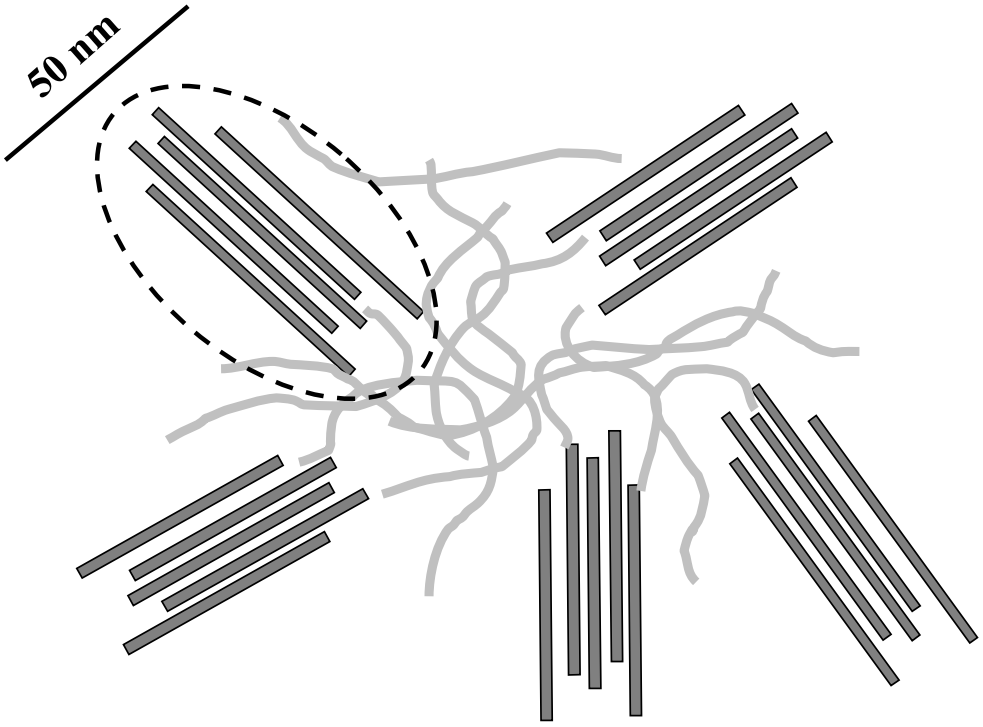

Figure 1.11. Elongated polymer aggregates model developed by Rubatat and coworkers. (Reprinted with permission from ref[75] *Macromolecules*, **37**, 7772 (2004). Copyright 2004, American Chemical Society.)

Using both SAXS and USAXS, the authors found two regimes of decreasing intensity in the scattering behavior, a q^{-1} power law at low angles and a q^{-4} power law at high angles. The high angle behavior is characteristic of a sharp interface between scattering particles, and the low angle behavior fits the expected scattering from rod-like particles over a q range defined by $2\pi/L$ to $2\pi/D$, where L and D are the particle length and diameter, respectively. Based on the scattering results the authors proposed that the intermediate q range provides information related to the size, shape, and spatial distribution of the

aggregates, while the ultra small *q* range was attributed to larger "bundles" of aggregates with long-range heterogeneous distributions.[74]

Scattering data of water swollen Nafion® with various polymer contents (Φp = 0.10-0.90), was collected in order to examine the position of both the ionomer and crystalline scattering peaks.[74] When plotting the polymer volume fraction versus the characteristic Bragg distance, *d*, of the ionomer and crystalline peak maxima, Rubatat et al. noticed two micrscopic swelling regimes in agreement with Gebel.[73] For low polymer volume fractions, below 60%, the ionomer peak maximum was found to follow a power law close to Φ^{-1}, as opposed to a power law of $\Phi^{-1/2}$ at polymer volume fractions above 60%. Based on the assumption that a power law of $\Phi^{-1/2}$ results in the dilution of cylindrical shaped particles, Rubatat et al. suggested the morphology of Nafion® aggregates are more representative of ribbon-like structures with a cross-sectional thickness close to 2 nm and a width of approximately 8 nm.[74]

Rubatat et al. also performed a series of WAXD, SAXS, and SANS on oriented Nafion® membranes to determine the validity of the elongated polymer aggregate model of Nafion®.[91, 92] The WAXD/SAXS analysis of Nafion® oriented between 100-272% draw ratios showed a trend of increasing intensity of the ionomer, amorphous, and crystalline peaks with increasing azimuthal angle. Based on these results, the Nafion® chains in the crystalline phase were determined to orient parallel to the draw direction of the membrane. It was determined that the overall crystallinity of Nafion® remained constant regardless of draw ratio, implicating that stress-induced crystallization was absent for Nafion®, possibly due to the influence of the ionic aggregates prohibiting the presence of large crystallites.[91]

Based on the Herman's orientation factor of the ionomer and crystalline peaks, the authors correlated the drawing effect on the polymer film at two different length scales.[91] The mesoscopic scale was used to characterize the ionomer peak and the molecular scale was used to characterize the crystalline peak. Due to the fact that the orientation factors between the ionomer and crystalline peaks differed between the mesoscopic and molecular scales, a cutoff size was determined to characterize two different structural orientation effects. While considering the elongated polymer aggregates model, the cutoff size corresponded to the diameter of the aggregates. A dual mechanism was postulated to occur during the orientation of Nafion®, corresponding to the rotation of large bundles (orientation factor of the ionomer peak) and sliding or disentangling of the aggregates within the bundles (orientation factor of the crystalline peak). The first mechanism was believed to occur mainly at low draw ratios, while the second mechanism was dominant at higher draw ratios.

Most recently, Schmidt-Rohr et al.[93, 94] have developed a parallel water-channel model for the morphology of Nafion® based on the simulation of various SAXS studies. The algorithm used to simulate various SAXS experiments involved calculating the scattering intensity I(q) by using two or three dimensional numerical Fourier transformations based on a user-defined scattering density, $\rho(x)$, on a lattice.[93] A representation of the parallel water-channel model of Nafion® can be seen in Figure 1.12.

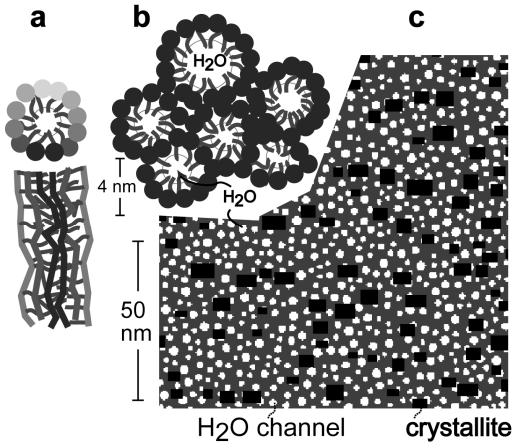

Figure 1.12. Parallel water-channel model of Nafion®. **a)** Top view and side view of an inverted micelle cylinder with water channel in the center. **b)** Hexagonal packing of several inverted micelle cylinders. **c)** Cross-section of scattering density distribution of inverted-micelle cylinders and Nafion® crystallites (black). (Reprinted with permission from ref[94] *Nature Materials*, **7**, 75 (2008). Copyright 2008, Nature Publishing Group.)

In order to develop the images seen in Figure 1.12, the authors assumed a hydration level of 20 vol% or 11 wt% water. Figure 1.12a, displays the top and side view of a single inverted micelle with the hydrophilic side chains facilitating a water channel through the center and the hydrophobic backbone of the polymer constructing the cylinder wall. Based on a 20 vol% of water, the simulated water channel diameters ranged from 1.8 to 3.5 nm with an average of 2.4 nm. Figure 1.12b, shows how several inverted micelle cylinders would approximately pack in a hexagonal fashion. Figure 1.12c displays a cross-sectional view of scattering density, $\rho(x)$, perpendicular to the channel axes. The water channels are displayed in white, the Nafion® amorphous region is gray, and Nafion® crystallites are black. The Nafion® crystallites used in the water-channel model simulation accounted for 13 vol%, were approximately 2-5 nm in thickness, and had x-y aspect ratios of 1 to 1.8. Based on the SAXS simulations, the water-channel model accurately depicted changes in the scattering profile with various water volumes, percent crystallinity, and changes in the thickness of the polymer layer surrounding the inverted

micelle cylinders.[94] An accurate depiction of the $I(q) \sim q^{-1}$ power law at small q values and the Porod region of q^{-4} at large q values was shown versus reported experimental data on the acid form Nafion® by Rubatat et al.[75, 94]

Physical Properties of PFSI's

The mechanical properties of PFSI's have not been heavily researched, with investigators primarily exploring morphology and transport properties. Due to the emergence of Nafion® and other PFSI's for industrial use in stationary and mobile fuel cell applications, the mechanical integrity of such membranes in extreme conditions must be taken into consideration. Dynamic mechanical analysis (DMA) of thermomechanical transitions of PFSI's, in particular Nafion®, has been the main focus in the literature on the physical properties of this class of ionomers.[13, 40, 41, 58, 95-97]

The earliest mechanical property data on Nafion® was presented by E. I. DuPont Co. and consists of tensile strength, tensile modulus, and elongation at yield as a function of cation type.[95] Since then, most of the mechanical property literature on Nafion® has involved dynamic mechanical analysis of tan δ, storage tensile modulus (E'), and loss tensile modulus (E"). In an early DMA study by Yeo and Eisenberg, a transition at maximum tan delta, labeled α, was observed for acid form Nafion® at 110 °C, and originally assigned to the glass transition of the nonionic component.[13] In preliminary studies, water was seen to have only a slight effect on the magnitude or position of the α-relaxation. A β-relaxation in the dry acid form was also observed at 20 °C, and shifted to lower temperatures with increasing water content. The β-relaxation was assigned to the glass transition of the ionic component. A low temperature γ-relaxation (-100 °C) was assigned to short range motions in the tetrafluoroethylene component, the same origin

assigned in pure PTFE. In a later examination of the results, Kyu and Eisenberg retained the assignment for the γ-relaxation yet reassessed their assignments of the α and β-relaxations.[15] The α-relaxation was reassigned to the glass transition of the ionic phase due to its sensitivity to counterion neutralization and water content. The β-relaxation was reassigned as the glass transition of the nonionic Nafion® matrix.

Cable and Moore used DMA studies to explore the behaviors of Nafion® membranes neutralized with a variety of counterions.[96, 98] It was concluded that the α-relaxation results from chain motions within and/or near ionic domains and the β-relaxation results from chain motions of amorphous fluorocarbon far removed from ionic aggregates, i.e. within the matrix. In this study, researchers referred to chain motions within an electrostatic network instead of polar and fluorocarbon components being discrete, isolated domains. This view is in agreement with Kyu and Eisenberg who demonstrated that effects on the behaviors of one phase result in strong effects on the other phase as the two are in intimate contact and are of small size.

In addition to examining the molecular origins of the mechanical relaxations, Moore and coworkers have examined the effect of counterion type and size on the mechanical properties of Nafion®.[98] Using both alkali metal and alkylammonium counterions, it was shown that counterion type has a profound impact on the thermomechanical properties of the membrane. In comparison to the acid form, small alkali metal counterions such as sodium, cause dramatic increases in both the α and β-relaxation temperatures due to the strong dipole-dipole interactions between sodium sulfonate groups, in comparison to the weak hydrogen bond interactions in the acid form. The use of alkylammonium counterions was found to provide a means to systematically

shift the α and β-relaxation temperatures.[96] Neutralization with large tetrabutylammonium (TBA^+) counterions caused the α and β-relaxation temperatures to shift below the α- relaxation temperature of the acid form. The decrease in relaxation temperatures was attributed to two contributing factors. First, the larger counterions significantly decreased the strength of the electrostatic interactions. Second, the bulky, organic counterions effectively plasticized the material, thus decreasing the relaxation temperatures.[41, 58] Using alkylammonium counterions ranging in size from tetramethylammonium to tetradecylammonium, the α and β-relaxation temperatures shift in a monotonic fashion over a temperature range from near that of the sodium form ionomer for tetramethylammonium to the α-relaxation temperature of the sulfonyl fluoride precursor for tetradecylammonium. The relative magnitudes of the two relaxations were also seen to vary with counterion type. Tan delta curves for membranes neutralized with small counterions were dominated by the α-relaxation and membranes neutralized with large counterions had more intense β-relaxation profiles.

Page and Moore[41, 99, 100] have used the current DMA results in conjunction with ^{19}F solid-state NMR and SAXS experiments to precisely define the molecular and morphological origins of the α and β-relaxations of Nafion® neutralized with a series of alkylammonium ions. SAXS analysis was used to monitor the ionomer morphology as a function of temperature and provided insight into the relationship between the strength of the electrostatic network and the relaxations observed using DMA. In relation, variable temperature ^{19}F solid-state NMR allowed the relaxations and morphological changes to be linked to the molecular motions of Nafion® neutralized with various counterions.

Initially, Page and Moore examined Nafion's® controversial DSC endothermic peaks during the initial heating. Various publications have attempted to correlate the endothermic events in DSC with the thermo-mechanical relaxations of Nafion® using DMA.[13-15, 67] Eisenberg and coworkers attributed the endothermic events to the glass transition temperature of the matrix of Nafion® (140 °C) and the ionic domains (240 °C).[15] Almeida et al. showed the existence of two endothermic events upon first heating of Nafion® occurring at 120 °C and 230 °C, respectively. Upon reheating, the peak at 120 °C was absent but reappeared gradually during annealing.[101] Page and Moore repeated this study using Nafion neutralized with either Na^+ or Cs^+ counterions.[41] As opposed to Almeida et al. only one endothermic event was seen at 240 °C, for both Na^+ and Cs^+-form Nafion®, and disappeared upon rescan after melt quenching from 330 °C. The peak at 240 °C reappeared after annealing at 200 °C for extended periods of time and increased in heat of fusion (ΔH) with longer annealing times. After 24 hours of annealing at 200 °C, the endothermic peak recovered half of the initial ΔH, meaning 50% of the initial crystallinity was recovered by isothermally crystallizing Nafion® at 200 °C. The assignment of the endothermic peak to the formation of crystallites was verified by the disappearance of the crystalline peak upon quenching from 330 °C at low q values using SAXS. In contrast to the Na^+-form DSC data, the Cs^+-form Nafion® displayed a 100% recovery in the ΔH upon annealing at 200 °C for 24 hours. By exchanging to the larger counterion, the dipole-dipole interactions were weakened throughout the electrostatic network, allowing for increased crystallization kinetics of Nafion® in the Cs^+-form. By annealing Cs^+-form Nafion® at temperatures ranging from 120 °C and 240 °C for two hours, Page and Moore noticed the appearance of multiple endothermic

events at lower annealing temperatures and one endothermic event at higher annealing temperatures. The endothermic peaks were attributed to multiple melting behaviors due to the shift of the low-temperature endotherm toward higher temperatures with increased annealing temperature. Thus, the low temperature endotherm was attributed to melting of small crystallites while the high temperature endotherm was due to the melting temperature of thicker lamellae.[41]

Based on variable temperature SAXS profiles of Nafion® in various alkylammonium counterion forms, Page and Moore examined the relationship between the strength of the electrostatic network and the mechanical relaxations observed using DMA.[41] The SAXS profiles revealed an abrupt decrease in the scattering intensity of the ionomer peak with increasing temperature. The temperature of the abrupt change in intensity also increased with decreasing counterion size. It was noted that the temperature at which the morphological transition occurred was strongly correlated with the α-relaxation temperature seen using DMA with the various alkylammonium counterions. The morphological transition was explained as a destabilization of the static electrostatic network into a dynamic network through the process of ion-hopping, where the thermally activated ion pairs "hop" from one aggregate to another in order to relieve local stress.[41]

In order to understand the link between the electrostatic network and the molecular motions, Page and Moore examined Nafion® in various alkylammonium counterions using variable temperature ^{19}F Solid-state NMR. By using spin-diffusion and sideband analyses over the same temperature range as both SAXS and DMA, a correlation was made between the transition from a static to a dynamic electrostatic

network and the corresponding changes on the molecular level. Changes in the spin-diffusion times were attributed to the mobility of polymer chains based on a constant distance between coupled side-chain and main-chain fluorine nuclei. In agreement with SAXS and DMA, an increase in the spin-diffusion time occurred near the morphological transition temperature for both TMA^+ and TBA^+ counterions, and was attributed to the onset of molecular motions. The sidebands associated with the ^{19}F resonances were also used to observe changes in mobility of Nafion®. The sidebands arise due to dipolar coupling and the intensity of the peaks correlate to the rigidity of the polymer. The sidebands for the fluorine nuclei of the side and main chains were shown to decrease with increasing temperature in TMA^+ and TBA^+-form Nafion®. The sidebands of the TBA^+-form Nafion® decreased more rapidly than the TMA^+-form Nafion® due to the increased mobility of the polymer in the TBA^+ form. By normalizing the sideband peak intensities of both the main and side chains, the side chains were determined to be more mobile than the main chains, supporting the NMR study of Schmidt-Rohr et al.[102] As a result of these studies, the α-relaxation was attributed to the onset of long-range mobility of both main and side chains through destabilization of the electrostatic network. Network destabilization is thought to occur through ion-hopping, the process of ion pairs transferring between aggregates to balance electrostatic and elastic forces.[103] In contrast, the low temperature β-relaxation was associated with the onset of chain motions, primarily in the backbone, within the concept of a static, physically crosslinked network of chains, similar to the traditional concept of a polymer glass transition.

Chemical Properties

The Department of Energy has currently set PEMFC durability targets of 5,000 hours for transportation applications and 40,000 hours for stationary power applications.[104] It has been shown that one of the weakest components in achieving extended fuel cell lifetimes is the proton exchange membrane.[105] Even though PFSI's are currently the benchmark materials for use in PEMFCs, chemical and mechanical degradation are the main causes of premature failure during operation.[104, 106] The PFSI Nafion®, with a thickness of 180 μm, was used by Stucki et al. to demonstrate that a fuel cell stack can last approximately 15,000 hours at 80 °C under continuous operating conditions.[107] Alternatively, Curtin et al. showed that 25 μm thick Nafion® last approximately 2,500 hours in a hydrogen/air fuel cell under a continuous load of 0.8 A/cm^2 at 65 °C, 100% RH, and ambient pressure.[108] Curtin et al. showed that even though fuel cell life expectancy decreases with thinner proton exchange membranes, a higher performance efficiency along with a decrease in material cost are driving the use of thinner proton exchange membranes in fuel cells.[108, 109]

The main two causes for membrane failure during fuel cell operation are chemical and physical degradation.[109] LaConti et al. proposed a chemical degradation mechanism within a hydrogen/oxygen fuel cell where molecular oxygen permeates through the membrane from the cathode and reduces to hydrogen peroxide by reacting with the Pt catalyst at the anode.[106, 110] A schematic of this mechanism is shown below in equations 1-10 through 1-12. Various authors have also documented the production of hydrogen

$$H_2 + Pt \rightarrow Pt\text{-}H \quad \text{(at anode)} \qquad \textbf{Eq. 1-10}$$

$$Pt\text{-}H + O_2 \rightarrow \bullet OOH \qquad \textbf{Eq. 1-11}$$

$$\bullet OOH + Pt\text{-}H \rightarrow H_2O_2 \qquad \textbf{Eq. 1-12}$$

peroxide at the cathode due to oxygen reduction on Platinum/Carbon catalysts.[111-114] The oxygen reduction reaction at the cathode is considered a multielectron reaction that proceeds via several elementary steps. Oxygen can go through a "direct", four electron reduction to water (Eq. 1-13), or a series of two electron reactions with an hydrogen peroxide intermediate (Eq. 1-14).[114] Paulus and coworkers verified the presence of

$$O_2 + 4H^+ + 4e^- \rightarrow 2H_2O \qquad \textbf{Eq. 1-13}$$

$$O_2 + 2H^+ + 2e^- \rightarrow H_2O_2 + 2H^+ + 2e^- \rightarrow 2H_2O \qquad \textbf{Eq. 1-14}$$

hydrogen peroxide by using a rotating ring-disk electrode (RRDE) where the oxygen reduction reaction takes place on the central disk electrode and H_2O_2 is produced on the concentric ring electrode, depending on the potential difference between the two electrodes.[112] By operating with potentials greater than 0.6 V, a relevant fuel cell cathode potential, Paulus et al. demonstrated that oxygen reduces exclusively to H_2O via a complete four-electron process as shown in equation 1-13.[112] On the other hand, by operating at potentials lower than 0.3 V (anodic potentials), up to 80% of the oxygen molecules were transformed to H_2O_2 when in contact with the Platinum/Carbon catalysts.[112, 113] Even though the absolute concentration of H_2O_2 remains questionable, various authors have confirmed the presence of H_2O_2 in the exhaust gas, drain water, and membrane of a PEMFC during operation.[115-117]

Due to the relatively long fuel cell operational times and low degradation rates, accelerated chemical degradation experiments were developed to examine PFSIs without waiting for membrane failure to occur during fuel cell operation.[104, 118, 119] Four common *in-situ* accelerated fuel cell life tests include testing; 1) elevated temperatures[120] , 2)

reduced humidity[121] , 3) cycling of humidity, temperature, or cell potential[122] , and 4) open circuit voltage (OCV)[123] . Changes in both gas crossover and fluoride-ion emission rate are monitored in order to accurately determine membrane degradation during accelerated in-situ testing.[109]

One of the most popular *in-situ* methods for testing the chemical degradation of a proton conducting electrolyte membrane is the OCV test.[39, 106, 115, 116, 123-128] By definition the OCV test involves operating a fuel cell with both reactant gases while maintaining an unclosed electrical circuit. Based on this condition, the fuel cell will not generate any current and the cell potential should be close to the theoretical potential based on changes in temperature, pressure, and concentration of reactant gases.[55] The theoretical cell potential for an H_2/O_2 fuel cell should be E° = 1.23 V at 25 °C and 1 atm based on equation 1-15, where ΔG is Gibbs free energy, n is the number of electrons per

$$E^{\circ} = \frac{-\Delta G}{nF} \qquad \textbf{Eq. 1-15}$$

molecule of hydrogen (n = 2), and F is Faraday's constant.[53, 55] However, the actual voltage under open circuit conditions is significantly lower than the theoretical cell potential based on parasitic electrochemical processes besides hydrogen oxidation at the anode and oxygen reduction at the cathode. Some voltage loss at the OCV is due to the permeation of hydrogen from the anode to the cathode where it competes with the oxygen reduction reaction, causing a mixed potential. Carbon corrosion of the electrodes may also cause a decrease in the potential under open circuit conditions.[53]

Endoh et al. performed an OCV test on the perfluorosulfonic acid ionomer Flemion manufactured by Asahi Glass Company.[129] Under normal OCV conditions, Endoh et al. noticed a voltage decay rate of 0.2 mV/hr, but when the humidity was

decreased from 100 to 30% the voltage decay increased by an order of magnitude to 2.0 mV/hr, verifying accelerated degradation within the fuel cell. Endoh and coworkers also saw a dramatic increase in the hydrogen crossover through the membrane between the normal and accelerated OCV tests, which they attributed to severe membrane degradation. In conjunction with LaConti et al., Endoh et al. concluded that the chemical degradation was due to hydroxyl radical attack on the membrane based on the formation of hydrogen peroxide via the permeation of oxygen from the cathode and reacting with Pt-H at the anode.[129]

Mittal et al. examined the chemical degradation of Nafion® in an H_2/O_2 fuel cell under open circuit conditions using various membrane electrode assembly configurations.[124] Mittal et al. noted that chemical degradation of Nafion® during fuel cell operation is negligible in the absence of either one of the reactant gases (H_2 or O_2). Similarly, the membrane degradation rates are minimal when exposed to H_2 and O_2 in the absence of a catalytic surface (Pt/C). Since all three variables (reactant gases and catalysts) must be present in order to induce chemical attack on the membrane, Mittal et al. designed three different membrane electrode assemblies (MEAs). The first MEA consisted of a membrane with catalyst applied only to the anode side. The second MEA was constructed with catalyst only on the cathode side of the membrane. The third MEA involved coating Nafion® 117 with a Pt/C catalyst and hot pressing Nafion® 112 on top of the previous membrane creating a catalyst layer sandwiched between two proton conducting layers. After operating all three types of MEAs at 90 °C and 30% relative humidity, Mittal et al. noticed minimal fluoride emission from the MEA with catalyst coated on the anode only and the MEA with the catalyst sandwiched between two

Nafion® films. On the contrary, the MEA with catalyst coated on the cathode side had a fluoride emission rate of approximately 3.0 μmol/h·cm^2 after fifteen hours of testing. Mittal and coworkers suggested that membrane degradation due to the formation of H_2O_2 at the anode followed by decomposition to radical species could not be the primary mechanism based on the significant degradation seen from the MEA coated with catalyst only on the cathode side. Fluoride emission rate of an MEA consisting of Nafion® 117 sandwiched between two Pt/C catalyst layers was examined at various current loadings as well as at OCV conditions. With current densities ranging from 0-150 mA/cm^2, Mittal et al. recorded an overall decrease in the fluoride emission rate with increasing current density, which they attributed to changes in the electrode surface properties at both the anode and cathode, as well as an increase in reactant crossover with decreasing current density. It should also be noted that the fluoride emission rate was dramatically higher when measured from the cathode condensate as opposed to the anode condensate.

Inaba and coworkers examined the chemical degradation of Nafion® in a PEMFC under open circuit conditions at 60 °C for 60 days with a reactant gas flow rate of 150 ml/min.[116] Throughout the entire 60 day OCV test, the open circuit voltage dropped from 960 to 840 mV with an average voltage degradation rate of 83 μV/hr. Every 24 hours the air to the cathode was replaced with argon and the hydrogen crossover current density was measured as a function of time. Throughout the first thirty days, the hydrogen crossover current density was approximately 0.8 mA/cm^2. Between 30 and 60 days the hydrogen crossover current density sharply increased from 0.8 to 11.0 mA/cm^2, indicating severe thinning and the formation of pinholes throughout the membrane. Inaba et al. suggested that reactant gas crossover increases under open circuit conditions

due to the lower consumption of reactant gases at the electrodes during the electrochemical fuel cell reactions. The fluoride ion release rate was also calculated from both the anode and cathode condensate as a function of time throughout the OCV test. The fluoride content in both the anode and cathode drain water increased from approximately 8.3 x 10^{-8} g/cm·h to 16.7 x 10^{-8} g/cm·h after 45 days under open circuit conditions. There was little differential between the fluoride ion release rates between the anode and cathode based on the assumption that the fluoride ions could move easily from side to side within the membrane. Inaba et al. also showed increased chemical degradation of the PEM by increasing the pressure of the oxygen being sent to the cathode. This coincides well with the study of LaConti et al. verifying that the primary formation of hydrogen peroxide in conjunction with hydroxyl radicals is due to the migration of oxygen from the cathode to the anode.[106] Based on this information, Inaba et al. concluded that hydrogen peroxide is produced at the anode catalyst upon the direct combustion between adsorbed hydrogen and crossover oxygen, upon which chemical degradation of the electrolyte membrane exist. Inaba and coworkers also pointed out that the concentration of hydrogen peroxide would increase with decreasing humidity within the fuel cell due to the difference in the boiling points of H_2O (100 °C) and H_2O_2 (150 °C).[116]

Ohma et al. performed transmission electron microscopy, micro-Raman spectroscopy, and ion chromatography to correlate Nafion® degradation within a PEMFC to the formation of a platinum (Pt) band within the membrane during OCV testing.[123, 125, 127] After 110 hours at open circuit voltage conditions, the fluoride ion emission rate at the anode was greater than at the cathode and the difference between the two electrodes

increased with increasing degradation time. Based on images of the MEA from scanning electron microscopy, Ohma et al. noticed the formation of a Pt band within the membrane, which was located closer to the anode than the cathode. Based on this observation, the authors suggested that the increase in fluoride ion release rate seen from the anode condensate was due to the location of the Pt band. Transmission electron microscopy images confirmed the presence of a Pt band located 12-22 μm from the anode catalyst layer and consisting of platinum clusters averaging 25 nm in diameter.[127] Ohma et al. assumed that the formation of a Pt band within Nafion® was based on the mixed potential profile seen during fuel cell testing which was described by Liu and coworkers[117] using a diffusion control theory. Based on the diffusion control theory, if the mixed potential is close to 1 V, deposited Pt is oxidized to Pt ions, which then diffuse into the membrane and are reduced back to the Pt nuclei. The reaction continues from the cathode to the anode until the mixed potential is approximately 0 V, upon which the dissolution reaction ceases and the Pt nuclei become stable.[123] Ohma et al. also note that the location of the Pt band within the polymer membrane is influenced by the partial pressures of both hydrogen at the anode and oxygen at the cathode, and their respective permeabilities throughout the membrane.[127] Since the mixed potential near the Pt band is close to 0 V, Ohma et al. believed that such a low potential favored the formation of hydrogen peroxide and hydroxyl radicals which increased the chemical degradation of the polymer electrolyte. Another aspect of increased hydrogen peroxide formation and chemical degradation is due to the Pt particle dispersion and apparent density. Inaba et al. have shown that there is an increase in the catalytic surface area of well dispersed Pt particles and hence an acceleration of hydrogen peroxide.[130] Ohma et al. suggest that since the Pt

particles in the Pt band are more uniformly dispersed, there should be a decrease in the oxygen reduction reaction activity (Eq. 1-13) and a higher rate of the two-electron hydrogen peroxide reaction (Eq. 1-14). By using micro-Raman spectroscopy, Ohma and coworkers verified that chemical degradation of Nafion® occurred more readily near the Pt band.[125, 127] A decrease in the relative intensities of the C-C, S-O, C-O, and C-F peaks, along with a decrease in the full width at half maximum of the C-C peak at the location of the Pt band (18 μm), proved that accelerated chemical degradation was occurring near the dispersed Pt particles. In conclusion, Ohma et al. observed the formation of a Pt band during OCV testing and verified that chemical degradation of the polymer electrolyte was accelerated within the vicinity of the Pt band.

Teranishi et al. examined the chemical and physical degradation of Nafion® after 24 hours of fuel cell operation under open circuit conditions.[115] A characteristic progressive decrease in the cell efficiency was documented during the OCV test. The rate of the decrease was 1.3 mV/hr for the fuel cell with 100% humidification and 5.8 mV/hr for the fuel cell with no humidification of the reactant gas streams. Further characterization of the MEA subjected to the 24 hour OCV test under 100% humidity was accomplished using both ac impedance and scanning electron microscopy. A Cole-Cole plot of the MEA before and after the OCV test was constructed and an increase in the low frequency cell resistance was observed, indicating that the voltage drop may be due to deterioration of the electrodes rather than the membrane. The scanning electron microscopy images of the MEA before and after the OCV test indicated that severe degradation occurred at the interface between the membrane and cathode catalyst layer. Teranishi and coworkers assume that the cathode degradation is due to the permeation of

H_2 through the membrane where it forms hydrogen peroxide on the cathode. Gas chromatography was used to verify that hydrogen gas permeability through the MEA increases with both temperature and humidity. Direct gas mass spectroscopy was also performed to examine the cathode exhaust after the OCV test. The direct gas mass spectroscopy results identified HF, H_2O_2, CO_2, SO, SO_2, H_2SO_2, and H_2SO_3 as compounds present in the cathode exhaust stream, indicating the onset of chemical degradation of Nafion® during the OCV test.

Merlo et al. performed an OCV test on the short-side chain perfluorosulfonic acid ionomer Hyflon® Ion.[39] For their first study, Merlo and coworkers examined the hydrogen crossover and OCV decay using three different reactant gas setups. The three fuel cell configurations consisted of the following anode/cathode reactant gas designations; hydrogen/air, hydrogen/nitrogen, and nitrogen/air. For all three fuel cell setups the cell temperature was 70 °C with a relative humidity of 50% for the reactant gases throughout the duration of the OCV test (at least 200 hours). In agreement with Mittal et al.[124] , Merlo and coworkers only observed hydrogen crossover or fuel cell performance degradation when both hydrogen and oxygen were used as reactant gases as opposed to the hydrogen/air and nitrogen/air systems. Based on this result, Merlo et al. concluded that H_2O_2 formation on the anode was feasible due to the permeation of oxygen through the polyelectrolyte membrane. In order to verify the influence of different operating conditions, Merlo et al. performed OCV tests on the Hyflon® Ion at 70 or 90 °C and either 50 or 100% relative humidity. Based on hydrogen crossover data, the membrane degradation rate increased with decreasing reactant gas humidity, but remained constant with changes in the fuel cell temperature. This result indicated that

high temperature operation alone will not reduce the lifetime of the Hyflon® Ion membranes.

Kundu and coworkers examined both reversible and irreversible voltage loss in a PEMFC during an OCV durability test.[128] OCV tests of 380 and 900 hours were completed with a cell temperature of 90 °C and 100% relative humidity. During both OCV tests, Kundu et al. noticed a rapid decrease in the voltage for the initial 50 hours followed by a slower voltage degradation rate beyond 50 hours of operation. The rapid degradation period was referred to as the transient decay period and beyond 50 hours the low voltage degradation was referred to as the steady decay period. It was suggested that reversible voltage degradation mainly occurred in the transient decay period. During this period, recoverable voltage losses could be due to various changes in operating conditions, such as cell and reactant gas temperature, and cathode flooding, both of which could decrease the open circuit voltage. Irreversible voltage degradation, witnessed in the steady decay period was attributed to membrane thinning and loss of catalytic surface area from platinum migration into the polymer electrolyte. In order to investigate irreversible voltage degradation, Kindu et al. examined polarization curves taken at various times throughout the OCV tests. Polarization curves were obtained at two different testing conditions, high pressure, high temperature (HPHT) and low pressure, low temperature (LPLT). The HPHT setup consisted of a cell temperature of 80 °C, 100 kPa pressure, and anode and cathode relative humidities of 65 and 50%, respectively. The LPLT setup involved the same relative humidities for both the anode and cathode, but a cell temperature of 65 °C and a pressure of 20 kPa. Along with examining the polarization curves, Kundu et al. performed crossover current and electrochemically

active surface area measurements to confirm the presence of irreversible voltage degradation during OCV conditions. The average rate of irreversible voltage degradation calculated from the polarization curves was 0.083 mV/hr for the HTHP curve and 0.141 mV/hr for the LTLP curve. Based on the loss of electrochemical surface area and increase in the crossover current, an average decay rate of 0.146 mV/hr was estimated. In comparison, voltage decay rates within the first 20 hours, or the transient decay period, were as high as 5.8 mV/hr, which is in agreement with the OCV data of Teranishi et al.[115] Overall, Kundu et al. concluded that voltage losses during OCV testing should be clarified when reported in the literature due to the large amount of reversible voltage degradation, which should be represented in any further voltage degradation models.[128]

As opposed to *in-situ* accelerated fuel cell life tests such as the OCV test, various authors have chosen to examine the chemical degradation of PEMs by an *ex-situ* method, most commonly referred to as the Fenton's Test.[39, 108, 110, 131-144] The Fenton's Test focuses mainly on the fact that the presence of H_2/O_2 in the fuel cell exhaust has been verified using direct gas mass spectroscopy.[115] By introducing Fe^{2+} or Cu^{2+} catalysts to aqueous H_2/O_2 (3-30%) at fuel cell operating temperatures, •OH and •OOH radicals are created, which in turn can attack various organic species used as proton exchange membranes.[104] The main reaction mechanisms for the creation of both •OH and •OOH radicals during the Fenton's Test are shown below in Equations. 1-16 and 1-17.[109]

$$H_2O_2 + Fe^{2+} \rightarrow Fe^{3+} + \bullet OH + OH^- \qquad \textbf{Eq. 1-16}$$

$$\bullet OH + H_2O_2 \rightarrow H_2O + \bullet OOH \qquad \textbf{Eq. 1-17}$$

Even though the Fenton's Test is an ex-situ chemical degradation method, it is based on the idea that various catalytic counterions are present during fuel cell operation

either by contaminated feed streams or hardware degradation. Pozio et al. have shown that using SS316L stainless steel as a material for bipolar plates within a fuel cell can cause membrane degradation and contamination based on residual iron, chromium, and nickel counterions leaching into both the hydrogen and oxygen feed and exhaust streams.[131] The authors examined both membrane degradation as well as fuel cell performance degradation based on the use of either stainless steel or aluminum bipolar plates. By comparing fuel cell voltage versus time, Pozio and coworkers noted a continual decrease in the fuel cell voltage when using stainless steel bipolar plates as opposed to minimal performance degradation with the aluminum bipolar plates. Coincidently, the average fluoride concentration in both the anode and cathode exhaust was significantly higher when stainless steel was used as opposed to aluminum. Upon removal of the stainless steel material, the contamination decreased by approximately 20%. With the aide of atomic absorption spectroscopy, Pozio et al. verified that the cathode exhaust contained trace amounts of chromium and nickel and a significant amount of iron, which was attributed to the decrease in fuel cell performance and increase in fluoride release or chemical degradation of the polymer membrane.

Based on the formation of hydroxyl and hydroperoxyl radicals via in-situ or ex-situ fuel cell degradation, Curtin et al. have recently proposed a chemical degradation mechanism for Nafion® involving abstraction of a hydrogen atom from residual carboxylic acid found on the ends of the polytetrafluoroethylene backbone.[108] Curtin's degradation scheme is shown in three parts using Equations 1-18 through 1-20. As shown, the hydrogen abstraction initiates a systematic chain oxidation to carbon dioxide

$$R_f{-}CF_2COOH + \bullet OH \rightarrow R_f{-}CF_2\bullet + CO_2 + H_2O \qquad \textbf{Eq. 1-18}$$

$$R_f{-}CF_2\bullet + \bullet OH \rightarrow R_f{-}CF_2OH \rightarrow R_f{-}COF + HF \qquad \textbf{Eq. 1-19}$$

$$R_f{-}COF + H_2O \rightarrow R_f{-}COOH + HF \qquad \textbf{Eq. 1-20}$$

and water. The perfluorocarbon radical then reacts with the hydroxyl radical forming an intermediate that rearranges to an acyl fluoride and one equivalent of hydrogen fluoride. The acyl fluoride then goes through hydrolysis to generate a second equivalent of hydrogen fluoride as well as regeneration of the carboxylic acid endgroup, causing an unzipping degradation mechanism continuing through the backbone of the proton exchange membrane.

The formation of various highly reactive radical species due to the decomposition of hydrogen peroxide has been examined by numerous authors.[145-149] Panchenko et al. were the first to examine a working fuel cell within an electron paramagnetic resonance (EPR) spectrometer.[145] With the aide of EPR, the authors were able to quantify changes in unpaired electrons in the catalyst layers with differing degrees of Pt content. The number of unpaired electrons reached a maximum when the Pt loading was approximately 0.35 mg/cm^2. Panchenko and coworkers also observed a dramatic decrease in the EPR signal intensity upon operating at both open and closed circuit as well as using fully humidified gas streams. The only explanation for the decreased EPR signal intensity was due to the formation of water during fuel cell operation which has been known to interfere with EPR signal acquisition. Despite the clear observation of unpaired carbon electrons during fuel cell operation, Panchenko et al. were unable to witness new signals due to chemical degradation of the polymer membrane. The authors note that due to the relatively short time frame of experiments, the organic radicals

present during chemical degradation were too low in quantity to be detected using in-situ EPR spectrometry.

In a separate study, Bosnjakovic et al. examined the presence of various free radical species present during the Fenton's Test using electron spin resonance (ESR).[146] For this particular study, Bosnjakovic and coworkers first neutralized Nafion® into the Titanium cation form and proceeded to measure the ESR signal at various temperatures as a function of membrane exposure time to 30% w/v H_2O_2. Ti^{3+} was chosen as the Nafion® counterion due to its ability to act as a catalyst during the Fenton's Test as well as being easily detected using ESR. After approximately 20 minutes of exposure to 30% w/v H_2O_2 at 200 K, an ESR signal appeared near g = 2, which was attributed to the •OOH. The signal intensity and resolution increased with peroxide exposure time and the isometric g value was determined to be g_{iso} = 2.0127. Even though the published g values of •OOH and •OH are relatively similar (2.0117 and 2.0102 respectively), Bosnjakovic and coworkers assume they observed the •OOH radical species during their ESR tests based on the calculated g value (2.0127) and the fact that •OH radicals can only be detected at temperatures below 77 K or by spin trapping.[146] Another reason for assuming a high quantity of •OOH radicals is due to the reaction in Equation 1-17, which shows that in the presence of excess H_2O_2, the •OOH will be the dominant species. By keeping the Ti^{+}-form Nafion® submersed in 30% w/v H_2O_2 and increasing the temperature from 250 to 320 K, the authors noticed the disappearance of the •OOH radical signal along with the appearance of an ESR peak with a g_{iso} value of 2.0122, which was attributed to the TiOO• radical. The formation of the TiOO• radical was

believed to occur through the mechanism shown in Equations 1-21 and 1-22. As shown in Equations 1-21 and 1-22, a superoxide radical is also created during

$$HOO\bullet + H_2O \leftrightarrow O_2^- + H_3O^+ \quad \textbf{Eq. 1-21}$$

$$O_2^- + Ti^{4+} \rightarrow TiOO\bullet \quad \textbf{Eq. 1-22}$$

the formation of the TiOO• species. Upon dehydration, or removal of the H_2O_2, Bosnjakovic et al. observed an ESR peak present between 160 and 360 K with a g_{iso} value of 2.0106 and was assigned to the O_2^- superoxide species. Finally, the authors examined the ESR signal of Ti^+-form Nafion® treated with 30% w/v H_2O_2 as a function of storage time from 0-92 days at ambient conditions. A signal at approximately g_{iso} = 2.0023 emerged and broadened over time to a line width of approximately 84 G. The authors concluded that the signal represented fluorinated alkyl radicals, which were formed by the attack of the TiOO• species on the polymer.

Continuing their previous work, Kadirov, Bosnjakovic, and Schlick used ESR to examine various chemical degradation species in both Nafion® and Hyflon Ion® perfluorosulfonate ionomers during the Fenton's Test as well as UV degradation.[147] In contrast to their previous study, the authors chose to neutralize the perfluorosulfonate ionomers with Cu(II), Fe(II), and Fe(III) counterions as opposed to titanium due to the increased catalytic activity of both the copper and iron species. Kadirov et al. first examined the effect of neutralization on the UV degradation of an Fe(II)/Nafion® system. After 60 minutes of UV irradiation at 77 K (in the absence of H_2O_2), Kadirov et al. noticed a signal intensity maximum for membranes with 10% neutralization. They also noticed a linear increase in the ESR signal intensity of 10% neutralized Fe^{2+}-form Nafion® as a function of UV irradiation time from 0-60 minutes. With the addition of

H_2O_2, prior to UV irradiation, the signal increased exponentially, mainly due to the homolytic cleavage of H_2O_2 into two •OH species. As a function of time, Kadirov et al. noticed an increase of the ESR signal with a g_{iso} value of 2.0023 and a decrease in the ESR signal at $g_{iso} = 4.31$. The first signal was attributed to the emergence of the chain-end perfluorinated radical $ROCF_2CF_2$•, which was determined based on its similar magnetic parameters to the propogating chain-end radical in polytetrafluoroethylene. The second signal was assumed to be the disappearance of the Fe(III) species as the chemical degradation proceeded as a function of time. The authors concluded, based on the quintet ESR signal, that the formation of the $ROCF_2CF_2$• species was due to the attack of the carbon backbone atom linked to the pendant side chain, accompanied by the loss of a fluorine atom.

Based on the confirmation of various radical species present during the Fenton's Test, several authors have used the ex-situ degradation technique to quantify membrane stability based on percent weight loss, fluoride loss, and membrane dissolution[39, 108, 110, 134-136, 138-144] Curtin et al. were the first to publish chemical degradation results via Fenton's Reagent for the new generation, chemically stable (CS), solution-cast NRE Nafion® membranes from DuPont.[108] DuPont has recently switched from extrusion to solution-casting Nafion® based on increased production rates, improved thickness control, and the ability to obtain thinner membranes. Along with switching the processing technique, DuPont has also decreased the number of carboxylic acid endgroups present in the solution-cast membrane by pre-treating the polymer with elemental fluorine, which decreased the number of measurable endgroups by 61%, hence increasing the chemical stability. Curtin et al. subjected both chemically stable

and non-chemically stable Nafion® to Fenton's Reagent for 55 hours and noticed a 56% decrease in the fluoride ion release rate between the two polymers, verifying the dramatic increase in chemical stability for the new generation Nafion®. This result confirmed that the carboxylic acid endgroups were the primary source for chemical degradation via hydroxyl and hydroperoxyl radical attack.

A later study by Escobedo et al. showed that even when the reactive endgroups are reduced close to zero, Nafion® fluoride loss is still present.[150] A secondary degradation mechanism was deemed essential to explain the additional loss of fluoride without the presence of carboxylic acid endgroups. Based on the data presented by Escobedo et al., Zhou and coworkers performed the Fenton's Test on Nafion® as well as several model compounds that mimic Nafion®'s backbone and sidechain in order to determine a secondary route for chemical radical attack.[132, 133, 140]

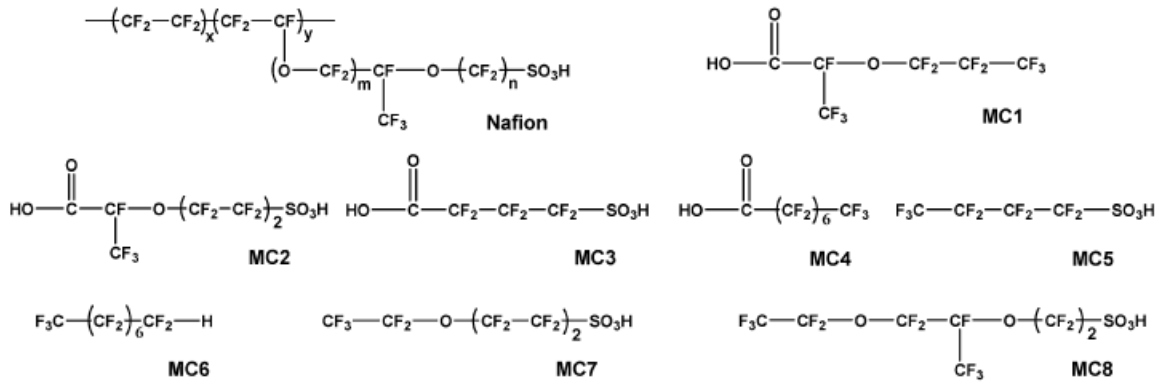

Figure 1.13. Structures of Nafion® and various model compounds. (Reprinted with permission from ref[140] *Macromolecules*, **40**, 8695 (2007). Copyright 2007, American Chemical Society.)

The structures of Nafion® and the various model compounds examined by Zhou et al. are shown in Figure 1.13. In order to conduct the Fenton's Test on the model compounds, Zhou et al. added a known concentration of Fe(II), H_2O_2, and model compound to ensure reproducibility between the various samples. The Fenton's Test on Nafion® was accomplished by exchanging the polymer into the Fe^{2+}-form prior to

subjection to the H_2O_2. The evaluation of fluoride loss was calculated for each model compound based on the atomic percentage ratio, which was the total fluoride released divided by the total fluorine atoms possible for each model compound. There was a significant increase in the fluoride loss between the model compounds with carboxylic acid endgroups and those without such functionality. Of the compounds without any carboxylic acid endgroups, the fluoride loss decreased in the following order; MC5 > MC7 > MC8 > MC6. Zhou et al. believe that MC5 had the highest fluoride loss ratio due to having the shortest chain or fewest fluorine atoms, which would increase the percentage of fluoride release. On the other hand, MC6 had the lowest fluoride loss mainly due to its insolubility in the aqueous media. Zhou et al. also note that even though the fluoride loss was approximately an order of magnitude higher for the model compounds containing carboxylic acid groups, the remaining compounds still displayed a loss of fluoride in the Fenton's Reagent, indicating that there must be a secondary degradation pathway. By performing liquid chromatography-mass spectroscopy (LC-MS) on the degradation product of MC4, Zhou et al. were able to clearly show the evolution of the perfluorinated eight carbon acid into various seven through three carbon analogues, giving further proof for the primary unzipping degradation mechanism. For a more direct comparison to Nafion®, LC-MS was performed on the degradation product of MC8. Based on the LC-MS results, MC8 appeared to degrade into four various perfluorinated species, primarily dominated by a fluorinated carboxylic acid compound similar to MC2. Zhou et al. clearly state that all of the major degradation products of MC8 involve the cleavage of the ether linkage, which would mimic the loss

of the sidechain in Nafion®. The authors also mention that there was no evidence of sulfonic acid loss in any of the degraded compounds.

As a corresponding publication to Zhou et al., Healy and coworkers incorporated ^{19}F NMR as well as mass spectroscopy to interpret both in-situ and ex-situ chemical degradation products of Nafion® membranes.[134] The authors overall goal was to determine if the degradation products could be identified as well as confirm the degradation mechanism of Curtin et al. and to determine the similarity between in-situ and ex-situ degradation products. By allowing severely degraded MEAs to soak in water for six days, Healy et al. were able to presumably extract any low molecular weight degradation species and compare them to the Fenton's degradation solution using ^{19}F NMR. From the ^{19}F NMR analysis, Healy et al. observed numerous peaks that coincided between the two degradation solutions. The peaks were believed to be associated with a single fluorinated organic compound based on the consistent intensity ratio observed between the different samples. With the aide of mass spectroscopy, Healy et al. determined that the principal degradation product was fluoro(3-oxapentane)-1sulfonic-4-carboxylic diacid, which is very similar to the MC2 compound examined earlier by Zhou et al.[140] Because the degraded compounds were so similar to the sidechain of Nafion®, Healy et al. postulated that their analytical results confirm the backbone unzipping degradation mechanism proposed by Curtin et al., upon which the sidechain is released during the process.

In a separate ex-situ Fenton's Test study, Kinumoto et al. used ion chromatography as well as ^{19}F NMR to examine the resulting degradation solution of Nafion® in various counterion forms.[135] Two main peaks were observed in the ion

chromatographs of degraded Fe^{2+}-form Nafion® after 12 hours at 80 °C and were assigned to the F^- ions as well as the SO_4^{2-} ions. The authors not that the fluoride ions are the result of both the backbone and sidechain degradation, while the SO_4^{2-} ions are due to degradation of the sulfonate moieties. Decomposition ratios of both ions were calculated as a function of time and counterion type. The authors determined that alkali and alkaline metal counterions had minimal effect on the chemical degradation, while both Fe^{2+} and Cu^{2+} had the largest influence on the release of the fluoride and SO_4^{2-} ions. The weight loss of the Fe^{2+}-form Nafion® membrane after five days of chemical degradation via Fenton's Reagent was approximately 40%, which significantly decreased the membranes mechanical and conductivity properties. Kinumoto et al. also examined Fe^{2+}-form Nafion® after chemical degradation using FTIR. Because the normalized absorbances of the backbone and sidechain peaks did not change after severe chemical degradation, the authors concluded that the hydroxyl and hydroperoxyl radicals attacked both the sidechain and backbone. On the other hand, the authors suspect that the sidechain of Nafion® degrades slightly faster than the backbone based on the larger integrated peak area for the backbone fluorine atoms measured using ^{19}F NMR.

In another accelerated ex-situ chemical degradation study, Liu et al. examined an in-situ Fenton's Test versus the conventional batch wise test.[106, 110] The in-situ Fenton's Test involved constructing a flow cell similar to a regular fuel cell where 10 wt% H_2O_2 flows to one side while the opposite side is purged with nitrogen gas. The H_2O_2 residence time was approximately three minutes and effluent water from both sides of the cell was used to measure fluoride loss. To examine the Fenton's degradation

mechanism, the Nafion® membrane was doped with 10% Fe^{3+} ions and ran in direct contact with the H_2O_2 solution at 90 °C for 48 hours. After completion of the in-situ Fenton's Test, the iron-doped membrane had a fluoride release rate similar to the chemical degradation observed using a regular hydrogen/oxygen fuel cell. The batch-wise or ex-situ Fenton's Test was conducted by again doping a Nafion® membrane with 10% Fe^{3+} ions and submersing it in 10wt% H_2O_2 at 68 °C for 24 hours. The fluoride release rate for the ex-situ Fenton's Test was approximately two orders of magnitude lower than the in-situ test. Liu et al. explain the discrepancy in the degradation results based on the constant supply of free radical generation during the in-situ test when compared to the batch-wise test, where the H_2O_2 concentration decreased over time and could be relatively ineffective after a few hours. In conclusion, Liu et al. recommend the in-situ Fenton's Test due to its similarity to actual fuel cell operation.

Tang and coworkers implemented the use of FTIR, ^{13}C NMR, and SEM to examine the chemical degradation of Nafion® NRE 111 membranes after 48, 72, and 96 hours in Fenton's Reagent.[138] All membranes were submersed in 30 wt% H_2O_2 at 80 °C with the addition of 12.3 ppm Fe, 6.1 ppm Cr, and 5.4 ppm Ni ions, which represented the combination of contaminants after subjecting stainless steel to a 0.5 M nitric acid solution. Based on the FTIR spectra of the polymer fragments collected from the Fenton's solution, Tang et al. observed the appearance of the C=O stretching band at 1700 cm^{-1} and the S=O stretching band at 930 cm^{-1}. Both of these bands were documented as being indicative of the loss of sulfonate moieties as well as carboxylic acid groups. After performing ^{13}C NMR analysis on the 96 hour Fenton's solution, Tang et al. identified four peaks which were C=O at 168 ppm, CF at 68.5 ppm, CF_2 at

63 ppm, and CF_3 at 61.5 ppm. The existence of the last three bands was not surprising since they make up both the backbone and sidechain of Nafion®. The appearance of the C=O band, coinciding with the FTIR data, helped confirm the presence of carboxylic acids in the degraded Nafion® fragments. SEM images of Nafion® subjected to the Fenton's Reagent for 48 hours showed severe physical degradation in the formation of bubbles and cracks on both the surface and throughout the cross section of the membranes. The authors comment on how the formation of the bubbles can lead to pinholes in the membrane which then increases the likelihood of gas crossover and ultimate membrane failure within a fuel cell. Overall, Tang and coworkers were in agreement with the primary degradation mechanism proposed by Curtin et al. involving the unzipping of the Nafion® backbone via radical attack of the carboxylic acid endgroups.

A more recent study by Merlo and coworkers focused on examining the ex-situ Fenton's Test degradation of the Hyflon Ion® produced by Solvey Solexis.[39] The Fenton's Test conditions were 36 ppm Fe^{2+} in a solution of 30 wt% H_2O_2 with 1 g of polymer at 55 °C for thirty hours, while replenishing the Fenton's solution every six hours. The total fluoride emission for the Hyflon Ion® was approximately the same when compared to both extruded Nafion® 112 and dispersion-cast Nafion® NR 112. A significant decrease in fluoride emission was noticed for an extruded, stabilized Hyflon Ion® membrane which is characteristic for membranes that have been pretreated with fluorine gas to help reduce the number of reactive carboxylic endgroups present in the polymer. As part of a continuing study, Merlo et al. chemically degraded both standard Hyflon Ion® and stabilized Hyflon Ion® for thirty hours, but instead of simply replacing

the Fenton's solution ever six hours, the authors removed the membrane, purified it with acid, followed by a washing treatment, and reinserted the membrane into fresh Fenton's solution. By measuring the amount of fluoride released during each six hour cycle, Merlo et al. were able to display a linear trend of increasing fluoride release for both stabilized and unstablized Hyflon Ion®. The authors also point out that there is no change in the rate of degradation throughout the thirty hour Fenton's Test. Due to the consistency of the degradation rate, Merlo and coworkers suggests that the number of chain sites which were attacked by the peroxide radicals remained constant, which was consistent with the unzipping mechanism proposed by Curtin et al.

Kundu et al. recently focused on the differences between performing a Fenton's Test on Nafion® using the solution method or exchange method.[142] The solution method involved subjecting a Nafion® membrane to a solution of both hydrogen peroxide and metal ions, while the exchange method involved first ion exchanging the membrane into the desired metal ion form followed by submersion in a hydrogen peroxide/water mixture. For this study, the solution method consisted of a 40 mL solution of 30 wt% H_2O_2 mixed with 16 mg/L of $FeCl_2 \cdot 4H_2O$ in a closed vessel with a 7.5 cm x 2.5 cm sample of Nafion® 112. The solution was kept at 72 °C and replenished every twelve hours to ensure a constant supply of free radicals. For the exchange method, Nafion® 112 with identical dimensions to the solution method was first submersed in a solution of $FeCl_2 \cdot 4H_2O$ for 24 hours to fully exchange the membrane into the Fe^{2+}-form. The sample was then rinsed and placed into vials with 40 mL of 30 wt% H_2O_2 at 72 °C and the peroxide was replenished every 24 hours. The overall goal of the study was to examine the differences between both methods as well

as accurately interpreting which method closely mimics in-situ chemical degradation during fuel cell operation. The first analytical method used to compare the two degradation procedures was percent weight loss of polymer from 0-120 hours. The first observation that Kundu et al. reported is that both methods succeeded in significantly degrading the membranes to the point where approximately 20% of the original weight was lost after approximately 80 hours. The authors thought this conclusion was surprising since both the solution replenishing times and total amount of iron were different between the solution and exchange methods. Their explanation for this phenomenon was that the majority of the radicals in the solution method were more than likely to terminate before ever reacting with any polymer fragment. On the other hand, with the exchange method, the concentration of iron present within the polymer membrane may be so small that the chemical degradation within the polymer may equal that of the solution method. In contrast to the percent weight loss results, Kundu et al. noticed a significantly higher cumulative fluoride loss for the solution method as opposed to the exchange method after 120 hours of chemical degradation. The authors explain this result based on the solution methods ability to continue degrading polymer fragments that break off of the polymer film and dissolve in the Fenton's media. Both ion exchange capacity and electron dispersive spectroscopy were performed on the chemically degraded membranes to determine if the ratio of backbone to sidechain groups had changed. The results showed no significant change in the ion exchange capacity or the atomic ratio of oxygen to fluorine or sulfur to fluorine over the exposure time for both the solution and exchange methods. The FTIR results were in agreement with the ion exchange capacity and electron dispersive spectroscopic results in that no

significant changes in the sidechain to backbone ratio was observed between the two degradation techniques. Despite the similarities in the degradation results of the solution method and exchange method, Kundu et al. noticed a significant visual difference between the two methods using SEM. SEM images of Nafion® degraded using the solution method were similar to images shown by Tang and coworkers where the presence of large bubbles and voids covered the exterior as well as the cross sections of the membrane.[138] The bubble density seemed to increase with degradation time and the diameters were reported on the order of hundreds of microns. In contrast, the membranes degraded using the exchange method displayed fewer defects and the bubbles or voids were much smaller in comparison to the solution method. The cross section of the membrane degraded using the exchange method was drastically different than the cross section of the film degraded using the solution method. The cross section images of Nafion® degraded using the exchange method appeared to be foam-like on the surface but relatively untouched or homogenous in the center. The authors attribute the differences in the degraded morphology of the membranes to how well the reactive species can diffuse into the membrane during either degradation method.

Rather than characterize PFSI degradation via the Fenton's Test, Hommura et al. chose to devise a method for accelerating and assessing the membrane degradation, while clarifying the chemical degradation mechanism during fuel cell operation.[143] A gas-phase H_2O_2 exposure method was devised, where 30 wt% H_2O_2 was maintained at 73 °C while nitrogen was used to purge the system and blow the heated peroxide to a chamber where a Fe^{2+}-form Flemion® membrane sat at 120 °C and 14% relative humidity. The gaseous decomposed products were then trapped in a potassium

hydroxide solution and new H_2O_2 was added every three days to maintain a constant 30 wt% throughout the experiment. The authors point out that the gas-phase H_2O_2 degradation method has the following advantages; uniform degradation, no membrane contamination, no effects from mechanical degradation, and temperature, relative humidity, and H_2O_2 concentration can all be evaluated independently throughout the experiment. Verification of the degradation method was observed by an increase in both the percent weight loss and fluoride release rate during exposure to gaseous H_2O_2 over a period of 700 hours. The degradation rate accelerated with time, indicating that a change in the number of carboxylic acids present in the membrane must change during the degradation test. The authors suggest that if the number of carboxylic acid endgroups is constant as in the degradation mechanism proposed by Curtin et al. then the degradation rate would remain constant throughout the chemical degradation timeframe. In contrast, since the chemical degradation rate increases with time, a secondary radical attack position must exist upon which more carboxyl groups are created to increase the rate of chemical degradation. Using FTIR, Hommura et al. observed an increased in the number of carboxyl groups present in the membrane as a function of degradation time from 0-700 hours, which had a direct correlation to the increase in the fluoride release rate over the same time period. Size exclusion chromatography (SEC) was also performed to examine changes in the molecular weight of Flemion® as a function of degradation time during exposure to aqueous H_2O_2. The SEC analysis showed an approximate 10% decrease in the number average molecular weight of Flemion® after 700 hours of chemical degradation. Hommura et al. attribute both a decrease in the molecular weight and increase in the number of carboxyl groups

to chain scission of the polymer backbone in Flemion®. Based on the SEC results, Hommura et al. suggests that the change in molecular weight is too large to be explained by the endgroup unzipping degradation mechanism alone. The authors finally conclude that PFSI membrane degradation proceeds via both the unzipping reaction at unstable polymer endgroups as well as scission of the main chain to form reactive carboxyl groups at the severed locations.

Morphological Manipulation

The physical properties of Nafion® and other PFSI's can be tailored with a fundamental understanding of the underlying morphology of the polymer membranes. The end morphology of PFSI's can be altered by using various processing methods, such as solution-processing,[66] melt-processing,[58] post-processing annealing,[151] and mechanical deformation.[27] The main goal of morphological manipulation of PFSI's is to attain the optimal morphology for the desired application of the polymer.

Nafion® is subjected to thermal treatment no matter what processing procedure is applied, whether it is solution-processing, melt-processing, or extrusion of the precursor. Aside from Nafion's® usual drying conditions, 60-100 °C under vacuum for 1-12 hours, various authors have examined the effects of additional high temperature annealing on the membrane's overall properties.

Effects of Annealing Nafion®

One of the earliest publications involving annealing at elevated temperatures was by Gierke et al.[27] Gierke and coworkers examined the effects of temperature on both the WAXD and SAXS profiles of the unhydrolyzed Nafion® precursor. Based on WAXD

results, the Nafion® precursor crystalline reflection at 18° 2θ gradually decreased in intensity from 50-250 °C and finally disappeared above 270 °C. On the contrary, the SAXS intercrystalline peak at 0.6° 2θ increased with increasing temperature and disappeared above 270 °C. Upon cooling, a reemergence of the small angle crystalline peak was noticed, verifying its relationship with the electron density difference between crystalline and amorphous polymer domains. Along with DSC measurements, the authors noted that the melting point of the Nafion® precursor crystallites is approximately 275 °C. It was assumed that Nafion® crystallites melt over a much broader range than the crystallites present in PTFE, which melt around 330 °C. After hydrolysis and conversion into the Ag^+ counterion form, Gierke et al. noticed the appearance of an ionomer peak in the SAXS profiles at approximately 2.0° 2θ. Minimal changes were seen in either peak shape or intensity after annealing the Ag^+-form Nafion® membranes from room temperature to 290 °C. The persistence of this peak above the Nafion® crystallite melting temperature provided strong evidence that the peak was due to the existence of ionic clustering.

Rather than examining Nafion's® precursor, Fujimura and coworkers followed up Gierke's study by looking into the effects of increased temperature on the SAXS and WAXD profiles of Nafion® in both the H^+ and Cs^+-forms.[68] Similar to Gierke's study of the Nafion® precursor, Fujimura et al. noticed a disappearance of the crystalline reflection in the WAXD profile of H^+-form Nafion® upon heating to 275 °C. Upon cooling back to room temperature the peak reappeared, confirming its association with the melting and recrystallization of the polymer. Fujimura et al. note that the melting point is well below that of PTFE due to the existence of sidechains in Nafion® which inhibit crystallization.

By neutralizing Nafion® into the Cs^+-form, Fujimura et al. were able to increase the scattering intensity of the ionomer peak, allowing for more accurate examination of the effects of temperature. A shift of the ionomer peak to larger *q* values was observed after increasing the temperature to 276 °C. The shift in the ionomer peak indicated that the intercluster distance decreases with temperature. The authors assume that the smaller distances between clusters is due to inherently smaller cluster sizes based on the increased thermodynamic work of elastic deformation of coils required for the cluster formation.

Roche et al. studied the morphology of as-received and quenched Na^+-form Nafion® membranes using SANS and SAXS.[69, 70] By annealing Na^+-form Nafion® at 330 °C for one hour and quenching to room temperature using hydrogen gas, Roche et al. were able to eliminate crystallinity based on the disappearance of the SANS intercrystalline scattering peak at approximately 0.04 $Å^{-1}$. Roche et al. also examined the ionomer peak of quenched Na^+-form Nafion® as a function of water content using SAXS. Scattering from the ionomer peak was absent for the sample quenched and then dried at 200 °C. The absence of the ionomer peak was attributed to the lack of water content, hence decreasing the scattering contrast between the ionomer domains in the dried Na^+-form membranes. After increasing the level of hydration, the ionomer peak reappeared and shifted to lower *q* values. Based on the author's annealing procedure, no changes to the ionomer peak occurred, but significant changes to the crystalline domain were documented based on melting of the crystallites after heating to 330 °C.

Kyu et al. indirectly studied the effects of annealing both Nafion® and its precursor.[15] In order to obtain partially neutralized Na^+-form precursor samples large

enough for DMA experiments, Kyu et al. melt pressed several membranes together at 250 °C for five minutes and cooled back to room temperature. Based on the previous studies of Gierke and Fujimura, by annealing at 250 °C, Kyu and coworkers melted the majority of crystallites present in the Nafion® precursor. Since all of the samples were prepared in the same manner, there was minimal change in the dynamic mechanical properties as a function of crystalline content. Because of the persistence of water in Nafion®, many scientists dry or anneal the membranes at elevated temperatures to obtain an accurate initial condition without postulating the ramifications on the crystalline or ionomer morphologies.

As opposed to annealing extruded Nafion®, Gebel et al. annealed Nafion® cast from high boiling point solvents.[152] Extruded Nafion® was exchanged into the Li^+-form and dissolved in a water/ethanol mixture under high pressure and temperature. A high boiling point solvent (NMF) was added to the Nafion® solution and a membrane was cast by allowing the solvent to evaporate at 80 °C. The authors noted that a clear, uncracked, but brittle, soluble membrane was obtained from this procedure. To increase the mechanical properties and solubility of the membrane, Gebel et al. annealed the "reconstructed membrane" under vacuum at 200 °C. A series of WAXS and SAXS studies were conducted to examine changes in the morphology of low temperature cast films compared to the annealed, reconstructed membranes. The WAXS profiles of the membrane cast at 80 °C and the reconstructed membrane were dramatically different. The membrane cast at 80 °C was rendered totally amorphous due to the disappearance of the crystalline reflection of Nafion® at 18° 2θ. After annealing the same membrane at 200 °C for three hours, the crystalline peak reappeared and was more intense than in the

as-received, extruded membrane. Further examination of the crystalline peak upon annealing was shown using WAXS of reconstructed Nafion® annealed for three hours at 80, 150, 200, and 250 °C. The crystalline reflection first appeared after annealing at 150 °C and continued to sharpen and become more intense as the annealing temperature increased. SAXS was conducted on the same membranes annealed at various temperatures for three hours and the same trend was noticed for the crystalline peak at low q values. Along with an increase in intensity and peak sharpening, Gebel et al. noticed a shift in the peak to lower q values, indicative of a longer repetition distance between electron scattering regions. The authors concluded that annealing increases the size of the lamellar crystallites, improves internal order, and allows for the development of long-range order throughout the film.

Silverman et al. examined the mechanical and barrier properties of Nafion® coated onto various substrates before and after annealing.[153, 154] The objective was to provide a protective coating of Nafion® onto both stainless steel and aluminum substrates, while improving the adhesion and barrier properties through annealing. The stainless steel specimens were dip coated with Nafion® at room temperature and allowed to dry overnight. The Nafion® coated substrate was then submersed in a 1M NaOH solution to exchange the ionomer into the Na^+-form. While under vacuum the coated substrate was annealed from room temperature to 210 °C over a period of 45 minutes and then held at 210 °C for 30 more minutes. To avoid contraction and cracking, or rapid crystallization of the polymer, the sample was cooled to room temperature between five and six hours. The aluminum coated specimens were coated using the same procedure as above except the Nafion® coating was annealed in the H^+-form instead of the Na^+-form. Both coated

substrates were then subjected to a 1M NaCl solution for 28-35 days. Silverman et al. documented that the nonannealed Nafion® coating had difficulty remaining adhered to the substrate and noticeable corrosion was observed underneath of the Nafion® laminate. On the contrary, the substrates coated with annealed Nafion® had no corrosion present and remained adhered throughout the duration of the test. Based on the WAXD results of Gebel et al.[152], Silverman et al. concluded that annealing Nafion® allowed for a more highly ordered molecular configuration, which improved the permselectivity and adhesion of the polymer to the substrate.[153]

Similar to the work of Silverman and coworkers, Ye et al. examined two post-casting treatments of Nafion® used as a protective coating on a platinum electrode.[155] The reference specimen used by Ye et al. was Nafion® cast at room temperature onto a Pt electrode from an alcohol/water solution. The two post-casting procedures involved converting the reference sample into the Na^+-form and annealing at 170 °C under vacuum for 40 mins, compared to drying an unannealed coating of Nafion® in a vacuum desiccator with P_2O_5 for 19 hours. Ye et al. utilized cyclic voltammetry to examine the effects of both post-casting treatments on the absorption of ferricyanide over 70 hours in both acidic and neutral pH environments. After one hour in the acidic solution, Ye et al. noticed that the cathode peak currents for the unannealed, desiccator cured, and annealed films were proportionally 6:4:1. In contrast, after one hour in the neutral pH solution, the peak current ratios were 7:1:0, where zero indicates that no peak current could be measured for the annealed membrane. From these results, Ye et al. concluded that annealing Nafion® coatings at elevated temperatures increased both the adhesion properties and anion-rejection capability as measured using cyclic voltammetry.

Following the work of Silverman et al. and Ye et al., Thomas and coworkers examined the effects of annealing Nafion® coated electrodes, neutralized with various quaternary ammonium counterions.[156] The selectivity, ion-exchange capacity (IEC), and mass transport of various species were examined as a function of annealing and quaternary ammonium counterion selection. The coated electrodes were prepared by pipetting 2.0 μl of 5 wt% quaternary ammonium exchanged Nafion® solution onto a glassy carbon electrode. The Nafion® solution was recast at room temperature, followed by annealing in an oven at 140 °C for 25 minutes. The various quaternary ammonium counterions included ammonium (NH_4^+) and tetramethylammonium ($N(CH_3)_4^+$) through tetrapentylammonium ($N(C_5H_{11})_4^+$). On average, Thomas et al. noticed a significant increase in the IEC of mixture-cast membranes after annealing at 140 °C for 25 minutes. The IEC of H^+-form Nafion® increased from 907 x 10^{-6} mol/g to 1023 x 10^{-6} mol/g after being thermally treated. Thomas et al. explain this phenomenon based on a restructuring of the membrane by annealing above the dynamic mechanical α-relaxation transition temperature. Along with a change in the IEC, Thomas et al. noticed a significant change in the diffusion of caffeine, $Ru(bpy)_3^{+2}$, and ferricyanide through Nafion® after annealing at 140 °C. The most significant change in flux for the caffeine molecule occurred after annealing H^+-form Nafion® at elevated temperatures. A decrease in diffusion of caffeine was also documented for annealed, quaternary ammonium exchanged Nafion® but was not as significant as through H^+-form Nafion®. Similar to caffeine, the flux of $Ru(bpy)_3^{+2}$ through Nafion® decreased upon annealing at 140 °C for 25 minutes. Unlike the diffusion of caffeine, $Ru(bpy)_3^{+2}$ was unable to diffuse through annealed Nafion® neutralized with tetrapropylammonium, tetrabutylammonium, or tetrapentylammonium

counterions. Similar to the diffusion of $Ru(bpy)_3^{+2}$, Nafion® neutralized with tetrapropylammonium, tetrabutylammonium, and tetrapentylammonium counterions were impervious to the penetration of ferricyanide after annealing at elevated temperatures. For the remaining counterions, a significant decrease in ferricyanide absorption was observed after annealing Nafion®. Similar to the results of Ye et al., Thomas et al. noticed a decrease in the absorption of ferricyanide after annealing H^+-form Nafion® at elevated temperatures.

Lee and coworkers used small and wide angle neutron scattering to examine the H-H and O-H correlations of Ni^+-form Nafion® after annealing at 300 °C for one hour and quenching in liquid nitrogen. The annealed Nafion® membrane was rendered amorphous based on the absence of the crystalline reflection at 18° 2θ using WAXD. Lee et al. removed the crystallinity present in Nafion® to avoid conflicting data at very low q values in SANS. Based on both small and wide angle neutron scattering, the authors were able to conclude that amorphous Nafion® is composed of a continuous aqueous network. If the morphology consisted of unconnected ionic spheres with a mean center to center separation of 70 Å, the membrane would only be able to theoretically accommodate 8 vol% of water instead of the measured 41 vol%.

Zawodzinski and coworkers examined the effect of drying H^+-form Nafion® at 105 °C and the subsequent water uptake at various temperatures.[157] As-received H^+-form Nafion®, without any thermal treatment, was noted as having a water uptake of (λ = 21 mol water/mol sulfonate) when subjected to water ranging from 27-94 °C. Upon annealing H^+-form Nafion® at 105 °C for an unspecified time, Zawodzinski et al. noticed a significant change in the rehydration properties of the membrane. Reexposure of the

annealed Nafion® membrane to liquid water at room temperature resulted in an equilibrium water uptake value of 12 mol water/mol sulfonate. A 50% decrease in water uptake was documented based on the effect of thermal history on the rehydration properties of Nafion®. Further studies showed that the equilibrium water uptake increased with increasing rehydration temperature. Annealed Nafion® membranes subject to water baths at 65 and 80 °C saw water uptake values of 14 and 16 mol water/mol sulfonate, respectively. Even after exposure to a water bath at 80 °C, annealed Nafion® membranes possessed less water than their as-received counterparts, which had been through no thermal treatments. Zawodzinski et al. concluded that the thermal history of Nafion® plays a crucial role in the membrane morphology as well as overall performance.

Zawodzinski and coworkers go on to point out the importance of the annealing step in fabricating state-of-the-art membrane electrode assemblies (MEAs) for fuel cell applications.[157] In a subsequent publication with Xie et al., Zawodzinski mentions how the majority of MEAs are fabricated using a "decal" process upon which a high temperature annealing procedure is employed.[158] The overall decal process is represented below in Figure 1.14. The first step in the decal process involves obtaining a clean substrate for the catalyst ink, which typically consists of either Teflon or Kapton.

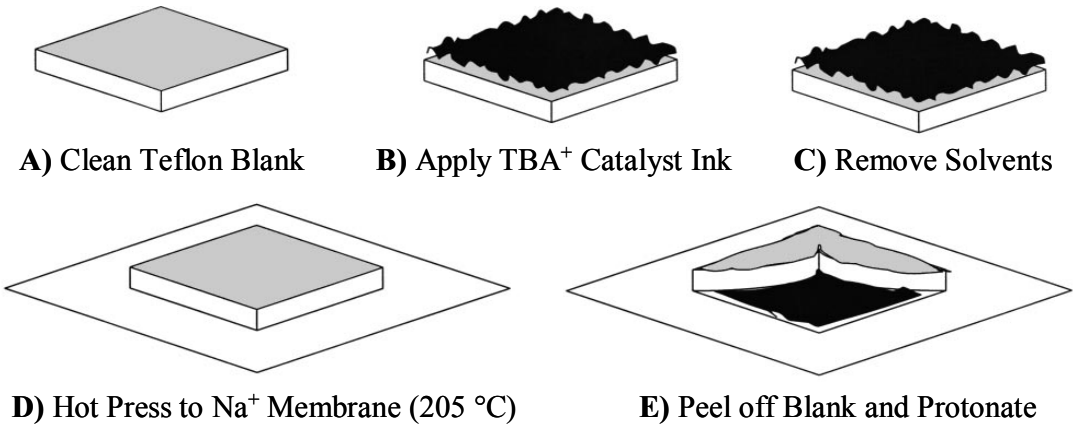

Figure 1.14. Schematic of decal process **A)** Teflon blank **B)** Apply catalyst ink onto decal through hand-painting or blade-coating **C)** Dry the catalyst in oven at 140 °C for 30 mins **D)** hot-press catalyst layer onto Na^+-form Nafion® membrane at 205 °C for 5 mins **E)** peel off decal and protonate final MEA. (Reprinted with permission from ref[158] *J. Electrochem. Soc.*, **151**, A1084 (2004). Copyright 2004, The Electrochemical Society.)

The second step involves applying the catalyst ink (Pt-C catalyst with glycerol, 5% Nafion® solution, and tetrabutylammonium hydroxide in methanol) to the blank decal using either a hand-painting or blade-coating technique. The ink is then dried in an oven at 140 °C for 30 minutes and weighed to determine if the appropriate amount of catalyst is present. From the work of Moore et al., it was shown that removing solvents from a Nafion® solution at temperatures below 170 °C can create a mud-cracked membrane with decreased mechanical properties.[66, 67] After removing the solvents from the ink, the decal is hot-pressed onto a Na^+-form Nafion® membrane at 205 °C for five minutes at 450 kq/cm^2. The final step is to peel the decal away from the membrane and reprotonate the MEA using 0.5M sulfuric acid. Based on Zawodzinski's previous publication, the thermal annealing steps present in the decal process should have profound effects on the water uptake of the resulting MEA. By annealing at 105 °C, it was shown that the water uptake at room temperature was approximately half of the water uptake from an as-received membrane. Using the decal method, Nafion® is subjected to annealing at both 140 and 205 °C, and the ionomer's ability to reach an optimum water uptake is reduced

along with a change in the crystalline morphology. Based on the findings of Gierke et al.[27] and Fujimura et al.,[68] annealing above 200 °C will cause a decrease in crystallinity of the as-received membrane based on the onset of crystalline melting around 150 °C. The main focus of Xie and coworkers was the choice of decal substrate (Teflon or Kapton) along with ink spreading procedures (hand-painting or blade-coating). The morphological impact of annealing Nafion® at either 140 or 205 °C was not examined and based on water uptake results, should have a dramatic effect on fuel cell performance.

Similar to the study done by Zawodzinski et al.,[157] Hinatsu and coworkers examined the water uptake of Nafion® after boiling in deionized water and thermally annealing at either 80 or 105 °C.[159] In agreement with Zawodzinski et al., the room temperature water uptake values decreased as the annealing temperature increased. Hinatsu and coworkers attributed this phenomenon to pore shrinkage and reorientation of the side chains, and could only be reversed by exposure to water at elevated temperatures. A significant increase in the water uptake of Nafion® annealed at either 80 or 105 °C was observed after increasing the water immersion temperature from 25 to 130 °C. The water uptake values of the membrane annealed at 80 °C followed a smooth second-order curve over the entire immersion temperature range. On the other hand, the water uptake of Nafion® annealed at 105 °C increased linearly with increasing immersion temperature up to 100 °C. The sample annealed at 80 °C absorbed more water than the respective sample annealed at 105 °C when subjected to immersion temperatures below 100 °C. Hinatsu et al. attribute this behavior to an easier ion hydration for the sample annealed at 80 °C based on a lesser degree of cluster breakup and reorientation of the polymer structure upon annealing. At immersion temperatures higher than 100 °C, the water

uptake values were identical for both membranes annealed at 80 and 105 °C, respectively. Hinatsu and coworkers believed that once the immersion temperature equals Nafion's® dynamic mechanical α-relaxation transition temperature, molecular motions could occur more easily and structural differences incurred during annealing at different temperatures would be eliminated.[159] Consequently, the effects of annealing during the decal process, shown by Xie et al., could be reversed based on rehydration of the ionomer at elevated temperatures.

In agreement with Zawodzinski et al. and Hinatsu et al., Sone and coworkers examined the proton conductivity of Nafion® annealed at 80, 105, and 120 °C.[160] After conducting proton conductivity measurements from 45-80 °C and 20-100% relative humidity, Sone et al. observed a trend in increasing conductivity with increasing cell temperature, regardless of annealing treatment. On the other hand, the proton conductivity, measured at 100% relative humidity, subsequently decreased with increasing annealing temperature, resulting in a change from 0.09 S/cm for commercial Nafion® to 0.03 S/cm for Nafion® annealed at 120 °C. Sone et al. concluded that by increasing the annealing temperature near the dynamic mechanical α-relaxation transition temperature, a significant decrease in both water uptake and proton conductivity is observed.

Zook and coworkers explored the effects of annealing recast Nafion® on both the density and solubility of the resulting ionomer.[161] Nafion® recast films were processed by evaporating commercial Nafion® solution (ethanol/water mixtures) onto polystyrene in a desiccator at room temperature. Various annealed films were created by subjecting the recast membranes to 140 °C in an oven for 10-60 minutes. The films were then

cleaned and reacidified using concentrated nitric acid. Densities of commercial, recast, and annealed Nafion® were recorded using a water displacement technique. The initial density of recast Nafion® without any thermal treatment was reported as 1.67 g/cm^3, which is much lower than the density of commercial Nafion® at 2.05 g/cm^3. Upon annealing in ten minute intervals, Zook et al. noticed an increase in the density from 1.67 g/cm^3 for recast Nafion® to 2.03 g/cm^3 for recast Nafion® annealed for 60 minutes at 140 °C. Based on these results, Zook et al. concluded that the density of recast Nafion® can be comparable to commercial Nafion® simply by annealing at 140 °C for at least 40 minutes. Percent solubility measurements in 50:50 ethanol/water mixtures were also conducted as a function of annealing time at 140 °C. Zook et al. noticed that all samples annealed at 140 °C for longer than 10 minutes were insoluble after sonicating in 50:50 ethanol/water mixtures for 60 minutes. The authors note that by utilizing an annealing temperature above Nafion's® dynamic mechanical α-relaxation transition temperature of 110 °C, significant mobility was imbibed, allowing for changes in the polymer solubility characteristics.

With the aide of small angle neutron scattering, Rollet et al. studied the influence of both counterion form and thermal treatment on the nanostructure of Nafion®.[89] By exchanging Nafion® into various monovalent (H^+, Na^+, Cs^+, and $N(CH_3)_4^+$) and multivalent (Th^{4+}, Eu^{3+}, and Ca^{3+}) counterions, Rollet et al. were able to use SANS to determine the dependence of ionomer cavity radius versus the volume fraction of solution in the membrane, Φ_w. The plot of cavity radius versus Φ_w displays two linear dependencies for both monovalent and multivalent counterions. For a given Φ_w, the cavity radius was smaller for multivalent counterions as opposed to monovalent

counterions. The authors explain the origin of this behavior based on the repulsive electrostatic interactions and polymer chain elasticity. Because monovalent and multivalent counterions behave differently when in solution, Rollet et al. confirmed that the ionic cavities are not a fixed shape and can change based on the size of the counterion, along with being reversible based on counterion exchange. Rollet et al. also used SANS to examine the effect of annealing Nafion® at 120 °C in both the tetramethylammonium (TMA^+) and Na^+ counterion forms. A significant decrease in the ionomer cavity radius with annealing temperature was observed for both counterion forms. Unlike the reversible reorganization of ionic domains with changing counterions, the effects of thermal annealing at 120 °C were irreversible and were believed to occur on a much larger size scale than the local exchange of counterions.

Lee et al. have recently examined the effect of annealing temperature on the diffusion and solubility of oxygen in recast, H^+-form Nafion®.[162] Recast Nafion® was created by evaporating a 5 wt% Nafion® in ethanol/water mixture at 50 °C for 12 hours. The effects of temperature were studied by annealing the recast Nafion® at 100, 120, 135, 150, and 180 °C for one hour at each temperature. By using an electrochemical cell, Lee et al. were able to perform chronoamperometric measurements on recast Nafion® from 25-60 °C. Both the diffusion and solubility of oxygen in the membranes were calculated using a modified Cottrell equation. The diffusion of oxygen was shown to decrease with annealing temperature up to 135 °C. The diffusion values between 135 and 180 °C remained constant, in agreement with extruded Nafion® 117. The diffusion of oxygen also increased as the electrochemical cell temperature increased from 25 to 60 °C, while maintaining a linear trend for all annealing temperatures. The solubility of oxygen in the

Nafion® membranes behaved completely opposite of the diffusion data. The solubility increased with increasing annealing temperature and decreased with increasing electrochemical cell temperature. A linear decrease in solubility was documented as the temperature of the electrochemical cell increased from 25 to 60 °C. Again, a plateau in the solubility values was seen for any samples annealed above 135 °C. It was very apparent that both the diffusion and solubility values heavily relied on the thermal pretreatment of Nafion®. Similar to the previous study by Zawodzinski et al., Lee et al. noticed a decrease in water uptake as a function of annealing temperature until leveling off above 135 °C. It should be noted that even after annealing for one hour at 180 °C, the water uptake was greater than extruded Nafion® 117. Lee et al. explain the changes in water uptake values with changes in the hydrophilic morphology at various annealing temperatures, and more importantly changes to the ionic clusters themselves. Lee et al. then used the bragg spacing from the ionomer peaks in SAXS profiles of annealed Nafion® to calculate an average ionic cluster diameter and correlate the cluster morphology to the water uptake values. A trend of decreasing cluster diameter was noticed as a function of annealing temperature, and again, the values plateaued after annealing the ionomer above 135 °C. An increase in the percent crystallinity of Nafion® with increasing annealing temperature was also documented using WAXD and helped elucidate a conclusion between morphological changes and macroscopic properties. Lee et al. concluded that if the crystallinity of the recast membrane is low due to a low recast temperature, the elastic energy of the PTFE matrix decreases, allowing for the electrostatic energy of the ionic clusters to dominate, which increases both water uptake and oxygen diffusion while decreasing oxygen solubility.[162]

Lin et al. used dynamic light scattering to correlate changes in various Nafion® solutions with SAXS data on membranes cast from the same solutions.[163] The Nafion® solutions consisted of 10 wt% Nafion® in dimethyl formamide (DMF), 4:1 methanol:water, 4:1 ethanol:water, and 4:1 2-propanol:water. Based on the different solubility parameters of the solvents chosen for the various Nafion® solutions, Lin et al. concluded using dynamic light scattering that hydrophobic aggregates present in Nafion® solution decrease in number and size as the solvent solubility parameter decreases. From dynamic light scattering, Nafion® in DMF was shown to have fewer chain entanglements and hydrophobic aggregates as opposed to Nafion® in various alcohol:water mixtures. SAXS was then used to examine the morphological properties of Nafion® cast from the various solutions. All three of the Nafion® alcohol:water solutions were cast at room temperature for 108 hours, followed by annealing under vacuum at 120 °C for one hour. Solutions of Nafion® dissolved in DMF were cast at 120 °C for 60, 70, and 80 minutes. Similar to previous SAXS studies of Nafion® solutions cast at room temperature[69, 152], no evidence of crystallinity was present. Upon annealing or casting at 120 °C, an intercrystalline peak appears at q = 0.6 nm^{-1}. By integrating $I(q)q^2$ over all of the scattering angles, Lin et al. were able to obtain the scattering invariant Q calculated from Equation 1-23. The invariant Q describes the electron density fluctuation of the polymer

$$Q = \frac{1}{2\pi}\int I(q)q^2 dq \qquad \textbf{Eq. 1-23}$$

and is a good representation of the overall degree of phase separation present in the Nafion® membranes. From the SAXS results, the Q values of Nafion® membranes cast from various alcohol:water solutions decreased as the aliphatic alcohol chains increased (methanol < ethanol < 2-propanol), indicating a decrease in the phase separation between

the hydrophobic and hydrophilic regions in the membranes. The same trend in decreasing Q values persists after annealing the Nafion® membranes at 120 °C for sixty minutes. On the otherhand, the Q value of Nafion® cast from DMF at 120 °C was nearly an order of magnitude lower than Nafion® cast at room temperature from various alcohol:water mixtures. The lower degree of phase separation seen in Nafion® cast from DMF is in agreement with the decreased entanglements and hydrophobic aggregation of the Nafion®:DMF solutions using dynamic light scattering. It was also interesting to note that Lin et al. saw an increase in the Q values of Nafion® cast from DMF with increasing casting time, 60-80 minutes. The increasing Q values with casting time suggests that annealing for longer periods of time allows for more molecular backbone movement and an increase in crystalline order. Lin and coworkers conclude that when Nafion® is cast from various alcohol:water solutions, a certain degree of phase separation between the hydrophobic backbone and hydrophilic side chains occurs before the membranes are annealed. On the contrary, due to the high boiling point of DMF (153 °C), the majority of phase separation in Nafion®:DMF solutions occurs during casting at 120 °C, due to the increased mobility of the Nafion® chains and aggregates.[163]

While creating a fundamental understanding of the molecular motions of Nafion®, Page et al. examined the effects of temperature using DSC, SAXS, and solid-state nuclear magnetic resonance (SS-NMR).[41] Thermal annealing of extruded Nafion® 117 was accomplished in the DSC after drying at 120 °C for two hours and erasing the thermal history by heating samples to 330 °C for five minutes and cooling back to room temperature. Nafion® in both the Na^+ and Cs^+-forms were then annealed in the DSC at 200 °C for 0.5, 2, 6, 12, and 24 hours. For both counterion forms of the ionomer, the

initial heating scan produced a broad endotherm between 200 and 250 °C. After quenching from 330 °C, the broad endotherm is erased but reappears upon annealing at 200 °C for various times. Based on the thermal behavior of semicrystalline polymers with slow crystallization kinetics, the broad endotherm was assigned to the melting of PTFE-like crystallites. For Na^+-form Nafion®, Page et al. observed an initial endotherm with a heat of fusion (ΔH) of 5 J/g. After quenching from the melt at 330 °C and annealing at 200 °C for 24 hours, the endothermic event reappeared with a ΔH of 2.7 J/g or approximately 50% of the original crystallinity. SAXS analysis verified the reconstitution of crystallinity due to the emergence of the crystalline peak at $q = 0.5$ nm^{-1} upon annealing Na^+-form Nafion® at 200 °C for 24 hours. The DSC results of Cs^+-form Nafion® quenched from the melt and annealed at 200 °C for 24 hours showed an endothermic event with a ΔH of 5.3 J/g, which was approximately 100% of the original endotherm before any thermal treatment. Based on the DSC data, Page et al. showed that changing the counterion drastically changes the crystallization kinetics due to manipulation of the dipole-dipole interactions between ionic moieties. Page et al. also examined the effect of annealing temperature on the crystallization of Cs^+-form Nafion® by annealing in the DSC for two hours at 120, 150, 180, 210, and 240 °C. The DSC data showed that two endothermic events appeared upon annealing Cs^+-form Nafion®. For each annealing treatment, the low temperature endotherm occurred at 20-30 °C above the respective annealing temperature, while the high temperature endotherm remained constant between 240-250 °C. Based on a shift of the low temperature endotherm to higher temperatures upon annealing, Page et al. concluded that the endothermic event

was attributed to melting of small, imperfect crystals similar to DSC data seen for other crystallizable copolymers.

In a separate but related study, Page and coworkers examined the thermal relaxation of various counterion forms of oriented Nafion®.[97, 100, 164] Nafion® membranes were uniaxially oriented to a draw ratio of $\lambda = 3$ at 190, 170, 100, and 80 °C for the TMA^+, TEA^+, TPA^+, and TBA^+ counterions, respectively. Variable temperature SAXS analysis was conducted on each oriented Nafion® sample from 50-300 °C. Page et al. noticed a dramatic decrease in the SAXS ionomer peak intensity with increasing temperature and decreasing counterion size. A comparison of the tan δ temperature from DMA and the intensity drop using variable temperature SAXS correlated well with the α-relaxation transition temperature of Nafion®. Page et al. concluded that annealing at elevated temperatures causes the elastic forces exerted on the side chains from the ionic aggregates to increase to a point that exceeds the electrostatic forces between ion pairs within the aggregate. As a result, the electrostatic network destabilizes and the morphology relaxes to an isotropic state, depending on counterion size and annealing temperature.

In a study on the effect of annealing temperature on the transport properties of Nafion®, Deluca et al. observed an interesting trend in that both the proton conductivity and methanol permeability had maximums versus annealing temperature.[165] The authors examined both extruded Nafion® 117 and Nafion® cast on Teflon at room temperature after 24 hours of alcohol/water solvent evaporation. Both sets of samples were then annealed at 120 and 150 °C for sixty minutes, along with annealing at 180, 210, 230, and 250 °C for ten minutes at each temperature. As opposed to an earlier study by Sone et

al.[160] , DeLuca and coworkers observed a proton conductivity maximum after annealing extruded Nafion® 117 at 210 °C for ten minutes.[165] A similar trend of increasing and then decreasing methanol permeability was also noticed for both extruded and solution-cast Nafion® after annealing at elevated temperatures. Along with the obscure proton conductivity and methanol permeability data, DeLuca et al. observed a lower selectivity (proton conductivity/methanol permeability) for all of the annealed, extruded Nafion® samples. This observation implied that the methanol permeabilities were actually higher for all of the annealed samples when compared to as-received Nafion®. DeLuca et al. conclude that the changes seen in the transport properties of both extruded and solution-cast Nafion® can be explained by morphological changes in the low temperature (< 210 °C) and high temperature (> 210 °C) transitions. The authors believed that by annealing below 210 °C, the percolation pathway reorients, leading to enhanced transport properties. On the other hand, by annealing at temperatures above 210 °C, the percolation pathway is negatively affected, resulting in lower proton conductivity and methanol permeability.[165]

Jung et al. examined the influence of annealing Nafion® on both the percent solubility of the recast form and MEA performance in a direct methanol fuel cell.[166] The recast Nafion®, used as a binder when attaching the catalyst onto the Nafion® film, was prepared by casting from a 5 wt% Nafion®/alcohol/water solution at 70 °C onto a glass substrate. The recast films were then annealed for 40 minutes at 110, 130, 150, and 200 °C. The percent solubilities were determined based on a procedure by Moore et al.[67] , and decreased as a function of annealing temperature with mechanical stability occurring above annealing at 150 °C. The authors note that the change in solubility is due to

annealing above the polymers dynamic mechanical α-relaxation transition temperature, which significantly changes the ionomer morphology. Similar to studies done by Fujimura et al.[68] and Gebel et al.[152], Jung and coworkers used both SAXS and WAXD to observe the reappearance of the crystallinity as a function of annealing temperature. A maximum in water uptake, proton conductivity, and electrochemical active surface was noticed after annealing recast Nafion® for 40 minutes at 130 °C. The authors do not give an explanation for this phenomenon, except for noting a change in the morphology of the membrane at 130 °C. The performance of an MEA annealed at 110, 130, 150, and 200 °C was also documented based on voltage and power density versus current density profiles. In agreement with the water uptake, proton conductivity, and electrochemical active surface results, the MEA annealed at 130 °C had the highest power and current densities at any given voltage. The authors concluded that annealing Nafion® at 130 °C for 40 minutes provided the best overall morphology for fuel cell performance and was attributed to an increase in the primary pores at the electrode interfaces.

Recently, Hensley et al. performed an extensive study on the effects of annealing extruded N111, N112, N115, and N117 Nafion® films, along with a hydrolyzed precursor of N111-F, which is designated as HP.[151] In order to determine the optimum annealing conditions, Hensley et al. annealed HP membranes between 100 and 165 °C for 0.5 to 12 hours. A significant increase (approximately 54%) in proton conductivity was observed for HP annealed at 165 °C for three hours when compared to membranes annealed at other temperatures and times. Based on these results, Hensley et al. adopted the procedure of annealing Nafion® at 165 °C for three hours in order to significantly improve the properties of extruded Nafion®. After performing proton conductivity

measurements on the various types of extruded, annealed Nafion®, Hensley et al. noticed an overall increase in proton conductivity along with an equilibrium being reached between all of the annealed membranes. Equilibrium was reached based on the significant decrease in the variability between different membranes after annealing at 165 °C for three hours. The authors note that under no circumstance did the proton conductivity decrease after annealing, indicating that, at best, any thermal pretreatment will only increase the overall proton conductivity. In agreement with the proton conductivity results, the water sorption and permeability of Nafion® increases upon annealing at 165 °C for three hours. The water uptake of the membranes was also dependent on film thickness. For thin membranes (1 mil, 25 μm) the water uptake plateaued at λ = 16-18 mol water/mol sulfonate, while for thick membranes (2-7 mil, 50-175 μm) the water uptake averaged between λ = 21-22 mol water/mol sulfonate. The authors suggest that rapid evaporation of water from thinner membranes during the experiment is plausible, but overall they believe thinner membranes do not require as much water to have comparable proton conductivity values, indicating a major advantage for future fuel cell work with thinner Nafion® membranes. Based on WAXD and SAXS results, Hensley et al. could not determine a correlation between annealing and changes in crystallinity of extruded Nafion® films. They noticed an increase in the crystallinity of thin membranes along with a subsequent decrease in the crystallinity of thicker films. From the crystallinity results, the authors conclude that changes in crystallinity had minimal influence on the previous trends seen for proton conductivity, water sorption, and water permeability. However, from the SAXS analysis, Hensley et al. noticed a shift of the ionomer peak to lower s values, for annealed Nafion® of increasing thicknesses. A

shift to lower s values indicated an increase in the average hydrated cluster size, which coincided well with the increase in water uptake for increasing membrane thicknesses. Finally, Hensley et al. used pulsed field gradient spin-echo NMR at 25 and 90 °C to examine the diffusion of water through various Nafion® membranes annealed at 165 °C for three hours. The diffusion of water increased on average 33% between annealed and unannealed Nafion® when the experiment was conducted at room temperature. By increasing the experimental temperature to 90 °C, the diffusion of water increased approximately 66% between as-received and Nafion® annealed for three hours at 165 °C. Hensley et al. conclude that annealing increases the diffusivity of water to such an extent that an increase in the long range diffusion of water and protons in the film is bound to improve. Overall, the annealing procedure was seen to vastly improve the proton conductivity, water uptake, permeability, and diffusion rates of extruded Nafion®.

Alberti and coworkers recently performed a detailed kinetic investigation on the water uptake of extruded Nafion® 117 after various hydrothermal and thermal treatments.[167] The first study involved submersing Nafion® 117, which had been annealed at 120 °C for 15 hours, in distilled water ranging from 20-140 °C and determining the water uptake equilibration values and times. The time needed for each sample to reach equilibrium in the respective water baths varied from 150-225 hours depending on the water temperature. The percent equilibrium reached after one hour of submersion was also drastically different depending on the water temperature. The percent equilibrium after one hour decreased dramatically from 95.4% for Nafion® subjected to room temperature water, compared to 39% for Nafion® submersed in water at 140 °C. Alberti et al. discussed both the long equilibration times and the decrease in

the kinetic rate with increasing water temperature based on a two-step process for the overall determination of water uptake. The first step was fast and attributed to the equilibrium necessary for the water to diffuse within the membrane, while the second step was slow and involved the modification of Nafion®'s conformation as a function of temperature. Plots of the equilibration values for Nafion® annealed at 120 °C for 15 hours were recorded as a function of temperature versus water uptake. In agreement with Hinatsu et al.[159] the equilibration values increased nonlinearly with increasing temperature and Alberti et al. documented an irreversible change in the hydration depending on the submersion temperature. By annealing Nafion® for various times (15-672 hours) and temperatures (100-140 °C), Alberti et al. observed a change in the degree of hydration shown in the equilibration values but the trend of increasing water uptake with increasing submersion temperature remained the same.

Alberti and coworkers also examined the effect of hydrothermal and thermal treatments on the mechanical properties of Nafion®.[167] Various thermally treated samples were examined ranging in annealing temperature (50-140 °C) and times (15-672 hours), and compared to the as-received state of extruded Nafion® 117. The hydration number (water uptake at 20 °C), along with tensile modulus and elongation at break (performed under 100% relative humidity) were all recorded for the annealed versus unannealed membranes. The authors observed a dramatic effect of the thermal memory of the membranes where the water uptake changed from a low of $\lambda = 9.0$ for the sample annealed at 120 °C for 672 hours compared to $\lambda = 82.7$ for the sample annealed at 140 °C for 96 hours while in water. Subsequently, the tensile modulus and elongation at break followed the same trend of decreasing mechanical properties with increasing water

uptake values. Because the water uptake and tensile modulus depended on the conformation of Nafion®, Alberti et al. concluded that various Nafion® conformations were created by thermally annealing the ionomer.

Maeda et al. developed a new method for reexamining the same area of the same sample using atomic force microscopy (AFM) and incorporated this technique into studying cast Nafion® before and after annealing.[168] Two methods were used to verify the original location of the AFM tip. The first method involved printing out a 10 x 10 mm grid consisting of colored characters and numbers in 250-500 μm spaces, which was then glued onto the back of the glass substrate so it was visible using an optical microscope. The second method involved the evaporation of chromium onto the back of the masked glass substrate, which allowed for the formation of a grid, and was verified using stereo-microscope images. Nafion® was then cast onto the top of the glass substrate by evaporating the residual water/alcohol solution at room temperature. Six trenches were scratched into the cast Nafion® film by utilizing the AFM in contact mode. The trench areas were labeled 1-6 and were scratched using a force of 25 nN for areas 1-3 and 50 nN for areas 4-6. The number of scans to create the areas consisted of two scans for areas 1 and 4, five scans for area 2, ten scans for areas 3 and 5, and finally 20 scans for area 6. The trenches were then analyzed using AFM in tapping mode, which allowed for accurate measurements of area and depth of the trenches without further deformation of the sample. The sample was then removed from the AFM and annealed in an oven at 130 °C for five minutes. With the aide of the alphabetical and numerical grid on the back of the glass substrate, Maeda et al. were able to relocate the exact location of the six trenches after the annealing step. Trenches 1-4 essentially disappeared after the short

annealing procedure. The two deepest trenches, 5 and 6, were visible but severely deformed. After characterization of the two trenches using AFM in tapping mode, Maeda et al. documented a decrease in the average depth for trench 5 from 120 nm to 20 nm and trench six decreased from 170 nm to 40 nm. Maeda et al. proclaimed that the changes seen using AFM was the first example of direct characterization of a structural change at the nanoscale level before and after annealing Nafion®. The authors conclude that Nafion® molecules rearranged and deformed during annealing at 130 °C for five minutes and the consequences of this deformation can be detrimental to increasing the efficiency of Nafion® for use in fuel cells at elevated temperatures.[168]

Luan et al. examined the effects of annealing cast Nafion® on the resulting proton conductivity and methanol permeability.[169] The sulfonyl fluoride precursor of Nafion® was first synthesized by Luan and coworkers, followed by conversion directly into the Na^+ counterion form. The Na^+-form Nafion® was then dissolved under high temperature and pressure in DMF and evaporated to a concentration of 21 wt % Nafion®. A 50 μm thick film of Na^+-form Nafion® was cast under vacuum at 125 °C over a period of 1.75 hours. The film was then cut into six equal sections and five of the samples were annealed for 1.5 hours at the following temperatures, 150, 170, 190, 210, 230, and 250 °C. Based on WAXD results, Luan et al. noticed a continual decrease in both the intensity and full width at half maximum of the crystalline reflection at 17.5 °, 2θ as a function of increasing annealing temperature. The change in percent crystallinity was calculated based on the deconvolution of an amorphous and crystalline peak from the WAXD profiles, resulting in a decrease in crystallinity from 22.0 to 7.4% with increasing annealing temperature from 150 to 230 °C. In contrast to the work of Jung et al. Luan

and coworkers observed a continual increase in proton conductivity with increasing annealing temperature as opposed to a maximum at lower temperatures. The higher proton conductivity values are explained based on the side chains being more mobile at higher temperatures, allowing the separated sulfonate groups to aggregate and form a more uniform network. Luan et al. also noticed a dramatic decrease in the methanol permeability of Nafion® annealed at elevated temperatures. In contrast to the proton conductivity, the authors suggest that the methanol permeates through both the ionic and hydrophobic domains. Upon annealing at high temperatures, the hydrophobic channels are assumed to contract, making it more difficult for methanol to permeate through the membrane, hence lower values of methanol permeability were recorded.

Effects of Orienting Nafion®

One of the more recent techniques employed in the literature to change the morphology of Nafion® is orientation of the membrane through mechanical deformation.[27, 83, 91, 97, 100, 164, 170-174] Gierke et al. were the first to report the effects of tensile drawing on the SAXS profile of both hydrolyzed and unhydrolyzed Nafion®.[27] For the oriented, unhydrolyzed precursor of Nafion® a periodicity of PTFE-like crystallites was observed in the meridional scan, implying equal distances in the long spacing along the fiber axis. In contrast, the ionomer form of Nafion® exhibited scattering of the ionomer peak perpendicular to the draw direction, implying a periodicity normal to the fiber axis.

During the same time period, Fujimura et al. used SAXS and small angle light scattering to examine the effects of orienting Nafion® in the carboxylic acid form.[68] Upon stretching the membrane, Fujimura et al. noticed a shift in the equatorial scattering

maximum to higher angles with increasing draw ratio (λ). In contrast, the meridional scattering maximum of the ionomer peak shifted toward lower angles and decreased in intensity with increasing elongation. A correlation was observed between the oriented SAXS pattern of carboxylic acid Nafion® and oriented spherulitic polyethylene films. A spherulitic structure was confirmed by the appearance of a four-leaf clover pattern using depolarized small angle light scattering. It was concluded that changes in the scattering profile of carboxylic acid form Nafion® upon orientation were due to changes in the interlamellar spacing of the spherulitic texture.[68]

As a continuation of the previous work, Fujimura et al. conducted analysis on cesium-neutralized Nafion® with orientations from $\lambda = 0$ to 1.5.[83] Over a range of orientations, the ionomer peak (located at approximately $s = 0.3$ nm^{-1}), was observed to shift to lower angles and decrease in intensity in the meridional or draw direction. In the equatorial direction, the ionomer peak shifted to higher angles and increased in intensity. By using the Bragg spacings calculated from the peak maxima, a nonaffine deformation behavior was observed between the microscopic expansion ratio, λ_d and the macroscopic expansion ratio, λ_B. Fujimura et al. concluded that the nonaffine behavior was inconsistent with an interparticle scattering model for the morphology of Nafion®, but on the otherhand, the deviation of the draw ratios was plausible if a core-shell morphology was employed, based on the ionomer particle being more rigid than the surrounding matrix phase.[83]

Elliot and co-workers performed a detailed SAXS investigation of the morphology of Nafion® membranes that were subjected to uniaxial and biaxial orientations.[171, 172] Extruded Nafion® membranes showed a distinct arcing of the cluster

or ionomer SAXS reflection in the direction perpendicular to the extruded machine direction. An interparticle morphology was used to explain the arcing of the ionomer peak in terms of an increase in coherence of the intercluster spacings perpendicular to the extrusion direction, as well as a corresponding reduction in coherence in the parallel direction.[171] By drawing an extruded Nafion® membrane to 50% strain parallel to the extrusion direction, Elliot et al. noticed an increase in the degree of arcing along with some elliptical distortion of the ionomer peak. Using a model-independent maximum entropy method (MaxEnt) for reconstructing a 2-dimensional electron density map in real space from that corresponding to the scattering data, the intercluster spacings parallel to the draw direction were found to be almost random, while the spacings in the transverse direction were observed to display distinct periodicity.[171] Along with the periodicity in the transverse direction, the clusters appeared to agglomerate relative to their distribution in the as-received membrane. Based on this observation, the anisotropic shape of the small-angle upturn in the SAXS profiles was attributed to scattering between oriented cluster agglomerates having periodic dimensions significantly larger than the intercluster spacings.

By drawing extruded Nafion® perpendicular to the extrusion direction, with a draw ratio of 0.5, Elliot et al. were able to demonstrate pseudo-isotropic SAXS behavior of biaxially oriented Nafion®.[171] Due to the persistence of anisotropy in the 2-D SAXS profiles of the biaxially oriented Nafion®, Elliot et al. decided to mimic true biaxial orientation by drawing extruded Nafion® at temperatures above its α-relaxation. After biaxially orienting as-received Nafion® at 120 °C, Elliot et al. succeeded in creating a

more isotropic ionomer morphology based on the reduction in the degree of arcing and significant decrease in the equivalent Bragg spacing of the ionomer peak reflection.[171]

In a subsequent publication, Elliot et al. examined the effects of swelling extruded Nafion® in various water/ethanol concentrations.[172] The SAXS analysis showed that the microscopic swelling decreased with increasing ethanol content, while the bulk swelling dramatically increased with increasing ethanol content. The maximum bulk swelling of extruded Nafion® was noticed at a 75/25 volume percent mixture of ethanol/water. By subjecting uniaxially oriented Nafion® to the 75/25 ethanol/water mixture, Elliot et al. were able to show a morphological relaxation of both the ionomer and crystalline peaks back to an almost isotropic state. In contrast, morphological relaxation was not observed for membranes swollen in water alone. Although no evidence of ethanol interacting with the fluorocarbon backbone of Nafion® was shown, the authors concluded that the relaxation behavior was attributed to the plasticization effect of ethanol on the fluorocarbon matrix. Elliot et al. concluded that chain entanglements in the fluorocarbon matrix were responsible for restricting the expansion of the ionomer morphology, hence maintaining the anisotropic spatial coherence under oriented conditions.[172]

Londono et al. with the aid of a synchrotron SAXS facility examined the effect of orienting H^+-form Nafion® from 0-150% elongation.[173] As the elongation of was increased to 150%, meridional scattering of the ionomer peak disappeared while the intensity profile narrowed azimuthally about the equatorial direction. An equatorial streak was seen at high elongations, which is typical in SAXS profiles of drawn fibers, due to the presence of a microfibril morphology. By collimating the x-ray beam to approximately 100 μm, Londono et al. were able to obtain edge-on SAXS profiles for

Nafion® oriented parallel and perpendicular to the stretching direction. Based on the observation of an isotropic scattering profile for the sample oriented parallel to the stretching direction, the authors concluded that the morphology of oriented Nafion® must be fiber-like. The authors also suggest that the morphology consists of either oriented cylindrical or lamellar domains rather than spherical clusters.

Londono et al. also performed simultaneous SAXS/WAXS during the in-situ orientation of H^+-form Nafion®.[173] Both the ionomer peak and PTFE crystalline peak (*hkl* = 100) were shown to orient equatorially during orientation. By correlating the full width at half height as a function of orientation, the authors noticed that the crystalline peak narrowed at twice the rate of the ionomer peak. From this result, it was concluded that the crystalline bilayers could not be intimately linked to the lamellar ionic domains, based on the nonlinear behavior of the peak widths during orientation.

Van der Heijden and coworkers have compared the orientations of both the ionomer and crystalline domains, with respect to draw ratio, of Nafion® using simultaneous SAXS/WAXD.[91] By examining the azimuthal angles from 0° (meridional) to 90° (equatorial) while drawing the sample from 0-272% elongation, the authors observed minimal change in the position of the crystalline peak (q = 1.24 $Å^{-1}$) seen in the WAXS profile. On the contrary, the ionomer peak (q = 0.15 $Å^{-1}$), amorphous peak (q = 1.1 $Å^{-1}$) and intrachain peak (q = 2.75 $Å^{-1}$) showed a decrease in q value in the meridional direction with increasing draw ratio.

The orientation of Nafion® was further discussed in terms of elongated polymeric aggregates and quantified by using the Hermans' orientation factor (f). The Hermans'

orientation factor is calculated using Equation 1-24, where φ is the angle between the molecular chain axis and the deformation axis. For a system with perfect orientation, the

$$f = \frac{3\cos^2 \varphi - 1}{2} \qquad \textbf{Eq. 1-24}$$

Hermans' orientation factor will be 1, isotropic systems will have a factor of 0, and a system with perfect orientation perpendicular to draw will be -0.5. Based on absolute calculations of the Herman's orientation factor, draw ratios of less than 200% created offset orientation where the ionomer domains oriented more readily than the crystalline domains. At draw ratios above 200%, the two domains began correlating with respect to elongation. The observed two-state orientation behavior was morphologically postulated based on Rubatat's elongated polymer aggregates model[75] of Nafion® consisting of a collection of bundled, elongated polymeric aggregates containing relatively extended chain crystals.[91] At small draw ratios, the large bundles begin to rotate, correlating the elongated aggregates during orientation and is described by the orientation factor of the ionomer peak. At large draw ratios, the alignment of individual elongated aggregates becomes more refined in the draw direction due to sliding or disentangling of the aggregates from each other and is described by the orientation factor of the crystalline peak.[91]

More recently, Moore and coworkers focused on studying the thermally induced relaxation of anisotropic Nafion® films due to their importance for operating proton exchange membrane fuel cells at elevated temperatures (80-120 °C). The authors found that Nafion's® morphology can be manipulated through high temperature uniaxial orientation of membranes neutralized with various alkylammonium counterions.[97, 98, 100] By using SAXS and WAXD analysis, the authors noticed a persistence of the

morphological manipulation after allowing the polymer to cool to room temperature from uniaxial orientation at temperatures above the, DMA verified, α-relaxation temperature. At relatively high orientations, elongations greater than 200%, only equatorial spots were observed for the ionomer peak as shown in Figure 1.15.

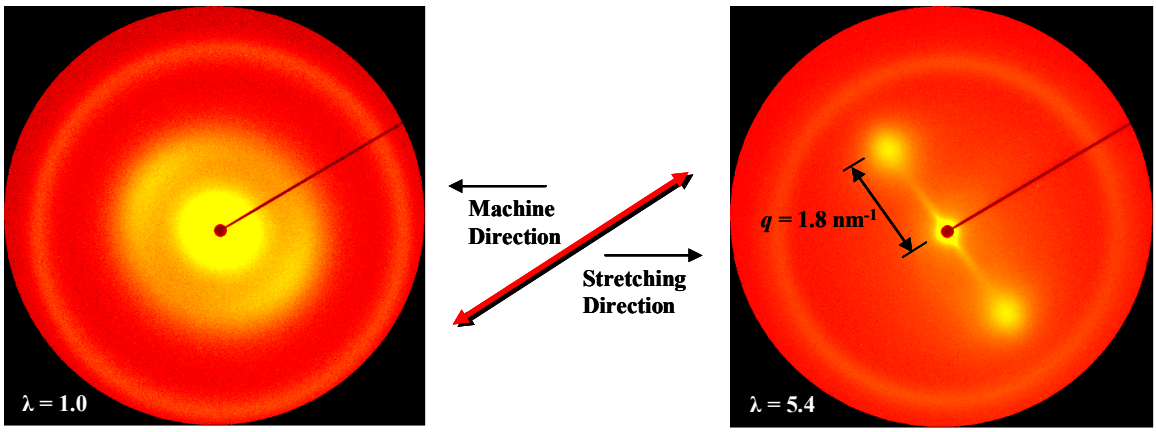

Figure 1.15. 2-D SAXS scattering patterns of **a)** As-received TBA^+-form Nafion®, displaying slight anisotropy in the ionic domains due to orientation during the calendaring process **b)** Uniaxially oriented TBA^+-form Nafion® ($\lambda = 5.4$)

A circular integration over all azimuthal angles of the SAXS patterns was performed to calculate the relative invariant, Q, for samples of various elongations. A significant increase in Q with elongation was attributed to an increase in the extent of ionic aggregation with elongation to yield a matrix with fewer lone pairs and a more uniform distribution of ionic aggregates.[174]

With the use of time-resolved synchrotron SAXS, Moore and coworkers were able to further examine the thermal relaxation behavior of oriented Nafion®.[97, 100] Figure 1.16 shows the SAXS profiles of Nafion® oriented in both the tetramethylammonium (TMA^+) and tetrabutylammonium (TBA^+) counterions during heating and cooling steps. Similar to earlier studies, the anisotropic scattering of the oriented samples at 50 °C contain two distinct equatorial spots, which are attributed to scattering from the ionomer domain, as well as equatorial streaking, which is due to the fibrillar-type morphology.

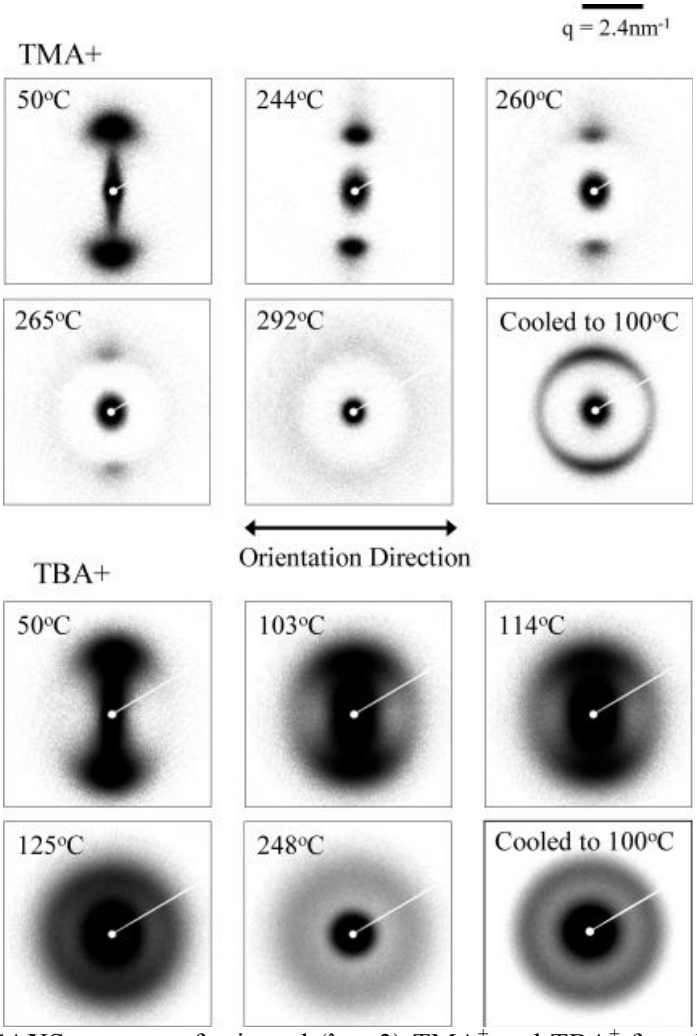

Figure 1.16. 2-D SAXS patterns of oriented (λ = 3) TMA^+ and TBA^+-form Nafion® during the heating process and after cooling to 100 °C (Reprinted with permission from ref[97] *Macromolecules*, **39**, 3939 (2006). Copyright 2006, American Chemical Society.)

By increasing the temperature from 50-300 °C, Page et al. observed a decrease in the anisotropy of the oriented Nafion® scattering profiles. A weak isotropic halo of the ionomer domain was noticed at 292 °C for TMA^+-form Nafion® and 125 °C for TBA^+-form Nafion®. Upon cooling the oriented samples to 100 °C, the ionomer regime reappears with increased intensity along with increased isotropy relative to the initial oriented profiles. This phenomenon suggests that the ionomer domain is significantly disrupted at elevated temperatures, yielding a more homogenous distribution of ion pairs, but the reconstitution of distinct aggregates is reversible upon cooling. It is also seen in

Figure 1.16 that as the size of the counterion increases, the equatorial arc due to orientation becomes broader in the azimuthal direction (χ), as well as a decrease in the temperature at which the anisotropic relaxation occurs. An enhanced understanding of the effects of counterion size and anisotropic relaxation of the orientation during heating were examined by plotting the azimuthal angle versus intensity as a function of temperature as shown in Figure 1.17. Similar to Figure 1.16, the oriented TMA^+ and TBA^+-form Nafion® samples display distinct equatorial scattering peaks located at approximately 90° and 270° (χ) with respect to the orientation direction.

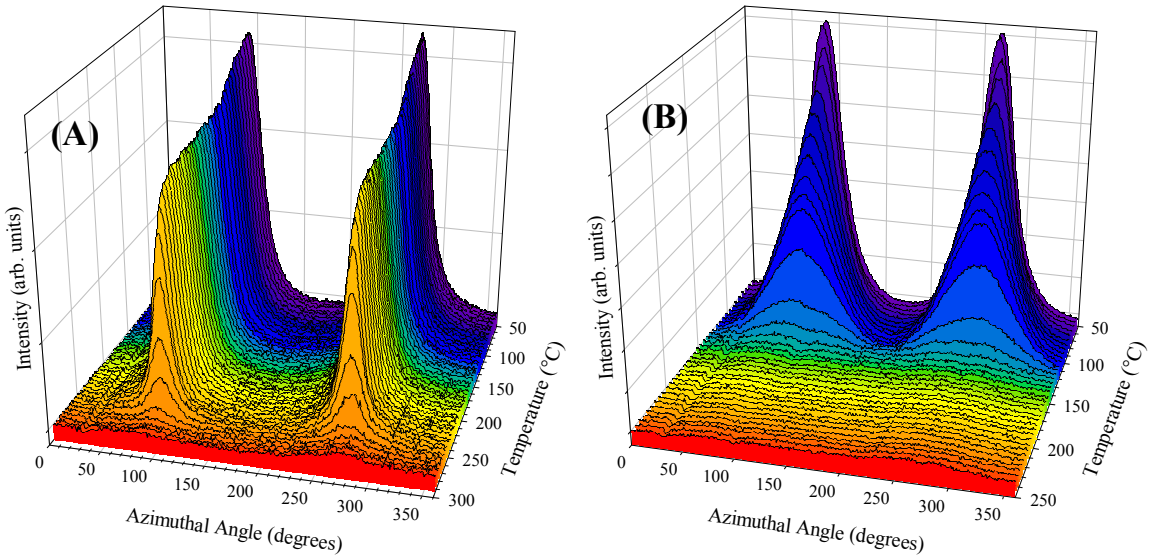

Figure 1.17. Variable temperature SAXS for scattering in the azimuthal direction (χ) for oriented Nafion® (λ = 3) in the **a)** TMA^+-form and **b)** TBA^+-form (Reprinted with permission from ref[97] *Macromolecules*, **39**, 3939 (2006). Copyright 2006, American Chemical Society.)

For both counterion forms, the anisotropic scattering transforms at elevated temperatures into isotropic profiles with a constant intensity throughout the range of azimuthal angles. From Figure 1.17, Page et al. correlated the temperature at which a rapid decrease in the intensity of the equatorial peaks was observed with the α-relaxation temperatures of the respective counterions, as seen using DMA.[41] The correlation of the anisotropic relaxation temperature of SAXS with the α-relaxation temperature of DMA has allowed

for a more precise description of the overall ionomer relaxation process. Page et al. denote that the α-relaxation allows for the onset of long-range mobility of both the main and side chains, which is facilitated by a profound weakening of the electrostatic interactions within the ionic aggregates. Based on this fundamental understanding of the origins of the thermo-mechanical relaxations in Nafion®, Page et al. have shown that oriented morphologies can persists at temperatures below the α-relaxation, allowing for a distinction in the operating temperature ranges for Nafion® in various counterion forms.

Lin et al. have recently examined the effects of orienting recast Nafion® on the properties of water in the membrane as well as proton conductivity and direct methanol fuel cell (DMFC) performance.[175-177] Draw ratios from 1-7 were obtained by orienting dimethylacetimide (DMAc) swollen Nafion® cast films at elevated temperatures (125 °C) and then annealing at 150 °C for two hours to remove any residual solvent. A persistence of the oriented morphology was noted based on the recast membranes ability to maintain orientation in a 75/25 methanol/water mixture at 60 °C for 12 hours. This is in contrast to an earlier study by Elliot et al. where oriented Nafion® ($\lambda = 1.5$) was immersed in a 75/25 ethanol/water mixture for one day, and based on SAXS analysis, relaxed back to an almost isotropic state.[172] Lin et al. assumed that the persistence of their oriented membranes in methanol/water mixtures was based on annealing after stretching, which increased the crystallinity, hence increasing solvent resistance.[175] The authors also note that without annealing, the recast membranes lack crucial mechanical properties, and the stretched recast membranes retract to their original dimensions after submersion in 60 °C methanol.[176] A slight increase in proton conductivity was also observed with increasing draw ratio along with a factor of 2.5 decrease in the methanol permeability of the oriented

recast membranes. Equilibrium water uptake results showed that the water uptake of stretched, recast Nafion® was independent of the draw ratio. No conclusion was given as to why the methanol permeability dramatically decreases with draw ratio and the water uptake remains constant. DSC thermograms of stretched, recast Nafion® showed a monotonic decrease in the size of the water melting peak as a function of draw ratio, indicating there is less freezable water present upon stretching.[176] A decrease in the freezable water melting temperature from 0 °C to -10 °C was also observed as the draw ratio increased for stretched, recast Nafion®. A similar trend in decreasing melting temperature was seen by Siu et al. involving unstretched Nafion® with a water content of 11-14 mol water/mol sulfonate.[178] As opposed to Sie et al., Lin and coworker's oriented Nafion® had a water content of 19 mol water/mol sulfonate, concluding that the depressed freezing point of bulk water was due to a morphological change during the stretching and annealing procedure.[176] A redistribution of ionic domains in the stretched Nafion®, where the domain size decreased and the number of domains increased, was assumed to cause the phenomenon of a constant water uptake and increasing draw ratio. Transmission electron microscopy images were taken on stretched, Nafion®, stained with lead acetate, to verify the change in both size and distribution of the ionic domains.[176]

Lin and coworkers also showed a significant increase in DMFC power output for stretched, recast Nafion® ($\lambda = 4$) versus nonstretched recast Nafion®.[175] It should also be noted that Lin et al. stacked three stretched films to obtain a total thickness of 180 μm as opposed to a single film thickness of 200 μm for the unstretched recast Nafion®. The thickness difference as well as MEA preparation with three layers as opposed to one could have a significant influence on the higher open-circuit voltage and lower resistance

losses seen for the stretched, recast membrane. Lin et al. also conducted DMFC tests on stretched, recast Nafion® using various methanol feed concentrations (0.5 and 1.0 M) as well as operating temperatures (60 and 80 °C). The changes in the concentration of the methanol input had minimal changes on the performance of stretched, recast Nafion® versus as-received Nafion® 117 in a DMFC. The most significant changes were observed when the operating temperature of the DMFC was increased from 60 to 80 °C. A far greater increase in power density was observed for stretched, recast Nafion® as opposed to as-received Nafion® 117 with an increase in DMFC temperature. At a cell voltage of 0.5, the power density increased by a factor of three (25 to 74 mW/cm^2) for stretched, recast Nafion® when the temperature of the cell was increased from 60 to 80 °C.

In a subsequent publication, Lin et al. compared two different methods for producing "pre-stretched recast Nafion®".[177] Method one was the same method used in the previous publication,[175] while method two involved creating thicker recast membranes by evaporating a larger quantity of solution and annealing at 180 °C for two hours instead of 150 °C to ensure complete evaporation of DMAc after orientation of the membranes. The proton conductivity and methanol permeability studies were repeated for as-received Nafion® 117, and prestretched, recast Nafion® created from methods 1 and 2. Similar to their first study, Lin et al. noticed constant proton conductivity between all three membranes, but a significant decrease in the methanol permeability with increasing drawing ratio. The membranes from method two followed a similar trend in methanol permeability as those from method one, with the exception of having higher permeability values. The higher methanol permeability values of membranes produced from method two were postulated due to changes in the morphology of DMAc-swollen

films of varying thicknesses. Rod-like polymer aggregates present in Nafion®/DMAc solutions were assumed to have better alignment in thinner films along with improved membrane nanostructure and greater crystallinity upon annealing, hence lower methanol permeability values for membranes produced from method one. Due to the discrepancy of using a multilayer MEA in their previous publication, Lin et al. chose to examine the DMFC performance of a multilayer MEA composed of method one membranes versus a single layer MEA composed of a thicker method two membrane. The initial study consisted of a three layer MEA of method one membranes (60 μm thick), compared to a single layer MEA of a 185 μm thick method two membrane. Both types of MEAs had similar direct methanol fuel cell performance and outperformed as-received Nafion® 117 over the entire voltage range. Since method two produced membranes with higher methanol permeabilities than method one, the authors examined the influence of the number of layers on the relative methanol permeability. By examining the open circuit voltage methanol crossover of MEAs consisting of 1-4 layers, the methanol permeability was shown to increase linearly with the number of Nafion® membranes. Similar to their previous publication, Lin et al. performed DMFC tests on a wide variety of prestretched membranes, all of which had higher performances than as-received Nafion® 117. Lin et al. also showed that membrane thickness plays a crucial role in optimizing DMFC performance. A series of DMFC tests were conducted on prestretched membranes ranging in thicknesses from 60-250 μm. All of the prestretched membranes had higher power densities at 0.4 V than their as-received Nafion® 117 counterparts, but a maximum power density of 84 mW/cm^2 was produced from a 150 μm thick prestretched membrane.

Chourdakis et al. examined the uniaxial orientation of both Nafion® and Teflon® by comparing DMA and UV-Raman data.[179] Polarized UV-Raman spectra were recorded using a 325 nm wavelength laser due to fluorescent problems in the visible and near infrared wavelength spectra. A significant change in the polarized UV-Raman spectra, both parallel and perpendicular to draw, was noticed between as-received and oriented Teflon®. Examination of the oriented Teflon® spectra revealed a dramatic increase in the intensity of the C-C stretching band (1377 cm^{-1}) parallel to draw, along with an increase in the intensity of the CF_2 stretching band (731 cm^{-1}) perpendicular to draw. The band at 1297 cm^{-1} remained unchanged throughout the orientation process and was assigned to a combination of C-C and C-F degenerate stretching. UV-Raman spectra were then recorded for extruded Nafion® samples oriented either parallel or perpendicular to the machine direction at draw ratios of 1, 2, 3.5, and 4.5. The as-received membranes, with a draw ratio of one, were shown to exhibit molecular anisotropy by the enhanced relative scattering intensities of the Raman bands at 731 and 1377 cm^{-1} parallel to the machine direction. Upon further orientation of the Nafion® membranes, an increase in the intensity of the C-C stretching band at 1377 cm^{-1} was documented, verifying preferred orientation parallel to draw. In contrast, the CF_2 stretching band at 731 cm^{-1} increased in intensity perpendicular to draw, implying an analogous increase in the molecular orientation. The authors also note a preferential orientation of two Nafion® side chain peaks (C-S stretch at 805 cm^{-1} and C-O-C stretch at 971 cm^{-1}) perpendicular to the draw direction. Dynamic mechanical analysis was also conducted on Teflon® oriented along the machine direction and Nafion® oriented both parallel and perpendicular to the machine direction. In all three cases, an increase in the storage

modulus with orientation draw ratio was observed. A more profound increase in modulus vales was noticed with Nafion® oriented parallel to the machine direction. The authors finally comment on the increased mechanical properties and solvent permeability of a membrane that was biaxially oriented to a thickness of 30 μm, which will be discussed in a later publication.[179]

Most recently, Rubatat et al. have used both SAXS and SANS to further characterize the morphology of uniaxially oriented Nafion® membranes.[92] Similar to the study of Londono et al.[173] , Rubatat and coworkers examined the 2D SAXS patterns of uniaxially oriented Nafion® along three different planes, MP_1, MP_2, and EP shown below in Figure 1.18.

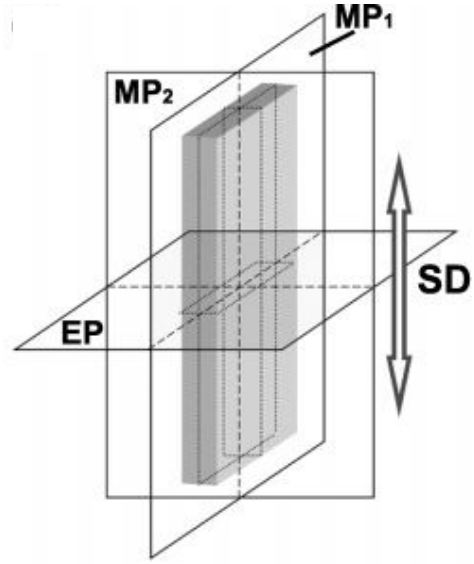

Figure 1.18. Configuration of geometrical planes examined during SAXS of uniaxially oriented Nafion®. SD is the stretching direction, EP is the equatorial plane relative to the SD, MP_1 and MP_2 are the two meridianol plans with respect to the SD. (Reprinted with permission from ref[92] *Macromolecules*, **40**, 9455 (2007). Copyright 2007, American Chemical Society.)

The SAXS profiles measured in the meridianol planes MP_1 and MP_2 displayed the typical anisotropic behavior of uniaxially oriented Nafion® as described earlier. On the other hand, the SAXS pattern through the equatorial plane, EP, remained isotropic after

orientation, verifying the results of Londono et al. on the uniaxiality of oriented Nafion®. Within a series of elongations (0-120%), Rubatat et al. examined the SAXS profiles in MP_1 both parallel and perpendicular to the stretching direction. It was shown that the scattering behavior was opposite for both directions. The intensity and *q*-position of the ionomer peak decreased with increased orientation parallel to the SD, and increased with increasing orientation perpendicular to draw. The authors also note a change in the power law of the crystalline peak (q = 0.07 nm^{-1}), from a slope of q^{-1} to q^{-2} for Nafion® parallel to draw in the MP_1 plane.

By utilizing contrast variation SANS, Rubatat et al. attempted to determine the shape of the scattering entities in oriented, swollen Nafion® membranes.[92] Based on the assumption that the ionomer peak intensity using SANS can be depicted by the product of a structure and form factor, Rubatat and coworkers divided the scattering profiles of Nafion® swollen in D_2O and H_2O, respectively, leading to the cancellation of the structure factors and subsequent ratio of the form factors. Examination of the resulting division curves showed a minimum value at 0.14 $Å^{-1}$ for both the as-received Nafion® as well as 120% elongated Nafion® measured perpendicular to the SD. The observation of the same minimum value for both of these curves meant that the scattering length density profile of the scattering entity remained constant perpendicular to draw after orientation. On the other hand, the minimum at 0.14 $Å^{-1}$ is absent in the division curve of Nafion® oriented parallel to draw in MP_1, indicating there is no longer variation in the scattering length density along the drawing axis. Based on this observation, Rubatat et al. eliminated the morphology consisting of deformed micelles or spheres based on the principle that the scattering objects are not deformed during the orientation process. To

validate their assumption, the authors compared the Nafion® division curves to perfectly oriented core-shell cylinder morphologies with a defined form factor. The theoretical curves displayed the same trend as the experimental data. The correlation is completely lost parallel to the stretching direction but the minimum appears consistent between both the perpendicular to drawn model and as-received model.

Conclusions

An introductory review of PFSI membranes involving processing procedures, complex morphologies, and various applications has been presented based on both recent and historical literature. The main driving force for the advancement of PFSI's is based on their excellent ionic conductivity and use as proton exchange membranes in fuel cells. The evolution of morphological models for this complex group of polymers has spanned decades with a detailed representation of the true structure still unknown. Once a fundamental understanding of the chemical microstructure and nanoscale morphology of PFSI's is achieved, then an increase in performance of the polymers will come with morphological and chemical manipulation.

References

(1) Connolly, D. J.; Gresham, W. F. *Fluorocarbon Vinyl Ether Polymers*. Patent US3282875, 1966.
(2) Grot, W. *Chemie Ingenieur Technik* **1978,** 50, 299-301.
(3) Mauritz, K. A.; Moore, R. B. *Chemical Reviews* **2004,** 104, (10), 4535-4585.
(4) Ezzell, B. R.; Carl, W. P.; Mod, W. A. *Novel polymers having acid functionality*. Patent US4330654, 1982.
(5) Ezzell, B. R.; Carl, W. P.; Mod, W. A. *Preparation of Vinyl Ethers*. Patent US4358412, 1982.
(6) Arcella, V.; Ghielmi, A.; Apostolo, M.; Abusleme, J. *Fluorinated ionomers*. European Patent Application 01114606.5, June 19, 2001.
(7) Guerra, M. A. *Preparation of perfluorinated vinyl ethers having a sulfonyl fluoride end-group*. US6624328, 2003.

(8) Hamrock, S. J.; Rivard, L. M.; Innes Moore, G. G.; Freemyer, H. T. *Polymer Electrolyte Membrane*. Patent Application, US20040121210, 2004.
(9) Hsu, W. Y.; Gierke, T. D. *Journal of Membrane Science* **1983,** 13, 307-326.
(10) Doyle, M.; Rajendran, G., Perfluorinated membranes. In *Handbook of Fuel Cells - Fundamentals, Technology and Applications*, Wolf Vielstich, A. L., and Hubert A. Gasteiger, Ed. John Wiley & Sons, Ltd, Chichester: 2003; Vol. 3 Part 3, pp 351-395.
(11) Ghielmi, A.; Vaccarono, P.; Troglia, C.; Arcella, V. *Journal of Power Sources* **2005,** 145, (2), 108-115.
(12) Grot, W. G. *Macromolecular Symposia* **1994,** 82, 161-172.
(13) Yeo, S.; Eisenberg, A. *Journal of Applied Polymer Science* **1977,** 21, 875-898.
(14) Hodge, I. M.; Eisenberg, A. *Macromolecules* **1978,** 11, (2), 289-293.
(15) Kyu, T.; Hashiyama, M.; Eisenberg, A. *Canadian Journal of Chemistry* **1983,** 61, 680-687.
(16) Boyle, N. G.; McBrierty, V. J.; Eisenberg, A. *Macromolecules* **1983,** 16, 80-84.
(17) Yeager, H. L.; Steck, A. *Journal of the Electrochemical Society* **1981,** 128, (9), 1880-1884.
(18) Lindheimer, A.; Molenat, J.; Gavach, C. *Journal of Electroanalytical Chemistry* **1987,** 216, 71-88.
(19) Ezzell, B. R.; Carl, W. P.; Mod, W. A. *Sulfonic acid electrolytic cell having flourinated polymer membrane with hydration product less than 22,000*. Patent US4358545, 1982.
(20) Ezzell, B. R.; Carl, W. P.; Mod, W. A. *Sulfonic acid electrolytic cell membranes*. Patent US4417969, 1983.
(21) Ezzell, B. R.; Carl, W. P.; Mod, W. A. *Electrolytic cell having an improved ion exchange membrane and process for operating*. Patent US4470889, 1984.
(22) Ezzell, B. R.; Carl, W. P.; Mod, W. A. *Sulfonic acid electrolytic cell membranes and use thereof in the electrolysis of sodium chloride*. Patent US4478695, 1984.
(23) Ezzell, B. R.; Carl, W. P.; Mod, W. A. *Process to produce novel fluorocarbon vinyl ethers and resulting polymers*. Patent US4834922, 1989.
(24) Tant, M. R.; Lee, K. D.; Darst, K. P.; Martin, C. W. *Polymeric Materials: Science and Engineering* **1988,** 58, 1074-1078.
(25) Tant, M. R.; Darst, K. P.; Lee, K. D.; Martin, C. W. *Multiphase polymers: blends and ionomers*, ACS Symposium Series 395, Washington, DC, 1989; pp 370-400.
(26) Moore, Robert B.; Martin, Charles B. *Macromolecules* **1989,** 22, 3594-3599.
(27) Gierke, T.D.; Munn, G.E.; Wilson, F.C. *Journal of Polymer Science: Polymer Physics Edition* **1981,** 19, 1687-1704.
(28) Tsou, Y. M.; Kimble, M. C.; White, R. E. *Journal of the Electrochemical Society* **1992,** 139, (7), 1913-1917.
(29) Zaluski, C.; Xu, G. *Macromolecules* **1994,** 27, (23), 6750-6754.
(30) Kohls, S. L.; Noble, R. D.; Koval, C. A. *Journal of Membrane Science* **1997,** 125, 61-73.
(31) Hill, T. A.; Carroll, D. L.; Czerw, R.; Martin, C. W.; Perahia, D. *Journal of Polymer Science Part B: Polymer Physics* **2002,** 41, 149-158.
(32) Gebel, G.; Moore, R. B. *Macromolecules* **2000,** 33, (13), 4850-4855.

(33) Dreyfus, B.; Gebel, G.; Pierre, A.; Pineri, M.; Escoubes, M.; Thomas, M. *Journal De Physique (Paris)* **1990,** 51, (12), 1341-1354.
(34) Prater, K. *Journal of Power Sources* **1990,** 29, 239-250.
(35) Arcella, V.; Ghielmi, A.; Tommasi, G. *Annals of the New York Academy of Sciences* **2003,** 984, 226-244.
(36) Arcella, V.; Troglia, C.; Ghielmi, A. *Industrial and Engineering Chemistry Research* **2005,** 44, 7646-7651.
(37) Arcella, V.; Ghielmi, A.; Merlo, L.; Gebert, M. *Desalination* **2006,** 199, 6-8.
(38) Merlo, L.; Ghielmi, A.; Cirillo, L.; Gebert, M.; Arcella, V. *Separation Science and Technology* **2007,** 42, 2891-2908.
(39) Merlo, L.; Ghielmi, A.; Cirillo, L.; Gebert, M.; Arcella, V. *Journal of Power Sources* **2007,** 171, 140-147.
(40) Osborn, S.; Hassan, M.; Divoux, G.; Rhoades, D.; Mauritz, K.; Moore, R. B. *Macromolecules* **2007,** 40, (10), 3886-3890.
(41) Page, K. A.; Cable, K. M.; Moore, R. B. *Macromolecules* **2005,** 38, (15), 6472-6484.
(42) Hamrock, S. J.; Yandrasits, M. A. *Journal of Macromolecular Science, Part C: Polymer Reviews* **2006,** 46, 219-244.
(43) Emery, M.; Frey, M.; Guerra, M.; Haugen, G. M.; Hintzer, K.; Lochhaas, K. H.; Pham, P.; Pierpont, D. M.; Schaberg, M.; Thaler, A.; Yandrasits, M. A.; Hamrock, S. J. *ECS Transactions* **2007,** 11, (1), 3-14.
(44) Meng, F.; Dec, S. F.; Williamson, D. L.; Frey, M. H.; Hamrock, S. J.; Turner, J. A.; Herring, A. M. *ECS Transactions* **2006,** 1, (6), 255-262.
(45) Haugen, G. M.; Meng, F.; Aieta, N.; Horan, J. L.; Kuo, M. C.; Frey, M. H.; Hamrock, S. J.; Herring, A. M. *ECS Transactions* **2006,** 3, (1), 551-559.
(46) Haugen, G. M.; Meng, F.; Aieta, N. V.; Horan, J. L.; Kuo, M. C.; Frey, M. H.; Hamrock, S. J.; Herring, A. M. *Electrochemical and Solid State Letters* **2007,** 10, (3), B51-B55.
(47) Yandrasits, M. A.; Aieta, N.; Stanis, R.; Hamrock, S. J.; Cookson, D. J.; Herring, A. M. *ECS Transactions* **2006,** 3, (1), 915-921.
(48) Aieta, N.; Leisch, J. E.; Santos, M. M.; Yandrasits, M. A.; Hamrock, S. J.; Herring, A. M. *ECS Transactions* **2007,** 11, (1), 1157-1164.
(49) Moore, R. B.; Wilkerson, J. E.; Martin, C. B. *Analytical Chemistry* **1984,** 56, 2572-2575.
(50) Gavach, C.; Pourcelly, G., Applications of perfluorinated proton conductors (Nafions). In *Proton Conductors Solids, membranes and gels - materials and devices*, Colomban, P., Ed. Cambridge University Press: Cambridge, 1992; pp 487-498.
(51) Grubb, Willard T. *Fuel Cell*. Patent US2913511, 1959.
(52) EG & G Technical Services, Inc. *Fuel Cell Handbook (Seventh Edition)*; U.S. Department of Energy: Morgantown, WV, 2004.
(53) Hoogers, G., *Fuel Cell Technology Handbook*. CRC Press: Boca Raton, 2003.
(54) O'Hayre, R.; Cha, S. W.; Colella, W.; Prinz, F. B., *Fuel Cell Fundamentals*. John Wiley & Sons: Hoboken, NJ, 2006.
(55) Barbir, F., *PEM Fuel Cells Theory and Practice*. Elsevier Academic Press: Amsterdam, 2005.

(56) Dyson, R. W., *Specialty Polymers*. Chapman and Hall: New York City, 1987.
(57) Eisenberg, A.; Hird, B.; Moore, R. B. *Macromolecules* **1990,** 23, 4098-4107.
(58) Moore, Robert B.; Cable, K. M.; Croley, T. L. *Journal of Membrane Science* **1992,** 75, (1), 7-14.
(59) Weiss, R. A.; Agarwal, P. K.; Lundberg, R. D. *Journal of Applied Polymer Science* **1984,** 29, (9), 2719-2734.
(60) Grot, W. G. *Production of a liquid composition containing a perfluorinated ion exchange polymer*. Patent EP0066369, 1982.
(61) Martin, Charles R.; Rhoades, Teresa A.; Ferguson, James A. *Analytical Chemistry* **1982,** 54, (9), 1639-1641.
(62) Yeo, R. S. *Polymer* **1980,** 21, (4), 432-435.
(63) Aldebert, P.; Bernard, D.; Pineri, M. *Macromolecules* **1986,** 19, 2651-2653.
(64) Aldebert, P.; Dreyfus, B.; Gebel, G.; Nakamura, N.; Pineri, M.; Volino, F. *Journal De Physique (Paris)* **1988,** 49, 2101-2109.
(65) Loppinet, B.; Gebel, G.; Williams, C. E. *Journal of Physical Chemistry B* **1997,** 101, 1884-1892.
(66) Moore, Robert B.; Martin, Charles R. *Analytical Chemistry* **1986,** 58, 2569-2570.
(67) Moore, Robert. B.; Martin, Charles R. *Macromolecules* **1988,** 88, (21), 1334-1339.
(68) Fujimura, M.; Hashimoto, T.; Kawai, H. *Macromolecules* **1981,** 14, (5), 1309-1315.
(69) Roche, E. J.; Pineri, M.; Duplessix, R.; Levelut, A. M. *Journal of Polymer Science: Polymer Physics Edition* **1981,** 19, 1-11.
(70) Roche, E. J.; Pineri, M.; Duplessix, R. *Journal of Polymer Science: Polymer Physics Edition* **1982,** 20, 107-116.
(71) Litt, Morton H. *Polymer Preprints* **1997,** 38, 80-81.
(72) Haubold, H. G.; Vad, T.; Jungbluth, H.; Hiller, P. *Electrochimica Acta* **2001,** 46, (10-11), 1559-1563.
(73) Gebel, G. *Polymer* **2000,** 41, (15), 5829-5838.
(74) Rubatat, L.; Rollet, A. L.; Gebel, G.; Diat, O. *Macromolecules* **2002,** 35, 4050-4055.
(75) Rubatat, L.; Gebel, G.; Diat, O. *Macromolecules* **2004,** 37, 7772-7783.
(76) Yeager, H. L.; Twardowski, Z.; Clarke, L. M. *Journal of the Electrochemical Society* **1982,** 129, (2), 324-327.
(77) Yeager, H. L.; Steck, A. *Analytical Chemistry* **1979,** 51, (7), 862-865.
(78) Lopez, M.; Kipling, B.; Yeager, H. L. *Analytical Chemistry* **1977,** 49, (4), 629-632.
(79) Yeager, H. L.; Kipling, B.; Dotson, R. L. *Journal of the Electrochemical Society* **1980,** 127, (2), 303-307.
(80) Yeager, H. L.; Kipling, B. *Journal of Physical Chemistry* **1979,** 83, (14), 1836-1839.
(81) Lee, P. C.; Meisel, D. *Journal of the American Chemical Society* **1980,** 102, (17), 5477-5481.
(82) Falk, M. *Canadian Journal of Chemistry* **1980,** 58, (14), 1495-1501.
(83) Fujimura, M.; Hashimoto, T.; Kawai, H. *Macromolecules* **1982,** 15, (1), 136-144.
(84) MacKnight, W. J.; Taggart, W. P.; Stein, R. S. *journal of Polymer Science: Polymer Symposia* **1974,** 45, (1), 113-128.

(85) Roche, E. J.; Stein, R. S.; Russell, T. P.; MacKnight, W. J. *Journal of Polymer Science: Polymer Physics Edition* **1980,** 18, (7), 1497-1512.
(86) Marx, C. L.; Caulfield, D. F.; Cooper, S. L. *Macromolecules* **1973,** 6, (3), 344-353.
(87) Gebel, Gerard; Lambard, Jacques. *Macromolecules* **1997,** 30, 7914-7920.
(88) Szajdzinska-Pietek, E.; Schlick, S.; Plonka, A. *Langmuir* **1994,** 10, (4), 1101-1109.
(89) Rollet, A. L.; Gebel, G.; Simonin, J. P.; Turq, P. *Journal of Polymer Science Part B-Polymer Physics* **2001,** 39, (5), 548-558.
(90) Rollet, A. L.; Diat, O.; Gebel, G. *Journal of Physical Chemistry B* **2002,** 106, (12), 3033-3036.
(91) van der Heijden, P. C.; Rubatat, L.; Diat, O. *Macromolecules* **2004,** 37, (14), 5327-5336.
(92) Rubatat, L.; Diat, O. *Macromolecules* **2007,** 40, 9455-9462.
(93) Schmidt-Rohr, K. *Journal of Applied Crystallography* **2007,** 40, 16-25.
(94) Schmidt-Rohr, K.; Chen, Q. *Nature Materials* **2008,** 7, (1), 75-83.
(95) Grot, W. G.; Munn, G. E.; Walmsley, P. N. Electrochemical Society Meeting, Houston, TX, May 7-11, 1972.
(96) Moore, R. B.; Cable, K. *Polymer Preprints* **1997,** 38, 272-273.
(97) Page, K. A.; Landis, F. A.; Phillips, A. K.; Moore, R. B. *Macromolecules* **2006,** 39, (11), 3939-3946.
(98) Cable, K.M.; Gatlin, M.E.; Mauritz, K.A.; Moore, R.B. *Polymer Preprints* **1995,** 36, 374-375.
(99) Page, K.A.; Moore, R.B. *Polymer Preprints* **2003,** 44, 1144-1145.
(100) Landis, F.A.; Moore, R.B.; Page, K.A.; Han, C.C. *Polymeric Materials: Science and Engineering* **2002,** 87, 121-122.
(101) Almeida, S.H.; Kawano, Y. *Journal of Thermal Analysis and Calorimetry* **1999,** 58, 569-577.
(102) Chen, Q.; Schmidt-Rohr, K. *Macromolecules* **2004,** 37, 5995-6003.
(103) Hird, B.; Eisenberg, A. *Macromolecules* **1992,** 25, 6466-6474.
(104) Schiraldi, D. A. *Polymer Reviews* **2006,** 46, (3), 315-327.
(105) Chalk, S. G.; Miller, J. F. *Journal of Power Sources* **2006,** 159, (1), 73-80.
(106) LaConti, A. B.; Liu, H.; Mittelsteadt, C. K.; McDonald, R. C. *ECS Transactions* **2006,** 1, (8), 199-219.
(107) Stucki, S.; Scherer, G. G. *Journal of Applied Electrochemistry* **1998,** 28, (10), 1041-1049.
(108) Curtin, D. E.; Lousenberg, R. D.; Henry, T. J.; Tangeman, P. C.; Tisack, M. E. *Journal of Power Sources* **2004,** 131, (1-2), 41-48.
(109) Borup, R.; Meyers, J.; Pivovar, B.; Kim, Y. S.; Mukundan, R.; Garland, N.; Myers, D.; Wilson, M.; Garzon, F.; Wood, D.; Zelenay, P.; More, K.; Stroh, K.; Zawodzinski, T.; Boncella, J.; McGrath, J. E.; Inaba, M.; Miyatake, K.; Hori, M.; Ota, K.; Ogumi, Z.; Miyata, S.; Nishikata, A.; Siroma, Z.; Uchimoto, Y.; Yasuda, K.; Kimijima, K.; Iwashita, N. *Chemical Reviews* **2007,** 107, 3904-3951.
(110) Liu, H.; Gasteiger, H.; Laconti, A. B.; Zhang, J. *ECS Transactions* **2006,** 1, (8), 283-293.
(111) Antoine, O.; Durand, R. *Journal of Applied Electrochemistry* **2000,** 30, 839-844.

(112) Paulus, U. A.; Schmidt, T. J.; Gasteiger, H. A.; Behm, R. J. *Journal of Electroanalytical Chemistry* **2001,** 495, 134-145.
(113) Inaba, M.; Yamada, H.; Tokunaga, J.; Matsuzawa, K.; Hatanaka, A.; Tasaka, A. *ECS Transactions* **2006,** 1, (8), 315-322.
(114) Shao, M.; Liu, P.; Adzic, R. R. *Journal of the American Chemical Society* **2006,** 128, 7408-7409.
(115) Teranishi, K.; Kawata, K.; Tsushima, S.; Hirai, S. *Electrochemical and Solid State Letters* **2006,** 9, (10), A475-A477.
(116) Inaba, M.; Kinumoto, T.; Kiriake, M.; Umebayashi, R.; Tasaka, A.; Ogumi, Z. *Electrochimica Acta* **2006,** 51, (26), 5746-5753.
(117) Liu, W.; Zuckerbrod, D. *Journal of the Electrochemical Society* **2005,** 152, (6), A1165-A1170.
(118) Knights, S.; Colbow, K.; St Pierre, J.; Wilkinson, D. *Journal of Power Sources* **2004,** 127, 127-134.
(119) Cho, E.; Ko, J.; Ha, H. Y.; Hong, S. A.; Lee, K. Y.; Lim, T. W.; Oh, I. H. *Journal of the Electrochemical Society* **2004,** 151, (5), A661-A665.
(120) Lakshmanan, B.; Huang, W.; Olmeijer, D.; Weidner, J. W. *Electrochemical and Solid State Letters* **2003,** 6, (12), A282-a285.
(121) Yu, J. R.; Matsuura, T.; Yoshikawa, Y.; Islam, M. N.; Hori, M. *Electrochemical and Solid State Letters* **2005,** 8, (3), A156-a158.
(122) Mathias, M. F.; Makharia, R.; Gasteiger, H.; Conley, J. J.; Fuller, T. F.; Gittleman, C. J.; Kocha, S. S.; Miller, D. P.; Mittelsteadt, C. K.; Xie, T.; Yan, S. G.; Yu, P. T. *The Electrochemical Society Interface* **2005,** 14, (3), 24-35.
(123) Ohma, A.; Suga, S.; Yamamoto, S.; Shinohara, K. *Journal of the Electrochemical Society* **2007,** 154, (8), B757-B760.
(124) Mittal, V. O.; Kunz, H. R.; Fenton, J. M. *Journal of the Electrochemical Society* **2006,** 153, (9), A1755-a1759.
(125) Ohma, A.; Yamamoto, S.; Shinohara, K. *ECS Transactions* **2007,** 11, (1), 1181-1192.
(126) Sethuraman, V. A.; Weidner, J. W.; Haug, A. T.; Motupally, S.; Protsailo, L. V. *Journal of the Electrochemical Society* **2008,** 155, (1), B50-B57.
(127) Ohma, A.; Yamamoto, S.; Shinohara, K. *Journal of Power Sources* **2008,** 182, 39-47.
(128) Kundu, S.; Fowler, M.; Simon, L. C.; Abouatallah, R. *Journal of Power Sources* **2008,** 182, 254-258.
(129) Endoh, E.; Terazono, S.; Widjaja, H.; Takimoto, Y. *Electrochemical and Solid State Letters* **2004,** 7, (7), A209-A211.
(130) Inaba, M.; Yamada, H.; Tokunaga, J.; Tasaka, A. *Electrochemical and Solid State Letters* **2004,** 7, (12), A474-A476.
(131) Pozio, A.; Silva, R. F.; De Francesco, M.; Giorgi, L. *Electrochimica Acta* **2003,** 48, (11), 1543-1549.
(132) Zhou, C.; Zawodzinski, T.; Schiraldi, D. *Polymer Preprints* **2004,** 45, (2), 760-761.
(133) Zhou, C.; Zawodzinski, T.; Schiraldi, D. *Polymer Preprints* **2006,** 47, (2), 485-486.

(134) Healy, J.; Hayden, C.; Xie, T.; Olson, K.; Waldo, R.; Brundage, A.; Gasteiger, H.; Abbott, J. *Fuel Cells* **2005,** 5, (2), 302-308.
(135) Kinumoto, T.; Inaba, M.; Nakayama, Y.; Ogata, K.; Umebayashi, R.; Tasaka, A.; Iriyama, Y.; Abe, T.; Ogumi, Z. *Journal of Power Sources* **2006,** 158, 1222-1228.
(136) Nosaka, A. Y.; Watanabe, S.; Toyoda, I.; Nosaka, Y. *Macromolecules* **2006,** 39, (13), 4425-4427.
(137) Duesterberg, C. K.; Waite, T. D. *Environmental Science & Technology* **2006,** 40, (13), 4189-4195.
(138) Tang, H.; Peikang, S.; Jiang, S. P.; Wang, F.; Pan, M. *Journal of Power Sources* **2007,** 170, 85-92.
(139) Rhoades, D.; Hassan, M.; Osborn, S.; Moore, R. B.; Mauritz, K. *Journal of Power Sources* **2007,** 172, 72-77.
(140) Zhou, C.; Guerra, M.; Qiu, Z. M.; Zawodzinski, T.; Schiraldi, D. *Macromolecules* **2007,** 40, 8695-8707.
(141) Mittal, V. O.; Kunz, H. R.; Fenton, J. M. *Journal of the Electrochemical Society* **2007,** 154, (7), B652-B656.
(142) Kundu, S.; Simon, L. C.; Fowler, M. *Polymer Degradation and Stability* **2008,** 93, 214-224.
(143) Hommura, S.; Kawahara, K.; Shimohira, T.; Teraoka, Y. *Journal of the Electrochemical Society* **2008,** 155, (1), A29-A33.
(144) Sethuraman, V. A.; Weidner, J. W.; Haug, A. T.; Protsailo, L. V. *Journal of the Electrochemical Society* **2008,** 155, (2), B119-B124.
(145) Panchenko, A.; Dilger, H.; Moller, E.; Sixt, T.; Roduner, E. *Journal of Power Sources* **2004,** 127, 325-330.
(146) Bosnjakovic, A.; Schlick, S. *Journal of Physical Chemistry B* **2004,** 108, (14), 4332-4337.
(147) Kadirov, M. K.; Bosnjakovic, A.; Schlick, S. *Journal of Physical Chemistry B* **2005,** 109, (16), 7664-7670.
(148) Bosnjakovic, A.; Schlick, S. *Journal of Physical Chemistry B* **2006,** 110, 10720-10728.
(149) Schlick, S.; Motyakin, M. *Electron Paramagnetic Resonance* **2007,** 20, 1-28.
(150) Escobedo, G. *Strategies to improve the durability of perfluorosulfonic acid membranes for PEM fuel cells*, KFTCA International Symposium, Washington, DC, December 8-9, 2005.
(151) Hensley, J. E.; Way, J. D.; Dec, S. F.; Abney, K. D. *Journal of Membrane Science* **2007,** 298, 190-201.
(152) Gebel, G.; Aldebert, P.; Pineri, M. *Macromolecules* **1987,** 20, 1425-1428.
(153) Silverman, D. C.; Lefelar, J. A.; Kinlen, P. J. *Metals coated with protective coatings of annealed perfluorinated cation-exchange polymers and method for making same*. Patent US5069974, 1991.
(154) Kinlen, P. J.; Silverman, D. C. *Journal of the Electrochemical Society* **1993,** 140, (11), 3140-3145.
(155) Ye, Jian-Hui; Fedkiw, P. S. *Electrochimica Acta* **1995,** 40, (3), 291-296.
(156) Thomas, T. J.; Ponnusamy, K. E.; Chang, N. M.; Galmore, K.; Minteer, S. D. *Journal of Membrane Science* **2003,** 213, 55-66.

(157) Zawodzinski, Thomas; Springer, Thomas E.; Uribe, Francisco; Gottesfeld, Shimshon. *Solid State Ionics* **1993,** 60, 199-211.
(158) Xie, J.; Garzon, F.; Zawodzinski, T.; Smith, W. *Journal of the Electrochemical Society* **2004,** 151, (7), A1084-A1093.
(159) Hinatsu, J. T.; Mizuhata, M.; Takenaka, H. *Journal of the Electrochemical Society* **1994,** 141, (6), 1493-1498.
(160) Sone, Y.; Ekdunge, P.; Simonsson, D. *Journal of the Electrochemical Society* **1996,** 143, (4), 1254-1259.
(161) Zook, L. A.; Leddy, J. *Analytical Chemistry* **1996,** 68, (21), 3793-3796.
(162) Lee, K.; Ishihara, A.; Mitsushima, S.; Kamiya, N.; Ota, K. *Journal Of The Electrochemical Society* **2004,** 151, (4), A639-A645.
(163) Lin, H. L.; Yu, T. L.; Huang, C. H.; Lin, T. L. *Journal of Polymer Science Part B-Polymer Physics* **2005,** 43, (21), 3044-3057.
(164) Cable, K.; Mauritz, K.; Moore, R. B. *Chemistry of Materials* **1995,** 7, 1601-1603.
(165) DeLuca, N. W.; Elabd, Y. A. *Journal of Membrane Science* **2006,** 282, (1-2), 217-224.
(166) Jung, H. Y.; Cho, K. Y.; Lee, Y. M.; Park, J. K.; Choi, J. H.; Sung, Y. E. *Journal of Power Sources* **2007,** 163, 952-956.
(167) Alberti, G.; Narducci, R.; Sganappa, M. *Journal of Power Sources* **2008,** 178, 575-583.
(168) Maeda, Y.; Gao, Y.; Nagai, M.; Nakayama, Y.; Ichinose, T.; Kuroda, R.; Umemura, K. *Ultramicroscopy* **2008,** 108, 529-535.
(169) Luan, Y.; Zhang, Y.; Zhang, H.; Li, L.; Li, H.; Liu, Y. *Journal of Applied Polymer Science* **2008,** 107, 396-402.
(170) van der Heijden, P. C.; de la Rosa, A.; Gebel, G.; Diat, O. *Polymers for Advanced Technologies* **2005,** 16, (2-3), 102-107.
(171) Elliott, J. A.; Hanna, S.; Elliott, A. M. S.; Cooley, G. E. *Macromolecules* **2000,** 33, 4161-4171.
(172) Elliott, J. A.; Hanna, S.; Elliott, A. M. S.; Cooley, G. E. *Polymer* **2001,** 42, (5), 2251-2253.
(173) Londono, J. D.; Davidson, R. V.; Mazur, S. *Polymeric Materials: Science and Engineering* **2001,** 85, 23.
(174) Cable, K.; Mauritz, K.; Moore, R. B. *Polymer Preprints* **1994,** 35, (1), 421.
(175) Lin, J.; Wycisk, R.; Pintauro, P. N.; Kellner, M. *Electrochemical and Solid State Letters* **2007,** 10, (1), B19-B22.
(176) Lin, J.; Wu, P.H.; Wycisk, R.; Pintauro, P. N.; Shi, Z. *Macromolecules* **2008,** 41, 4284-4289.
(177) Lin, J.; Wu, P.H.; Wycisk, R.; Trivisonno, A.; Pintauro, P. N. *Journal of Power Sources* **2008,** 183, 491-497.
(178) Siu, A.; Schmeisser, J.; Holdcroft, S. *Journal of Physical Chemistry B* **2006,** 110, (12), 6072-6080.
(179) Chourdakis, N.; Voyiatzis, G. A. *Journal of Polymer Science Part B: Polymer Physics* **2007,** 45, 2509-2517.

CHAPTER 2

GLASS TRANSITION TEMPERATURE OF PERFLUOROSULFONIC ACID IONOMERS

Introduction

The perflurosulfonic acid ionomer Nafion® is the current benchmark material for proton exchange membrane fuel cells (PEMFCs) and consist of a polytetrafluoroethylene (PTFE) backbone with perfluorovinylether side chains that terminate with a sulfonic acid functionality.[1] Nafion® is currently available commercially from E.I. du Pont de Nemours and Company and has the following structure:

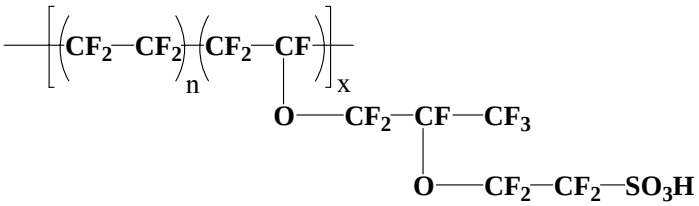

Due to the difference in polarity between the nonpolar fluorocarbon matrix and polar ionic moieties, the ionic groups tend to phase separate and form what is referred to as ionic aggregates.[2] Along with the aggregate structures are the crystalline domains involving runs of polytetrafluoroethylene, which have unit cell dimensions virtually identical to that of pure PTFE.[3, 4] In the interest of accurately describing Nafion's® complex, phase-separated network of both ionic aggregates and crystalline domains, the majority of investigations have focused on characterizing both the morphological[4-9] and thermo-mechanical[1, 10-19] properties. For use in PEMFCs, Nafion®, must possess excellent proton transport properties along with mechanical integrity. PEMFC conditions subject polymer films to various pressure gradients, swelling/dehydration cycles, creep,

and extreme temperatures, which must be taken into account when examining the physical properties of a proton exchange membrane for use in fuel cells.[1]

With the recent interest in high temperature (> 100 °C) fuel cell operations,[20] a common misconception that Nafion® has a glass transition temperature (T_g) at 100 °C has led to concern regarding the mechanical stability of these membranes at elevated temperatures. Surprisingly, however, the fundamental concept of a true glass transition temperature of this exhaustively studied ionomer has yet to be precisely defined and widely accepted for the most commonly applied H^+-form of the polymer.

The earliest mechanical property data on Nafion® was presented by E.I. du Pont de Nemours and Company and consisted of tensile strength, tensile modulus, and elongation at yield as a function of cation type.[21] Since then, most of the literature on Nafion's® mechanical properties have involved dynamic mechanical analysis (DMA) of tan δ, storage modulus (E'), and loss modulus (E"). The prevailing confusion regarding the assignment of a T_g for Nafion® stems back to the early work of Eisenberg and coworkers.[12, 13, 22] In their early study, three dynamic thermo-mechanical temperature relaxations (γ, β, and α) were observed for the acid form of Nafion® between -160 and 150 °C. The γ-relaxation occurred around -100 °C and was attributed to short-range motions of the $–CF_2–$ backbone. The β-relaxation was observed around 20 °C and shifted toward lower temperatures with increasing water content. The β-relaxation was therefore attributed to the relaxation of the ionic domains based on the strong effect of water on the pendant sulfonate moieties present on the side chain of Nafion®. The α-relaxation occurred around 110 °C and was considered to be the glass transition of the nonionic phase due to the minor role that water played in effecting the position and magnitude of

the peak. Eisenberg et al. also studied the effects of ionization and partial neutralization on the DMA properties of 1200 equivalent weight Nafion®, where equivalent weight is equal to the grams of polymer per equivalent of sulfonate groups.[12] Upon neutralization with alkali metal salts, the α and β-relaxation temperatures increased by approximately 100 °C, while the γ-relaxation temperature remained constant. Upon partial neutralization with the Cs^+ counterion, the β-relaxation temperature increased along with a dramatic increase in peak intensity. The authors then re-examined their earlier interpretations of the α and β-relaxations. The α-relaxation was reassigned to the glass transition of the ionic regions and the β-relaxation was reassigned to the glass transition of the matrix. For twenty years, these revised assignments suggesting that the α and β relaxations are associated with the glass transitions of the matrix and the ionic domains, respectively, have remained unconfirmed for the H^+-form of the ionomer.

The thermo-mechanical relaxations of Nafion® have also been widely studied using dielectric spectroscopy (DS).[11, 23-30] Due to the strong dependence on having dipoles present in the polymer sample, dielectric spectroscopy has been shown to be a powerful tool in the study of chain dynamics in glass-forming polymers and should be used complimentary to DMA to maximize the strengths of both techniques.[11, 31-33] DS probes the molecular dynamics of polymers over a broad range of frequencies and temperatures, allowing for the examination of motional processes which take place on vastly different time scales.[34] Furthermore, information on the chemical structure, molecular chain length, phase separation, and glass and sub-glass transitions can be extracted using DS.[34]

Coinciding with their DMA studies, Yeo and Eisenberg also examined the dielectric properties of 1365 EW H^+-form Nafion® using dielectric relaxation spectroscopy.

Similar to the results obtained using DMA, a bimodal β-relaxation peak was observed from dielectric spectroscopy, which consisted of a minor and major component.[12] At a frequency of 100 Hz, Yeo et al. examined the effects of water content on the β-relaxation of H^+-form Nafion® using DS from -190 to 150 °C. Both the major and minor components of the β-relaxation peak shifted to lower temperatures with increasing water content present in the Nafion® membrane. An interesting phenomenon was observed where the minor and major components of the β-relaxation peak switched positions when the water content present in Nafion® went above 1.7 H_2O/SO_3H. Below 1.7 H_2O/SO_3H, the minor and major components were recorded as low as -125 and -100 °C respectively at a water content of 15 H_2O/SO_3H. Above 1.7 H_2O/SO_3H, the minor and major components were reversed but were observed as high as 20 and 50 °C at a water content of 0.7 H_2O/SO_3H. Due to such a strong effect of moisture on the location of the β-relaxation peak, Yeo et al. concluded that the β-relaxation was directly related to the ionic domains. However, as mentioned previously with the DMA studies of Yeo and Eisenberg, the assignment of the β-relaxation being directly correlated to the ionic domains was reversed in a later publication by Kyu and Eisenberg, where the β-relaxation became known as the glass transition of the matrix of Nafion®.[12, 13]

More recent DMA data collected by Cable and Moore explored the behavior of Nafion® membranes neutralized with a variety of counterions.[16, 35] It was concluded that the α-relaxation results from chain motions within and/or near ionic domains and the β-relaxation results from chain motions of amorphous fluorocarbons far removed from ionic aggregates, i.e. within the matrix. In this study, researchers referred to chain motions within an electrostatic network instead of polar and fluorocarbon components

being discrete, isolated domains. This view is in agreement with Kyu and Eisenberg who demonstrated that effects on the behavior of one phase results in strong effects on the other phase as the two are in intimate contact and are of small size.

In addition to examining the molecular origins of the mechanical relaxations, Moore and coworkers have examined the effect of counterion type and size on the mechanical properties of Nafion®.[35] Using both alkali metal and alkylammonium counterions, it was shown that counterion type has a profound impact on the thermo-mechanical properties of the membrane. In comparison to the acid form, small alkali metal counterions such as sodium, caused dramatic increases in both the α and β-relaxation temperatures due to the strong dipole-dipole interactions between sodium sulfonate groups, in comparison to the weak hydrogen bond interactions in the acid form. The use of alkylammonium counterions was found to provide a means to systematically shift the α and β-relaxation temperatures.[16] Neutralization with large tetrabutylammonium (TBA^+) counterions caused the α and β-relaxation temperatures to shift below the α-relaxation temperature of the acid form. The decrease in relaxation temperatures was attributed to two contributing factors. First, the larger counterions significantly decreased the strength of the electrostatic interactions. Second, the bulky, organic counterions effectively plasticized the material, thus decreasing the relaxation temperatures.[15, 19] Using alkylammonium counterions ranging in size from tetramethylammonium (TMA^+) to tetradecylammonium, the α and β-relaxation temperatures shifted in a monotonic fashion over a temperature range from near that of the sodium form ionomer for tetramethylammonium to the α-relaxation temperature of the sulfonyl fluoride precursor for tetradecylammonium. The relative magnitudes of the two relaxations were also seen to vary with counterion type.

Tan delta curves for membranes neutralized with small counterions were dominated by the α-relaxation and membranes neutralized with large counterions had more intense β-relaxation profiles.

Recently, through a correlation of DMA, variable temperature ^{19}F solid-state NMR and small angle x-ray scattering (SAXS), Page and Moore were able to precisely define the molecular and morphological origins of the α and β-relaxations of Nafion® neutralized with a series of alkylammonium ions.[19, 36-38] SAXS analysis was used to monitor the ionomer morphology as a function of temperature and provided insight into the relationship between the strength of the electrostatic network and the relaxations observed using DMA. In relation, variable temperature ^{19}F solid-state NMR allowed the relaxations and morphological changes to be linked to the molecular motions of Nafion® neutralized with various counterions.

Initially, Page and Moore examined Nafion's® controversial differential scanning calorimetry (DSC) endothermic peaks during the initial heating. Various publications have attempted to correlate the endothermic events in DSC with the thermo-mechanical relaxations of Nafion® observed using DMA.[4, 11-13] Eisenberg and coworkers attributed the endothermic events to the glass transition temperature of the matrix of Nafion® (140 °C) and the ionic domains (240 °C), respectively.[13] Almeida et al. showed the existence of two endothermic events upon first heating of Nafion® occurring at 120 °C and 230 °C, respectively. Upon reheating, the peak at 120 °C was absent but reappeared gradually during annealing.[39] Page and Moore repeated this study using Nafion neutralized with either Na^+ or Cs^+ counterions.[19] As opposed to Almeida et al. only one endothermic event was observed at 240 °C, for both Na^+ and Cs^+-form Nafion®, and

disappeared upon rescan after melt quenching from 330 °C. The peak at 240 °C reappeared after annealing at 200 °C for extended periods of time and increased in heat of fusion (ΔH) with longer annealing times. After 24 hours of annealing at 200 °C, the endothermic peak recovered half of the initial ΔH, meaning 50% of the initial crystallinity was recovered by isothermally crystallizing Nafion® at 200 °C. The assignment of the endothermic peak to the formation of crystallites was verified by the disappearance of the crystalline peak upon quenching from 330 °C at low *q* values using SAXS. In contrast to the Na^+-form DSC data, the Cs^+-form Nafion® displayed a 100% recovery in the ΔH upon annealing at 200 °C for 24 hours. By exchanging to the larger counterion, the dipole-dipole interactions were weakened throughout the electrostatic network, allowing for increased crystallization kinetics of Nafion® in the Cs^+-form. By annealing Cs^+-form Nafion® at temperatures ranging from 120 °C and 240 °C for two hours, Page and Moore noticed the appearance of multiple endothermic events at lower annealing temperatures and one endothermic event at higher annealing temperatures. The endothermic peaks were attributed to multiple melting behaviors due to the shift of the low temperature endotherm toward higher temperatures with increased annealing temperature. Thus, the low temperature endotherm was attributed to melting of small crystallites while the high temperature endotherm was due to the melting temperature of thicker lamellae.[19]

Based on variable temperature SAXS profiles of Nafion® in various alkylammonium counterion forms, Page and Moore examined the relationship between the strength of the electrostatic network and the mechanical relaxations observed using DMA.[19] The SAXS profiles revealed an abrupt decrease in the scattering intensity of the ionomer peak with

increasing temperature. The temperature of the abrupt change in intensity also increased with decreasing counterion size. It was noted that the temperature at which the morphological transition occurred was strongly correlated with the α-relaxation temperature seen using DMA with the various alkylammonium counterions. The morphological transition was explained as a destabilization of the static electrostatic network into a dynamic network through the process of ion-hopping, where the thermally activated ion pairs "hop" from one aggregate to another in order to relieve local stress.

In order to understand the link between the electrostatic network and the molecular motions, Page and Moore examined Nafion® in various alkylammonium counterions using variable temperature ^{19}F solid-state NMR.[19, 38] By using spin-diffusion and sideband analyses over the same temperature range as both SAXS and DMA, a correlation was made between the transition from a static to a dynamic electrostatic network and the corresponding changes on the molecular level. Changes in the spin-diffusion times were attributed to the mobility of polymer chains based on a constant distance between coupled side chain and main chain fluorine nuclei. In agreement with SAXS and DMA, an increase in the spin-diffusion time occurred near the morphological transition temperature for both TMA^+ and TBA^+ counterions, and was attributed to the onset of molecular motions. The sidebands associated with the ^{19}F resonances were also used to observe changes in mobility of Nafion®. The sidebands arise due to dipolar coupling, and the intensity of the peaks correlates to the rigidity of the polymer. The sidebands for the fluorine nuclei of the side and main chains were shown to decrease with increasing temperature in TMA^+ and TBA^+-form Nafion®. The sidebands of the TBA^+-form Nafion® decreased more rapidly than the TMA^+-form Nafion® due to the

increased mobility of the polymer in the TBA^+ form. By normalizing the sideband peak intensities of both the main and side chains, the side chains were determined to be more mobile than the main chains, supporting the NMR study of Schmidt-Rohr et al.[40] As a result of these studies, the α-relaxation was attributed to the onset of long-range mobility of both main and side chains through destabilization of the electrostatic network. Network destabilization is thought to occur through ion-hopping, the process of ion pairs transferring between aggregates to balance electrostatic and elastic forces.[41] In contrast, the low temperature β-relaxation was associated with the onset of chain motions, primarily in the backbone, within the concept of a static, physically crosslinked network of chains, similar to the traditional concept of a polymer glass transition.

Although the studies performed by Moore and coworkers of Nafion® containing alkylammonium ions have provided fundamental information regarding the influence of electrostatic interactions on chain dynamics in these complex polymeric materials, it is recognized that these counterion forms have little relevance in the context of proton transport in PEMFC applications.[42] However, in order to understand the thermo-mechanical response of these ionomers in fuel cell operations, it is now possible to build upon this fundamental information in order to accurately define and confirm the true glass transition temperature of perfluorosulfonic acid membranes. Thus, the purpose of this investigation is to identify and verify the true glass transition temperature of H^+-form Nafion® through correlations of relaxation behavior as probed mainly by DMA and dielectric spectroscopy.

Experimental

Materials. Extruded Nafion® 112 and 117 films (1100 g/equivalent, sulfonic acid form) were obtained from E.I. du Pont de Nemours and Company. Tetrabutylammonium hydroxide (TBAOH), 1M in methanol, was obtained from Aldrich Chemical Co. and used without further purification.

Preparation of Perfluorosulfonate Ionomer Membranes. To remove impurities, the membranes were cleaned in refluxing 8M HNO_3 for two hours, then rinsed three times with deionized water, and finally boiled in deionized water for an additional hour. Partial neutralization of the Nafion® samples was performed by stirring the membranes in TBAOH/methanol solutions containing specified quantities of TBAOH for 12 hours followed by boiling in pure methanol for one hour. Based on the equivalent weight of dry Nafion®, the following ratios of H^+-form to TBA^+-form were prepared: 100/0, 90/10, 85/15, 75/25, 65/35, 50/50, 25/75, 0/100. All membranes were subsequently dried in a vacuum oven overnight at 70 °C after the neutralization step.

Humidity Chamber Preparation. Samples were suspended over various LiCl and water solutions in sealed humidity chambers. The chambers were calibrated at 40, 78, 90, 96, and 98% relative humidity. All samples requiring specific humidity conditions were allowed to equilibrate in the chambers for one week prior to testing. The presented lambda values are calculated averages based on ten tensile samples run at each humidity. Equation 2-1 shows how the water content was calculated throughout the experiment, where m_h represents the mass of the hydrated polymer, m_d is the mass of the dry polymer, 18 is the molecular weight of water, and 1100 is the equivalent weight of the polymeric membrane.

$$\lambda = \frac{\left(m_h - m_d\right)/18}{\left(m_d/1100\right)} \qquad \textbf{Eq. 2-1}$$

The lambda values for the experiment ranged from zero for the dry sample to 21.02 for the boiled membranes.

Tensile Analysis of Nafion® 112 Membranes. Following cleaning of the membranes, 70 dogbone shaped tensile bars of acid form Nafion® 112 were punched along the machine direction using a stainless steel die (38 x 5 mm). In order to reduce experimental error, ten samples were tested for each humidity setting. The following conditions were tested: dry, 40, 78, 90, 98, 100% humidity (submersed), and boiled. All samples were tested on an MTS Alliance RT/10 at a rate of 25.4 mm/min in tensile mode.

Dynamic Mechanical Analysis. Dynamic mechanical analysis of the membranes was performed on a TA Instruments DMA Q800 Analyzer in tensile mode using clamps for thin film samples. All samples were cut from dried membranes (70 °C vacuum, overnight) with a width of 5.3 mm and run in triplicate to verify results and reduce experimental error. Samples of pure H^+-form Nafion® 112 and 50/50 H^+/TBA^+ Nafion® 117 were prepared under the following conditions prior to DMA: dry, 40, 78, 90, 96, 98% humidity, and boiled. All other H^+/TBA^+ partial neutralizations were examined using DMA only in the dried and boiled states. The membranes were analyzed at a frequency of 1 Hz from -120 °C to 200 °C with a heating ramp of 2 °C/min. The temperature range was chosen in order to span all three thermo-mechanical relaxations, α, β, and γ.

Dielectric Spectroscopy. Dielectric spectra were recorded using a Novocontrol GmbH Concept 40 Broadband Dielectric Spectrometer over the frequency range of 0.01 Hz to 1 MHz. The range of isothermal temperatures tested, to within ±0.2 °C, was -50 °C

to 130 °C in increments of 5 °C. Samples 0.178 mm or 7 mil thick were punched with a 25.4 mm diameter circular die and tightly pressed between 20 mm diameter brass electrodes. In order to determine the characteristic relaxation times at each temperature,[43] isothermal dielectric permittivity data were first fitted (using the Novocontrol WinFit program) to the Havriliak-Negami equation[44] shown below.

$$\varepsilon^*(\omega) = \varepsilon'(\omega) - i\varepsilon''(\omega) = -i\left(\frac{\sigma_0}{\varepsilon_0 \omega}\right)^S + \sum_{k=1}^{n}\left[\frac{\Delta\varepsilon}{\left(1+\left(i\omega\tau_{HN}\right)^{\alpha}\right)^{\beta}} + \varepsilon_{\infty}\right] \qquad \textbf{Eq. 2-2}$$

In this equation, ε*(ω) is the complex dielectric constant, ε′(*ω*) is the real component associated with material polarizability, ε″(*ω*) is the imaginary component associated with energy loss per signal cycle, σ_0 is the dc conductivity having units of S/cm, *ω* is the angular frequency = 2πf, and ε_0 is the vacuum permittivity. The exponent *s* ($0 < s \leq 1$) characterizes the nature of the conduction process in terms of charge hopping pathways. The symbol *n* in the summation is the number of relaxation peaks fitted (*n* = 1 in this case) to the data. The dielectric strength Δε is equal to $\varepsilon_R - \varepsilon_\infty$ which is the difference between the relaxed and unrelaxed dielectric constants at low and high frequencies, respectively. τ_{HN} is the Havriliak-Negami relaxation time, which is related to the actual relaxation time $\tau_{max} = 1/2\pi f_{max}$, where f_{max} is the frequency at the maximum dielectric loss and *α* and *β* are constants that quantify breadth and asymmetry in the distribution of relaxation times, respectively. Given these three data-fitted parameters, Equation 2-3 was used to determine the relaxation time for the peak maximum for each isothermal peak, using the following relationship.[43]

$$\tau_{\max} = \tau_{\mathrm{HN}}\left[\sin\frac{\pi\alpha\beta}{2(\beta+1)} \Big/ \sin\frac{\pi\alpha}{2(\beta+1)}\right]^{1/\alpha} \qquad \textbf{Eq. 2-3}$$

Results and Discussion

Mechanical Properties of H^+-form Nafion® 112. Figure 2.1a shows the stress versus strain profiles for H^+-form Nafion® 112 preconditioned at various humidities. Based on the data shown in Figure 2.1a, the highest mechanical properties for H^+-form Nafion® 112 are achieved after drying at 70 °C for approximately 12 hours under vacuum. It can also be seen that the initial modulus of each sample decreases with increasing humidity or water content present within the membrane. This decrease in modulus suggests that water is weakening the physical network of clusters by hydrating the $-SO_3^-H^+$ junction points within the ionomer membrane. Similar mechanical properties were observed by Kawano et al. where H^+-form Nafion® membranes were soaked in water for 24 hours or boiled in water for 1 hour prior to testing.[45] Kawano et al. comment on how the high water content swells the membrane and works as a plasticizer, mainly reducing the ionic intermolecular forces, hence weakening the initial mechanical properties of the polymer.[45] In Figure 2.1b the strain at break versus humidity data are fit to a nonlinear regression that shows a minimum strain value occurring at a preconditioned humidity of 40%. This phenomenon has not been documented in the literature and is somewhat surprising considering the plasticization effect of water mentioned by Kawano et al.[45] Even though Kawano et al. were unable to examine the strain at break throughout their studies, they assumed that the samples boiled in water would have higher elongations at break due to the weakened ionic network. It must also be noted that given the large amount of statistical error associated with measuring the elongation at break of Nafion® samples preconditioned at various humidities, the minimum could occur anywhere between 40 and 90% relative humidity. Either way, it is

apparent based on the data shown in Figure 2.1b that a minimum does occur between the samples dried overnight at 70 °C under vacuum and those boiled in deionized water for one hour prior to testing. Based on this information, the elongation at break of H^+-form Nafion® can be drastically manipulated depending on changes in relative humidity as well as direct contact with water at various temperatures.

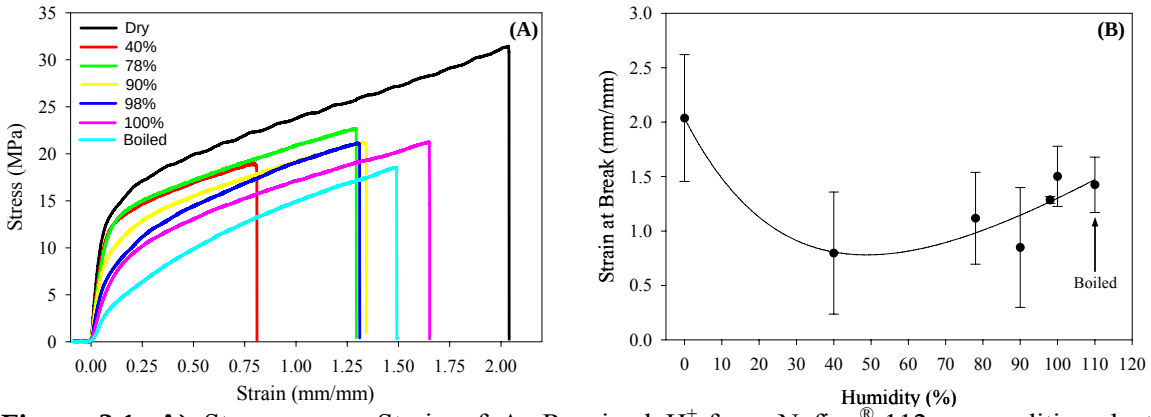

Figure 2.1. A) Stress versus Strain of As-Received H^+-form Nafion® 112 preconditioned at various humidities. **B)** Strain at break versus preconditioned percent humidity for As-Received H^+-form Nafion® 112.

A decrease in the Young's modulus of H^+-form Nafion® 112 is observed in Figures 2.2a and 2.2b with both increasing humidity and water content. In Figure 2.2a an approximate 20% decrease in the modulus is achieved after preconditioning H^+-form Nafion® samples at 40% humidity for one week. The modulus values continue to decrease slightly until 90% humidity, upon which a significant decrease of approximately 85% of the original modulus occurs after boiling the sample in deionized water for one hour prior to testing. The loss of mechanical properties of Nafion® at various humidities was also documented by Huang et al. who examined the tensile properties of Nafion® membrane electrode assemblies (MEAs). As opposed to our results, Huang and coworkers noticed a systematic decrease in the modulus values of Nafion® MEAs with increasing relative humidity from 3-75%.[46] Our data suggest more of a plateau effect, where the

preconditioned humidity does not incur catastrophic decreases in the modulus of H^+-form Nafion® until above 90%. It should be noted that our studies were conducted on preconditioned, pure Nafion® membranes, while Huang et al. examined Nafion® MEAs, which consist of a Nafion® membrane sandwiched between two Pt/C catalyst layers.

Figure 2.2b displays the tensile modulus of H^+-form Nafion® 112 versus water content (λ) calculated using Equation 2-1. In agreement with other studies,[47] the ionomer modulus decreases exponentially as water content (λ) increases from 0.86 to 21.02 for the 40% RH equilibrated and boiled samples, respectively. The data verify that the water is behaving as a plasticizer in the membrane within the elastic region and severely weakening the mechanical properties prior to reaching a yield point.

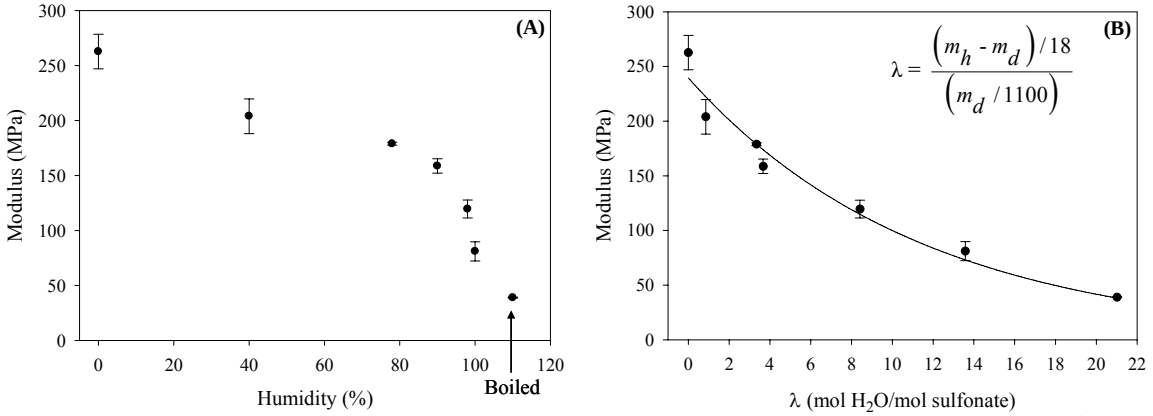

Figure 2.2. A) Modulus versus preconditioned percent humidity of As-Received H^+-form Nafion® 112. **B)** Modulus versus water uptake (λ) for As-Received H^+-form Nafion® 112 after preconditioning at various humidities as well as boiling in deionized water.

Figures 2.3a and 2.3b show that the yield stress of the ionomer decreases in a similar fashion with increasing humidity or water content. The difference in yield stress (shown in both figures) between the dry and boiled samples is approximately 10 MPa. It should be noted that a significant source of error could be due to the lack of a distinct yield point in the stress versus strain curves of H^+-form Nafion® hydrated at various levels. The MTS Alliance RT/10 software was used to choose the most appropriate yield

point based on the deviation from linearity of the stress vs. strain curves at low strain values. Overall, the trend in decreasing mechanical properties shown in Figures 2.2a and 2.2b are further verified based on the yield stress versus humidity and water content shown below in Figures 2.3a and 2.3b.

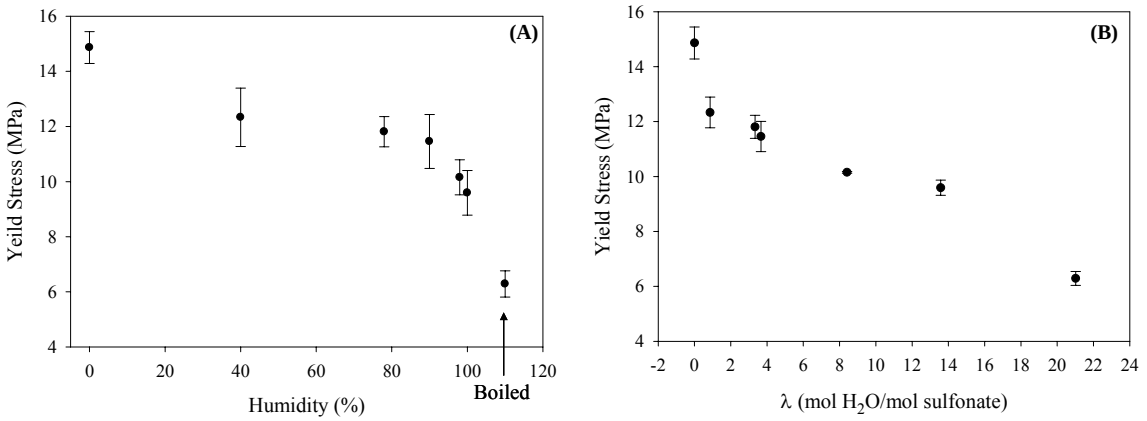

Figure 2.3. A) Yield Stress versus preconditioned percent humidity of As-Received H^+-form Nafion® 112. **B)** Yield Stress versus water uptake (λ) for As-Received H^+-form Nafion® 112 after preconditioning at various humidities as well as boiling in deionized water.

Dynamic Mechanical Analysis. As demonstrated in our previous work,[10, 15, 19] the principle dynamic mechanical relaxations of Nafion® are strongly dependent on the strength of interactions between the side chain terminal $–SO_3X$ groups. For the neutralized ionomers, the α-relaxation can vary over 250 °C depending on counterion (X^+) size (e.g., α (Na^+) = ca. 230 °C versus α (TBA^+) = 115 °C). As the counterion size increases, the weakened electrostatic interactions yield progressively lower α and β-relaxation temperatures. For the H^+-form of Nafion®, the interactions are principally hydrogen-bonding interactions, which are significantly weaker than the corresponding electrostatic interactions in neutralized samples. Thus, the α-relaxation of H^+-form Nafion® is observed at a relatively low temperature near 100 °C.[13, 19]

Figure 2.4 compares DMA data, plotted as the loss tangent (tan δ) vs. temperature, for TBA^+-form and H^+-form Nafion®. For the TBA^+-form sample, distinct α and

β-relaxations are observed at ca. 115 °C and 75 °C, respectively. In contrast, the H^+-form sample appears to show only one principal relaxation in the vicinity of 100 °C. Upon closer inspection of the DMA data for the H^+-form sample, a weak peak near -20 °C is observed. In addition, both samples show a γ-relaxation at ca. -80 °C, which is independent of neutralization or counterion type and has been attributed to local motions of the fluorocarbon $–CF_2–$ backbone chains.[13]

By convention, the peak at -20 °C observed for the H^+-form sample is assigned as a β-relaxation. While this relaxation is similar in temperature to the β-relaxation observed for 1200 EW Nafion® in the early work of Eisenberg,[13] it is not reasonable, however, to attribute this relaxation (without further analysis) to the same molecular motions as those known to occur at the β-relaxation for the neutralized samples (i.e., the glass transition).[19] To further clarify the molecular origins of this weak relaxation, we invoke rule-of-mixture concepts common to studies of polymer blends[48] or copolymers. By evaluating the dynamic mechanical behavior of samples prepared with partial neutralization, and assuming that the TBA^+ counterions are homogeneously distributed among the sulfonate groups, the β-relaxation should show a clear compositional dependence if both relaxations are of a similar molecular origin.

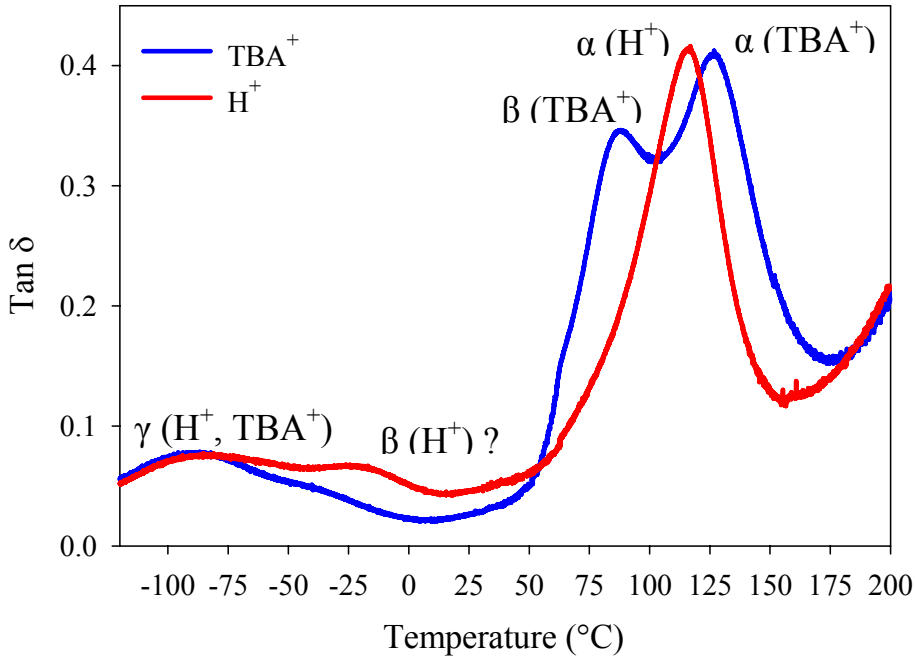

Figure 2.4. Dynamic mechanical tan δ versus temperature plots of Nafion® 117 for H^+-form and TBA^+-form samples.

Figure 2.5 shows the DMA data for all seven partially neutralized samples, ranging from pure TBA^+-form Nafion® to pure H^+-form Nafion®. As the composition of TBA^+ counterions in the samples decreases, the β-relaxation is observed to shift systematically to lower temperatures and decrease uniformly in magnitude. In contrast, the α-relaxation remains in the range of 120 °C to 100 °C with only a modest decrease in intensity between 75% and 50% neutralization. The continual decrease in the β-relaxation peak intensity as TBA^+ content decreases suggests that fewer populations of chains are capable of activated motion at lower temperatures.[19] Within the context of a nanophase-separated morphology, this behavior may be attributed to very weak associations between ion pairs for the systems containing the large TBA^+ counterions (i.e., a weak electrostatic network). With weakened interactions between the ionic groups, the efficiency of the physical cross-links to locally restrict the mobility of chains decreases, yielding a relatively larger population of chains in a more mobile state.

Furthermore, the γ-relaxation temperature and magnitude is independent of the degree of neutralization – consistent with the assignment of local backbone motions[13] that should be fairly insensitive to changes in side-chain interactions.

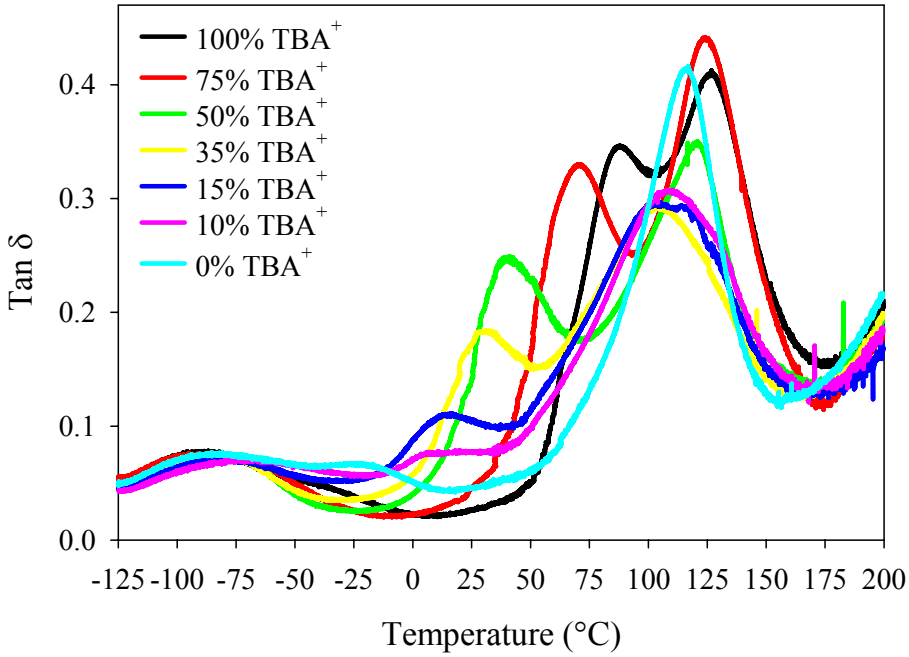

Figure 2.5. Dynamic mechanical tan δ versus temperature of partially neutralized Nafion® 117 for 100, 75, 50, 35, 15, 10, and 0% TBA^+ counterion compositions.

By plotting the peak maxima versus TBA^+ composition (shown in Figure 2.6), a strong and uniform compositional dependence is observed for the β-relaxation, while the α-relaxation remains relatively independent of composition. This behavior strongly suggests that the molecular origin of the β-relaxation in H^+-form Nafion® is the same as that of the β-relaxation in TBA^+-form Nafion®. Therefore, based on our fundamental understanding of the origin of the β-relaxation in neutralized Nafion® samples,[19] we now assign the β-relaxation as the glass transition of H^+-form 1100 EW Nafion® with a temperature in the vicinity of ca. -20 °C. In a manner consistent with the defined behavior of the neutralized ionomers, this glass transition of H^+-form Nafion® is

attributed principally to main chain (backbone) motions within the framework of a *static* physically-crosslinked (hydrogen-bonded) network.[19]

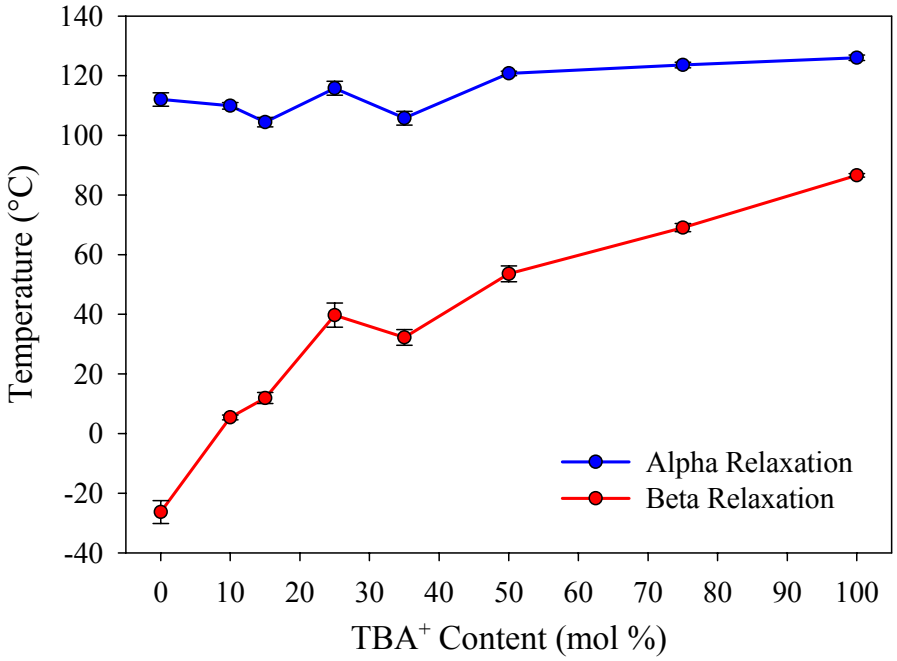

Figure 2.6. α and β-relaxation temperatures as a function of TBA^+ content from the dynamic mechanical analysis of Nafion® 117.

Figure 2.7 displays the dynamic mechanical analysis of all partially neutralized H^+/TBA^+ Nafion® samples after boiling for one hour in deionized water. The alpha relaxation shows minimal change with partial neutralization as well as being subjected to boiling before testing. The beta relaxation shows a shift to lower temperatures along with a dramatic decrease in magnitude. The beta relaxation for the pure TBA^+ sample remains constant between dry and boiled conditions, which is attributed to the hydrophobic nature of the TBA^+ counterion and the corresponding water uptake or lambda value of 1.05. As opposed to the pure TBA^+-form sample, the rest of the partially neutralized membranes have a β-relaxation that is very susceptible and easily manipulated in the presence of water.

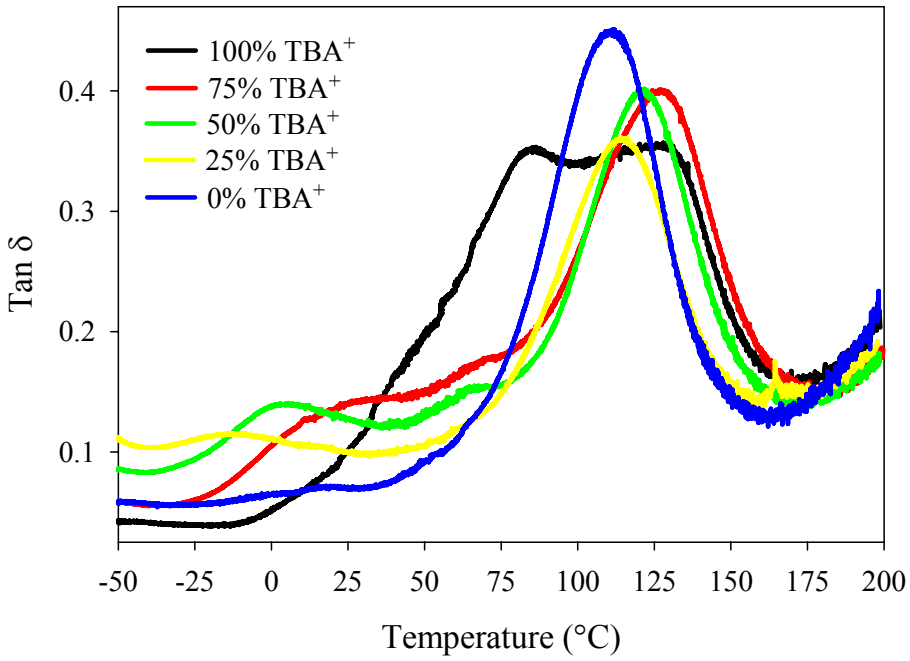

Figure 2.7. Dynamic mechanical tan δ versus temperature of partially neutralized Nafion® 117 for 100, 75, 50, 25, and 0% TBA^+ counterion compositions after boiling in deionized water for one hour.

Figures 2.8a and 2.8b display the tan delta and storage modulus (MPa) versus temperature for the 50/50 H^+/TBA^+ neutralized Nafion® 117 membrane preconditioned at various humidities. Similar to the behavior seen in Figure 2.7, Figure 2.8a shows a dramatic decrease in both the intensity and temperature of the β-relaxation with increasing water content. Also the α-relaxation remains independent of water content, which is believed to be due to the relaxation temperature (121 °C) being well above the boiling point of water. By the time the alpha relaxation is reached during the DMA experiment, all of the samples should be in a fairly dry state. The drying behavior of Nafion® within the DMA is also verified by the data shown in Figure 2.8b. The storage modulus curves appear to merge from 100 °C to 200 °C for all sample humidities. This behavior is to be expected since the water is evaporating from the samples at temperatures above 100 °C. As the films dehydrate, the DMA behavior begins to resemble that of the initially dry sample. Prior to evaporation of the water near 100 °C,

the storage modulus dramatically decreases from 1850 MPa to 760 MPa between the dried and boiled samples at -50 °C. In agreement with the previous tensile data for pure H^+-form Nafion® preconditioned at various humidities, the storage modulus behaves similarly to the Young's modulus in that they both see a dramatic decrease in MPa due to the plasticization effect of water throughout the membrane. It is important to note that the decrease in modulus values during the DMA experiment is approximately 60% while the decrease in the modulus values of the tensile test is 85%. A reasonable explanation for the discrepancy in the percent change in modulus after boiling in deionized water for one hour is due to the hydrophobicity of the TBA^+ counterion. All of the DMA data was performed on samples that were 50% neutralized with TBA^+ counterions, which in turn lowered the amount of water the membranes could absorb after boiling for one hour. Due to the decreased amount of water present in the 50/50 H^+/TBA^+ membrane, the change in modulus observed using DMA was lower than the change in modulus observed for the pure H^+-form membranes during the tensile test.

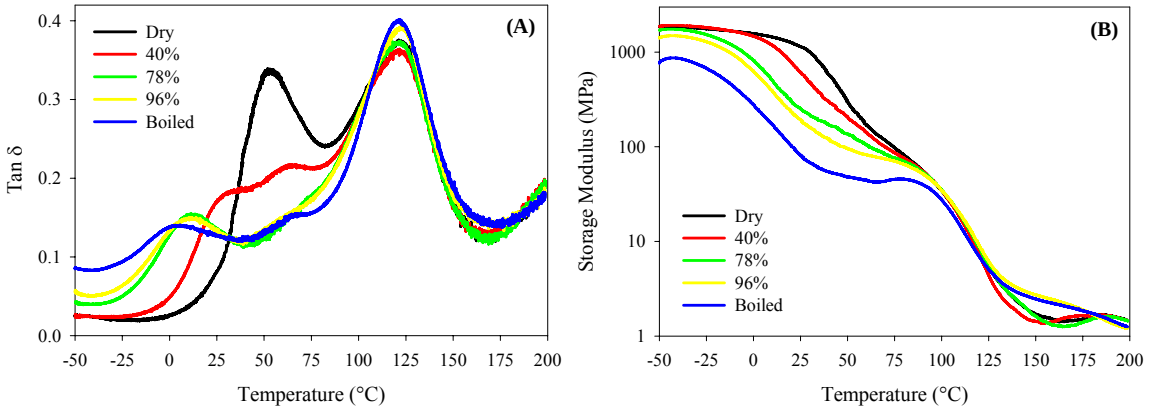

Figure 2.8. A) Dynamic mechanical tan δ versus temperature of 50/50 H^+/TBA^+ partially neutralized Nafion® 117 after preconditioned at various humidity levels. **B)** Dynamic mechanical storage modulus versus temperature of 50/50 H^+/TBA^+ partially neutralized Nafion® 117 after preconditioned at various humidity levels.

Mechanical Properties of Partially Neutralized H^+/TBA^+ Nafion® 117. Evaluation of the mechanical properties of samples prepared with partial neutralization, and assuming that the TBA^+ counterions are homogeneously distributed among the sulfonate groups, was conducted using room temperature tensile tests. Figure 2.9a shows the stress versus strain profiles for Nafion® 117 of 0, 25, 50, 75, and 100% TBA^+ content. It can be seen from this figure that strain at break decreases with higher percentages of TBA^+ content, while the modulus increases with increasing TBA^+ content. It is also important to note the emergence of a sharp yield point with increasing TBA^+ content, which may have various explanations. Wilkes and coworkers also observed the emergence of a distinct yield point in their tensile data on blends of poly(tetrafluoroethylene) PTFE and poly(tetrafluoroethylene-co-vinylidene fluoride-co-hexafluoropropylene) (KFM) before and after thermally curing.[49] Wilkes et al. observed that as the weight percent of PTFE increased from 0-70% in the polymer blends, a distinct yield point emerged and increased in intensity. Along with the appearance of a yield point, the modulus of the blends greatly increased with PTFE content, which coincides with our data shown in Figure 2.9b. Granted, Wilkes et al. were studying a nonionic polymer blend, but the trend observed with our polymer blend was ironically similar. Wilkes and coworkers came to the conclusion that as the PTFE began to form the majority of the matrix, it also became more important in determining the modulus of the final membrane. Wilkes et al. point out that as the PTFE content increases, the character of the polymer blends shifts from elastomeric deformation behavior to having more plastic character. The same is true for the partially neutralized H^+/TBA^+ Nafion® membranes shown in Figures 2.9a and 2.9b. As the TBA^+ content increases, the

membrane mechanical properties shift from elastomeric to plastic. The indication of more plastic behavior involves the distinct formation of a yield point along with easier recognition of the irrecoverable flow region. Wilkes et al. point out that similar behavior has been observed in elastomeric systems that have been reinforced with various inorganic fillers.[50] In these systems, the change in elastomeric behavior is due to closer packing of fillers at higher filler contents. So, as the filler content increased, stress concentration increased, and large scale deformation was impeded. In the case of the H^+/TBA^+ form Nafion® membranes, the TBA^+ counterion behaves as a filler, but at the same time introduces ionic interactions, which are stronger than the subsequent hydrogen-bonding displayed by the pure H^+-form of the ionomer. The TBA^+/SO_3^- interaction leads to a stronger electrostatic network, creating more physical crosslinks as the TBA^+ content is increased. These physical crosslinks help strengthen the polymer membrane by increasing the modulus but simultaneously impede large scale deformation.

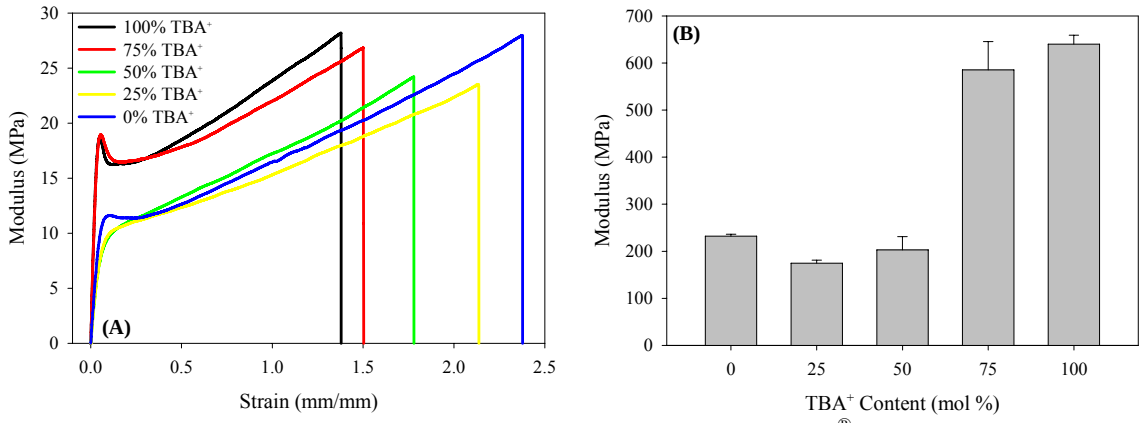

Figure 2.9. A) Modulus versus Strain of partially neutralized Nafion® 117 for 100, 75, 50, 25, and 0% TBA^+ counterion compositions. **B)** Modulus of partially neutralized Nafion® 117 for 100, 75, 50, 25, and 0% TBA^+ counterion compositions.

Coinciding with the modulus data shown in Figure 2.9b, the yield stress versus TBA^+ content displays a similar trend of dramatically increasing at TBA^+ levels beyond 75%, as shown in Figure 2.10a. The increase in yield stress at elevated TBA^+ contents is due to

the increasing strength of Nafion's® electrostatic network with the addition of more ionic TBA^+/SO_3^- interactions. An interesting trend of decreasing strain at break versus increasing TBA^+ content is displayed in Figure 2.10b. Wilkes et al. observed a similar trend of decreasing strain at break with increasing PTFE content within their PTFE/KFM polymer blend.[49] The strain at break was determined to decrease as the percentage of PTFE filler increased and was attributed to the rigid PTFE portion not allowing the polymer to deform at large strains. In our example, the interaction of the TBA^+ with the sulfonate moiety creates a stronger electrostatic interaction than with hydrogen alone, hence decreasing large scale mobility at increasing strains. Another interesting observation to consider is the role of temperature and the β-relaxation on the resulting tensile properties. As mentioned in the previous section, based on our fundamental understanding of the origin of the β-relaxation in neutralized Nafion® samples, we now attribute this relaxation to the true glass transition of the polymer. Based on this assignment it was shown that as the TBA^+ content increased within the membrane, the β-relaxation temperature also increased. Based on the tensile data of partially neutralized H^+/TBA^+ Nafion® shown in Figures 2.9 and 2.10, we see that the mechanical properties of the membrane are greatly affected by changes to the glass transition temperature. As mentioned previously, based on DMA results, the β-relaxation temperature resides at approximately -20 °C. Since all of the tensile experiments were conducted at room temperature, which is well above the β-relaxation temperature of H^+-form Nafion®, the polymer exhibited increased ductility and extended elongation at break. On the opposite side of the spectrum, the pure TBA^+-form Nafion® has a β-relaxation temperature of 126 °C, which would place the polymer in the glassy state during the room temperature

tensile experiments. Based on this observation, one would expect the TBA^+-form Nafion® sample to exhibit decreased long range mobility due to being frozen in the glassy state, but also exhibit increased strength in the elastic region.

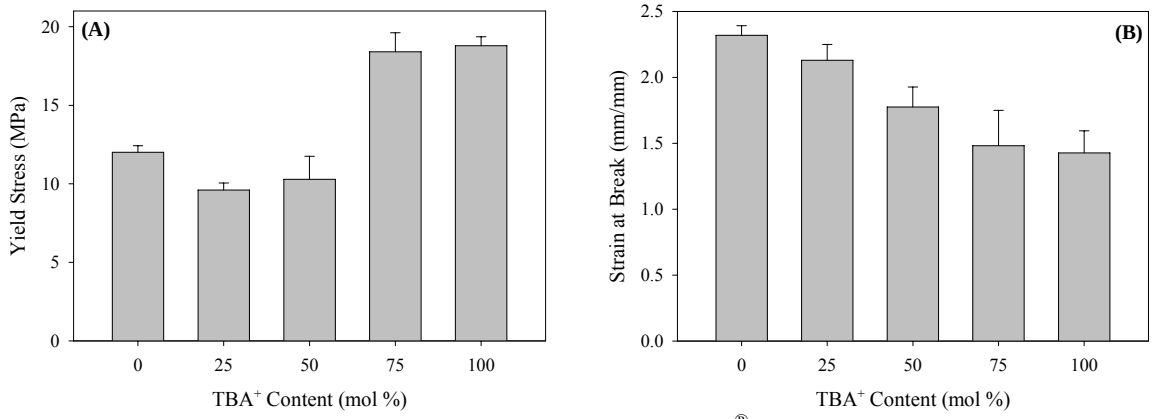

Figure 2.10. A) Yield Stress of partially neutralized Nafion® 117 for 100, 75, 50, 25, and 0% TBA^+ counterion compositions. **B)** Strain at break of partially neutralized Nafion® 117 for 100, 75, 50, 25, and 0% TBA^+ counterion compositions.

Dielectric Spectroscopy. Dielectric spectroscopy (DS) has been a powerful tool in the study of chain dynamics in glass-forming polymers and yields information that is complementary to DMA. To confirm the assignment of the β-relaxation in H^+-form Nafion® as the true glass transition, the relaxation behavior of dry samples of pure H^+-form Nafion® were probed using DS in both the temperature and frequency regimes. Figure 2.11 displays the loss permittivity of the β-relaxation as a function of frequency and temperature. Relative to the DMA data in Figure 2.4, the β-relaxation peak observed with DS is quite pronounced. The β-relaxation first appears at approximately -20 °C at 0.01 Hz and shifts to higher frequencies with increasing temperature as a consequence of a thermally-activated relaxation process.

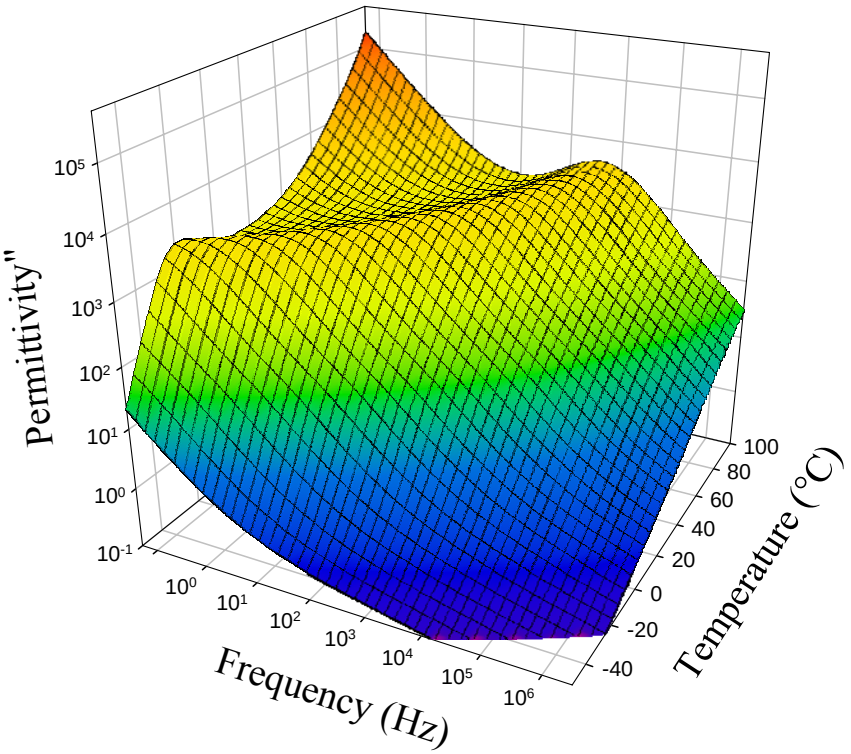

Figure 2.11. Dielectric Loss Permittivity data of H^+-form Nafion® 117 β-relaxation as a function of frequency and temperature.

To clearly illustrate the presence of the β-relaxation, 2D plots of loss permittivity versus temperature and frequency are shown in Figures 2.12a and 2.12b. The β-relaxation is clearly identifiable in Figure 2.12a and first appears at approximately -20 °C at 0.01 Hz on the ε" vs temperature plot at various fixed frequencies. The observed peak shift to higher temperatures with increasing frequency is interpreted in the usual sense: as the oscillatory period = 1/f decreases, the characteristic dipole motions must be more rapid by heating to be detected within a shorter experimental time frame, i.e., (1/2f). The curves at the lowest frequencies should be compared with the dynamic mechanical data for which the perturbation frequency is low (1Hz). In Figure 2.12b, the peak in the ε" vs. f curves monotonically shifts to higher frequencies, and the associated relaxation time correspondingly shifts to lower values with increased temperature.

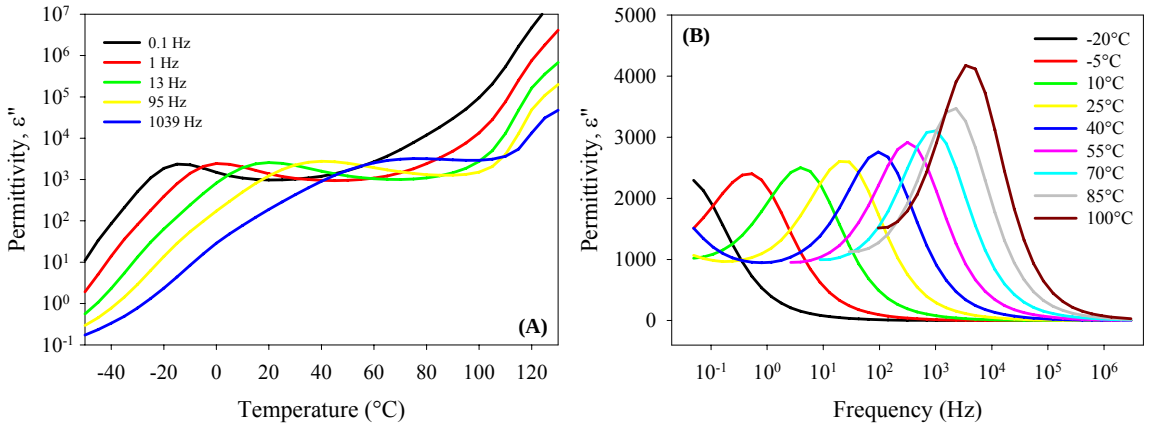

Figure 2.12. **A)** ε" versus temperature curves at various frequencies in the region of the β-relaxation for H^+-form Nafion®. **B)** Isothermal ε" versus frequency curves for temperatures above the β-relaxation for H^+-form Nafion®.

By fitting Equation 2-2 to the loss permittivity data points in Figure 2.12b, τ_{HN}, α, and β were obtained and substituted into Equation 2-3 to calculate τ_{max} over the range of temperatures. Figure 2.13 is a plot of ln τ_{max} versus inverse Kelvin temperature. First, it is seen that the points define a plot with upward curvature rather than a straight line that would characterize an activated rate (i.e., Arrhenius-like) process such as observed for short range motions.

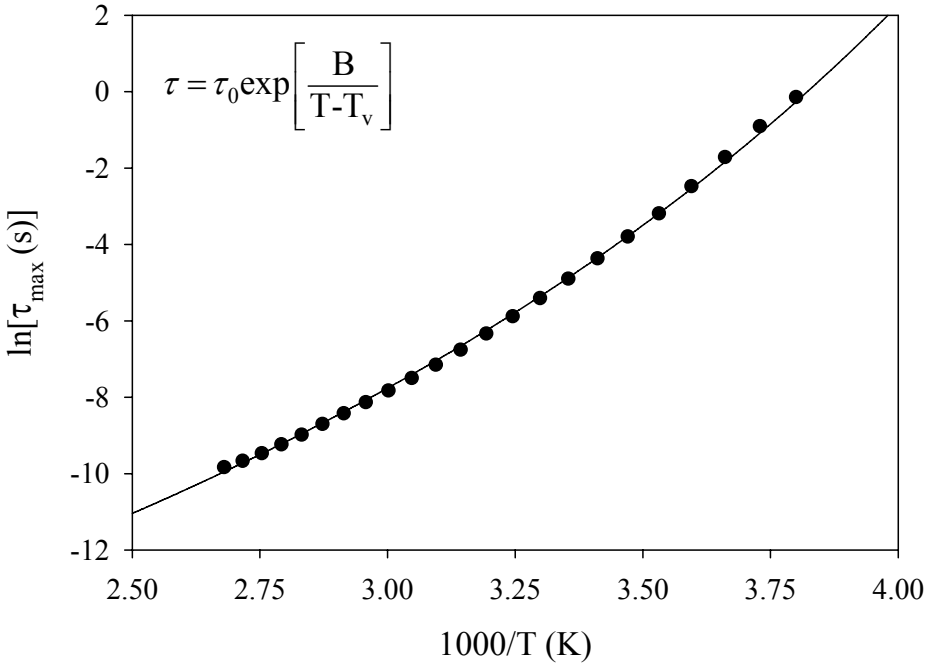

Figure 2.13. ln τ_{max} versus inverse temperature for the β-relaxation of H^+-form Nafion® 117. The continuous curve is a plot of the best fit of theVFT equation to the data points.

The Vogel-Fulcher-Tammann (VFT) equation, shown below, can be well-fitted to the data.[51-53]

$$\tau = \tau_0 \exp\left[\frac{B}{T\text{-}T_v}\right] \qquad \textbf{Eq. 2-4}$$

τ_0 is a hypothetical relaxation time at infinite temperature, and B is a fitted parameter that is sometimes related to an apparent activation energy. T_v is the Vogel temperature that is often interpreted as a temperature that is reached upon quasi-static cooling and at which chain segments become immobile. At temperatures above this frozen-in state, the free volume is dynamic and constantly redistributed with no change in energy according to simple liquid state theories, the most notable being based on the concepts of Cohen and Turnbull.[54, 55] While the VFT equation is empirical in origin, it has often been interpreted in terms of free volume fluctuations in a liquid-like state in the same way as

used in the rationalization of the WLF equation for the rubbery state of polymers.[56] In fact, T_v in some instances, has been called an 'ideal glass transition temperature'.[57]

The data points in Figure 2.13 fit very well with the VFT equation over the range of tested temperatures for the β-relaxation for H^+-form Nafion®, as it does for many polymers at temperatures above the dynamic glass transition.[58] The extracted values from the fit of the VFT equation for τ_0 and T_v are 1.63 x 10^{-9} sec and 146 K (-127 °C), respectively. T_v is usually lower than T_g by as much as 100 °C so that this value is realistic in comparison with the relaxation centered at -20 °C.

In order to account for systematic deviation of the data points in Figure 2.13 from the VFT fit, a derivative analysis, as performed by Stickel et al.,[59, 60] was undertaken. In this analysis, the behavior of the first derivative of the VFT equation versus temperature is observed in Equation 2-5.

$$\frac{d\log\left(\frac{\tau_0}{\tau_{\max}}\right)}{dT} = \frac{B}{\left(T - T_V\right)^2} \qquad \textbf{Eq. 2-5}$$

This equation is linearized as follows:

$$\left[\frac{d\log\left(\frac{\tau_0}{\tau_{\max}}\right)}{dT}\right]^{-\frac{1}{2}} = B^{-\frac{1}{2}}\left(T - T_V\right) \qquad \textbf{Eq. 2-6}$$

Thus, when the quantity on the left side of the equation is plotted against time and the plot is linear, it can be concluded that the VFT equation is indeed a good representation of the relaxation data in this temperature range. The actual data fit, seen in Figure 2.14,

shows considerable agreement with VFT behavior over the temperature range from 260 K to 350 K.

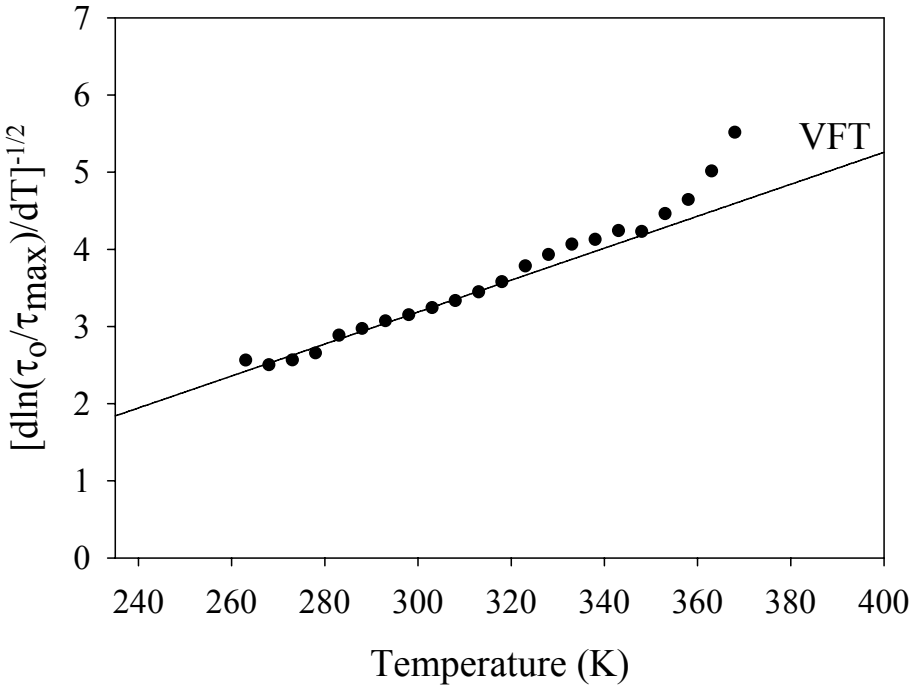

Figure 2.14. Temperature derivative data vs. temperature and fit of Equation 2-6 for the β-relaxation of H^+-form Nafion®.

As further confirmation of the consistency of the experimental data with the VFT equation over this temperature range, it is important to note that the derivative of equation 2-6 with respect to T, shown as equation 2-7, yields a temperature invariant value of B over the range 260 K < T < 360 K.

$$\frac{d\left[\frac{d\log\left(\frac{\tau_0}{\tau_{\max}}\right)}{dT}\right]^{-\frac{1}{2}}}{dT} = B^{-\frac{1}{2}} \qquad \textbf{Eq. 2-7}$$

Figure 2.15 shows the second derivative of the VFT equation (Eq. 2-4) with respect to temperature as a function of temperature between 260 and 360 K. The dashed line in Figure 2.15 represents the average B value calculated from Eq. 2-4 at every experimental

temperature and relaxation time. In agreement with the analysis of Stickel et al.,[59, 60] this representation of the experimental data clearly indicates a reasonable VFT fit over the temperature range of 270 to 350 K. Beyond 350 K, the experimental data begin to deviate from both the first and second derivatives of the VFT equation.

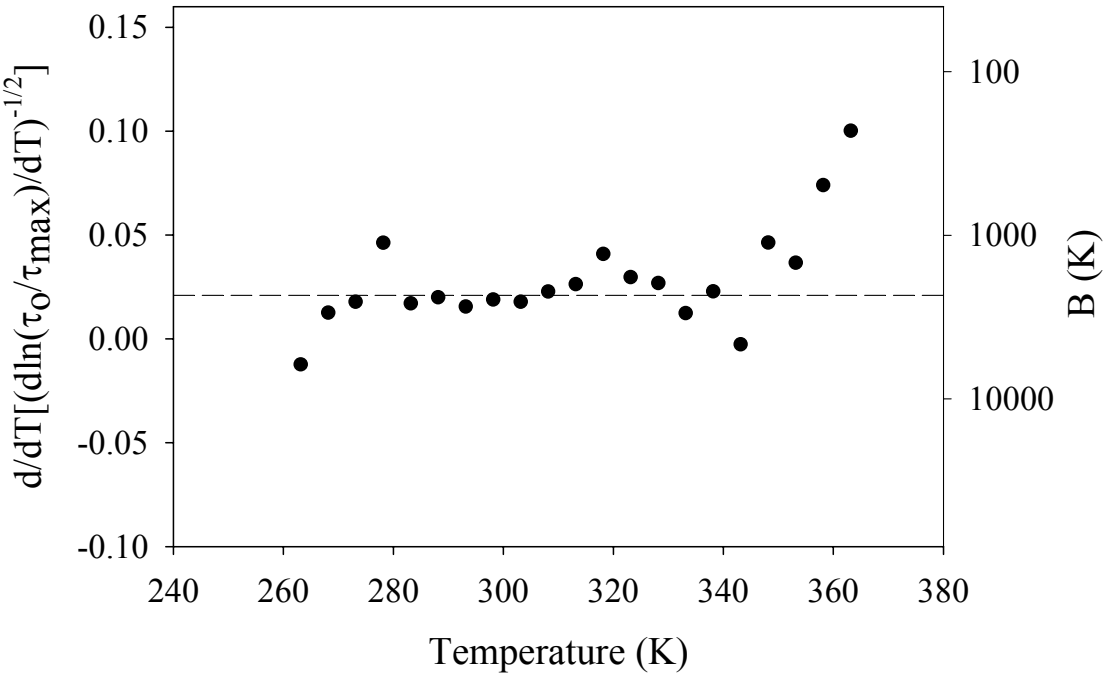

Figure 2.15. Second derivative of the VFT equation with respect to temperature and the invariant value B vs. temperature for the β-relaxation of H^+-form Nafion®.

VFT behavior is characteristic, and is a signature of long-range segmental motions not requiring an activation energy in glass forming liquids.[57] In contrast, the Arrhenius equation does not involve a lower limit on temperature (T_v) at which long range motions are frozen-in. The relaxation time vs. temperature behavior, the existence of a T_v, as well as the magnitude of the frequencies above the β-transition, coupled with the DMA results, strongly suggest that this is a glass transition in the usual sense. While the conformance of the VFT equation to relaxation data over a temperature range is not sufficient proof of a liquid-like state as in rubbery polymers, it is a necessary condition given the large volume of evidence for numerous polymers. Given this rationale, and in

agreement with the latter assignment of Eisenberg and coworkers,[13] it is concluded that the β-relaxation of H^+-form Nafion® is a *genuine* glass transition involving long range segmental motions.

Conclusions

Through a correlation of dynamic mechanical analysis and dielectric spectroscopy, the glass transition temperature of H^+-form Nafion® is assigned to the weak β-relaxation centered at -20 °C. Building upon our previous studies[10, 19, 38] of the molecular and morphological origins of the dynamic mechanical relaxations of Nafion® containing large organic ions, a strong compositional dependence of the β-relaxation in partially neutralized samples suggests that the β-relaxation of H^+-form Nafion® and the neutralized ionomers have the same molecular origin, namely backbone segmental motions. In the dielectric spectroscopy studies, the relaxation time versus temperature behavior, the existence of a Vogel temperature, and the magnitude of the frequencies above the beta transition, coupled with the DMA results, strongly suggest that the β-relaxation is a glass transition in the usual sense, rather than a short range, secondary relaxation with Arrhenius temperature dependence.

With this understanding of the glass transition in H^+-form Nafion®, it remains important to recognize that the β-relaxation is significantly weaker than the dominant α-relaxation observed near 100 °C. At temperatures between -20 °C and 100 °C, main-chain segmental motions are significant; however, the morphological organization of the hydrophobic and hydrophilic domains is likely to be pinned within a static physical network.[19] At temperatures above the α-relaxation, the hydrogen-bonded network

becomes dynamic, resulting in considerable molecular mobility. Under these conditions, it is reasonable to consider the possibility of morphological reorganization;[10, 61] however, the extent of this potential change in structure and the impact on membrane properties remains to be determined.

Acknowledgements

We would like to thank E.I. du Pont De Nemours and Company for supplying the extruded Nafion® 112 and 117 samples. Funding for this work was provided by DuPont Fuel Cells and DOE Office of Energy Efficiency and Renewable Energy; contract # DE-FC36-03GO13100 and DE-FG36-06GO86065.

References

(1) Mauritz, K. A.; Moore, R. B. *Chemical Reviews* **2004,** 104, (10), 4535-4585.
(2) Eisenberg, A.; Hird, B.; Moore, R. B. *Macromolecules* **1990,** 23, 4098-4107.
(3) Starkweather, H. W. *Macromolecules* **1982,** 15, (2), 320-323.
(4) Moore, Robert. B.; Martin, Charles R. *Macromolecules* **1988,** 88, (21), 1334-1339.
(5) Gierke, T.D.; Munn, G.E.; Wilson, F.C. *Journal of Polymer Science: Polymer Physics Edition* **1981,** 19, 1687-1704.
(6) Gebel, Gerard; Lambard, Jacques. *Macromolecules* **1997,** 30, 7914-7920.
(7) Gebel, G. *Polymer* **2000,** 41, (15), 5829-5838.
(8) Fujimura, M.; Hashimoto, T.; Kawai, H. *Macromolecules* **1981,** 14, (5), 1309-1315.
(9) Schmidt-Rohr, K.; Chen, Q. *Nature Materials* **2008,** 7, (1), 75-83.
(10) Page, K. A.; Landis, F. A.; Phillips, A. K.; Moore, R. B. *Macromolecules* **2006,** 39, (11), 3939-3946.
(11) Hodge, I. M.; Eisenberg, A. *Macromolecules* **1978,** 11, (2), 289-293.
(12) Yeo, S.; Eisenberg, A. *Journal of Applied Polymer Science* **1977,** 21, 875-898.
(13) Kyu, T.; Hashiyama, M.; Eisenberg, A. *Canadian Journal of Chemistry* **1983,** 61, 680-687.
(14) Miura, Y.; Yoshida, H. *Thermochimica Acta* **1990,** 163, 161-168.
(15) Moore, Robert B.; Cable, K. M.; Croley, T. L. *Journal of Membrane Science* **1992,** 75, (1), 7-14.
(16) Moore, R. B.; Cable, K. *Polymer Preprints* **1997,** 38, 272-273.
(17) Young, S.; Mauritz, K. *Journal of Polymer Science: Polymer Physics Edition* **2001,** 39, 1282-1295.

(18) Doyle, M.; Rajendran, G., Perfluorinated membranes. In *Handbook of Fuel Cells - Fundamentals, Technology and Applications*, Wolf Vielstich, A. L., and Hubert A. Gasteiger, Ed. John Wiley & Sons, Ltd, Chichester: 2003; Vol. 3 Part 3, pp 351-395.
(19) Page, K. A.; Cable, K. M.; Moore, R. B. *Macromolecules* **2005,** 38, (15), 6472-6484.
(20) Song, Y.; Xu, H.; Wei, Y.; Kunz, H. R.; Bonville, L. J.; Fenton, J. A. *Journal of Power Sources* **2006,** 154, (1), 138-144.
(21) Grot, W. G.; Munn, G. E.; Walmsley, P. N. Electrochemical Society Meeting, Houston, TX, May 7-11, 1972.
(22) Kyu, T.; Eisenberg, A. *Journal of Polymer Science, Polymer Symposia* **1984,** 71, 203-219.
(23) Damay, F.; Klein, L. C. *Solid State Ionics* **2003,** 162, 261-267.
(24) Tsonos, C.; Apekis, L.; Pissis, P. *Journal of Materials Science* **2000,** 35, 5957-5965.
(25) Su, S.; Mauritz, K. A. *Macromolecules* **1994,** 27, 2079-2086.
(26) Starkweather, H. W.; Chang, J. J. *Macromolecules* **1982,** 15, 752-756.
(27) Deng, Z. D.; Mauritz, K. A. *Macromolecules* **1992,** 25, 2369-2380.
(28) Deng, Z. D.; Mauritz, K. A. *Macromolecules* **1992,** 25, 2739-2745.
(29) Mauritz, K. A.; Fu, R. M. *Macromolecules* **1988,** 21, 1324-1333.
(30) Mauritz, K. A. *Macromolecules* **1989,** 22, 4483-4488.
(31) Zhang, Shihai; Painter, P.C.; Runt, J. *Macromolecules* **2002,** 35, 8478-8487.
(32) Osborn, S.; Hassan, M.; Divoux, G.; Rhoades, D.; Mauritz, K.; Moore, R. B. *Macromolecules* **2007,** 40, (10), 3886-3890.
(33) Rhoades, D.; Hassan, M.; Osborn, S.; Moore, R. B.; Mauritz, K. *Journal of Power Sources* **2007,** 172, 72-77.
(34) Schonhals, A.; Kremer, F., *Broadband Dielectric Spectroscopy*. Springer: Berlin, 2003.
(35) Cable, K.M.; Gatlin, M.E.; Mauritz, K.A.; Moore, R.B. *Polymer Preprints* **1995,** 36, 374-375.
(36) Page, K.A.; Moore, R.B. *Polymer Preprints* **2003,** 44, 1144-1145.
(37) Landis, F.A.; Moore, R.B.; Page, K.A.; Han, C.C. *Polymeric Materials: Science and Engineering* **2002,** 87, 121-122.
(38) Page, K.; Jarrett, W.; Moore, R. B. *Journal of Polymer Science Part B: Polymer Physics* **2007,** 45, 2177-2186.
(39) Almeida, S.H.; Kawano, Y. *Journal of Thermal Analysis and Calorimetry* **1999,** 58, 569-577.
(40) Chen, Q.; Schmidt-Rohr, K. *Macromolecules* **2004,** 37, 5995-6003.
(41) Hird, B.; Eisenberg, A. *Macromolecules* **1992,** 25, 6466-6474.
(42) Kreuer, K. D. *Chemisty of Materials* **1996,** 8, (3), 610-641.
(43) Zhang, S.; Painter, P. C; Runt, J. *Macromolecules* **2004,** 37, 2636-2642.
(44) Havriliak, S.; Negami, S. *J. Polym. Sci., Polym. Symp.* **1966,** 14, 99-117.
(45) Kawano, Y.; Wang, Y.; Palmer, R. A.; Aubuchon, S. R. *Polimeros: Ciencia e Tecnologia* **2002,** 12, (2), 96-101.

(46) Huang, X. Y.; Solasi, R.; Zou, Y.; Feshler, M.; Reifsnider, K.; Condit, D.; Burlatsky, S.; Madden, T. *Journal of Polymer Science Part B-Polymer Physics* **2006,** 44, (16), 2346-2357.
(47) Bauer, F.; Denneler, S.; Willert-Porada, M. *Journal of Polymer Science Part B-Polymer Physics* **2005,** 43, (7), 786-795.
(48) Fox, T. G. *Bull. Am. Phys. Soc.* **1956,** 2, (1), 123.
(49) Kaushiva, B. D.; Wilkes, G. L.; C., Comeaux.; Socha, L. *Polymer* **2001,** 42, 4619-4633.
(50) Nielsen, L. E.; Landel, R. F., *Mechanical Properties of Polymers and Composites*. Marcel Dekker, Inc.: New York, 1994; Vol. 2.
(51) Vogel, H. *Physik. Zeit.* **1921,** 22, 645.
(52) Fulcher, G. S. *Journal of the American Ceramic Society* **1925,** 8, (6), 339-355.
(53) Tammann, V. G.; Hesse, W. Z. *Zeitschrift fur Anorganische und Allgemeine Chemie* **1926,** 156, 245-257.
(54) Cohen, M. H.; Turnbull, D. *Journal of Chemical Physics* **1959,** 31, (5), 1164-1169.
(55) Turnbull, D.; Cohen, M. H. *Journal of Chemical Physics* **1961,** 34, (1), 120-125.
(56) Williams, M. L.; Landel, R. F.; Ferry, J. D. *Journal of the American Chemical Society* **1955,** 77, 3701-3707.
(57) Kremer, F.; Schoenhals, A., *In Broadband Dielectric Spectroscopy*. Springer-Verlag: Berlin, 2003.
(58) McCrum, N. G.; Read, B. E.; Williams, G., *Anelastic and Dielectric Effects in Polymeric Solids*. Dover Publications: New York, 1991.
(59) Stickel, F.; Fischer, E. W.; Richert, R. *Journal of Chemical Physics* **1995,** 102, (15), 6251-6257.
(60) Stickel, F.; Fischer, E. W.; Richert, R. *Journal of Chemical Physics* **1996,** 104, (5), 2043-2055.
(61) Nosaka, A. Y.; Watanabe, S.; Toyoda, I.; Nosaka, Y. *Macromolecules* **2006,** 39, (13), 4425-4427.

CHAPTER 3

COUNTERION COMPOSITION AS A MEANS TO CONTROL MEMBRANE PROPERTIES OF PERFLUOROSULFONATE IONOMERS

Introduction

The perflurosulfonic acid ionomer Nafion® is the current benchmark material for proton exchange membrane fuel cells (PEMFCs) and consists of a polytetrafluoroethylene (PTFE) backbone with perfluorovinylether side chains that terminate with a sulfonic acid functionality.[1] Nafion® is currently available commercially from E.I. du Pont de Nemours and Company and has the following structure, shown in Figure 3.1.

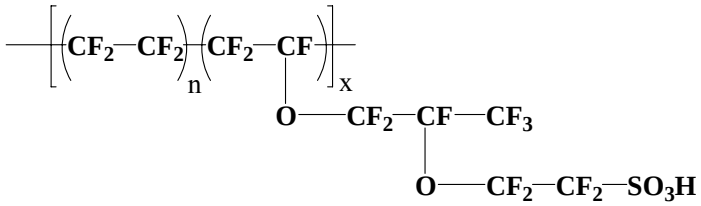

Figure 3.1. Chemical structure of Nafion®.

The extent of branching is displayed in terms of equivalent weight (EW), which is defined as the grams of polymer per equivalent of sulfonic acid.[2] The equivalent weight can be determined by acid-base titration, analysis of atomic sulfur, and Fourier transform infrared spectroscopy.[3] Determination of EW for Nafion® is shown in Equation 3-1, where 100 is the molecular weight of one $(CF_2\text{-}CF_2)$ unit and 443 is the molecular weight of the sidechain.

$$EW = 100(n) + 443 \qquad \textbf{Eq. 3-1}$$

The most common EW for Nafion® reported in the literature is 1100 g/mol SO_3^-.[1] Based on a complete random copolymerization, an EW of 1100 would yield an *n* value of approximately 6.57, or twelve to fourteen CF_2 units in the backbone, capable of forming "teflon-like" crystallites.[4, 5]

Due to the difference in polarity between the nonpolar fluorocarbon matrix and polar ionic moieties, the ionic groups tend to phase separate and form what is referred to as ionic aggregates.[6] In the interest of accurately describing Nafion's® complex, phase-separated network of both ionic aggregates and crystalline domains, the majority of investigations have focused on characterizing both the morphological[5, 7-11] and thermo-mechanical[1, 3, 12-20] properties. For use in PEMFCs, Nafion® must possess excellent proton transport properties along with mechanical integrity. PEMFC conditions subject polymer films to various pressure gradients, swelling/dehydration cycles, creep, and extreme temperatures, which must be taken into account when examining the physical properties of a proton exchange membrane for use in fuel cells.[1]

Dupont has shown that the production method used in creating Nafion® membranes plays a crucial role in the inherent properties of the film.[21, 22] For the past forty years, the main method for producing Nafion® membranes was through melt extrusion of a sulfonyl fluoride (SO_2F) precursor. This was followed by hydrolysis to convert the precursor into the sulfonate ionomer (SO_3^-).[1, 3] DuPont has recently introduced dispersion-cast membranes which exhibit lower thicknesses and higher water uptake values when compared to their extruded counterparts.[23] To date, DuPont has yet to disclose the exact solvent system or casting conditions used to create the dispersion-cast membranes.

In contrast to the dispersion-cast method of DuPont, Moore and Martin developed a "solution-processing" procedure for Nafion®, shown in Figure 3.2.[5, 24]

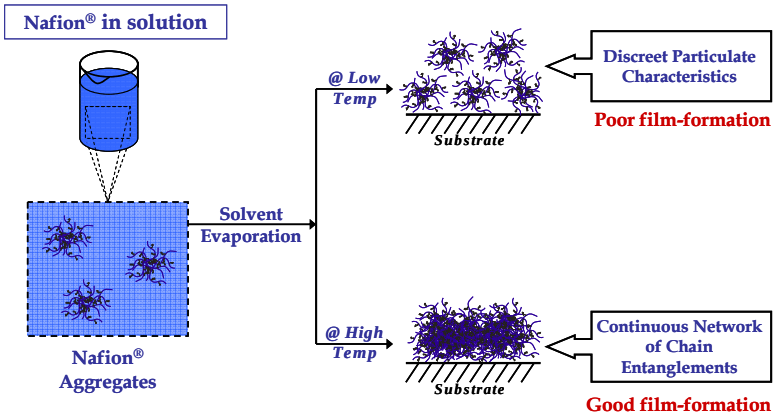

Figure 3.2. Effect of solution-processing temperature and solvent on film formation of Nafion® membranes.

The first step in Moore and Martin's solution-processing procedure involves dissolving extruded Nafion® in an alcohol/water mixture under high pressure and high temperature as developed by Grot[25] and Martin[26] . Figure 3.2 shows that membranes cast at room temperature from ethanol/water Nafion® dispersions were classified as recast films due to their brittleness, presence of mud cracks, and solubility in various polar organic solvents at room temperature. In contrast, the as-received Nafion® membranes were tough, pliable, and insoluble in virtually all solvents at temperatures below 200 °C. Moore and Martin's solution-processing procedure incorporated high boiling solvents such as dimethylsulfoxide (DMSO) or dimethylformamide (DMF) to the alcohol-water system to disrupt the colloidal particles and allow casting at elevated temperatures. Combination of the elevated casting temperature and the plasticizing effect of the solvent provided the chain mobility necessary to facilitate macromolecular organization of the Nafion® chains in solution, thereby producing mechanically stable membranes with similar attributes to their extruded, as-received counterparts.

Another method to manipulate the morphology and mechanical properties of Nafion® involves neutralization with various alkali metal and alkylammonium counterions. To date, numerous authors have examined the effect of completely neutralizing Nafion® with various alkali metal counterions (Li^+, Na^+, K^+, Cs^+) and alkylammonium counterions (TMA^+, TEA^+, TPA^+, TBA^+) on both the morphology and mechanical properties of the ionomer.[14, 20, 27-30] However, very few authors have published the effects of partial neutralization or mixed counterion systems on the morphology and mechanical properties of Nafion®.[15, 31, 32] The earliest experiments involving the partial neutralization of Nafion® were performed by Kyu and coworkers.[15] Kyu et al. examined the dynamic mechanical properties of Nafion®'s sulfonyl fluoride precursor as a function of Na^+ counterion content, as well as the H^+-form of Nafion® as a function of partial conversion to the Cs^+ counterion form. For the purpose of this publication, we will focus on Kyu's study of partial neutralization of H^+-form Nafion® with cesium counterions rather than discuss the ramifications of partial conversion of the precursor into the Na^+-form of Nafion®. To achieve partial H^+/Cs^+ neutralization of Nafion®, Kyu et al. immersed the membranes in a 0.1 M CsOH solution for various time periods, consequently neutralizing the acid form of the ionomer with 39, 50, 76, and 90% cesium counterions. The authors assume a homogenous distribution of Cs^+ counterions throughout the membrane based on the rapid diffusion coefficient of the cesium cation throughout the solution. With the aid of dynamic mechanical analysis (DMA), Kyu et al. observed three tan delta versus temperature relaxations (γ, β, and α) present for all partially neutralized membranes. The γ-relaxation, which is associated with short-range motions of the $–CF_2–$ units in the backbone of Nafion®, was relatively unaffected by

partial neutralization into the Cs^+-form. On the other hand, both the β and α-relaxations increased in temperature with increasing cesium neutralization. Kyu et al. classified the β-relaxation as the glass transition of the matrix of the polymer based on previous assignments of the thermo-mechanical relaxations of Nafion® by Yeo and coworkers.[14] Recent efforts from our group have determined that the β-relaxation is actually the true glass transition of the perfluorosulfonate ionomer, which affects both the fluorocarbon matrix and ionomer regions.[32] Kyu et al. also noticed a decrease in the β-relaxation peak intensity with increasing neutralization, which was noted as being a common attribute among hydrocarbon based ionomers. The increase in temperature and decrease in intensity of the β-relaxation was explained by an enhancement of the ionic interaction strength, which in turn reduced the mobility of the fluorocarbon matrix. The α-relaxation, which Kyu attributes to the glass transition of the ionic region, and we associate with the destabilization of the electrostatic network, also increased in temperature as a function of cesium neutralization. Based on the uniform shifting of both the β and α-relaxations to higher temperatures with increasing cesium neutralization, Kyu et al. concluded that the Cs^+ counterions were homogeneously mixed throughout the membranes.

A more recent publication involving the effects of various counterions on the phase separation behavior of Nafion®/polyvinyldiene fluoride (PVDF) blends was conducted by Landis and Moore.[33] Incorporation of either Na^+ or tetrabutylammonium (TBA^+) counterions into Nafion® prior to blending with PVDF, allowed Landis and Moore to characterize the phase separation and polymer miscibility using optical microscopy, small angle laser light scattering, scanning electron microscopy, and small

angle x-ray scattering. Landis and Moore incorporated a pseudo solution-processing technique in order to create Na^+ and TBA^+-form Nafion®/PVDF blends. The authors first made solutions of both pure Na^+ and TBA^+-form Nafion® according to the procedure of Martin et al., by dissolving the membranes at elevated temperature and pressure in various alcohol/water mixtures.[26] Landis and Moore then proceeded to obtain both counterion forms of Nafion® in the dry state in order to blend with PVDF powder in various weight ratios. Dry powder of Na^+-form Nafion® was obtained by pouring the alcohol/water/Nafion® solution onto a hot crystallizing dish, which rapidly flashed off the solvents, leaving behind a Na^+-form Nafion® residue. Obtaining a dry state of TBA^+-form Nafion® was achieved by incorporating a "steam stripping" technique, which was described elsewhere by Moore and Cable.[17] Steam stripping of TBA^+-form Nafion® involves slowly pouring the alcohol/water/Nafion® solution into boiling water, where the alcohols are flashed off and, due to the hydrophobic nature of the TBA^+ counterion, the Nafion® precipitates as a fluffy, white solid on top of the solution. Both the Na^+ and TBA^+-forms of Nafion® were then ground into a fine powder and mixed with PVDF powder with proper weight fractions and dissolved in a 40/60 N,N-dimethylacetamide/acetone solution. The various polymer blends were then achieved by casting the membranes on glass plates at 130 °C. Based on the differences in the strength of the electrostatic interactions between the Na^+ and TBA^+ counterions, Landis and Moore observed drastically different blended Nafion®/PVDF morphologies. Small angle laser light scattering results indicated that Na^+-form Nafion®/PVDF blends underwent irreversible phase separation upon heating above the PVDF crystalline melting

temperature, while TBA^+-form Nafion®/PVDF blends remained homogeneously mixed during the heating and cooling procedure.

Due to the extremely different behavior between Na^+ and TBA^+-form Nafion® when blended with PVDF, Phillips and Moore decided to continue the work of Landis and Moore, by exploiting the differential strengths of electrostatic interactions as a means to control morphology-property relationships in Nafion® membranes.[31] Rather than focus on blending Nafion® with a nonionic polymer such as PVDF, Phillips and Moore turned their attention to manipulating the phase behavior within Nafion® by composing a system of mixed Na^+ and TBA^+ counterions. By applying the same pseudo solution-processing technique of Landis and Moore, Phillips et al. mixed various weight fractions of dry Na^+ and TBA^+-form Nafion®, followed by dissolution in dimethylsulfoxide (DMSO), and finally cast at 180 °C to create membranes with the following Na^+/TBA^+ ratios: 0/100, 25/75, 50/50, 75/25, and 100/0. With the aid of DMA, differential scanning calorimetry, ^{23}Na solid-state NMR, and small angle x-ray scattering, Phillips and Moore were able to thoroughly characterize the mechanical and morphological properties of Nafion® with variable compositions of Na^+ and TBA^+ counterions. Despite the distinct differences in chain dynamics of Na^+ and TBA^+-form Nafion® at elevated temperatures, the DMA results indicated that the mixed counterion membranes behaved as a uniform, molecularly mixed system. Coinciding with the DMA data, ^{23}Na solid-state NMR spectra of the mixed counterion membranes showed that the local organization of the ionic aggregates was essentially identical to the as-received membrane. The data supports the concept of mixed ionic aggregates containing both Na^+ and TBA^+ counterions, which is in agreement with uniform shift in the mechanical relaxation peaks

observed using DMA. Upon reacidification of the 50/50 Na^+/TBA^+ membrane to the H^+-form, Phillips and Moore documented an unusual phenomenon of high proton conductivity with minimal water uptake. In conclusion, Phillips and Moore suggest that specific interactions during processing of Nafion® can affect the organization of the ionic domains and yield persistent structures that can have a significant influence on the final transport properties of the film.

Even though the previous studies by Landis and Phillips on Nafion® containing either Na^+ or TBA^+ counterions or a mixture of both, provided fundamental information regarding the influence of electrostatic interactions on the mechanical and transport properties of these complex polymeric materials, our goal is to expand upon their work and compare our true solution-processing technique to their recast/dissolution, pseudo solution-processing method. In conclusion, we will perform an in-depth analysis of the mixed counterion systems after reacidification and attempt to manipulate the morphology of Nafion® to optimize the transport properties and PEMFC performance.

Experimental

Materials. Extruded Nafion® 117 CS (1100 g/equivalent, sulfonic acid form, 7 mil or 0.178 mm thick, CS = chemically stable) was provided by E.I. du Pont de Nemours and Company. Tetrabutylammonium hydroxide (1M in methanol), sodium hydroxide, and dimethylsulfoxide were obtained from Aldrich Chemical Co. and used without any further purification.

Preparation of Perfluorosulfonic Ionomer Solutions. To remove impurities, the Nafion® 117 CS film was cleaned in refluxing 8M HNO_3 for two hours, then rinsed three times with deionized water, and finally boiled in deionized water for one hour. Upon

drying overnight at 70 °C in a vacuum oven, the clean Nafion® membranes were ion exchanged to either sodium (Na^+) or tetrabutylammonium (TBA^+) forms by stirring for 24 hours in sodium hydroxide (1.0 M aqueous solution) or tetrabutylamonium hydroxide (1.0 M solution in methanol). After neutralization, the Na^+ form membranes were boiled in deionized water for one hour and TBA^+ form membranes were boiled in methanol for one hour, followed by drying overnight under vacuum at 70 °C. Nafion® solutions were prepared using a PARR pressure reactor following the procedure by Martin and coworkers.[26] Seven grams of Na^+-form Nafion® were added to a 200 ml solution of 50:50 deionized water and ethanol, which was then placed into the high pressure reactor and stirred at 250 °C for two hours at approximately 1000 psi. The same procedure was followed for seven grams of TBA^+ form Nafion® in a mixture of deionized water, methanol, and isopropanol at a ratio of 40:30:30 by volume. After cooling, each solution was filtered under vacuum through Whatman number four filter paper. The average solution concentration was determined by extracting one milliliter of solution into three separate scintillation vials and obtaining the dry weight of the polymer after evaporating the residual solvent.

Solution-Processing Procedure. The following ratios of solution-processed Na^+/TBA^+ Nafion® membranes were created: 0/100, 25/75, 50/50, 75/25, 100/0. The various ratios of Na^+/TBA^+ were obtained by calculating the appropriate amount of either Na^+ or TBA^+ Nafion® solution prior to casting a membrane. Na^+ and TBA^+ Nafion® solutions were assumed to have an average density of 2.1 g/mL based on the studies of Takamatsu et al.[34] Using 2.1 g/mL as an average density, the volume needed to produce a 2 mil (0.05 mm) thick membrane with a surface area of 25 cm^2 was determined to be

0.125 cm^3. The appropriate volume of either Na^+ or TBA^+-form Nafion® solution necessary to construct films with various counterion compositions was determined based on the corresponding weight percent Nafion® present in each solution. To ensure optimum film properties as shown by the casting procedure of Moore and coworkers,[5, 24] dimethylsulfoxide (DMSO) was chosen as the high boiling point solvent for solution-processing of various Na^+/TBA^+ Nafion® films. A combination of the elevated casting temperature along with the plasticizing effect of DMSO provided the chain mobility necessary to facilitate macromolecular organization of both the Na^+ and TBA^+-form Nafion® chains in solution, thereby producing mechanically stable membranes. A solution of Na^+/TBA^+ Nafion® in DMSO was obtained after addition of appropriate quantities of both DMSO and Nafion®/water/alcohol into a 25 mL scintillation vial, followed by evaporation of the low boiling point solvents for 12 to 20 hours at 90 °C. After evaporation of the water and alcohols, the Nafion®/DMSO solution was poured onto a leveled borosilicate glass plate and maintained at 110 °C to evaporate any residual trace of low boiling point solvents that could lead to the formation of bubbles. The glass plate was then heated from 110 °C to 180 °C in five minutes and held at 180 °C for an additional fifteen minutes to ensure the evaporation of any residual DMSO. The temperature of the solution on the glass plate was measured in five different locations with an infrared thermometer in order to accurately document changes in temperature during solution-processing. The film was then peeled away from the glass plate after immersion in hot deionized water for a few minutes. The film thickness was measured in five different locations using micrometers to determine a uniform thickness of approximately 0.05 mm. The solution-processed membranes were then dried under

vacuum at 70 °C for 12 hours prior to analysis. Prior to membrane electrode assembly (MEA) and fuel cell testing, all Na^+/TBA^+ films were reacidified by refluxing in methanolic 4M H_2SO_4 solution for two hours, followed by boiling in deionized water for an additional hour.

Water Uptake Analysis. Weight fraction of water in the membranes was determined gravimetrically on solution-processed Na^+/TBA^+ films before and after reacidification. Five membranes were solution-processed at each Na^+/TBA^+ counterion composition to verify accurate water uptake results and minimize experimental error. Equation 3-2 shows how the weight fraction of water was calculated throughout the experiment, where m_h represents the mass of the hydrated polymer and m_d is the mass of the dry polymer.

$$Wt\ \ frac\ water = \frac{m_h - m_d}{m_d} \qquad \textbf{Eq. 3-2}$$

The dry weight of the polymer was determined after drying the membranes in a vacuum oven overnight at 70 ºC. The hydrated polymer mass was determined after boiling each sample individually in deionized water for two hours. After cooling to room temperature, the solution-processed membranes were removed from the deionized water, where excess water was wiped off and the final hydrated weight was determined (m_h). The water content (λ) of the solution-processed membranes was calculated using Equation 3-3, where 18 is the molecular weight of water and 1100 is the equivalent weight of the polymeric membrane. Water content is displayed as a ratio of moles of water per moles of sulfonate groups $-SO_3^-$.

$$\lambda = \frac{\left(m_h - m_d\right)/18}{\left(m_d/1100\right)} \qquad \textbf{Eq. 3-3}$$

Proton Conductivity Analysis. Prior to analysis, the solution-processed membranes were reacidified by refluxing in methanolic 4M H_2SO_4 solution for one hour, boiled in deionized water for one hour, and immersed in deionized water at 80 °C for 12 hours. In-plane membrane proton conductivity was conducted on solution-processed films using a 4-point conductivity cell developed by Bekktech which was submersed in deionized water at 80 °C. Measurements were taken from 0.1 to 500,000 Hz using a 1255 HF frequency analyzer coupled with a 1286 electrochemical interface, both from Solatron. Data analysis was carried out using both Zplot and Zview software purchased from Scribner and Associates, Inc. The in-plane conductivity was then calculated using the definition of the resistance in terms of the bulk resistivity and the cell geometry, shown in Equation 3-4 where ρ is the membrane resistivity (Ω·cm), A is the cross-sectional area perpendicular to the current flow, W is the width of the sample, L is the distance between the two reference electrodes and T is the thickness of the film.

$$R = \frac{\rho \times L}{A} = \frac{\rho \times L}{W \times T} \qquad \textbf{Eq. 3-4}$$

Since conductivity is the inverse of resistivity, Equation 3-4 can be rewritten in terms of conductivity as shown in Equation 3-5 where σ is the conductivity (S/cm), ρ is the membrane resistivity (Ω.cm), and R is the membrane resistance (Ω).

$$\sigma = \frac{1}{\rho} = \frac{L}{R \times W \times T} \qquad \textbf{Eq. 3-5}$$

The membrane resistance is determined by taking the real Z-axis intercept of the complex impedance plot or the real Z value for which the phase, Φ, is equal to zero.

Dynamic Mechanical Analysis. Dynamic mechanical analysis was performed on a TA Instruments DMA Q800 Analyzer in tensile mode using clamps for thin film samples.

The following ratios of solution-processed Na^+/TBA^+ Nafion® membranes were examined using DMA before and after reacidification: 0/100, 25/75, 50/50, 75/25, 100/0. All samples were dried for 12 hours at 70 °C under vacuum and stored in a desiccator for 24 hours prior to analysis. Samples were then cut to a width of 5.3 mm and run in triplicate to verify results and reduce experimental error. The membranes were annealed in the DMA by heating from room temperature to 110 °C followed by quenching to -130 °C prior to analysis. The samples were then analyzed at a frequency of 1 Hz from -130 to 300 °C with a heating rate of 2 °C/min. The temperature range was chosen in order to span all three thermo-mechanical relaxations, α, β, and γ.

Small and Wide Angle X-ray Scattering (SAXS-WAXS). Samples included solution-processed Na^+/TBA^+ Nafion® of the following weight percent compositions: 0/100, 25/75, 50/50, 75/25, 100/0 before and after reacidification. Simultaneous SAXS-WAXS was performed at the Argonne National Laboratory Advanced Photon Source on the DND-CAT 05-ID-D beamline. A monochromatic x-ray beam was derived from an insertion device and a double-crystal monochromator. The incident energy was set to 15 keV and the resulting x-ray wavelength was 0.82656 Å. Two-dimensional scattering images of SAXS data were collected on a high resolution Mar CCD detector (8.1 cm radius) at a distance of 294.35 cm from the sample. Two-dimensional scattering images of WAXS data were collected on a Roper Scientific detector (14.1 cm radius) at a distance of 23.6 cm from the sample. Four, one second exposures (2D images of each sample) were averaged prior to integration. All scattering profiles were corrected for incident beam flux, background scatter due to air, and the variable thickness of each sample. The scattering profiles are displayed as absolute intensity (cm^{-1}) versus the

scattering vector, q, which is a function of the scattering angle through the relationship in Equation 3-6 where λ is the wavelength of radiation (0.82656 Å) and θ is half of the scattering angle (2θ).

$$q = \frac{4\pi}{\lambda}\sin(\theta) \qquad \textbf{Eq. 3-6}$$

Wide Angle X-ray Diffraction (WAXD). Samples included solution-processed Na^+/TBA^+ Nafion® of the following weight percent compositions: 0/100, 25/75, 50/50, 75/25, 100/0 before and after reacidification. X-ray analysis was repeated on the same samples examined during the simultaneous SAXS-WAXS at Argon National Laboratory in order to increase the resolution of the data as well as verify any morphological changes. All membranes were first dried under vacuum at 70 °C for 12 hours and placed in a desiccator prior to analysis. WAXD was performed at the University of Southern Mississippi using a Rigaku Ultima III x-ray diffractometer in reflection mode. A Copper K_α radiation source was used with a beam wavelength of 1.54 Å. The one-dimensional diffraction images were recorded using a computer controlled scintillation counter. Diffraction data was collected every 0.05°, 2θ from 4-25°, 2θ at a scan rate of 0.1°, 2θ per minute. The scattering profiles are displayed as relative intensity as a function of the scattering angle, 2θ. PeakFit® analysis software was used to deconvolute the crystalline peak from the amorphous halo and to determine the percent crystallinity present in the film. First, a linear two-point baseline subtraction was applied to the WAXD profiles followed by fitting the data with three gaussian/lorentzian peaks. The three peaks represented a broad amorphous scattering peak, a distinct amorphous halo, and a crystalline reflection. The three artificial peaks were then numerically fit to the experimental data to obtain the best r^2 value relative to the experimental data. Finally the

percent crystallinity was determined from the ratio of the integrated crystalline peak area versus the entire integrated area under the curve.

MEA Fabrication. The decal technique, as documented in the literature, was used to prepare all MEAs in this study.[35-37] The catalyst inks were prepared by mixing a carbon supported catalyst (30% HP Platinum on Vulcan XC-72) purchased from E-Tek, with 5 wt% TBA^+-form Nafion® solution and isopropanol while stirring overnight to form a "homogeneous" dispersion. The ink was prepared to obtain a Nafion® ionomer content of 30 wt% of the total composition of the dry catalyst ink. The catalyst ink was then coated using a mechanical drawdown drive from BYK Gardner equipped with a vacuum hot plate and a 2 mil multi clearance applicator onto a 0.0762 mm thick decal substrate made of polytetrafluoroethylene-coated fiberglass fabric purchased from McMaster-Carr. The decal was then heated to 90 °C for 15 minutes to fully dry the ink by evaporating the low boiling point alcohols. The process of applying the catalyst ink and heating was repeated on the substrate until the desired Platinum loading was reached (0.5 mg/cm^2). The catalyst layer was transferred from the substrate to the various reacidified solution-processed membranes by hot pressing at 125 °C and 10 MPa for five minutes. The catalyst was decaled in a one step operation on both sides of the membrane. After hot pressing, the two decal blanks were peeled off from the membrane and the Platinum loading was checked by calculating the residual weight of catalyst left on the decaling substrates. The membrane coated with the catalyst was then immersed in methanolic 8M H_2SO_4 for six hours and moderate temperature (60 °C), followed by washing in slightly boiling deionized water for two hours. The geometrically active area of all MEAs prepared was 5 cm^2. Finally, prior to fuel cell testing, gas diffusion layers (GDLs) were

applied to both sides of the catalyst coated membrane. The GDLs, consisting of Carbon paper 2050A, were purchased from the Fuel Cell Store and subsequently washed with acetone to remove any impurities. In order to increase the hydrophobicity of the GDL, they were coated with aqueous fluoropolymer dispersion, TE 3859, provided by E.I. du Pont de Nemours and Company with a target loading of 15-20 wt%. The fluoropolymer coated GDL was then sintered in a convection oven at 320 °C for two hours to allow the fluoropolymer to cover the entire carbon paper. Finally, the GDL was applied to the catalyst coated membrane at 110 °C and 800 psi for 3 mins using a Carver Laboratory Press.

PEMFC Testing. After application of the GDL, the completed MEAs were placed in single-cell fuel cell hardware consisting of two graphite plates with a triple serpentine flow channel pattern machined on the side facing the MEA. The single cell hardware and the MEA were assembled using a micrometric torque wrench adjusted to 5 N·m. In all single-cell experiments, the cathode was fed with high purity grade oxygen at a stoichiometric ratio of 2. The oxygen was humidified by passing through a humidifier set at 55 °C, creating a relative humidity of 80% upon arrival at the cathode side of the MEA. The anode was fed with high purity grade hydrogen at a stoichiometric ratio of 1.5. The hydrogen was humidified by passing through a humidifier set at 70 °C, creating a relative humidity of 100% upon arrival at the anode side of the MEA. The back pressure of the fuel cell was kept at atmospheric pressure at both the anode and cathode, with the operating temperature set at 60 °C throughout the lifetime of the experiment. Prior to fuel cell performance testing, all MEAs equilibrated through an activation period of 12 hours at a constant load of 0.5 V. The fuel cell performance curves were obtained using a

Medusa RD fuel cell test station from Teledyne, coupled with an 890CL fuel cell test system from Scribner, and interfaced with fuel cell software from Scribner.

Results and Discussion

Dynamic Mechanical Analysis (DMA). Dynamic mechanical spectra of solution-processed, mixed counterion membranes before and after reacidification are shown in Figures 3.3 A and B.

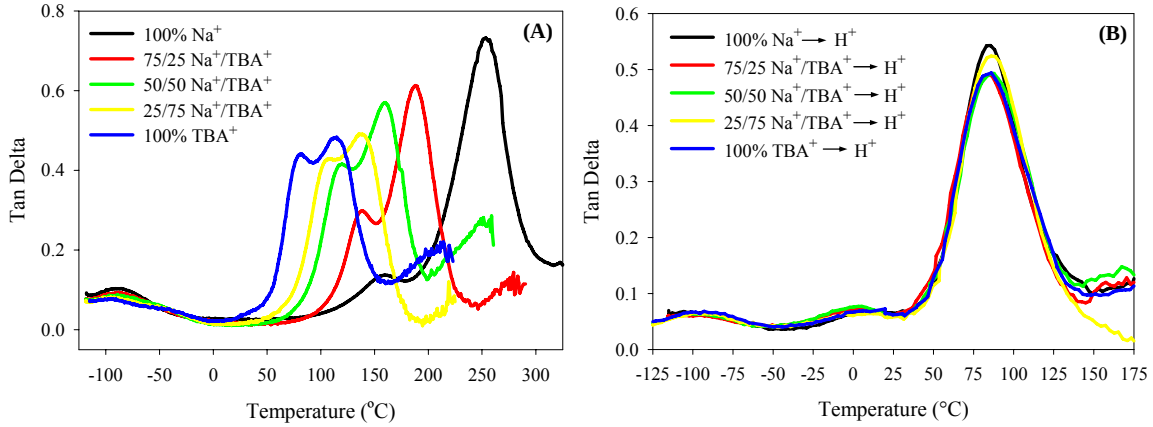

Figure 3.3. **A)** Dynamic mechanical tan delta versus temperature of solution-processed membranes containing mixed counterions Na^+/TBA^+ in the following ratios: 0/100, 25/75, 50/50, 75/25, 100/0. **B)** Dynamic mechanical tan delta versus temperature of solution-processed Na^+/TBA^+ membranes in the following ratios: 0/100, 25/75, 50/50, 75/25, 100/0 after reacidification back into the H^+-form.

The DMA data in Figure 3.3A shows that pure Na^+-form Nafion® displays a strong α-relaxation at 252 °C and low intensity β-relaxation at 160 °C. In the pure TBA^+-form Nafion®, a pair of relaxations are observed with the higher temperature α-relaxation at 112 °C and the lower temperature β-relaxation at 80 °C. The α and β-relaxation temperatures of both Na^+ and TBA^+ form Nafion® are in agreement with previous work from our group investigating the molecular origins of both dynamic mechanical relaxations.[20] Our current understanding of the dynamic mechanical relaxations of Nafion® involves assigning the high temperature α-relaxation to long range motions of

both main and side chains through destabilization of the electrostatic network. The low temperature β-relaxation is assigned as the true glass transition of the polymer and is attributed to the onset of segmental motions, primarily within the backbone, in the context of a static, physically crosslinked matrix.[20, 32, 38]

As the ratio of mixed counterions shifts from pure TBA^+-form to pure Na^+-form Nafion®, as shown in Figure 3.3A, the α and β-relaxations shift to higher temperatures in a uniform fashion. In agreement with Kyu et al.'s study on the partial neutralization of Nafion®, the α and β-relaxation peak intensities increase and decrease, respectively, with increasing neutralization, which in our study involves transitioning from pure TBA^+-form to pure Na^+-form Nafion®.[15] Kyu et al. concluded that the increase in temperature and decrease in intensity of the β-relaxation was explained by an enhancement of the ionic interaction strength, which in turn reduced the mobility of the fluorocarbon matrix. This conclusion also holds true for our mixed counterion system. As the counterion composition changed from pure TBA^+ to pure Na^+-form, a monotonic shift in the strength of the ionic interactions was observed, hence increasing the temperature necessary to induce significant polymer mobility within the static electrostatic network. The data shown in Figure 3.3A are also in agreement with the DMA of Na^+/TBA^+ mixed counterion systems produced by Phillips and Moore.[31] Phillips and Moore comment on how the systematic, compositional increase in the relaxation temperatures with increasing Na^+ content is characteristic behavior of molecularly mixed polymer blends. They assume homogeneous mixing of the ionic aggregates based on the systematic shift in DMA relaxation temperatures, along with elevated temperatures (180 °C) and the ability

of the polar organic solvent (DMSO) to effectively plasticize Nafion® during solution-processing.[39, 40]

DMA was also performed on the various Na^+/TBA^+ mixed counterion membranes after reacidification, as shown in Figure 3.3B. The dynamic mechanical properties of the reacidified films appear to be identical regardless of prior mixed counterion concentration. This data shows that on the macroscopic scale, morphological manipulation of the ionomer domains had no influence on the mechanical properties of the membranes once converted back into the H^+-form. Since Nafion® is currently primarily used in the H^+-form, the DMA data shown in Figure 3.3B is highly relevant.

Small and Wide Angle X-ray Scattering (SAXS-WAXS). Small and wide angle x-ray scattering was incorporated in order to examine the effect of mixed counterions on the organization of both the ionic and crystalline domains. Figure 3.4 displays the SAXS profiles of solution-processed Nafion® containing various ratios of Na^+/TBA^+ counterions.

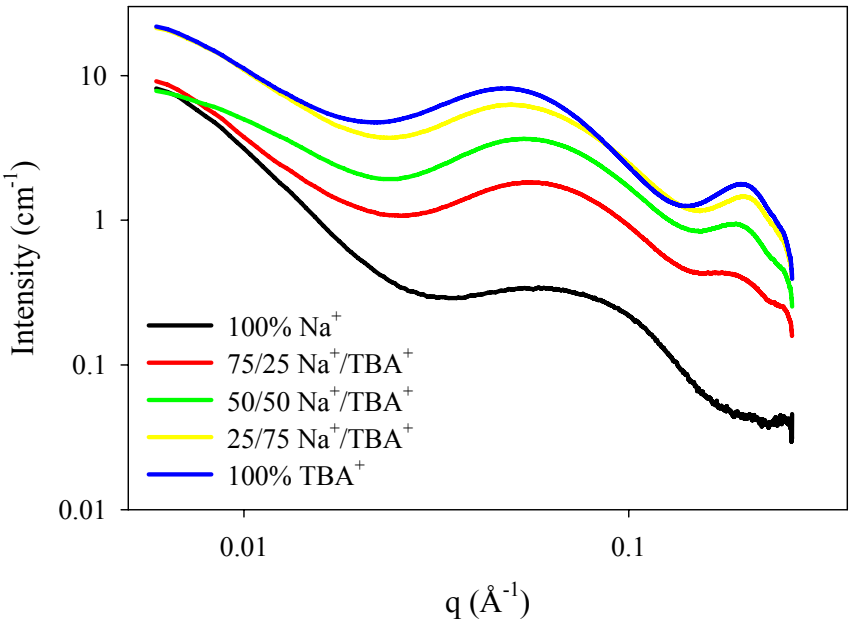

Figure 3.4. SAXS profiles of solution-processed Na^+/TBA^+ mixed counterion membranes.

The solution-processed, TBA^+-form Nafion® SAXS profile contains three typical Nafion® scattering components, the small angle upturn, intercrystalline peak, and ionomer peak. The small angle upturn ($q < 0.02$ Å^{-1}) has been examined by Gebel et al. and is attributed to large scale heterogeneities between the ionomer domain and polymer matrix.[8] The intercrystalline peak ($q \approx 0.05$ Å^{-1}) is often referred to as the scattering between crystalline domains or the crystalline long period.[12] The ionomer peak ($q \approx 0.2$ Å^{-1}) is attributed to the scattering from the interparticle interference between ionic aggregates that are spatially distributed throughout the membrane.[20] Examination of the intercrystalline peak between the five scattering profiles in Figure 3.4 shows a relatively constant peak shape and q spacing, indicating minimal change in the crystalline domain as a function of inorganic/organic mixed counterion content. On the other hand, the overall intensity of the profiles increases along with the emergence of an ionomer peak with increasing TBA^+ content. The increasing scattering intensity and emergence of an ionomer peak is believed to be due to the high scattering contrast between the TBA^+-form ionic aggregates and Nafion®'s fluorocarbon matrix. The disappearance of the SAXS ionomer peak in the Na^+-form has been documented by Fujimura et al., who attributed the disappearance to a small electron density difference between the ionic aggregates and the surrounding scattering medium.[10] To prove this theory, Fujimura and coworkers exchanged the membrane back into the H^+-form, where the electron density of the aggregates became lower than that of the surroundings, and the scattering due to the ionomer peak returned. They also exchanged the membrane into the cesium, Cs^+-form, which increased the electron difference, resulting in an increase in the ionomer peak

intensity. This phenomenon is also evident when examining the ionomer peak at $q \approx 0.2$ Å^{-1} in Figure 3.4 as a function of increasing TBA^+ counterion content.

Further examination of the SAXS profiles, in particular the ionomer peaks, of solution-processed Na^+/TBA^+ mixed counterion membranes after reacidification, are shown in Figures 3.5 A and B.

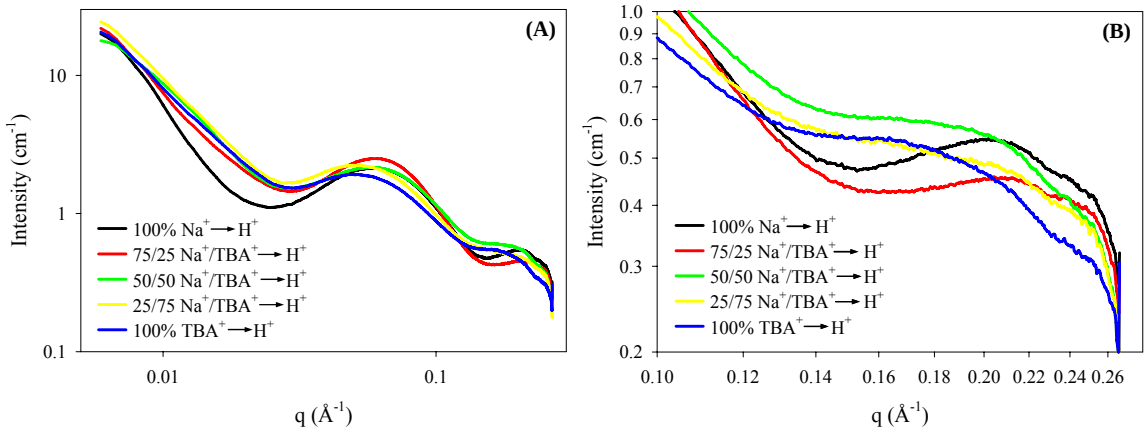

Figure 3.5. A) SAXS profiles of solution-processed Na^+/TBA^+ mixed counterion membranes after reacidification. **B)** SAXS profiles of ionomer region of solution-processed Na^+/TBA^+ mixed counterion membranes after reacidification.

Figure 3.5A displays the SAXS profiles of solution-processed Nafion® with various Na^+/TBA^+ counterion contents after conversion back to the H^+-form. Similar to the SAXS data of the various Na^+/TBA^+ form membranes, the intercrystalline peak ($q \approx 0.05$ Å^{-1}) shape and q spacing remains relatively constant after reacidification. In contrast, the ionomer peak ($q \approx 0.2$ Å^{-1}) appears distorted between the various Na^+/TBA^+ mixed counterion ratios after reacidification. Closer examination of the ionomer peak of reacidified Na^+/TBA^+ mixed counterion membranes is shown in Figure 3.5B as a truncation of the original SAXS profile from Figure 3.5A. From Figure 3.5B, we observe drastic changes to the ionomer peak of mixed Na^+/TBA^+ membranes after reacidification. Upon reacidification of the pure Na^+-form Nafion® membrane, a distinct ionomer peak appears at approximately $q \approx 0.20$ Å^{-1}. The ionomer peak then begins to broaden and

shift to lower q values as the original TBA^+ counterion content of the membranes increases. Reacidification of the pure TBA^+-form membrane yields an ionomer peak maximum at approximately $q \approx 0.17$ $Å^{-1}$, indicating that the distance between the ionic aggregates increases as a function of increasing TBA^+ counterion content within the original solution-processed, mixed counterion membranes. Based on the information displayed in Figure 3.5B, we conclude that the ionic domain of H^+-form Nafion® can be morphologically manipulated by the introduction of mixed inorganic/organic counterion systems prior to reacidification.

Wide angle x-ray scattering was also performed on the mixed Na^+/TBA^+ counterion systems before and after reacidification, shown in Figures 3.6 A and B. Figure 3.6A displays changes to the WAXS profile of solution-processed Nafion® as a function of Na^+/TBA^+ ratio.

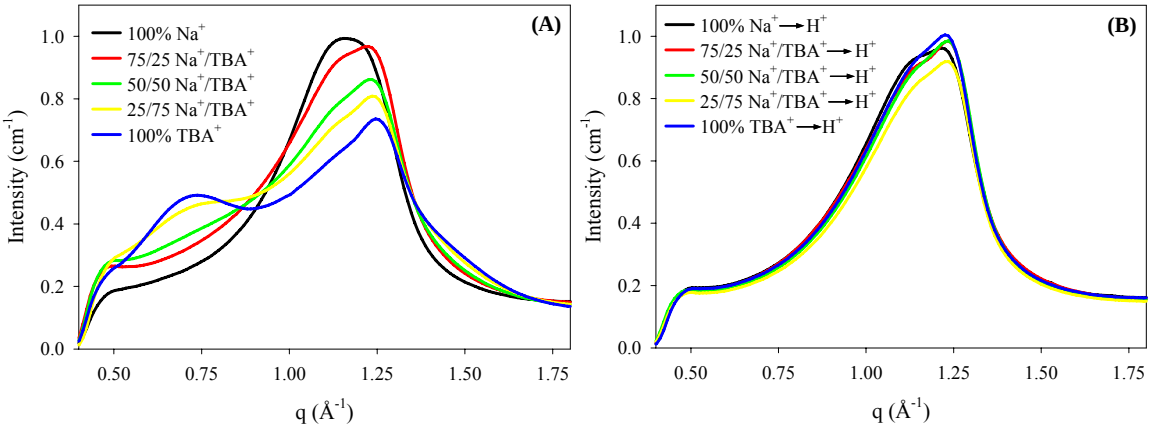

Figure 3.6. A) WAXS profiles of solution-processed Na^+/TBA^+ mixed counterion membranes. **B)** WAXS profiles of solution-processed Na^+/TBA^+ mixed counterion membranes after reacidification.

The WAXS profile for pure Na^+-form Nafion® is in agreement with Fujimura et al., where a broad amorphous halo is present between 0.8-1.4 q, and a faint crystalline reflection exists at 1.26 q.[10] It is apparent based on the data shown in Figure 3.6A, that an extra peak appears at approximately 0.7 q and increases in intensity with increasing

TBA^+ counterion content. Previous work in our research group[41] has shown that the WAXS extra peak may be attributed to counterion condensation of the rod-like aggregates in Nafion®, based on the studies of Diat[42, 43] and Hoffman[44]. Page et al. also determined that the presence of the extra WAXS peak did not influence the position or shape of the amorphous halo or crystalline peak.[41] The data shown in Figure 3.6B verifies that the extra peak is due solely to the presence of TBA^+ counterions based on the disappearance of the peak after reacidification of the membrane. It should be pointed out that the WAXS profiles of the reacidified membranes are in excellent agreement with various WAXS patterns of extruded Nafion® that are widely reported in the literature.[4, 7, 10] The general H^+-form, Nafion® WAXS profile consists of a broad amorphous halo from 0.85-1.42 q along with a distinct crystalline reflection near 1.26 q. The membranes shown in Figure 3.6B have the same amorphous and crystalline morphologies and appear to be identical. However, due to the poor resolution of the WAXS data, we were unable to quantify changes in the crystalline domain of solution-processed, mixed counterion Nafion® membranes before and after reacidification.

Due to the poor WAXS resolution observed in Figures 3.6 A and B, we conducted similar wide angle x-ray diffraction (WAXD) studies at the University of Southern Mississippi in order to quantitatively determine changes in the percent crystallinity of solution-processed, Na^+/TBA^+, mixed counterion Nafion® membranes before and after reacidification. The WAXD results of the mixed counterion membranes before and after reacidification are shown in Figures 3.7 A and B.

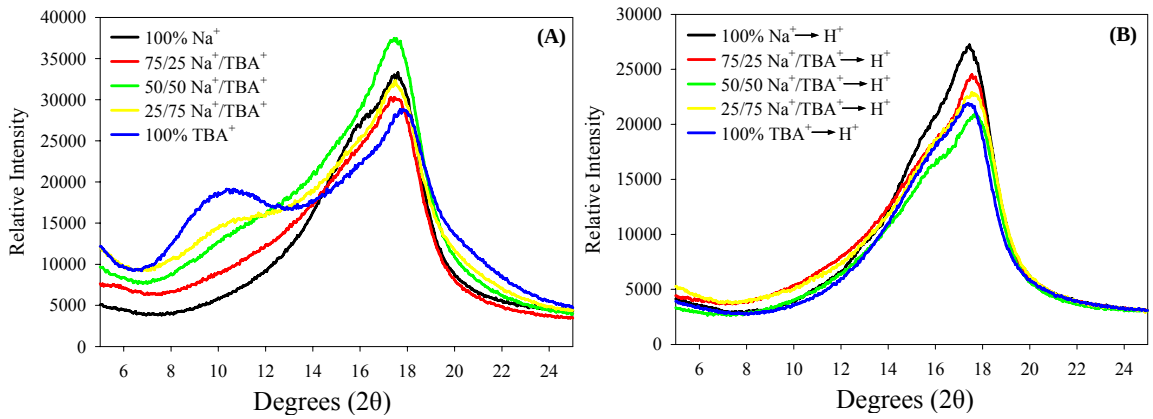

Figure 3.7. A) WAXD profiles of solution-processed Na^+/TBA^+ mixed counterion membranes. **B)** WAXS profiles of solution-processed Na^+/TBA^+ mixed counterion membranes after reacidification.

Similar to the data shown in Figure 3.6, we observe the emergence of an extra peak in Figure 3.7A due to the presence of increasing TBA^+ content within the solution-processed membranes. The peak also disappears after reacidification as shown in Figure 3.7B, further verifying the initial results shown in Figure 3.6. The H^+-form solution-processed Nafion® WAXD profiles are also in agreement with those reported in the literature, consisting of a broad amorphous halo from 12-20°, 2θ and a distinct crystalline reflection near 18°, 2θ.[4, 7, 10] Due to the increased resolution of the crystalline reflection in Figures 3.7 A and B, we were able to deconvolute the crystalline peak from the amorphous halo using PeakFit® analysis and calculate the percent crystallinity present in each membrane. Deconvolution of the crystalline peaks of solution-processed, Na^+/TBA^+, mixed counterion membranes before and after reacidification is shown in Figures 3.8 A and B.

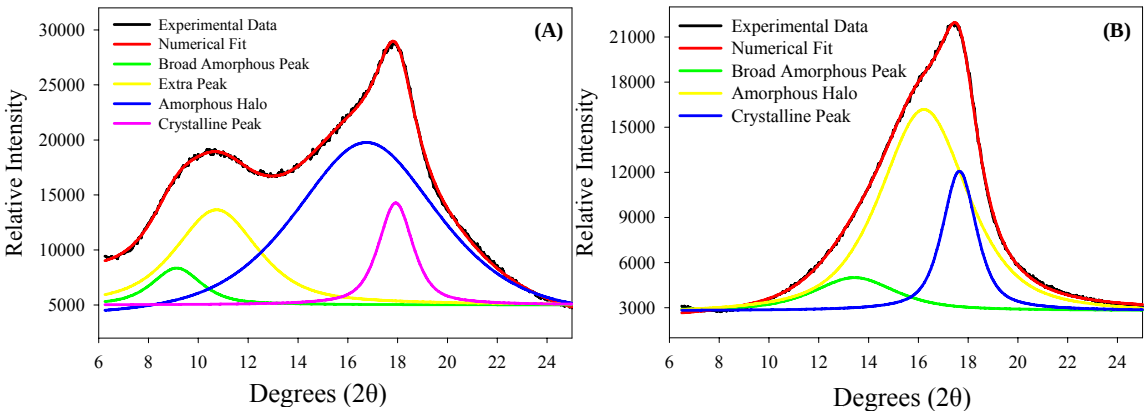

Figure 3.8. WAXD data of **A)** solution-processed Na^+/TBA^+ mixed counterion membranes before and after **B)** reacidification, displaying the deconvolution of the crystalline peak using PeakFit® analysis software.

As shown in Figure 3.8A, four peaks were deconvoluted in order to accurately resolve the entire WAXD profile. The four peaks included the broad amorphous peak, amorphous halo, crystalline peak, and the extra peak, which was only incorporated whenever TBA^+ counterions were present in the membrane. On the other hand, the deconvolution of the data shown in Figure 3.8B involved only the broad amorphous peak, amorphous halo, and crystalline peak due to the absence of TBA^+ counterions contributing to an extra peak. The deconvolution results allowed us to determine the full width at half maximum (FWHM) of the crystalline peak as well as determine the percent crystallinity of each membrane based on the integrated area of the crystalline peak divided by the entire area under the curve. The FWHM and percent crystallinity of the solution-processed, Na^+/TBA^+, mixed counterion membranes before and after reacidification are shown in Tables 3-1 and 3-2, respectively.

Sample	% Xc	FWHM
100% Na^+	21.20	1.76
75/25 Na^+/TBA^+	20.42	1.86
50/50 Na^+/TBA^+	21.10	1.96
75/75 Na^+/TBA^+	17.26	1.83
100% TBA^+	9.97	1.64

Table 3-1. Percent crystallinity and full width at half maximum (FWHM) of solution-processed, Na^+/TBA^+, mixed counterion Nafion® membranes.

From the data shown in Table 3-1, we can conclude that the percent crystallinity of the mixed Na^+/TBA^+ counterion membranes is relatively constant between 20 and 21% until solution-processed with 75 wt% or more of TBA^+-form Nafion® solution. We do not currently have an explanation for the sudden decrease in the percent crystallinity of the pure TBA^+-form membrane other than possible influence of the extra peak on the deconvolution of the crystalline peak in the WAXD profile. The percent crystallinity and FWHM of the crystalline peak, after reacidification of the membranes, are displayed in Table 3-2.

Sample	% Xc	FWHM
100% $Na^+ \rightarrow H^+$	26.02	1.84
75/25 $Na^+/TBA^+ \rightarrow H^+$	20.73	1.60
50/50 $Na^+/TBA^+ \rightarrow H^+$	20.00	1.66
25/75 $Na^+/TBA^+ \rightarrow H^+$	21.02	1.76
100% $TBA^+ \rightarrow H^+$	19.58	1.62

Table 3-2. Percent crystallinity and full width at half maximum (FWHM) of solution-processed, Na^+/TBA^+, mixed counterion Nafion® membranes after reacidification.

Other than the pure Na^+-form Nafion® membrane, the other four mixed counterion membranes exhibit roughly the same quantity of crystallinity after reacidification back to the H^+-form. The percent crystallinity of all of the membranes increased as a function of reacidification, except for the 50/50 Na^+/TBA^+ mixed counterion film, which decreased slightly after conversion to the H^+-form. The largest change in crystallinity occurred for

the pure TBA^+-form membrane, which went from approximately 10 to 20% crystalline after refluxing in methanolic 4M H_2SO_4. We currently cannot explain such a large increase in percent crystallinity during reacidification, especially due to the process occurring at relatively low temperatures compared to the melting point of Nafion® crystallites.[7] Overall, the crystalline and amorphous regions of the solution-processed, Na^+/TBA^+, mixed counterion membranes appear to be morphologically similar after reacidification. We conclude that even though dramatic differences are observed in the WAXD profiles of the various Na^+/TBA^+ mixed counterion membranes, Nafion® is typically utilized in the H^+-form, and upon reacidification the WAXD profiles of the membranes appear to be identical, suggesting similar morphologies.

Water Uptake and Proton Conductivity Analysis. The percent water uptake and moles of water/moles of sulfonate (λ) for solution-processed, Na^+/TBA^+, mixed counterion membranes before and after reacidification are displayed in Figure 3.9.

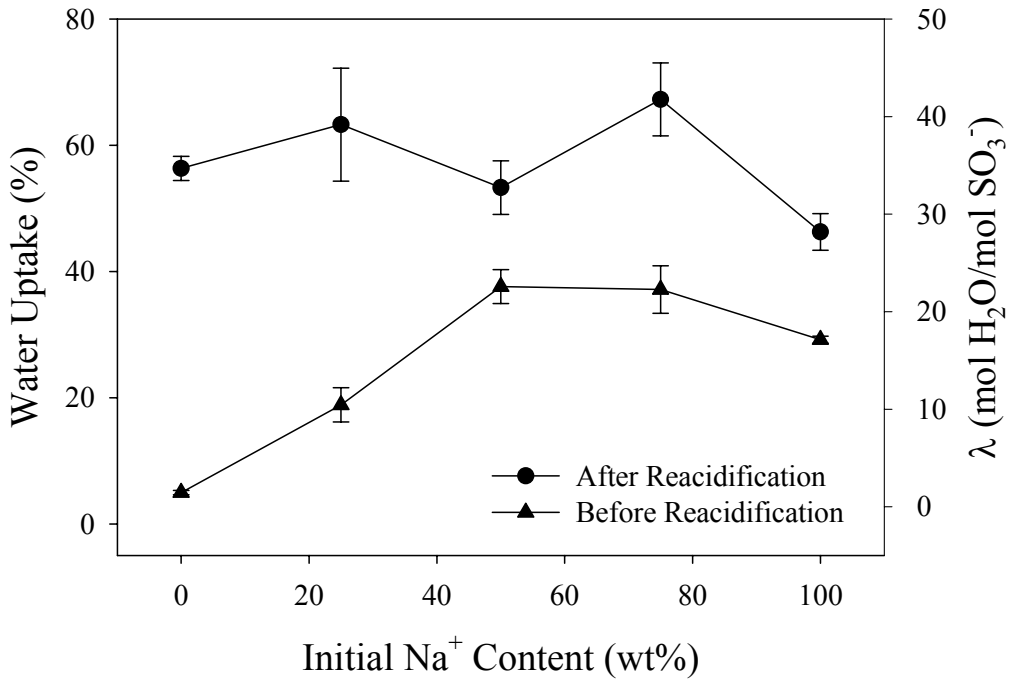

Figure 3.9. Percent water uptake and water content (λ) of solution-processed Na^+/TBA^+ Nafion® membranes before and after reacidification as a function of initial Na^+ counterion content.

The water uptake and λ values of the solution-processed, Na^+/TBA^+, mixed counterion membranes reach a plateau at 50% Na^+ counterion content and decrease slightly after 100% neutralization into the Na^+-form, shown in Figure 3.9. This trend is similar to the results of Phillips and Moore and is attributed to the hydrophobic character of the TBA^+ counterion along with the relative uniform distribution of the Na^+ and TBA^+ ions within the aggregates.[31] After reacidification of the mixed counterion membranes, the water uptake and lambda values appear to reach an equilibrium of approximately 60% or λ = 36 except for the reacidified pure Na^+-form film, which has a water uptake of 46% and λ = 28. The relatively constant water uptake of the H^+-form membranes, with the exception of the reacidified, pure Na^+-form membrane, is drastically different than the results of Phillips and Moore, who observed maximum lambda values of approximately 50 for membranes previously in the pure Na^+ and pure TBA^+-forms. They also witnessed a minimum lambda value of 34 for H^+-form membranes originally composed of a 50/50 Na^+/TBA^+ composition. Phillips and Moore concluded that the water uptake values of the reacidified membranes are surprisingly dependent on the original counterion composition used during solution-processing of the membrane. Our results, shown in Figure 3.9, display that the solution-processing counterion content has minimal impact on the resulting water uptake of the membranes after reacidification.

Figure 3.10 shows the proton conductivity of the solution-processed, Na^+/TBA^+, mixed counterion membranes after reacidification.

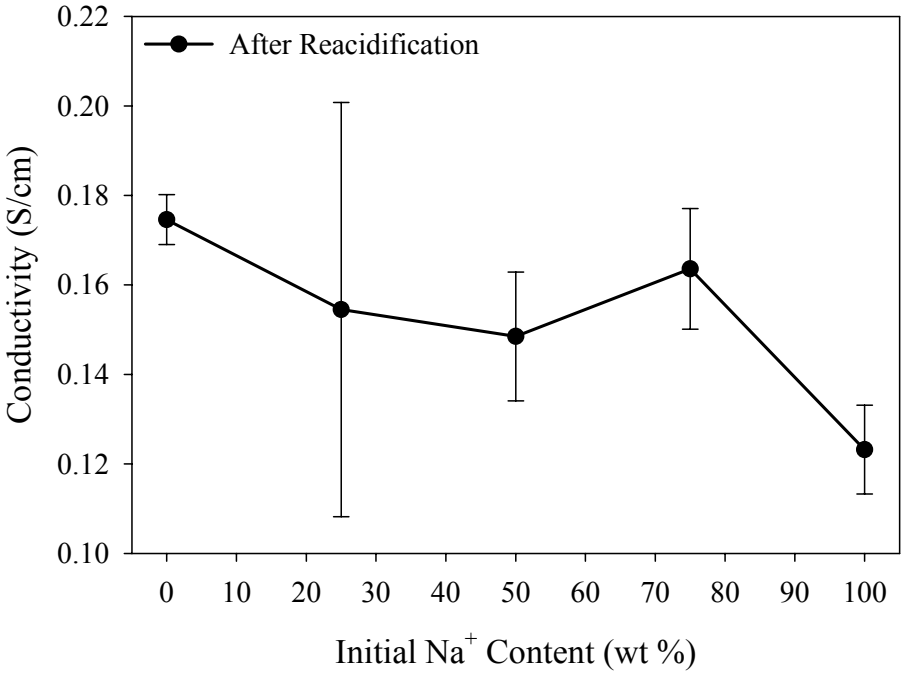

Figure 3.10. Proton conductivity of solution-processed Na^+/TBA^+ Nafion® membranes after reacidification as a function of initial Na^+ counterion content. Bekktech 4-pt conductivity cell was submersed in deionized water at 80 °C throughout test.

From Figure 3.10, a minimum average proton conductivity (σ = 0.123 S/cm) is observed for the reacidified, pure Na^+ counterion membrane, while a maximum average proton conductivity (σ = 0.175 S/cm) occurs for the reacidified, pure TBA^+ counterion film. Based on this data, we assume a more favorable proton percolation pathway is achieved after reacidification of the pure TBA^+-form membrane. In agreement with Phillips and Moore, this behavior suggests that during solution-processing, the nature of ion-ion and/or ion-solvent interactions influence the organization of the ionic domains in the resulting polymer film. The data shown in Figure 3.10 can also be related to changes in the ionomer morphology upon reacidification of the membranes, previously shown in Figure 3.5B. The SAXS data in Figure 3.5B showed that the H^+-form ionic domain of Nafion® can be manipulated via solution-processing with various Na^+/TBA^+ mixed counterion solutions. The reacidified ionomer peak appeared to broaden and shift to

lower *q* values with increasing TBA^+ content within the original membrane. The change in the ionomer peak shape and position appears to have a major influence on the resulting proton conductivity of the membrane, as shown in Figure 3.10. Further studies are necessary in order to verify whether the SAXS ionomer peak shape or *q* spacing has the largest influence on the resulting proton conductivity of H^+-form Nafion®.

Proton Exchange Membrane Fuel Cell (PEMFC) Testing. Figure 3.11 shows the performance and power density curves of solution-processed, Na^+/TBA^+, mixed counterion membranes after reacidification as a function of current density. The data in Figure 3.11 indicate that the fuel cell performance after reacidification increases with increasing TBA^+ content of the solution-processed membrane.

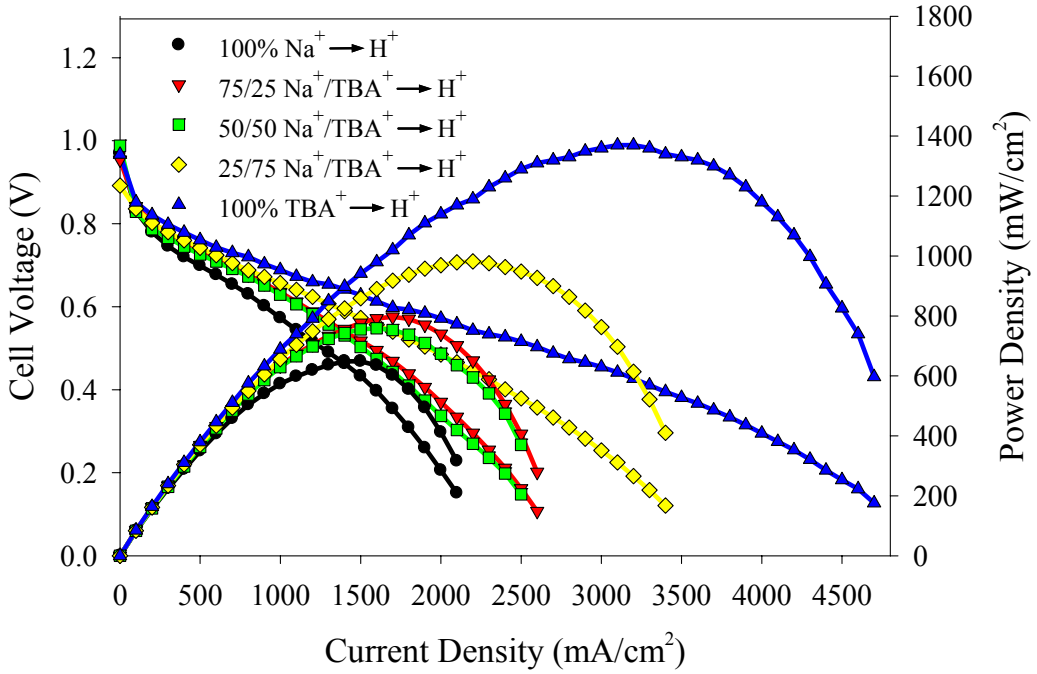

Figure 3.11. H_2/O_2 fuel cell polarization and power density curves of solution-processed Na^+/TBA^+ mixed counterion membranes after reacidification. (T cell = 60 °C, T anode tank = 70 °C, T cathode tank = 55 °C, 100% relative humidity at anode, 80% relative humidity at cathode, H_2/O_2 stoichiometry = 1.5:2)

The reacidified, pure Na^+-form membrane's maximum power density is 620 mW/cm^2 at a current density of approximately 1500 mA/cm^2, while the reacidified, pure TBA^+-form

membrane's maximum power density is 1400 mW/cm^2 at 3500 mA/cm^2, which is more than twice that of the reacidified Na^+-form membrane. In agreement with previously mentioned SAXS and proton conductivity data, it appears that the morphology of the H^+-form membranes can be manipulated through the incorporation of various Na^+/TBA^+ counterions during solution-processing, allowing for drastic fluctuations in the resulting fuel cell properties. The dramatic increase in fuel cell performance of the reacidified TBA^+-form membrane is believed to be contributed to the more efficient proton percolation pathway created during solution-processing. This is direct evidence indicating that Nafion® membrane properties can be controlled through morphological manipulation of the ionic domain during solution-processing with various organic or inorganic counterions.

Conclusions

Solution-processing Nafion® membranes containing various mixtures of Na^+ and TBA^+ counterions resulted in a vast array of mechanical and morphological properties. Dynamic mechanical analysis results showed that the mixed counterion membranes behave as a molecularly mixed system. Both the α and β-relaxations were observed at temperatures intermediate of either pure TBA^+ or Na^+, and shifted based on the counterion composition incorporated during solution-processing. SAXS analysis of the mixed counterion membranes after reacidification showed that the resulting ionomer morphology is dependent on the initial counterion composition during solution-processing. Upon reacidification of the pure TBA^+-form membrane, the SAXS ionomer peak broadened and shifted to lower q values. In contrast, the SAXS ionomer peak of reacidified, Na^+-form Nafion® appeared narrower and was shifted to a higher q value in

relation to the reacidified TBA^+ peak. Manipulation of the ionic domain of solution-processed Nafion® was evident based on the proton conductivity analysis of the H^+-form of the membrane. The reacidified, TBA^+-form membrane exhibited an average proton conductivity 30% higher than that of reacidified, Na^+-form solution-processed Nafion®. The dramatic change in proton conductivity between the two membranes is believed to be attributed to the morphological manipulation of the ionic domain during solution-processing. Solution-processing membranes in the pure TBA^+-form allowed for a more efficient percolation pathway for protons to travel, hence higher proton conductivity. Similar results were also observed during hydrogen/oxygen fuel cell performance tests. The reacidified, TBA^+-form membrane significantly outperformed the reacidified, Na^+-form membrane by achieving higher current and power densities under the same load conditions. The fuel cell performance properties, changes to the SAXS ionomer peak, and proton conductivity results are all examples of how the manipulation of the morphology of H^+-form Nafion® is possible via incorporation of various mixtures of organic and inorganic counterions during initial solution-processing of the polymer.

Acknowledgements

Portions of this work were performed at the DuPont-Northwestern-Dow Collaborative Access Team (DND-CAT) located at Sector 5 of the Advanced Photon Source (APS). DND-CAT is supported by E.I. DuPont de Nemours & Co., The Dow Chemical Company and the State of Illinois. Use of the APS was supported by the U. S. Department of Energy, Office of Science, Office of Basic Energy Sciences, under Contract No. DE-AC02-06CH11357.

The authors would also like to acknowledge the assistance of the Polymer Science Department at the University of Southern Mississippi for the use of their wide angle x-ray diffractometer.

References

(1) Mauritz, K. A.; Moore, R. B. *Chemical Reviews* **2004,** 104, (10), 4535-4585.
(2) Hsu, W. Y.; Gierke, T. D. *Journal of Membrane Science* **1983,** 13, 307-326.
(3) Doyle, M.; Rajendran, G., Perfluorinated membranes. In *Handbook of Fuel Cells - Fundamentals, Technology and Applications*, Wolf Vielstich, A. L., and Hubert A. Gasteiger, Ed. John Wiley & Sons, Ltd, Chichester: 2003; Vol. 3 Part 3, pp 351-395.
(4) Starkweather, H. W. *Macromolecules* **1982,** 15, (2), 320-323.
(5) Moore, Robert. B.; Martin, Charles R. *Macromolecules* **1988,** 88, (21), 1334-1339.
(6) Eisenberg, A.; Hird, B.; Moore, R. B. *Macromolecules* **1990,** 23, 4098-4107.
(7) Gierke, T.D.; Munn, G.E.; Wilson, F.C. *Journal of Polymer Science: Polymer Physics Edition* **1981,** 19, 1687-1704.
(8) Gebel, Gerard; Lambard, Jacques. *Macromolecules* **1997,** 30, 7914-7920.
(9) Gebel, G. *Polymer* **2000,** 41, (15), 5829-5838.
(10) Fujimura, M.; Hashimoto, T.; Kawai, H. *Macromolecules* **1981,** 14, (5), 1309-1315.
(11) Schmidt-Rohr, K.; Chen, Q. *Nature Materials* **2008,** 7, (1), 75-83.
(12) Page, K. A.; Landis, F. A.; Phillips, A. K.; Moore, R. B. *Macromolecules* **2006,** 39, (11), 3939-3946.
(13) Hodge, I. M.; Eisenberg, A. *Macromolecules* **1978,** 11, (2), 289-293.
(14) Yeo, S.; Eisenberg, A. *Journal of Applied Polymer Science* **1977,** 21, 875-898.
(15) Kyu, T.; Hashiyama, M.; Eisenberg, A. *Canadian Journal of Chemistry* **1983,** 61, 680-687.
(16) Miura, Y.; Yoshida, H. *Thermochimica Acta* **1990,** 163, 161-168.
(17) Moore, Robert B.; Cable, K. M.; Croley, T. L. *Journal of Membrane Science* **1992,** 75, (1), 7-14.
(18) Moore, R. B.; Cable, K. *Polymer Preprints* **1997,** 38, 272-273.
(19) Young, S.; Mauritz, K. *Journal of Polymer Science: Polymer Physics Edition* **2001,** 39, 1282-1295.
(20) Page, K. A.; Cable, K. M.; Moore, R. B. *Macromolecules* **2005,** 38, (15), 6472-6484.
(21) E. I. Dupont De Nemours & Co Inc. *DuPont™ Nafion® PFSA Membranes NRE-211 and NRE-212*. http://www.fuelcellmarkets.com/content/images/articles/nae201.pdf (January 3, 2009).
(22) E. I. Dupont De Nemours & Co Inc. *DuPont™ Nafion® PFSA Membranes N-115, N-117, NE-1110*.

http://www.fuelcellmarkets.com/content/images/articles/nae101.pdf (January 3, 2009).
(23) Curtin, D. E.; Lousenberg, R. D.; Henry, T. J.; Tangeman, P. C.; Tisack, M. E. *Journal of Power Sources* **2004,** 131, (1-2), 41-48.
(24) Moore, Robert B.; Martin, Charles R. *Analytical Chemistry* **1986,** 58, 2569-2570.
(25) Grot, W. G. *Production of a liquid composition containing a perfluorinated ion exchange polymer*. Patent EP0066369, 1982.
(26) Martin, Charles R.; Rhoades, Teresa A.; Ferguson, James A. *Analytical Chemistry* **1982,** 54, (9), 1639-1641.
(27) Yeager, H. L.; Kipling, B.; Dotson, R. L. *Journal of the Electrochemical Society* **1980,** 127, (2), 303-307.
(28) Yeager, H. L.; Steck, A. *Journal of the Electrochemical Society* **1981,** 128, (9), 1880-1884.
(29) Bosnjakovic, A.; Schlick, S. *Journal of Physical Chemistry B* **2004,** 108, (14), 4332-4337.
(30) Cable, Kevin M.; Mauritz, Kenneth A.; Moore, Robert B. *Journal of Polymer Science Part B: Polymer Physics* **1995,** 33, 1065-1072.
(31) Phillips, A. K.; Moore, R. B. *Journal of Polymer Science Part B-Polymer Physics* **2006,** 44, (16), 2267-2277.
(32) Osborn, S.; Hassan, M.; Divoux, G.; Rhoades, D.; Mauritz, K.; Moore, R. B. *Macromolecules* **2007,** 40, (10), 3886-3890.
(33) Landis, F. A.; Moore, R. B. *Macromolecules* **2000,** 33, (16), 6031-6041.
(34) Takamatsu, T.; Eisenberg, A. *Journal of Applied Polymer Science* **1979,** 24, 2221-2235.
(35) Xie, J.; Garzon, F.; Zawodzinski, T.; Smith, W. *Journal of the Electrochemical Society* **2004,** 151, (7), A1084-A1093.
(36) Xie, J.; More, K. L.; Zawodzinski, T. A.; Smith, W. H. *Journal of the Electrochemical Society* **2004,** 151, (11), A1841-a1846.
(37) Ren, X. M.; Wilson, M. S.; Gottesfeld, S. *Journal of the Electrochemical Society* **1996,** 143, (1), L12-L15.
(38) Page, K.; Jarrett, W.; Moore, R. B. *Journal of Polymer Science Part B: Polymer Physics* **2007,** 45, 2177-2186.
(39) Yeo, R. S. *Polymer* **1980,** 21, (4), 432-435.
(40) Belmares, M.; Blanco, M.; Goddard, W. A.; Ross, R. B.; Caldwell, G.; Chou, S. H.; Pham, J.; Olofson, P. M.; Thomas, C. *Journal of Computational Chemistry* **2004,** 25, (15), 1814-1826.
(41) Page, K. A. The Influence of Electrostatic Interactions on Chain Dynamics and Morphological Development in Semi-Crystalline Perfluorosulfonate Ionomers. University of Southern Mississippi, Hattiesburg, 2005.
(42) Rollet, A. L.; Diat, O.; Gebel, G. *Journal of Physical Chemistry B* **2002,** 106, (12), 3033-3036.
(43) Diat, O.; Lyonnard, S.; Gebel, G.; Rollet, A. L. *Physica B: Condensed Matter* **2004,** 350, e959-e962.
(44) Hoffmann, H.; Wurtz, J. *Journal of Molecular Liquids* **1997,** 72, 191-230.

CHAPTER 4

EFFECT OF THERMAL TREATMENTS ON THE MORPHOLOGY AND MECHANICAL PROPERTIES OF DISPERSION-CAST NAFION®

Introduction

Developed by DuPont de Nemours & Co. in the 1960's, Nafion® is a copolymer of tetrafluoroethylene (TFE) and a perfluorinated vinyl ether monomer.[1] Recognized for its high ionic conductivity and excellent stability, Nafion® has gained high acclaim for its performance as a Polymer Electrolyte Membrane (PEM) and is currently the benchmark ionomer used in chlor-alkali cells[2] and PEM Fuel Cells (PEMFCs).[3] However, many properties of Nafion® have not been fully explored and therefore render the perfluorosulfonate ionomer the focus of this research. It is our particular goal to elucidate the relationship of solution-processing temperatures upon the morphological and mechanical properties of the resulting membranes.

Nafion® is capable of forming "teflon-like" crystallites based on the ratio of perfluorovinyl ether side chains to polytetrafluoroethylene backbone units shown in Figure 4.1 as (*n*/*x*).

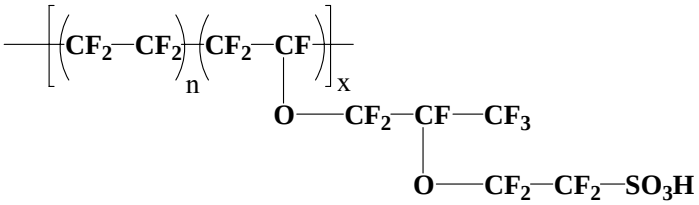

Figure 4.1. Chemical structure of Nafion®.

The extent of branching is displayed in terms of equivalent weight (EW), which is defined as the grams of polymer per equivalent of sulfonic acid.[4] The equivalent weight

can be determined by acid-base titration, analysis of atomic sulfur, and Fourier transform infrared spectroscopy.[5] Determination of EW for Nafion® is shown in Equation 4-1, where 100 is the molecular weight of one $(CF_2\text{-}CF_2)$ unit and 443 is the molecular weight of the sidechain.

$$EW = 100(n) + 443 \qquad \textbf{Eq. 4-1}$$

The most common EW for Nafion® reported in the literature is 1100 g/mol SO_3^-.[3] Based on a complete random copolymerization, an EW of 1100 would yield an *n* value of approximately 6.57, or twelve to fourteen CF_2 units in the backbone, capable of crystallization.

An application of great interest for Nafion® is the proton exchange membrane fuel cell. PEMFCs rely on the excellent chemical and mechanical stability of perfluorosulfonate ionomers, such as Nafion®, to serve as a separator membrane between an anode and cathode.[6] The main two types of PEMFCs used for portable and transportation power are the hydrogen/oxygen (H_2/O_2) and direct methanol fuel cells (DMFC).[7] The purpose of both types of fuel cells is to convert chemical energy into electrical energy.[8] To maximize the energy efficiency during fuel cell operation, the proton exchange membrane must be able to minimize the diffusion of water for an H_2/O_2 fuel cell, or water and methanol for a DMFC between the anode and the cathode. It has been demonstrated that methanol crossover during DMFC operation causes depolarization losses at the cathode as well as overall fuel conversion losses.[9] Furthermore, perfluorosulfonate ionomers which exhibit a high affinity for methanol and water can lead to decreased mechanical properties[10] as well as increased stresses due to the hydration/dehydration cycles during fuel cell operation.[11]

Dupont has shown that the production method used in creating Nafion® membranes plays a crucial role in the water uptake of the film.[12, 13] For the past forty years, the main method for producing Nafion® membranes was through melt extrusion of a sulfonyl fluoride (SO_2F) precursor. This was followed by hydrolysis to convert the precursor into the sulfonate ionomer (SO_3^-).[3, 5] Dupont has recently introduced dispersion-cast membranes which exhibit lower thicknesses and higher water uptake values when compared to their extruded counterparts.[14] The casting procedure involves applying the polymer dispersion onto a base film, drying both materials, applying a coversheet, and winding onto a master roll. The focal point of this publication will be to discuss the effects of thermal treatments on the mechanical integrity of dispersion-cast Nafion® when subjected to boiling methanol.

In the early 1980's, two publications by Grot[15] and Martin[16] detailed a procedure for dissolving Nafion® membranes in water/alcohol mixtures at elevated temperatures and pressures. Martin et al. developed a procedure for the dissolution of Nafion® based on the solvent swelling studies of Yeo and coworkers on 1100 and 1200 EW Nafion®.[17] Martin et al. demonstrated that high temperature and pressure were necessary to obtain high degrees of swelling and to melt the polytetrafluoroethylene crystallites present in the membrane.[16]

Even though Nafion® solutions have been utilized for a variety of applications, it has been assumed that the morphologies, physical properties, and chemical characteristics of the cast membranes were identical to the as-received films. Based on various casting procedures of Nafion® solutions, Moore and Martin discovered that cast Nafion® is drastically different from as-received Nafion®.[18-20]

Membranes cast at room temperature from ethanol/water Nafion® dispersions were classified as recast films due to their brittleness, presence of mud cracks, and solubility in various polar organic solvents at room temperature. In contrast, the as-received Nafion® membranes were tough, pliable, and insoluble in virtually all solvents at temperatures below 200 °C. Moore and Martin then developed a "solution-processing" procedure to reconstitute the desired mechanical properties of as-received Nafion® from recast Nafion®.[18, 19] Solution-processing, shown schematically in Figure 4.2, involved adding a high boiling point solvent (ie. dimethylsulfoxide or dimethylformamide) to the alcohol-water system to disrupt the colloidal particles and allow casting at an elevated temperature.

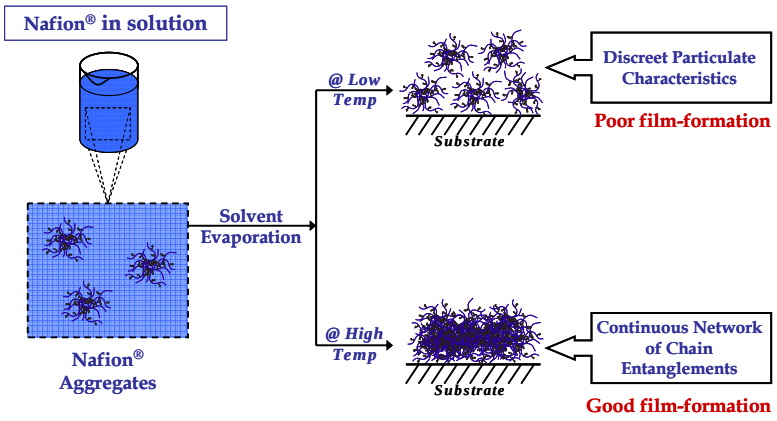

Figure 4.2. Effect of solution-processing temperature and solvent on film formation of Nafion® membranes.

Combination of the elevated casting temperature and the plasticizing effect of the solvent provided the chain mobility necessary to facilitate macromolecular organization and increased chain entanglement of Nafion® within the solution, thereby producing mechanically stable membranes.

Moore and Martin also documented the percent solubility of solution-processed membranes by determining the percent weight loss after sonicating the films in a 50:50

ethanol/water mixture for one hour. Membranes with a percent solubility below 5% were considered satisfactory in terms of mechanical properties in comparison to the as-received membranes. Membranes with less than 5% solubility were obtained by solution-processing in dimethylsulfoxide (DMSO) at 170 °C, ethylene glycol (EG) at 185 °C, or *N*,*N*' dimethylformamide (DMF) at 130 °C.[19] The authors, therefore, concluded that the percent solubility of the Nafion® membranes was critically dependant on the solvent evaporation temperature.

Gebel et al. reported a casting procedure for Nafion® where a high boiling point solvent was added to an ethanol/water/Nafion® solution and allowed to evaporate to completeness at room temperature.[21] The room temperature dried membrane was noted to be clear and uncracked, but soluble in various polar solvents. Gebel and coworkers then annealed the membrane under vacuum at approximately 200 °C, producing a film with properties similar to the solution-processed membranes of Moore and Martin. Various publications studying the morphology, proton transport, and water uptake of solvent cast Nafion® using either the solution-processing technique of Moore and Martin or the thermal annealing technique of Gebel et al. have played a critical role in the assessment of the ionomer.[19, 21-32]

Although the effect of thermal treatments on cast Nafion® has been well documented, it is surprising to notice the lack of information on annealing extruded or dispersion-cast Nafion®. One of the first publications involving annealing of extruded Nafion® was published by Gierke et al.[33] Gierke and coworkers examined the effects of annealing temperature on both the wide angle x-ray diffracation (WAXD) and small angle x-ray scattering (SAXS) profiles of the unhydrolyzed Nafion® precursor. Based on

WAXD results, the Nafion® precursor crystalline reflection at 18°, 2θ gradually decreased in intensity from 50-250 °C and finally disappeared above 270 °C. On the contrary, the SAXS intercrystalline peak at 0.6°, 2θ increased with increasing temperature and disappeared above 270 °C. Upon cooling, a reemergence of the small angle crystalline peak was noticed, verifying its relationship with the electron density difference between crystalline and amorphous polymer domains. Along with DSC measurements, the authors noted that the melting point of the Nafion® precursor crystallites is approximately 275 °C. It was assumed that Nafion® crystallites melt over a much broader range than the crystallites present in PTFE, which melt around 330 °C. After hydrolysis and conversion into the Ag^+ counterion form, Gierke et al. noticed the appearance of an ionomer peak in the SAXS profiles at approximately 2.0°, 2θ. Minimal changes were seen in either peak shape or intensity after annealing the Ag^+-form Nafion® membranes from room temperature to 290 °C. The persistence of this peak above the Nafion® crystallite melting temperature provided strong evidence that the peak was due to the existence of ionic clustering. Since Gierke's work, various publications have directly or indirectly involved examining the effects of annealing as-received Nafion®.[34-45]

Fujimura and coworkers went beyond the study of Gierke et al. by examining the effects of increased temperature on the SAXS and WAXD profiles of both H^+ and Cs^+-form Nafion®.[34] Similar to Gierke's study of the Nafion® precursor, Fujimura et al. noticed a disappearance of the crystalline reflection in the WAXD profile of H^+-form Nafion® upon heating to 275 °C. Upon cooling back to room temperature the peak reappeared, confirming its association with the melting and recrystallization of the

polymer. Fujimura et al. note that the melting point is well below that of PTFE due to the existence of sidechains in Nafion® which inhibit crystallization. By neutralizing Nafion® into the Cs^+-form, Fujimura et al. were able to increase the scattering intensity of the ionomer peak, allowing for more accurate examination of the effects of temperature. A shift of the ionomer peak to larger *q* values was observed after increasing the temperature to 276 °C. The shift in the ionomer peak indicated that the intercluster distance decreases with temperature. The authors assume that the smaller distances between clusters is due to inherently smaller cluster sizes based on the increased thermodynamic work of elastic deformation of coils required for the cluster formation.

Thomas and coworkers examined the effects of annealing Nafion® coated electrodes neutralized with a series of quaternary ammonium counterions: ammonium (NH_4^+) and tetramethylammonium ($N(CH_3)_4^+$) through tetrapentylammonium ($N(C_5H_{11})_4^+$).[37] On average, Thomas et al. noticed a significant increase in the ion-exchange capacity (IEC) of the cast membranes after annealing at 140 °C for 25 minutes. The IEC of H^+-form Nafion® increased from 907 x 10^{-6} mol/g to 1023 x 10^{-6} mol/g after being thermally treated. Thomas et al. explain this phenomenon based on a restructuring of the membrane by annealing above the dynamic mechanical α-relaxation transition temperature (110 °C).

Zawodzinski and coworkers examined the effect of drying H^+-form Nafion® at 105 °C and the subsequent water uptake at various temperatures.[38] As-received H^+-form Nafion®, without any prior thermal treatment, was noted as having a water uptake of λ = 21 mol water/mol sulfonate when subjected to water temperatures ranging from 27-94 °C. Upon annealing H^+-form Nafion® at 105 °C for an unspecified time, Zawodzinski et al.

noticed a significant change in the rehydration properties of the membrane. Reexposure of the annealed Nafion® membrane to liquid water at room temperature resulted in an equilibrium water uptake value of 12 mol water/mol sulfonate. A 50% decrease in water uptake was documented based on the effect of thermal history on the rehydration properties of Nafion®. Further studies showed that the equilibrium water uptake increased with increasing rehydration temperature. Annealed Nafion® membranes subjected to water baths at 65 and 80 °C saw water uptake values of 14 and 16 mol water/mol sulfonate, respectively. Even after exposure to a water bath at 80 °C, annealed Nafion® membranes possessed less water than their as-received counterparts, which had undergone no thermal treatments. Zawodzinski et al. concluded that the thermal history of Nafion® plays a crucial role in the membrane morphology as well as overall performance.[38]

Coinciding with the study by Zawodzinski et al., Sone and coworkers examined the proton conductivity of Nafion® annealed at 80, 105, and 120 °C.[40] The proton conductivity, measured at 100% relative humidity, subsequently decreased with increasing annealing temperature, resulting in a change from 0.09 S/cm for commercial Nafion® to 0.03 S/cm for Nafion® annealed at 120 °C. Sone et al. concluded that by increasing the annealing temperature near the dynamic mechanical α-relaxation transition temperature, a significant decrease in both water uptake and proton conductivity was observed.

With the aid of SANS, Rollet et al. studied the influence of both counterion form and thermal treatment on the nanostructure of Nafion®.[41] By exchanging Nafion® into both the tetramethylammonium (TMA^+) and Na^+ counterion forms and annealing at

120 °C, Rollet et al. observed a significant decrease in the ionomer cavity radius with annealing temperature. Unlike the reversible reorganization of ionic domains during counterion exchange, the effects of thermal annealing at 120 °C were irreversible and were believed to occur on a much larger size scale than the local exchange of counterions.

While creating a fundamental understanding of the molecular motions of Nafion®, Page et al. examined the effects of thermal treatments on extruded Nafion® 117 using DSC, SAXS, and solid-state nuclear magnetic resonance (SS-NMR).[42] Thermal annealing of extruded Nafion® 117 was accomplished in the DSC after drying at 120 °C for two hours and erasing the thermal history by heating samples to 330 °C for five minutes and cooling back to room temperature. Nafion® in both the Na^+ and Cs^+-forms were then annealed in the DSC at 200 °C for 0.5, 2, 6, 12, and 24 hours. For both counterion forms of the ionomer, the initial heating scan produced a broad endotherm between 200 and 250 °C. After quenching from 330 °C, the broad endotherm was erased but reappeared upon annealing at 200 °C for various times. Based on the thermal behavior of semicrystalline polymers with slow crystallization kinetics, the broad endotherm was assigned to the melting of PTFE-like crystallites. For Na^+-form Nafion®, Page et al. observed an initial endotherm with a heat of fusion (ΔH) of 5 J/g. After quenching from the melt at 330 °C and annealing at 200 °C for 24 hours, the endothermic event reappeared with a ΔH of 2.7 J/g or approximately 50% of the original crystallinity. SAXS analysis verified the reconstitution of crystallinity due to the emergence of the crystalline peak at $q = 0.5$ nm^{-1} upon annealing Na^+-form Nafion® at 200 °C for 24 hours. The DSC results of Cs^+-form Nafion® quenched from the melt and annealed at 200 °C for 24 hours showed an endothermic event with a ΔH of 5.3 J/g, which was approximately

100% of the original endotherm before any thermal treatment. Based on the DSC data, Page et al. showed that changing the counterion drastically changes the crystallization kinetics due to manipulation of the dipole-dipole interactions between ionic moieties. Page et al. also examined the effect of annealing temperature on the crystallization of Cs^+-form Nafion® by annealing in the DSC for two hours at 120, 150, 180, 210, and 240 °C. The DSC data showed that two endothermic events appeared upon annealing Cs^+-form Nafion®. For each annealing treatment, the low temperature endotherm occurred 20-30 °C above the respective annealing temperature, while the high temperature endotherm remained constant between 240-250 °C. Based on a shift of the low temperature endotherm to higher temperatures upon annealing, Page et al. concluded that the endothermic event was attributed to melting of small, imperfect crystals similar to DSC data seen for other crystallizable copolymers.

In a study on the effect of annealing temperature on the transport properties of Nafion®, Deluca et al. observed an interesting trend in that both the proton conductivity and methanol permeability had maximums when plotted as a function of annealing temperature.[43] Deluca et al. examined extruded Nafion® 117 after annealing at 120 and 150 °C for sixty minutes, and 180, 210, 230, and 250 °C for ten minutes. As opposed to an earlier study by Sone et al.,[40] DeLuca and coworkers observed a proton conductivity maximum after annealing extruded Nafion® 117 at 210 °C for ten minutes.[43] A similar trend of increasing and then decreasing methanol permeability was also noticed for extruded Nafion® after annealing at elevated temperatures. Along with the obscure proton conductivity and methanol permeability data, DeLuca et al. observed a lower selectivity (proton conductivity/methanol permeability) for all of the annealed, extruded

Nafion® samples. This observation implied that the methanol permeabilities were actually higher for all of the annealed samples when compared to as-received Nafion®. DeLuca et al. concluded that changes seen in the transport properties of extruded Nafion® could be explained by morphological changes occurring both below and above the annealing temperature of 210 °C. The authors believed that by annealing below 210 °C, the percolation pathway reorients, leading to an enhancement in transport properties. On the other hand, by annealing at temperatures above 210 °C, the percolation pathway is negatively affected, resulting in lower proton conductivity and methanol permeability.[43]

An in-depth publication on the annealing of commercially extruded Nafion® was done by Hensley et al.[46] This study showed that an increase in proton conductivity was possible for all extruded samples regardless of thickness after annealing at 165 °C for 3 hours. In agreement with the proton conductivity results, the water sorption and permeability of Nafion® increased upon annealing at 165 °C for three hours. The water uptake of the membranes was also dependent on film thickness. For thin membranes (1 mil, 25 μm) the water uptake plateaued at λ = 16-18 mol water/mol sulfonate, while for thick membranes (2-7 mil, 50-175 μm) the water uptake averaged between λ = 21-22 mol water/mol sulfonate. The authors suggested that rapid evaporation of water from thinner membranes during the experiment was plausible, but overall they believed thinner membranes would not require as much water to have comparable proton conductivity values, indicating a major advantage for future fuel cell work with thinner Nafion® membranes. The authors also concluded that annealing had mixed results on the crystallinity of extruded membranes of various thicknesses. Thinner membranes exhibited an increase in crystallinity while thicker membranes decreased in overall

crystallinity. An explanation of this phenomenon was not given, although a decrease in the crystallinity of thicker films coincided well with an increase in the proton conductivity and water uptake values as shown by Moore and Martin.[22]

As the fuel cell industry moves towards the use of thinner membranes, DuPont's dispersion-cast method of forming Nafion® will be preferred over extrusion due to ease of processing and lower obtainable thicknesses. Although relevant annealing studies have been completed on the as-received, extruded form of Nafion®, we will also focus on the influence of various thermal annealing procedures on the mechanical stability of both H^+ and Na^+-form dispersion-cast Nafion® membranes in methanol. Neutralization of the dispersion-cast membranes into the Na^+-form will be used to evaluate the influence of electrostatic interactions on the mechanical integrity of the ionomer in boiling methanol.

Experimental

Materials. Extruded H^+-form Nafion® 117 (1100 g/equiv) and Dispersion-cast H^+-form Nafion® NRE 212CS were obtained from E.I. DuPont de Nemours & Co. Methanol was purchased from Fisher Scientific without further purification. Sodium hydroxide was obtained from Aldrich Chemical Co. and dissolved in deionized water to form a 1M solution for counterion exchange of the membrane samples.

Preparation of Nafion® Membranes for Thermal Treatment. H^+-form NRE 212CS membranes were cut into 2.54 cm^2 squares and used in their as-received form during thermal annealing and characterization. Neutralization of NRE 212CS membranes into the Na^+-form counterion was completed by soaking in a 1M NaOH/deionized water solution for twelve hours, followed by boiling in deionized water for one hour to rinse off the excess base. The Na^+-form membranes were placed between

Kimwipes and allowed to dry at room temperature for twelve hours prior to the thermal annealing treatment.

Thermal Treatment of H^+ and Na^+-form NRE 212CS Membranes. All membranes were sandwiched between Kapton® films and annealed between stainless steel plates with 0.10 mm shims to avoid unnecessary pressure during the thermal treatment. After thermal annealing, membranes were quenched to room temperature by removing the Nafion® and Kapton® films from the heated plates. The H^+-form membranes were annealed for one hour at the following temperatures; 100, 125, 150, 175, and 200 °C. Na^+-form membranes were annealed for one hour at the following temperatures: 100, 125, 150, 175, 200, 225, 250, 275, and 300 °C. H^+ and Na^+-form samples were also annealed at 175 °C and 275 °C, respectively, for 1, 2, 5, 10, 15, and 20 minutes.

Mechanical Stability of Thermally Annealed Membranes. All thermally annealed NRE 212CS membranes were placed in scintillation vials filled with methanol and boiled at 65 °C. The membranes were removed from the boiling methanol every five minutes to verify physical integrity. Based on visual inspection, NRE 212CS membranes were determined to be mechanically stable in boiling methanol if the membrane swelled but did not disintegrate after four hours.

Equivalent Weight of Annealed H^+-form NRE 212CS Membranes. H^+-form NRE 212CS membranes were cut into 2.54 cm^2 squares and used in their as-received form during thermal annealing and equivalent weight determination. Sodium hydroxide 0.01 M and sodium chloride were purchased from Fisher Scientific and used without further purification. The exact molarity of the NaOH solution was determined to be 0.00984 M

± .0002 based on direct titration of benzoic acid in triplicate. Five H^+-form membranes were annealed for one hour at each annealing temperature (100, 125, 150, 175, and 200 °C) to verify equivalent weight reproducibility and minimize experimental error. After thermal treatments, all of the membranes were dried under vacuum at 70 °C for 12 hours to obtain a dry weight (m_d). Each membrane was then submersed in a 1.0 M aqueous NaCl solution overnight to allow for the conversion of the ionomer into the Na^+-form along with the formation of residual HCl in the solution. The residual HCl was then titrated using the 0.00984 M NaOH solution with phenolphthalein as an indicator. Since the moles of HCl are equivalent to the moles of sulfonate groups, the resulting EW of the polymer was determined using Equation 4-2; where m_d is the membrane dry weight and V_{NaOH} and C_{NaOH} are the volume and concentration of sodium hydroxide solution used to titrate.

$$EW = \frac{m_d}{V_{NaOH}(C_{NaOH})} \qquad \textbf{Eq. 4-2}$$

Water Uptake Analysis of Annealed NRE 212CS Membranes. All membranes were dried under vacuum at 70 °C for 12 hours to obtain a dry weight (m_d). The films were then submersed in boiling water for one hour, patted dry, and weighed to obtain the hydrated membrane weight (m_h). Equation 4-3, shown below, was used to calculate the water uptake (λ) values of NRE 212CS before and after annealing. The molecular weight of water (18 g/mol) and the equivalent weight of NRE 212CS (1100 g/equiv) were used in calculating the λ values as moles of water per moles of sulfonate groups.

$$\lambda = \frac{(m_h - m_d)/18}{(m_d/1100)} \qquad \textbf{Eq. 4-3}$$

The water uptake values are representative of calculated averages based on three samples before and after thermal treatment at each annealing temperature.

Percent Solubility of Annealed H^+-form NRE 212CS Membranes. To calculate the percent solubility, all membranes were first dried under vacuum at 70 °C for 12 hours to obtain a dry weight (m_d). The solubilities of dispersion-cast Nafion® NRE 212CS were assessed by adding 0.05 g of Nafion® into a scintillation vial containing 15 mL of a 50:50 deionized water:ethanol solution. The solutions were ultrasonicated for one hour, which caused the water:ethanol mixture to increase in temperature to approximately 50 °C. After sonication, the water:ethanol solution was filtered under vacuum using a Whatman no. 1 filter paper to remove undissolved solids. The filtered solution was evaporated to dryness at 50 °C and the dry weight of the resulting residue (r_d) was obtained. Using the dry weight of the polymer sample and the dry weight of the remaining filtered residue, the percent solubility was calculated for both H^+ and Na^+-form NRE 212CS using Equation 4-4. The percent solubility values are representative of calculated averages of at least four samples thermally treated at each annealing temperature.

$$\% \text{ soluble} = \frac{r_d}{m_d}(100) \qquad \textbf{Eq. 4-4}$$

Tensile Analysis of H^+-form NRE 212CS Membranes. As-received Nafion® NRE 212CS membranes were first cut into 75 mm by 5.5 mm strips and annealed at 100, 125, 150, 175, and 200 °C for one hour. In order to reduce experimental error, ten samples were annealed at each temperature and tested on an Instron 5500R at ambient conditions with a crosshead speed of 25.4 mm/min and a gauge length of 25 mm.

Small Angle X-ray Scattering (SAXS) of NRE 212CS Membranes. Small angle X-ray scattering was performed at the Argonne National Laboratory Advanced Photon Source on the DND-CAT 05-ID-D beamline. A monochromatic x-ray beam was derived from an insertion device and a double-crystal monochromator. The incident energy was set to 15 keV and the resulting x-ray wavelength was 0.82656 Å. Two-dimensional scattering images of SAXS data were collected on a high resolution Mar CCD detector (8.1 cm radius) at a distance of 294.35 cm from the sample. Four, one second exposures (2D images of each sample) were averaged prior to integration. All scattering profiles were corrected for incident beam flux, background scatter due to air, and the variable thickness of each sample. The scattering profiles are displayed as intensity (cm^{-1}) versus the scattering vector, q, which is a function of the scattering angle through the following relationship:

$$q = \frac{4\pi}{\lambda}\sin(\theta) \qquad \textbf{Eq. 4-5}$$

where λ is the wavelength of radiation (0.82656 Å) and θ is half of the scattering angle (2θ).

Wide Angle X-ray Diffraction (WAXD) of NRE 212CS Membranes. WAXD was performed at the University of Southern Mississippi using a Rigaku Ultima III x-ray diffractometer in reflection mode. A Copper K_α radiation source was used with a beam wavelength of 1.54 Å. The one-dimensional diffraction images were recorded using a computer controlled scintillation counter. Diffraction data was collected every 0.05°, 2θ between 4-25°, 2θ at a scan rate of 0.1°, 2θ per minute. The scattering profiles are displayed as relative intensity as a function of the scattering angle, 2θ. PeakFit® analysis software was used to deconvolute the crystalline peak from the amorphous halo and aid

in determining the percent crystallinity present in the film. First, a linear two-point baseline subtraction was applied to the WAXD profiles followed by fitting the data with three gaussian/lorentzian peaks. The three peaks represented a broad amorphous scattering peak, a distinct amorphous halo, and a crystalline reflection. The three artificial peaks were then numerically fit to the experimental data to obtain the best r^2 value relative to the experimental data. Finally the percent crystallinity was determined from the ratio of the integrated crystalline peak area versus the entire integrated area under the curve.

Results and Discussion: Effects of Solution-Processing

Dissolution of Nafion®. Both dispersion-cast and extruded Nafion®, in the acid form, were lowered into boiling methanol for up to five minutes while images were taken every thirty seconds to visually inspect the mechanical integrity of the perfluorosulfonic acid membranes. Figures 4.3A-D show the disintegration of dispersion-cast Nafion® NRE 212CS, displayed on the right in each figure, after submersing in boiling methanol for up to 330 seconds. Throughout the five minute submersion test, NRE 212CS began disintegrating almost immediately and mechanically failed between 60 and 120 seconds as shown in Figures 4.3 A and B. Complete disintegration of the dispersion-cast membrane is shown in Figure 4.3D after boiling in methanol for 330 seconds. On the other hand, the extruded Nafion® 112, displayed on the left in each figure, dramatically swelled in the presence of boiling methanol, but remained intact after several hours of boiling.

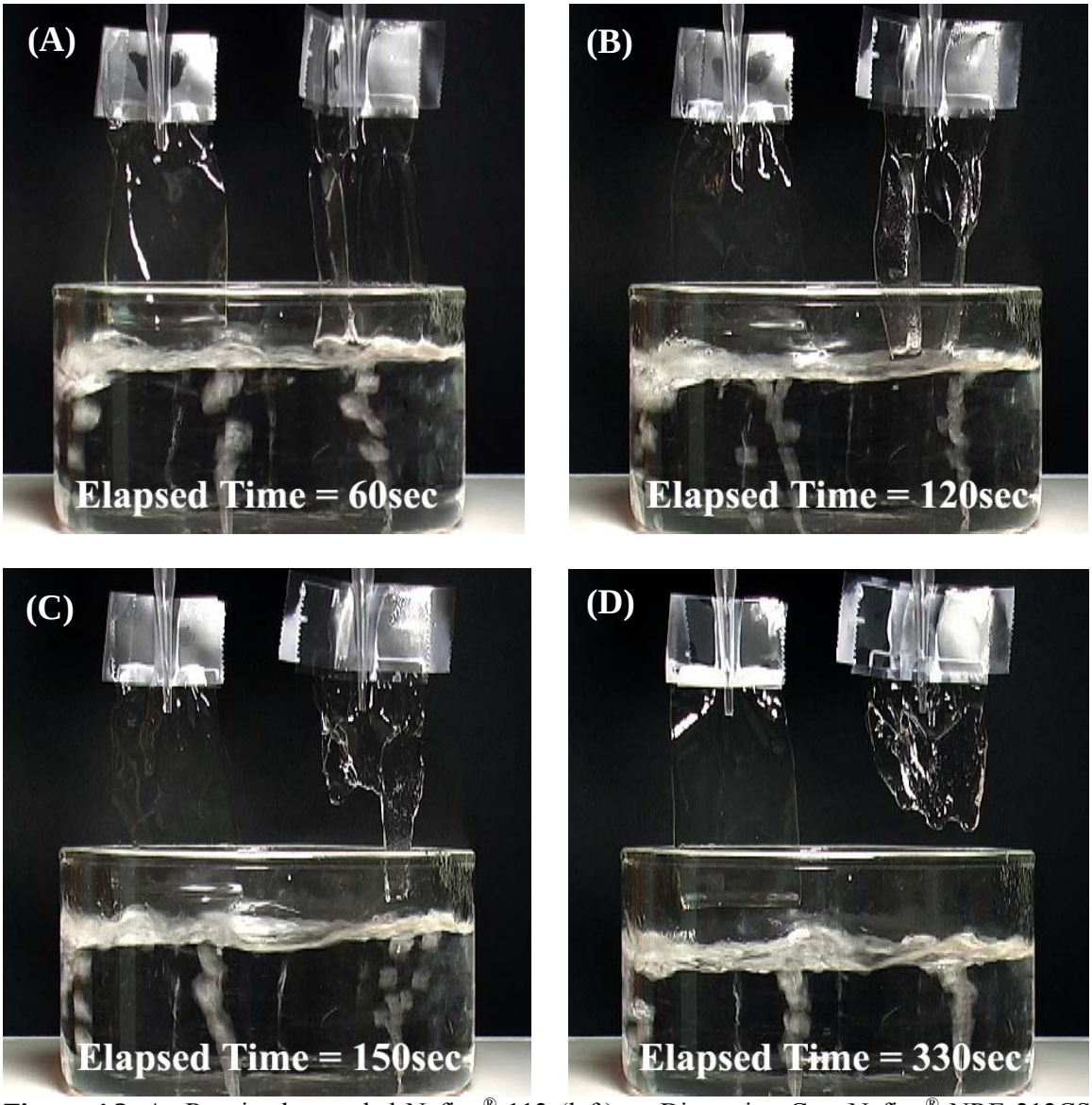

Figure 4.3. As-Received extruded Nafion® 112 (left) vs Dispersion-Cast Nafion® NRE 212CS (right) in boiling methanol after **A)** 60 seconds **B)** 120 seconds **C)** 150 seconds **D)** 330 seconds

Based on this visual evidence, dispersion-cast Nafion® may not be suited for use in direct methanol fuel cells based on the Department of Energy's target operation temperature of 60 °C. With the boiling point of methanol being 64.7 °C, dispersion-cast Nafion® may exhibit catastrophic failures in a direct methanol fuel cell, if held at 60 °C for prolonged periods of time.

Mechanical Stability of NRE 212CS in Binary Solvent Mixtures. Based on the undesirable disintegration of dispersion-cast H^+-form Nafion® in boiling methanol, a series of solvent uptake experiments were conducted in order to determine the optimum binary alcohol/water mixture necessary to avoid Nafion® dissolution. Table 4-1 displays the percent solvent uptake of H^+-form NRE 212CS after refluxing in various binary solvent mixtures for one hour at their respective boiling points.

Volume Ratio of Binary Solvent Mixtures	Percent Solvent Uptake
100/0 MeOH/H_2O	Disintegrated
75/25 MeOH/H_2O	Disintegrated
50/50 MeOH/H_2O	Stable 537% ± 9.1
25/75 MeOH/H_2O	Stable 121% ± 4.2
0/100 MeOH/H_2O	Stable 52% ± 2.3
100/0 EtOH/H_2O	Disintegrated
75/25 EtOH/H_2O	Disintegrated
50/50 EtOH/H_2O	Disintegrated
25/75 EtOH/H_2O	Stable 510% ± 13.3

Table 4-1. Disintegration and percent solvent uptake of H^+-form NRE 212CS after refluxing in various methanol/water and ethanol/water mixtures.

Verifying the results shown in Figures 4.3 A-D, Table 4-1 displays the dissolution of H^+-form NRE 212CS membranes in both refluxing methanol and ethanol. The swelling effect of both alcohols in binary mixtures with deionized water is also observed in Table 4-1. When subjected to a 50/50 volume percent binary mixture of methanol/water, H^+-form NRE 212CS absorbs approximately 537 wt%, but when subjected to a mixture of 50/50 volume percent ethanol/water the membrane disintegrates or falls apart in solution. Due to the discrepancy in the results, it can be concluded that ethanol has more of a swelling effect on Nafion® than methanol. Yeo and coworkers proved this theory by examining the solubility parameters of various solvents on the uptake and solubility of Nafion®.[17] The volume fraction of swollen polymer increased when subjected to ethanol

rather than methanol. Yeo et al. concluded that Nafion® exhibits a dual solubility parameter with maximum solubilities at 9.5 and 18.1 Hb. The solubility envelope at 9.5 Hb was attributed to swelling of Nafion's® organic phase, while the solubility envelope at 18.1 Hb was attributed to swelling of the ionic aggregate domain. The increased swelling of Nafion® with ethanol as opposed to methanol was attributed to ethanol's solubility parameter (12.7 Hb) being closer to the organic phase solubility maximum value of 9.5 Hb as opposed to methanol's solubility parameter of (14.5 Hb). With respect to direct methanol fuel cell performance, the data represented in Table 4-1 concludes that at least 50 vol% of water must be present in the methanol feed stream for NRE 212CS to resist mechanical dissolution within the fuel cell environment. On the other hand, with a 50/50 volume percent binary mixture of methanol/water the membrane would swell excessively (537 wt% solvent uptake), hence increasing the chances of mechanical failure during fuel cell operation.

Thermal Annealing of Dispersion-Cast H^+-form Nafion® NRE 212CS. A series of annealing experiments were conducted in an attempt to increase the physical stability of NRE 212CS in boiling methanol. Table 4-2 displays the methanol dissolution time of H^+-form NRE 212CS before and after annealing for one hour at various temperatures.

Annealing Procedure	**H^+ NRE 212CS Dissolution Time**
Unannealed	1 min
100°C	3 min
125°C	5 min
150°C	25 min
175°C	Intact after 4 hrs
200°C	Intact after 4 hrs

Table 4-2. Dissolution time of H^+-form NRE 212CS in boiling methanol after annealing for one hour at 100, 125, 150, 175, and 200 °C.

The time necessary for complete dissolution of NRE 212CS increased with increasing annealing time, as seen in Table 4-2. The unannealed, or as-received membrane disintegrated in boiling methanol after submersion for approximately one minute. In order to obtain physical stability in boiling methanol, the H^+-form NRE 212CS membranes had to be annealed at 175 °C for at least one hour.

Figure 4.4 displays the effect of thermally annealing H^+-form NRE 212CS for one hour at 100, 125, 150, 175, and 200 °C.

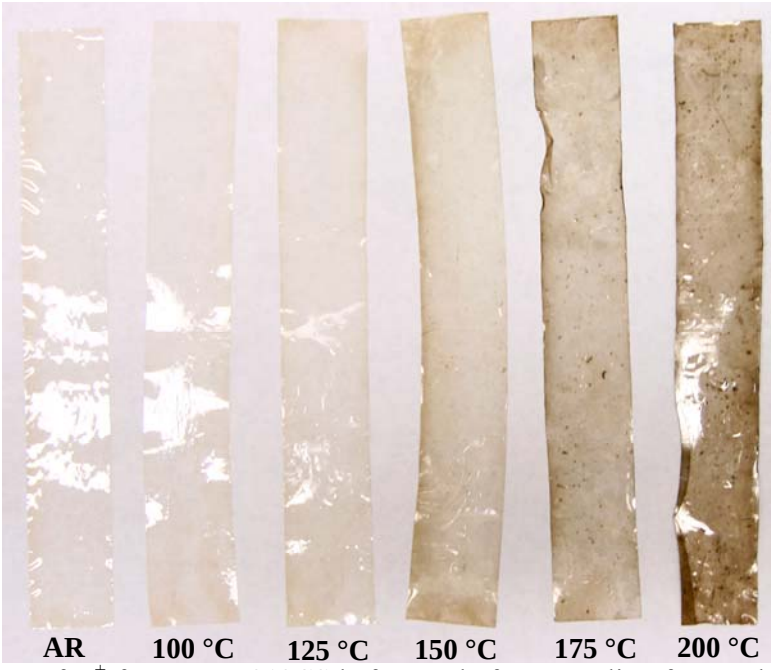

Figure 4.4. Image of H^+-form NRE 212CS before and after annealing for one hour at 100, 125, 150, 175, and 200 °C.

As the annealing temperature increases, the onset of discoloration also increases. The observation of H^+-form Nafion® discoloration has been previously observed by other scientists, but the source has yet to be determined.[21, 46, 47] Most researchers ignore the discoloration of Nafion® due to the ability to reclaim transparent membranes after treating the films with nitric acid or hydrogen peroxide. Another way to avoid the

discoloration of Nafion® during thermal treatments is to convert the membrane into an alkali metal counterion form (i.e. Na^+) prior to annealing.[47]

Due to the disintegration of H^+-form NRE 212CS in boiling methanol, water uptake instead of methanol uptake was measured before and after annealing at various temperatures. Figure 4.5 shows the water uptake (λ) of H^+-form NRE 212CS after annealing for one hour at various temperatures.

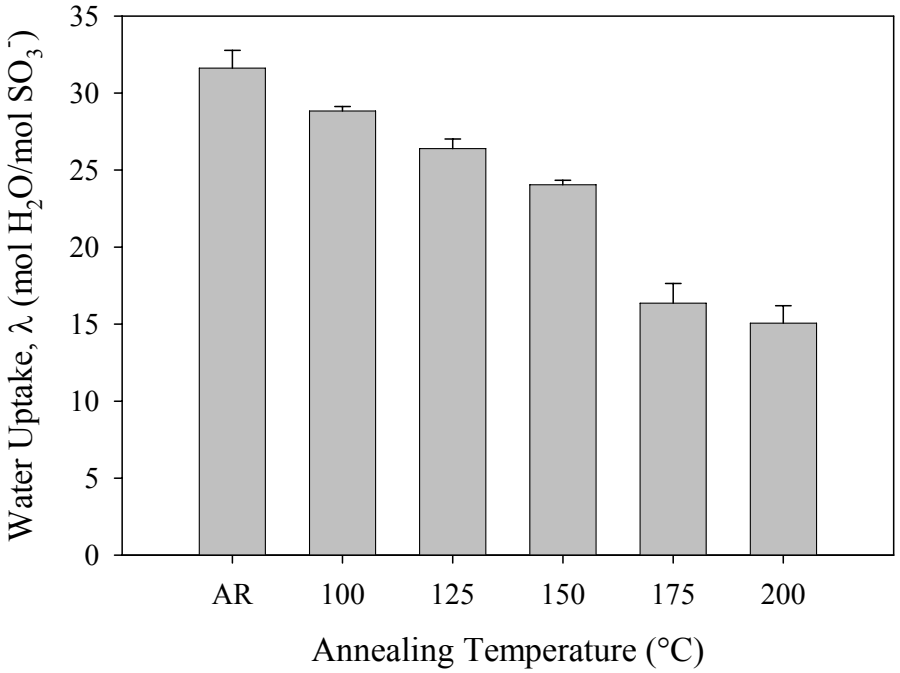

Figure 4.5. Water uptake of H^+-form NRE 212CS before and after annealing for one hour at 100, 125, 150, 175, and 200 °C.

The initial water uptake of H^+-form NRE 212CS is 31 mol water/mol sulfonate and is approximately 10 λ above the water uptake of extruded Nafion®, which is 21 mol water/mol sulfonate.[45, 48] Gebel et al. documented that recast or reconstructed perfluorosulfonate ionomer membranes had higher water uptakes than the extruded membranes due to more uniform swelling. The extruded membranes did not swell as much in the laminating direction due to the onset of polymeric chain orientation in the extrusion direction.[21] By annealing H^+-form NRE 212CS for one hour at 200 °C, the

water uptake continuously decreased from an as-received value of 31 to approximately 15 mol water/mol sulfonate. In a similar study, Lee and coworkers showed that annealing recast Nafion® at various temperatures had a dramatic effect on the water uptake of the membranes.[26] By annealing recast membranes at 150 °C, Lee et al. obtained a water uptake of 24.4, which is in agreement with our values. Hinatsu et al. also noticed a decrease in water uptake values after annealing extruded Nafion® for two hours at 80 and 105 °C.[49] The decreased water uptake values were contributed to a significant decrease in the degree of shrinkage of the ion cluster microstructure. Mauritz and Moore suggest that the water uptake values were lower based on improved main and side chain packing or a decrease in the free volume by the increase in thermal kinetic energy.[3] It should also be noted that a significant decrease in the water uptake of H^+-form NRE 212CS occurred between annealing at 150 and 175 °C. The membranes became stable in boiling methanol after annealing at 175 °C for one hour. These annealing conditions yielded a water uptake value of 16 mol water/mol sulfonate and is lower than the water uptake of as-received extruded Nafion® ($\lambda = 21$).

An examination of the equivalent weight of the polymer before and after annealing was conducted to determine if there was a correlation between the loss of sulfonate moieties and the dramatic 50% decrease in water uptake values of H^+-form NRE 212CS after annealing at elevated temperatures. Figure 4.6, shown below, displays the average equivalent weight values of H^+-form NRE 212CS before and after annealing as well as after drying overnight under vacuum at 70 °C.

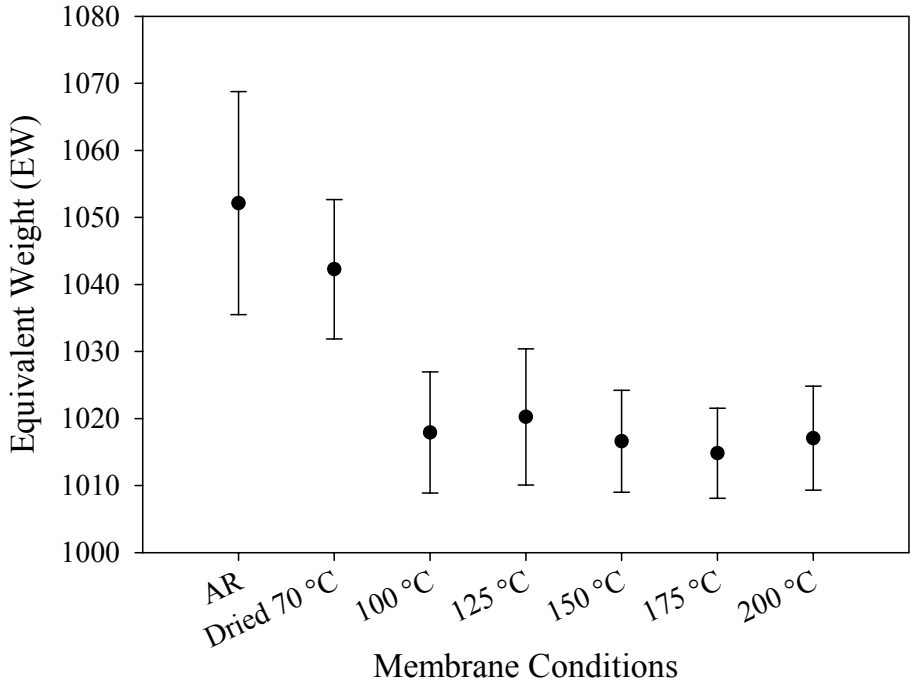

Figure 4.6. Equivalent weight (EW) as a function of various thermal treatments on H^+-form NRE 212CS films. Membranes were tested in their as-received (AR) state, dried at 70 °C for 12 hours, and annealed for one hour at 100, 125, 150, 175, and 200 °C.

The initial equivalent weights of 1052 and 1042 g/mol for as-received and dried H^+-form NRE 212CS are in agreement with DuPont's titration results wherein the equivalent weight could not be greater than 1087 g/mol.[12] After annealing at 100, 125, 150, 175, and 200 °C for one hour, the equivalent weight of H^+-form NRE 212CS decreased to approximately 1017 g/mol for each annealing temperature. The sudden decrease between the as-received and dried membranes and those annealed at elevated temperatures may be attributed to residual water in the membrane, which would cause an inaccurate dry weight and equivalent weight determination. Since the equivalent weight does not change between annealing at 100 and 200 °C, we conclude that the dramatic decrease in water uptake as a function of annealing temperature is not attributed to the loss of sulfonate moieties during the thermal treatment.

Figure 4.7 displays the percent solubility of H^+-form NRE 212CS before and after thermal annealing for one hour at 100, 125, 150, 175, and 200 °C.

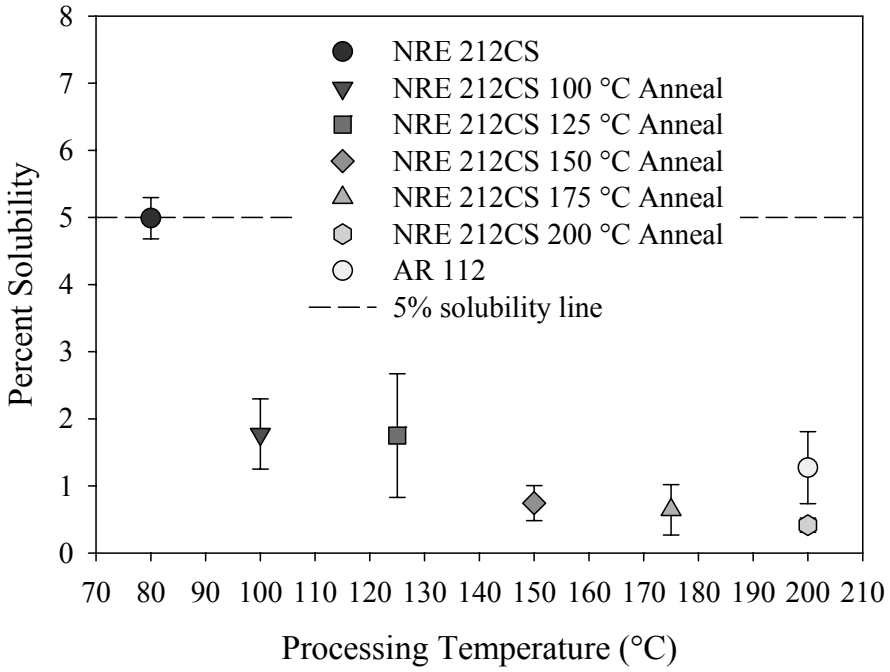

Figure 4.7. Percent solubility of H^+-form NRE 212CS before and after annealing for one hour at 100, 125, 150, 175, and 200 °C, as well as the percent solubility of extruded Nafion® 112 as a function of processing temperature.

The dashed line represents the solubility limit of 5%, where mechanical integrity is lost by subjecting the membranes to various solvents.[18] Solubility of less than 5% generally indicates stable membranes in various water/ethanol mixtures. Extruded Nafion® AR 112 is less than 2% soluble in 50/50 ethanol/water, while the new, dispersion-cast membrane (NRE 212CS) is approximately 5% soluble. After thermally annealing the membranes for one hour at elevated temperatures, a trend of decreasing percent solubility with increasing annealing temperature was observed. The decrease in percent solubility mimics the trend of decreasing water uptake with increasing annealing temperature. The two membranes annealed at 175 and 200 °C are both stable in boiling methanol and have percent solubilities well below that of the extruded Nafion® AR 112. Hence, the

mechanical integrity of dispersion-cast membranes annealed at either 175 or 200 °C are similar to the as-received solubility properties of extruded Nafion®.

In comparison, Zook and coworkers explored the effects of annealing recast Nafion® on the solubility of the resulting ionomer.[32] Nafion® recast films were processed by evaporating commercial, *previous-generation* Nafion® dispersions (ethanol/water mixtures) onto polystyrene in a desiccator at room temperature. Various annealed films were created by subjecting the recast membranes to 140 °C in an oven for 10-60 minutes. Zook et al. noticed that all samples annealed at 140 °C for longer than 10 minutes were insoluble after sonicating in 50:50 ethanol/water mixtures for 60 minutes. The authors note that by utilizing an annealing temperature above Nafion's® dynamic mechanical α-relaxation transition temperature of 110 °C, significant mobility was achieved, allowing for changes in the polymer solubility characteristics. Zook's results differ from ours based on the grade of Nafion® used throughout the study. Our focus was on new-generation NRE 212CS membranes, while Zook and coworkers were using solutions based on the extruded Nafion®, which had no previous problems with dissolution in boiling methanol. Unfortunately, Zook et al. only annealed the recast Nafion® at 140 °C, so a trend with increasing or decreasing annealing temperature was not available for comparison.

On the other hand, Jung et al. examined the percent solubility of recast Nafion® annealed for 40 minutes at 110, 130, 150, and 200 °C.[44] Similar to Zook et al., Jung and coworkers were examining the solubility characteristics of Nafion® recast from the previous generation solution. In agreement with our studies, Jung et al. noticed a continual decrease in the percent solubility as a function of annealing temperature with

mechanical stability occurring after annealing at 150 °C. Jung et al., also note that the change in solubility was due to annealing above the polymer's dynamic mechanical α-relaxation transition temperature, which significantly changed the ionomer morphology.

Mechanical Properties of Annealed H^+-form NRE 212CS. Figure 4.8A displays the stress versus strain of H^+-form Nafion® NRE 212CS before and after annealing at 100, 125, 150, 175, and 200 °C. Based on the data shown in Figure 4.8A, the plastic modulus or slope of the experimental stress-strain curve beyond the yield point, is increasing as a function of temperature.[50] Since the slope is positive, it is commonly referred to as experimental strain hardening.[51] Satterfield et al. performed tensile tests on extruded Nafion® as well as recast Nafion®/titania composites and observed a slight decrease in the strain hardening slope with increasing testing temperature.[50] The authors also note that the water content within the membranes had minimal influence on the change in strain hardening behavior. Gilbert et al. observed an increase in experimental strain hardening of the sulfonyl fluoride precursor to Nafion® after annealing at 70 °C.[52] The authors witnessed an increase in tensile strength along with a decrease in elongation at break of annealed samples, which was attributed to improvement of the crystalline structure. On the other hand, van der Heijden et al. documented no significant change in the crystallinity of Nafion® with increasing draw ratio or elongation when stretching at room temperature.[53] The authors concluded that the frequently observed phenomenon of stress-induced crystallinity was absent in Nafion® due to the orientation temperature being well below the α-relaxation of the membrane and the presence of ionic moieties inhibiting the formation of large crystalline domains. Based on the studies of Satterfield and van der

Heijden, we attribute the increase in experimental strain hardening to an increase in the ability of the polymer backbone to align or orient after annealing at elevated temperatures.

Figure 4.8B displays the tensile modulus as a function of annealing temperature. The modulus values of the samples within the elastic region remained relatively unchanged with increasing annealing temperature prior to testing. It is interesting to notice that the modulus values of the samples did not change between annealing at 150 °C and annealing at 175 °C. As mentioned earlier, by annealing at 175 °C for one hour, we were able to achieve mechanical stability for NRE 212CS membranes when subjected to boiling methanol. Based on the data shown in Figure 4.8B, the onset of mechanical integrity after annealing at 175 °C for one hour had no influence on the modulus values of the membranes.

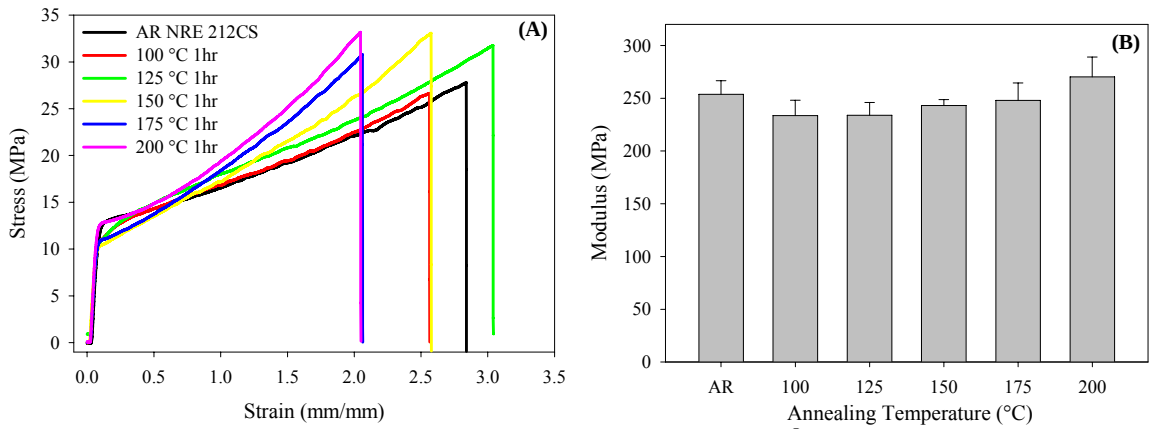

Figure 4.8. A) Stress versus strain of as-received H^+-form Nafion® NRE 212CS before and after annealing for one hour at 100, 125, 150, 175, and 200 °C. **B)** Modulus versus annealing temperature of H^+-form Nafion® NRE 212CS before and after annealing for one hour at 100, 125, 150, 175, and 200 °C.

The stress at break, like the modulus data, was relatively constant after annealing H^+-form NRE 212CS membranes at various temperatures, as shown in Figure 4.9A. Similar to the discussion of the modulus values, the stress at break was not influenced by the change in annealing temperature or the onset of mechanical stability in boiling

methanol at 175 °C. On the other hand, the strain at break decreased by approximately 25% after annealing at 175 °C or higher. The dramatic decrease in strain at break could be due to the morphological changes occurring while annealing at 175 °C. One theory, which will be mentioned throughout this publication, for the decrease in strain at break and the increase in mechanical stability in boiling methanol after annealing at 175 °C for one hour includes complex manipulation of chain entanglement, crystallinity, and the ionic domain.

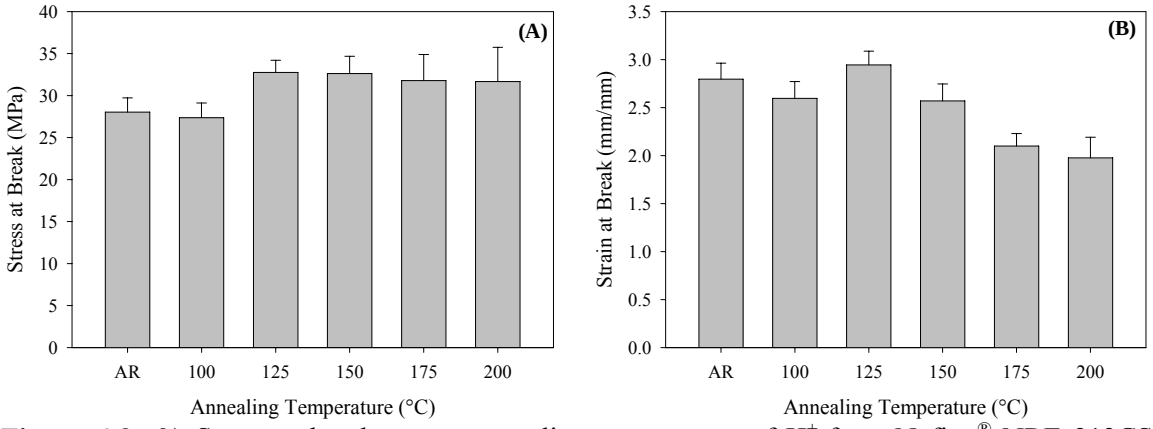

Figure 4.9. A) Stress at break versus annealing temperature of H^+-form Nafion® NRE 212CS before and after annealing for one hour at 100, 125, 150, 175, and 200 °C. **B)** Strain at break versus annealing temperature of H^+-form Nafion® NRE 212CS before and after annealing for one hour at 100, 125, 150, 175, and 200 °C.

Small and Wide Angle X-ray Analysis of Annealed H^+-form NRE 212CS. Figure 4.10 shows the absolute intensity as a function of the scattering vector, *q*, from radial integration of the two-dimensional scattering patterns of H^+-form NRE 212CS annealed at various temperatures.

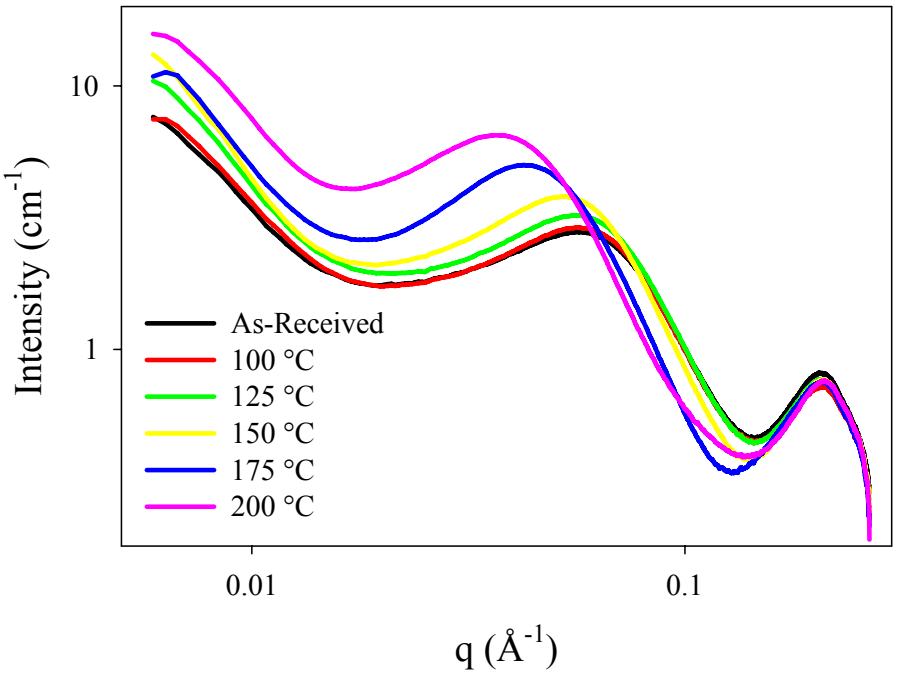

Figure 4.10. Small Angle X-ray Scattering (SAXS) profile of H^+-form NRE 212CS membranes before and after annealing for one hour at 100, 125, 150, 175, and 200 °C.

The as-received H^+-form NRE 212CS scattering profile is in agreement with previous SAXS patterns of extruded Nafion®.[33, 34] The three main components of a typical Nafion® SAXS pattern include the small angle upturn, intercrystalline peak, and ionomer peak. The small angle upturn ($q < 0.02$ Å^{-1}) has been examined by Gebel et al. and is attributed to large scale heterogeneities between the ionomer domain and polymer matrix.[54] The intercrystalline peak ($q \approx 0.05$ Å^{-1}) is often referred to as the scattering between crystalline domains or the crystalline long period.[55] The ionomer peak ($q \approx 0.2$ Å^{-1}) is attributed to the scattering from the interparticle interference between ionic aggregates that are spatially distributed throughout the membrane.[42] In Figure 4.10, a dramatic shift in the intercrystalline peak to lower q values with increasing annealing temperature is documented. The shift of the intercrystalline peak from $q = 0.05$ to $q = 0.03$ is indicative of larger scattering distances between Nafion® crystallites or electron dense domains. It is also important to note that the largest shift in the intercrystalline

peak occurred at annealing temperatures above 175 °C, which were the conditions necessary to obtain mechanical stability of H^+-form NRE 212CS in boiling methanol. Although dramatic changes to the crystalline domain of H^+-form NRE 212CS were seen after annealing at elevated temperatures, the ionomer peak remained constant, meaning that the distance between ionic aggregates was unchanged along with the overall size of the ionomer domain.

Wide Angle X-ray Diffraction (WAXD) was also performed on H^+-form NRE 212CS in order to verify changes to the crystalline morphology after annealing at elevated temperatures. Figure 4.11 shows the WAXD pattern of relative intensity versus degrees, 2θ for H^+-form NRE 212CS before and after annealing between 100 and 200 °C.

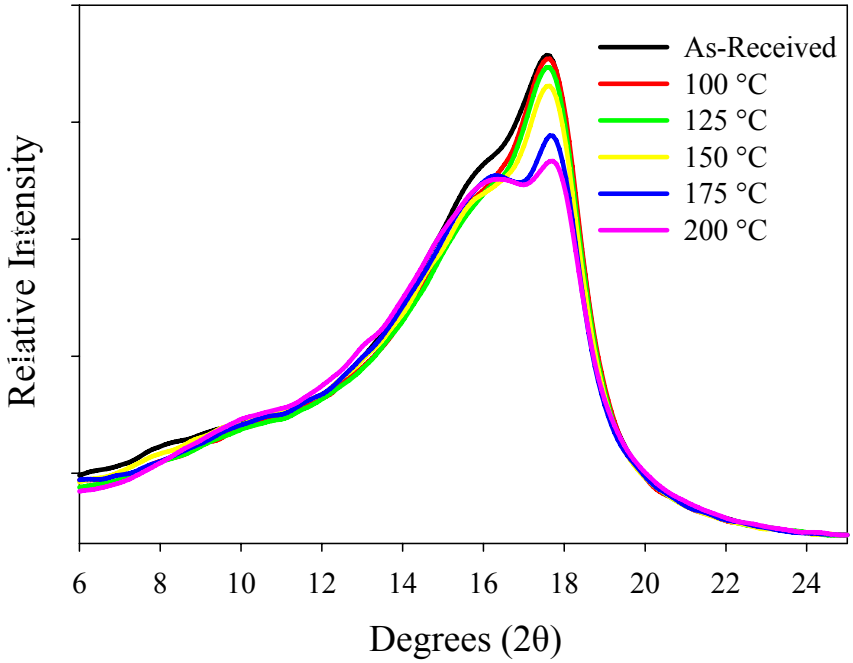

Figure 4.11. WAXD profile of H^+-form NRE 212CS membranes before and after annealing for one hour at 100, 125, 150, 175, and 200 °C.

The WAXD profile of as-received H^+-form NRE 212CS is in agreement with various WAXD patterns of extruded Nafion® that are widely reported in the literature.[33, 34, 56] The general Nafion® WAXD profile consists of a broad amorphous halo from 12-22°, 2θ

along with a distinct crystalline reflection at 18°, 2θ. A simple deconvolution of the crystalline peak from the amorphous halo was done using PeakFit® analysis software (an example is shown in Figure 4.12).

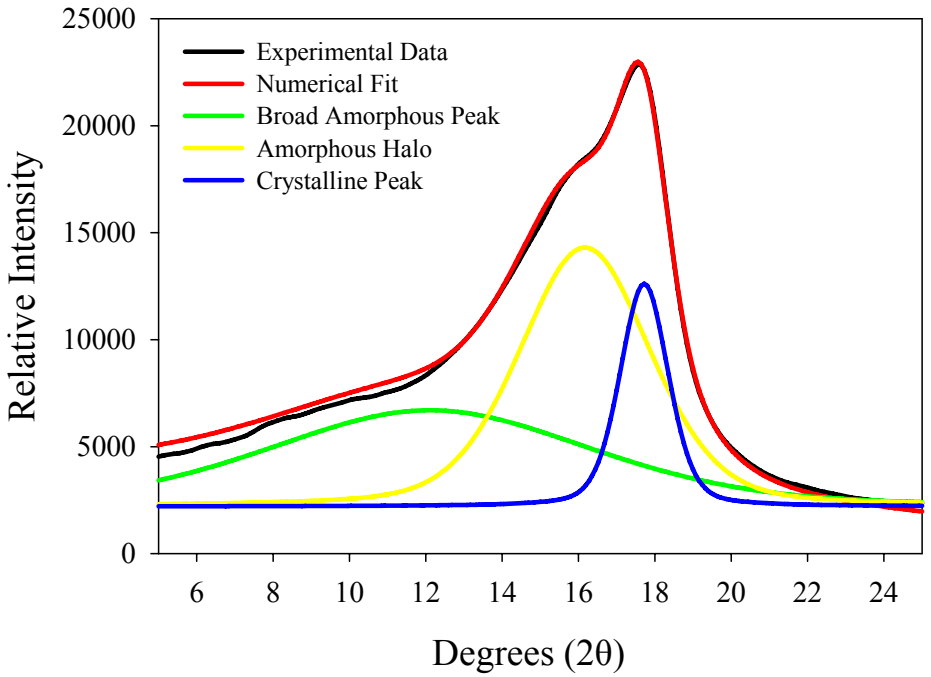

Figure 4.12. WAXD data of as-received, H^+-form NRE 212CS displaying the deconvoluation of the crystalline peak and amorphous peaks using PeakFit® analysis software.

Based on deconvolution analysis of the crystalline peak from the amorphous halo, decreases in percent crystallinity and full width at half maximum (FWHM) were observed after annealing H^+-form NRE 212CS at 100, 125, 150, 175, and 200 °C, as shown in Table 4-3. It is interesting to note that both the percent crystallinity and FHWM remain relatively constant while annealing at temperatures below 175 °C. By annealing at temperatures beyond 175 °C, a significant change in the morphology of the membrane occurs, which also aids in increasing the mechanical stability of NRE 212CS when subjected to boiling methanol.

T_{Anneal}	H^+-form $\%X_c$	FWHM
AR	14.2	1.5
100 °C	15.2	1.4
125 °C	15.3	1.4
150 °C	13.1	1.4
175 °C	8.7	1.2
200 °C	6.8	1.2

Table 4-3. Percent crystallinity and full width at half maximum (FWHM) of H^+-form NRE 212CS before and after annealing for one hour at 100, 125, 150, 175, and 200 °C.

The overall decrease in percent crystallinity with increasing annealing temperature is also in agreement with the shift of the intercrystalline peak observed in the SAXS profiles in Figure 4.10. By increasing the annealing temperature, the smaller crystallites were allowed to melt, leaving a more uniform crystalline domain consisting of larger crystallites. Based on the SAXS analysis, the distance between the crystallites grew as the smaller, imperfect crystallites were melted. It was then believed that the H^+-form NRE 212CS membranes' mechanical integrity increased due to a more uniform crystalline domain allowing for less solubility in boiling methanol.

Electrostatic Network Manipulation. As opposed to annealing H^+-form NRE 212CS membranes at elevated temperatures to increase the mechanical stability in boiling methanol, the addition of Na^+ counterions was anticipated to increase the strength of the electrostatic network. Based on previous work by Moore et al., alkali metal counterions have been shown to increase the dynamic mechanical properties of Nafion® by increasing the strength of the ionic interactions and thereby strengthening the electrostatic network.[42, 57-59] Table 4-4 shows necessary annealing procedures for obtaining mechanical stability of Na^+-form NRE 212CS in boiling methanol.

Annealing Procedure	Na^+ NRE 212CS Dissolution Time
Unannealed	3 min
100°C	3 min
125°C	3 min
150°C	5 min
175°C	5 min
200°C	7 min
225°C	10 min
250°C	180 min
275°C	Intact after 4 hrs
300°C	Intact after 4 hrs

Table 4-4. Dissolution time of Na^+-form NRE 212CS in boiling methanol before and after annealing for one hour at 100, 125, 150, 175, 200, 225, 250, 275, and 300 °C.

Although simply exchanging NRE 212CS into the Na^+-form had no effect on the mechanical integrity in boiling methanol, mechanical stability was achieved after annealing Na^+-form NRE 212CS at 275 °C for one hour. It should also be noted that the Na^+-form membranes had to be annealed 100 °C higher than the H^+-form membranes in order to achieve mechanical stability and the effects of discoloration during annealing at elevated temperatures was minimal.

Small and Wide Angle X-ray Analysis of Na^+-form NRE 212CS. SAXS and WAXD analysis was completed to examine any changes in the morphology of Na^+-form NRE 212CS before and after annealing and to determine the difference between the annealing temperatures at which mechanical stability occurs in both H^+ and Na^+-form NRE 212CS membranes. Figure 4.13 displays the SAXS profile of Na^+-form NRE 212CS before and after annealing at various temperatures.

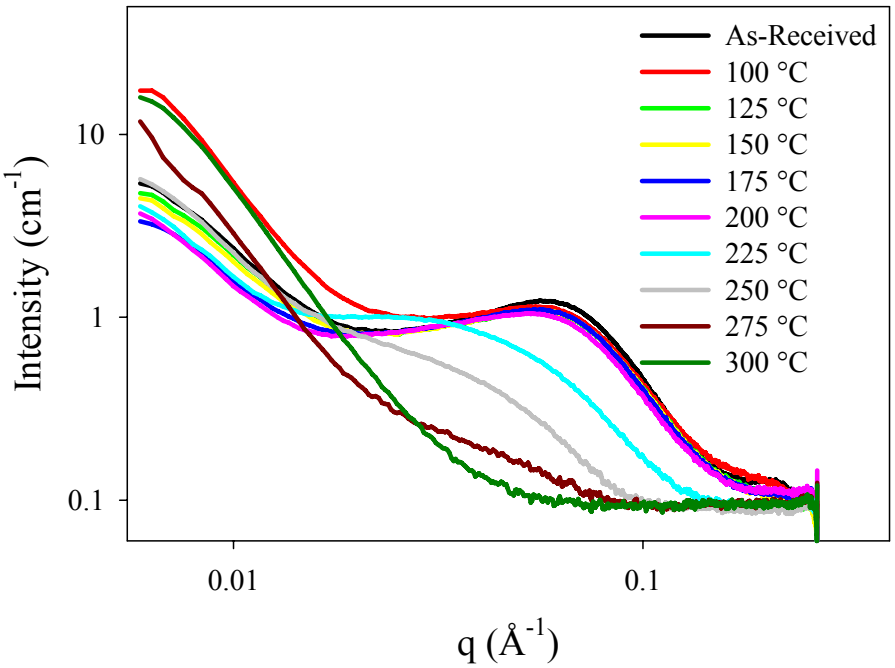

Figure 4.13. SAXS profile of Na^+-form NRE 212CS membranes before and after annealing for one hour at 100, 125, 150, 175, 200, 225, 250, 275, and 300 °C.

The intercrystalline peak ($q \approx 0.05$ Å^{-1}) shifts to lower *q* values and decreases in intensity after annealing at 225 °C for sixty minutes and then disappears due to melting of the crystallites after sixty minutes at 275 °C. The Na^+-form membranes become stable in boiling methanol after annealing at 275 °C for one hour in the absence of crystallinity, as opposed to the H^+-form membranes which become stable in boiling methanol with crystallinity present. The ionomer peak is absent in the SAXS profiles of Na^+-form NRE 212CS due to similarities in electron density between the ionomer domain and polymer matrix. To elucidate the effects of annealing Nafion® in other counterion forms, we have provided supplemental SAXS information on NRE 212CS and AR 117CS annealed for 10-1440 minutes from 50-300 °C (see Supplemental Information 4A).

Figure 4.14 shows the WAXD profile of relative intensity versus degrees, 2θ for Na^+-form NRE 212CS before and after annealing between 100 and 300 °C.

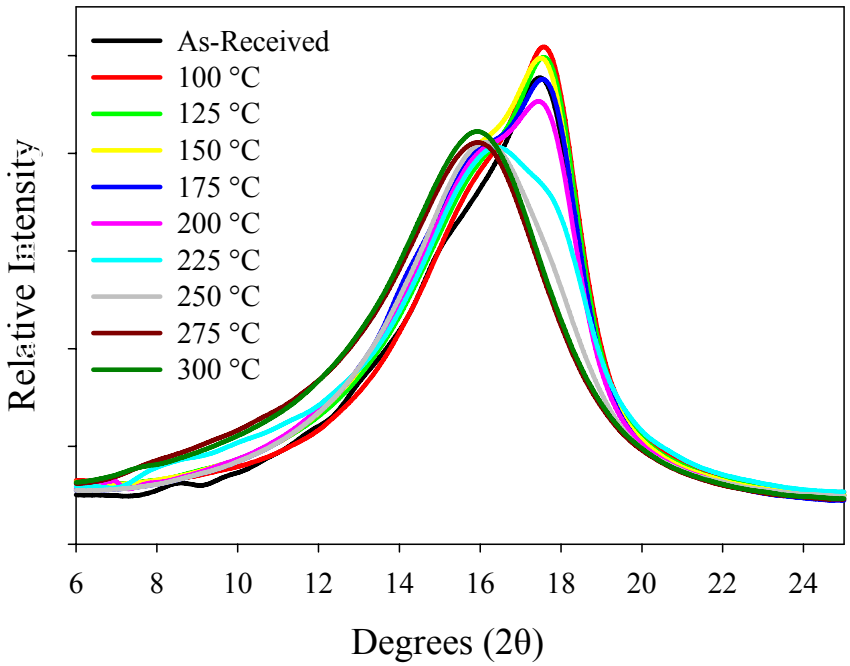

Figure 4.14. WAXD profile of Na^+-form NRE 212CS membranes before and after annealing for one hour at 100, 125, 150, 175, 200, 225, 250, 275, and 300 °C.

The WAXD profiles of Na^+-form NRE 212CS after annealing at elevated temperatures verifies the disappearance of crystallinity seen in the SAXS analysis at annealing temperatures above 275 °C. In a similar study, Luan et al. examined the effects of annealing on the resulting crystallinity and methanol permeability for cast Nafion® membranes.[60] The sulfonyl fluoride precursor of Nafion® was first synthesized by Luan and coworkers, and then converted directly into the Na^+ counterion form. The Na^+-form Nafion® was then dissolved under high temperature and pressure in dimethylformamide and cast under vacuum at 125 °C over a period of 1.75 hours. The film was then cut into six equal sections, and five of the samples were annealed for 1.5 hours at the following temperatures: 150, 170, 190, 210, 230, and 250 °C. Based on WAXD results, Luan et al. noticed a similar decrease in both the intensity and full width at half maximum of the

crystalline reflection at 17.5 °, 2θ as a function of increasing annealing temperature as compared to our results. The change in percent crystallinity was calculated based on the deconvolution of an amorphous and crystalline peak from the WAXD profiles, resulting in a decrease in crystallinity from 22.0 to 7.4% with increasing annealing temperature from 150 to 230 °C. These results are in agreement with our percent crystallinity deconvolutions of Na^+-form NRE 212CS, shown in Table 4-5. The only difference between our results and Luan's is that we annealed at temperatures high enough to melt all of the crystallites present in Nafion® (275 °C) and Luan et al. only annealed up to 230 °C.

T_{Anneal}	Na^+-form $\%X_c$	FWHM
AR	21.4	1.7
100 °C	17.5	1.5
125 °C	16.3	1.5
150 °C	13.9	1.4
175 °C	15.1	1.5
200 °C	12.8	1.5
225 °C	3.45	1.3
250 °C	2.22	1.6
275 °C	0	0
300 °C	0	0

Table 4-5. Percent crystallinity and full width at half maximum (FWHM) of Na^+-form NRE 212CS before and after annealing for one hour at 100, 125, 150, 175, 200, 225, 250, 275, and 300 °C.

Based on the observation that Na^+-form NRE 212CS membranes are stable in boiling methanol in an amorphous state, the role of crystallinity can be neglected as influencing the mechanical integrity of either H^+ or Na^+-form NRE 212CS membranes.

It is interesting to note that Luan et al. also noticed a dramatic decrease in the methanol permeability of Nafion® annealed at elevated temperatures.[60] The authors

suggest that the methanol permeates through both the ionic and hydrophobic domains and upon annealing at high temperatures the hydrophobic channels contract, making it more difficult for methanol to permeate through the membrane.

Figure 4.15 displays the Dynamic Mechanical Analysis (DMA) of both H^+ and Na^+-form extruded Nafion® membranes as well as the Differential Scanning Calorimetry (DSC) of Na^+-form extruded Nafion®.

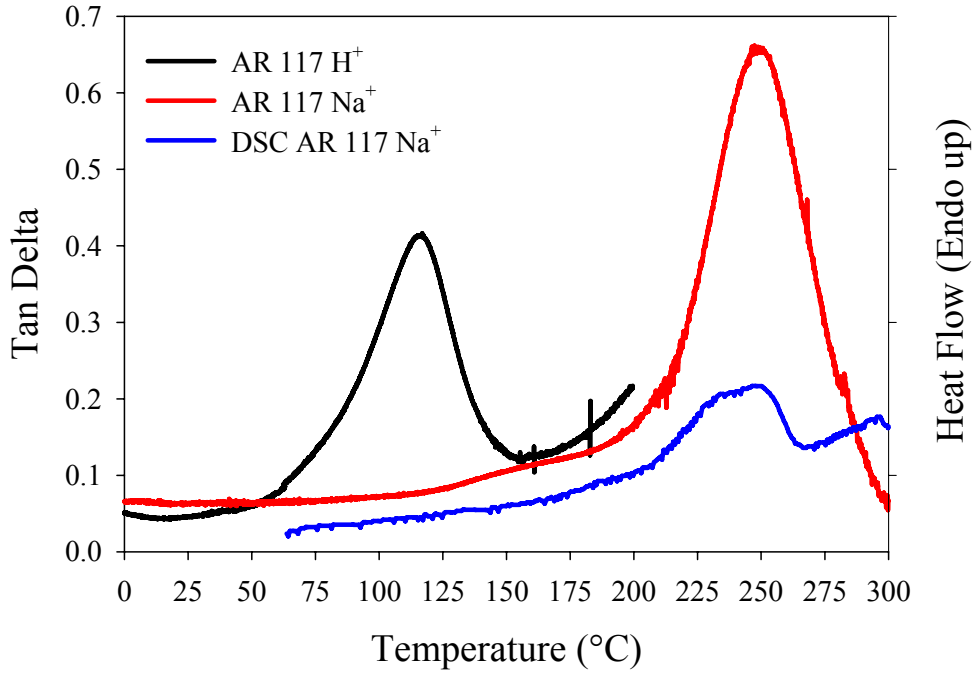

Figure 4.15. Tan delta of H^+ and Na^+-form extruded Nafion® versus temperature along with heat flow of Na^+-form extruded Nafion® as a function of temperature.

It can be seen in Figure 4.15 that the annealing temperatures which yield mechanical stability (175 °C and 275 °C for H^+ and Na^+-form NRE 212CS membranes, respectively) are well above the α-relaxation temperatures displayed in the tan delta profiles. Based on previous assignments of the α-relaxation of Nafion®, it can be concluded that significant ion-hopping as well as chain mobility is present at the respective annealing temperatures of 175 °C for H^+-form and 275 °C for Na^+-form membranes.[42] Based on the DSC heat flow trace of extruded Na^+-form Nafion®, the crystalline domain exists between 215 and

260 °C. Beyond 260 °C, the Teflon-like crystallites melt, and the membrane is rendered amorphous. Hence annealing Na^+-form NRE 212CS membranes at 275 °C for one hour eliminated any crystallinity present although mechanical integrity was enhanced. From Figure 4.15, we can conclude that crystallinity played a minor role in increasing the mechanical integrity of dispersion-cast Nafion®. Furthermore, annealing above the α-relaxation temperature allowed for increased mobility and chain entanglement which was responsible for the stability in boiling methanol.

Conclusions

Dispersion-cast Nafion® NRE 212CS have been shown to disintegrate when subjected to boiling methanol. In an attempt to mitigate this undesirable behavior, we have performed a series of annealing experiments on both the H^+ and Na^+-forms of the ionomer. H^+-form NRE 212CS membranes were rendered mechanically stable in boiling methanol after annealing at 175 °C for one hour. Characterization of these membranes showed a decrease in percent solubility, water uptake, and percent crystallinity. By simply converting the membranes into the Na^+-form, hence creating a stronger electrostatic network, we were unsuccessful in increasing the mechanical integrity of the membrane in boiling methanol. Mechanical integrity of the Na^+-form membrane was only achieved after annealing at 275 °C for one hour. The WAXD data indicated that at 275 °C, the Nafion® membrane was rendered amorphous; therefore, we conclude that the amount of crystallinity present in the film has minimal influence on the membrane's ability to withstand dissolution in boiling methanol. In conclusion, annealing at temperatures well above the respective α-relaxation for either counterion form induces a significant amount of mobility within the polymer, allowing for increased chain

entanglement, and therefore aids in increasing the mechanical integrity of the membrane when subjected to boiling methanol.

Acknowledgements

Portions of this work were performed at the DuPont-Northwestern-Dow Collaborative Access Team (DND-CAT) located at Sector 5 of the Advanced Photon Source (APS). DND-CAT is supported by E.I. DuPont de Nemours & Co., The Dow Chemical Company and the State of Illinois. Use of the APS was supported by the U. S. Department of Energy, Office of Science, Office of Basic Energy Sciences, under Contract No. DE-AC02-06CH11357.

The authors would also like to acknowledge the assistance of the Polymer Science Department at the University of Southern Mississippi for the use of their wide angle x-ray diffractometer.

Supplemental Information 4A

The following data sets include small angle x-ray scattering (SAXS) of dispersion-cast Nafion® NRE 212CS and extruded Nafion® 117CS in various counterion forms, annealed for 10-1440 minutes at temperatures from 50-300 °C.

Figures 4.16 A-C display SAXS data of H^+-form NRE 212CS annealed at 175 °C for various times (4.16A) and annealed at various temperatures for both 15 minutes (4.16B) and 60 minutes (4.16C). Based on our initial experiments, H^+-form NRE 212CS membranes became mechanically stable in boiling methanol after annealing at 175 °C for one hour. A subsequent experiment on annealing time at 175 °C was conducted and it was determined that the threshold of mechanical stability actually occurred at

approximately 15 minutes. The data shown in Figures 4.16 A-C display the shift of the intercrystalline peak ($q \approx 0.05$ Å^{-1}) to lower q values with increased annealing time and temperature. Figures 4.16 B and C show that the morphological difference between annealing for 15 minutes and annealing for 60 minutes is negligible.

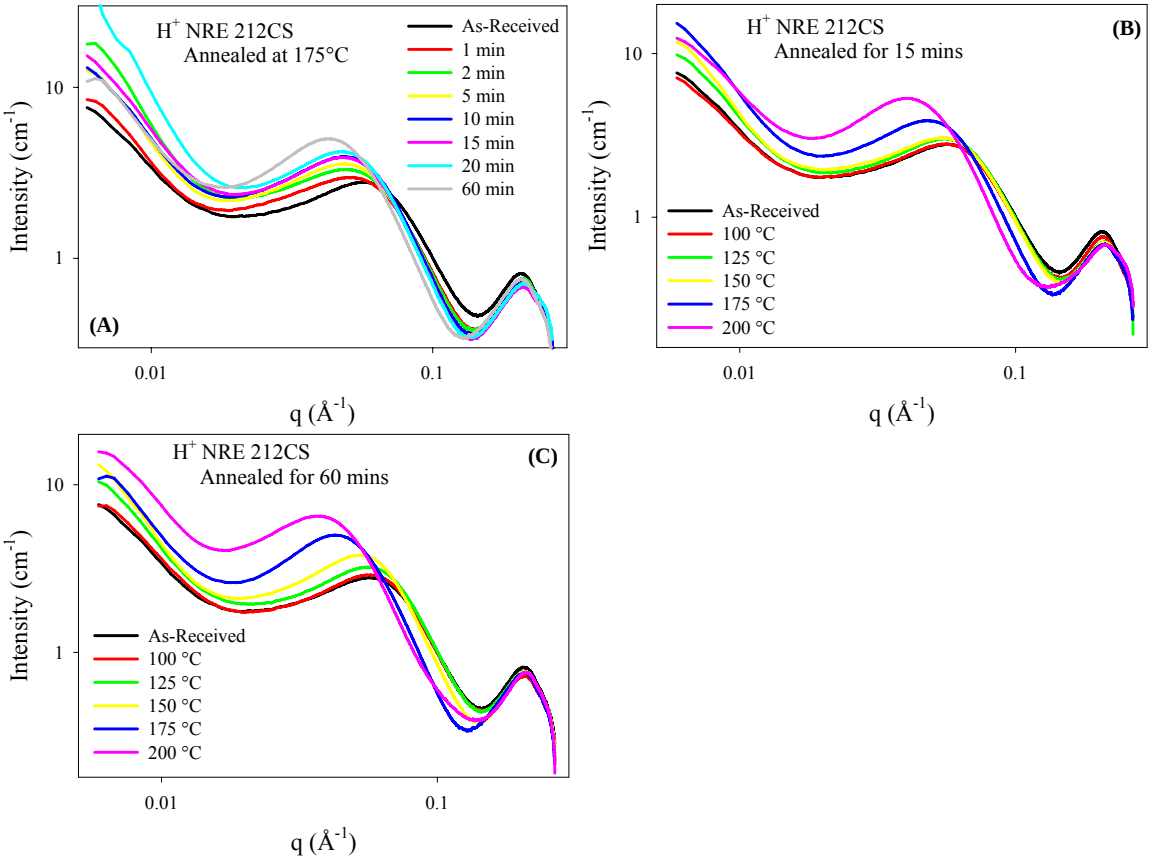

Figure 4.16. A) SAXS profile of H^+-form NRE 212CS membranes before and after annealing at 175 °C for 1, 2, 5, 10, 15, 20, and 60 minutes. **B)** SAXS profile of H^+-form NRE 212CS membranes before and after annealing for fifteen minutes at 100, 125, 150, 175, and 200 °C. **C)** SAXS profile of H^+-form NRE 212CS membranes before and after annealing for sixty minutes at 100, 125, 150, 175, and 200 °C.

Figures 4.17 A-D display SAXS data of Na^+-form NRE 212CS annealed at 250 °C for various times (4.17A), 275 °C for various times (4.17B), fifteen minutes at various temperatures (4.17C), and sixty minutes at various temperatures (4.17D). Similar to the trend seen in Figure 4.16, the intercrystalline peak of Na^+-form NRE 212CS also changes intensity and q spacing with increasing annealing temperature or time. In

agreement with the previous study on H^+-form membranes, the mechanical stability of Na^+-form membranes in boiling methanol was also achieved after annealing for fifteen minutes as opposed to the original experimental criteria of sixty minutes. It is also important to notice the same trend of decreasing crystallinity with increasing annealing temperature as shown in Figures 4.17 C and D.

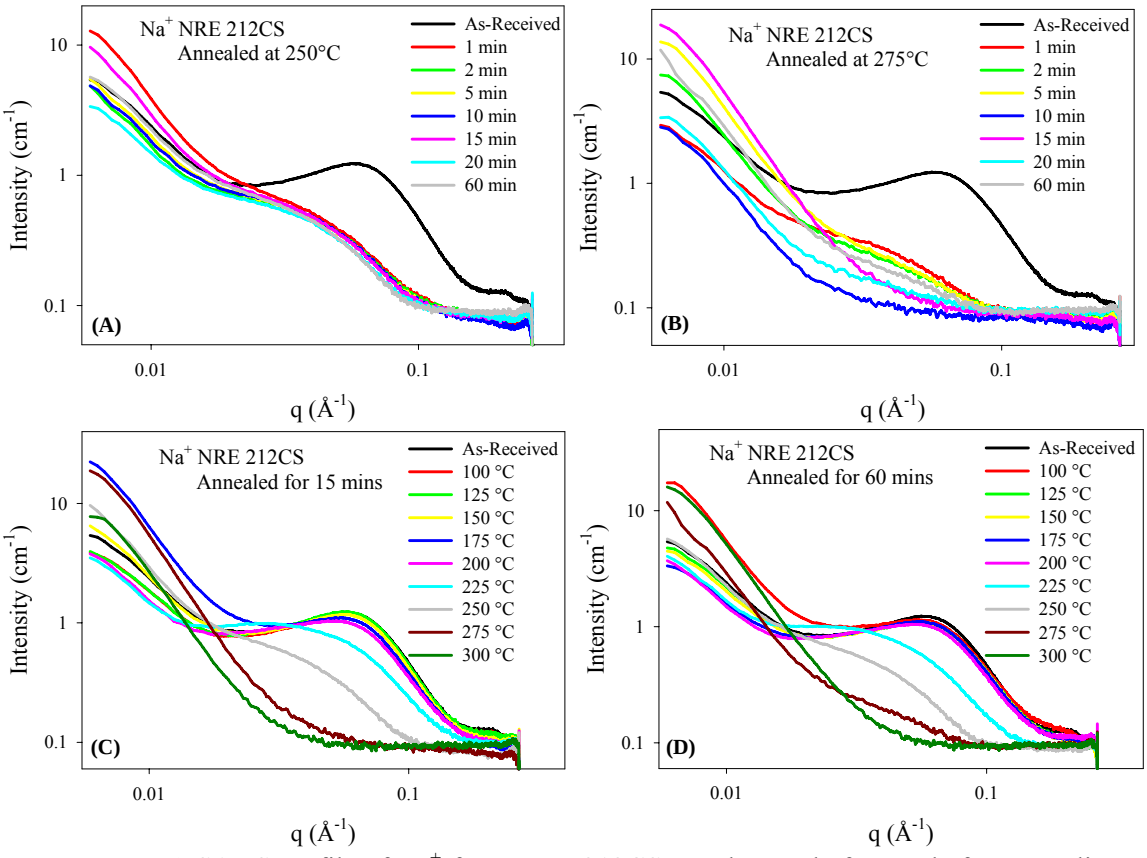

Figure 4.17. A) SAXS profile of Na^+-form NRE 212CS membranes before and after annealing at 250 °C for 1, 2, 5, 10, 15, 20, and 60 minutes. **B)** SAXS profile of Na^+-form NRE 212CS membranes before and after annealing at 275 °C for 1, 2, 5, 10, 15, 20, and 60 minutes. **C)** SAXS profile of Na^+-form NRE 212CS membranes before and after annealing for fifteen minutes at 100, 125, 150, 175, 200, 225, 250, 275, and 300 °C. **C)** SAXS profile of Na^+-form NRE 212CS membranes before and after annealing for sixty minutes at 100, 125, 150, 175, 200, 225, 250, 275, and 300 °C.

Figures 4.18 A-I display SAXS profiles of the 1000 equivalent weight, sulfonyl fluoride Nafion® precursor before and after annealing for 10-1440 minutes at various temperatures. The most striking observation from Figure 4.18 is that the ionomer peak,

located at $q \approx 0.2$ Å^{-1} is absent due to the lack of ionic character in the Nafion® precursor. The intercrystalline peak, located at $q \approx 0.05$ Å^{-1} is observed to sharpen in intensity and shift to lower q values as the annealing temperature is increased, similar to the behavior of H^+-form NRE 212CS membranes.

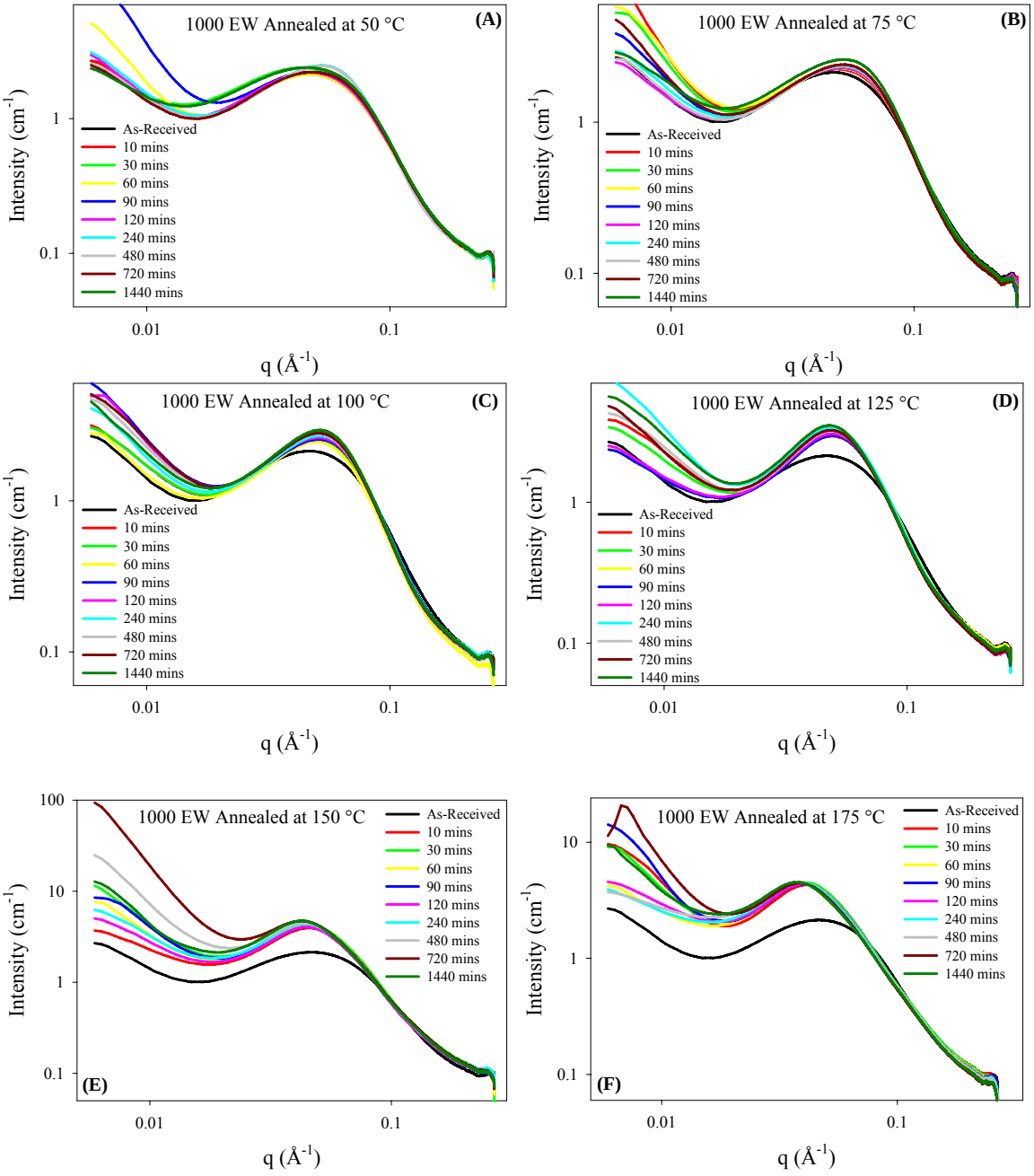

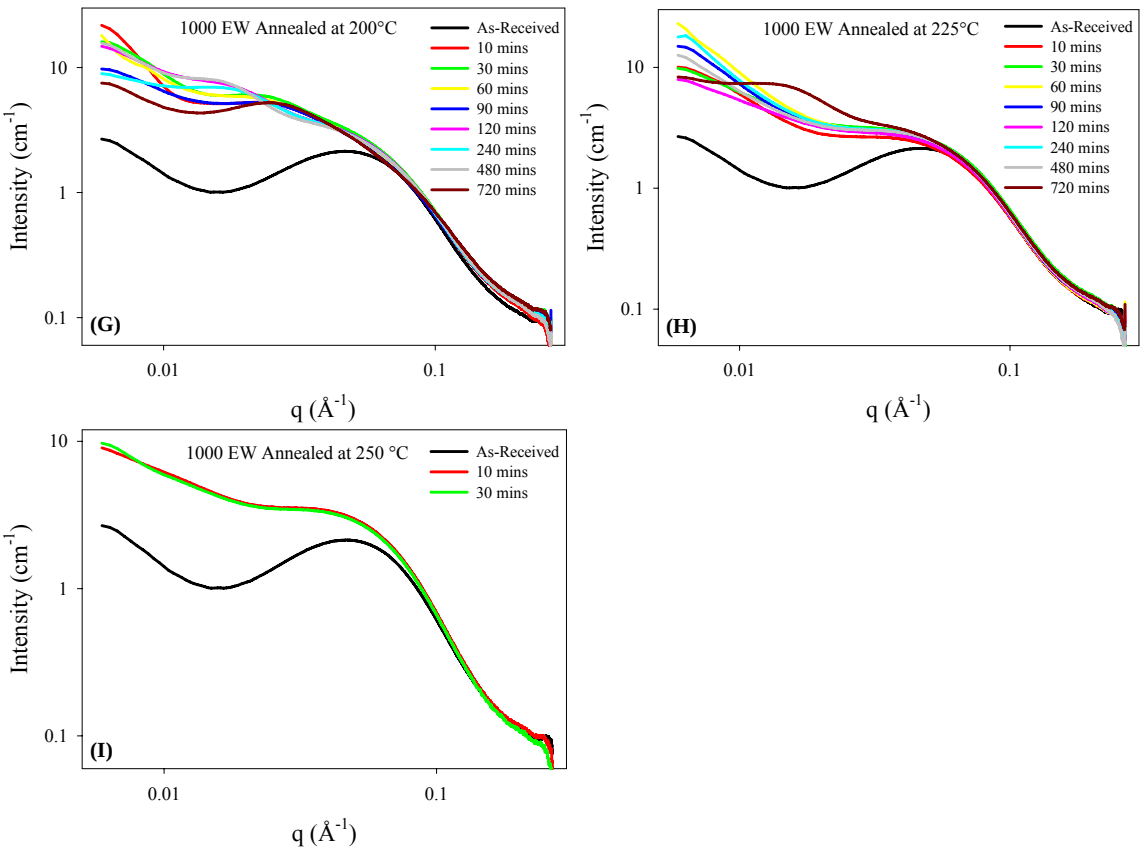

Figure 4.18. SAXS profiles of 1000 equivalent weight, sulfonyl fluoride Nafion® precursor before and after annealing from 10-1440 minutes at **A)** 50 °C, **B)** 75 °C, **C)** 100 °C, **D)** 125 °C, **E)** 150 °C, **F)** 175 °C, **G)** 200 °C, **H)** 225 °C, **I)** 250 °C.

Figures 4.19 A-I display SAXS profiles of the 1100 equivalent weight, sulfonyl fluoride Nafion® precursor before and after annealing for 10-1440 minutes at various temperatures. Similar to the SAXS data of the 1000 equivalent weight, Nafion® precursor, there is no scattering contrast due to an ionic domain and the intercrystalline peak is observed at $q \approx 0.05$ Å^{-1}. In agreement with the lower equivalent weight precursor data, the intercrystalline peak shifts to lower q values along with a decrease in the full width at half maximum with increasing annealing temperature. At temperatures greater than 225 °C, the intercrystalline peak becomes less visible as it shifts to q values within the small angle upturn region ($q < 0.03$).

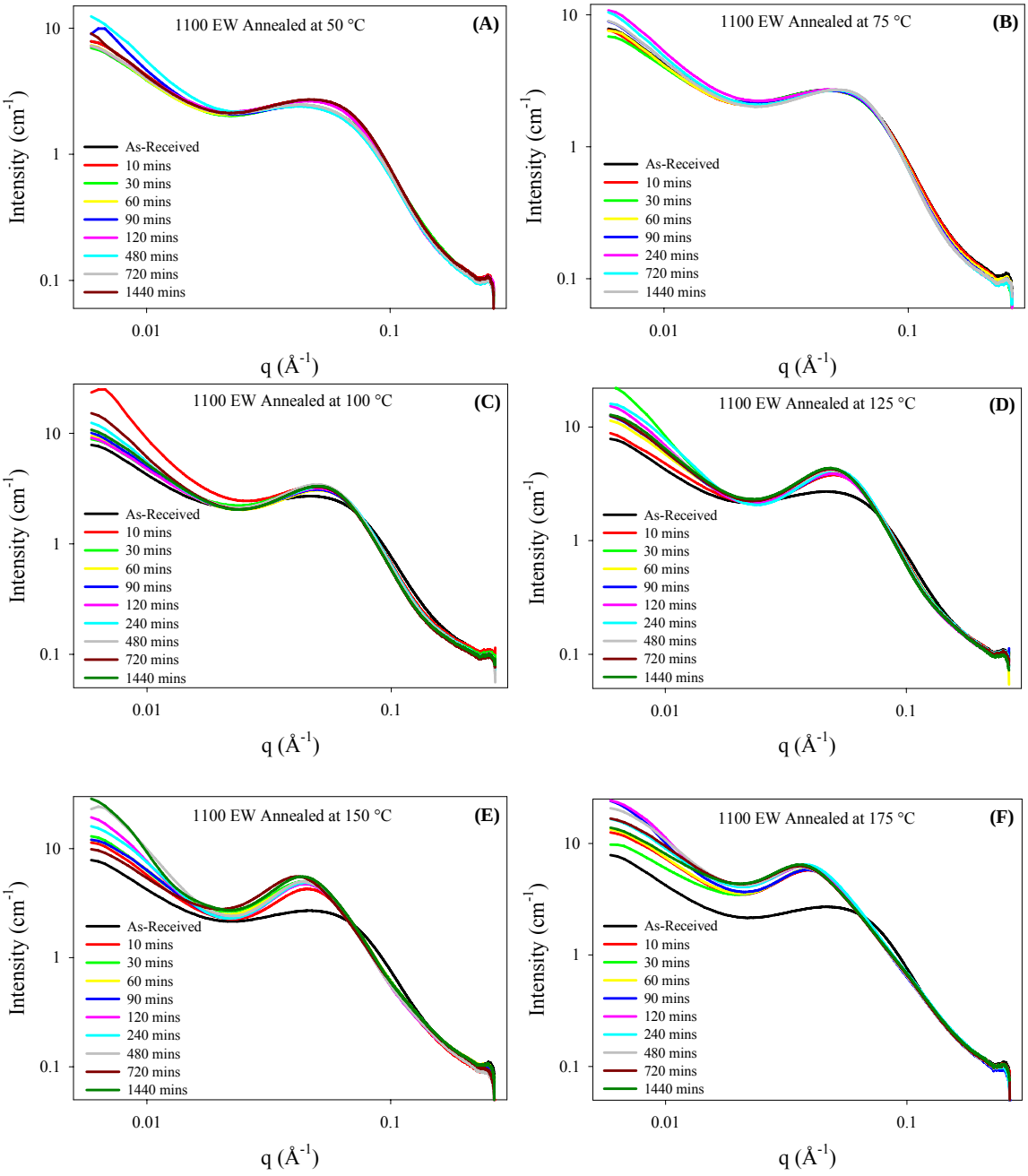
1100 EW Annealed at 50 °C
(A)
1100 EW Annealed at 75 °C
(B)
1100 EW Annealed at 100 °C
(C)
1100 EW Annealed at 125 °C
(D)
1100 EW Annealed at 150 °C
(E)
1100 EW Annealed at 175 °C
(F)
Intensity (cm-1)
q (Å-1)
10
1
0.1
0.01
0.1
As-Received
10 mins
30 mins
60 mins
90 mins
120 mins
240 mins
480 mins
720 mins
1440 mins

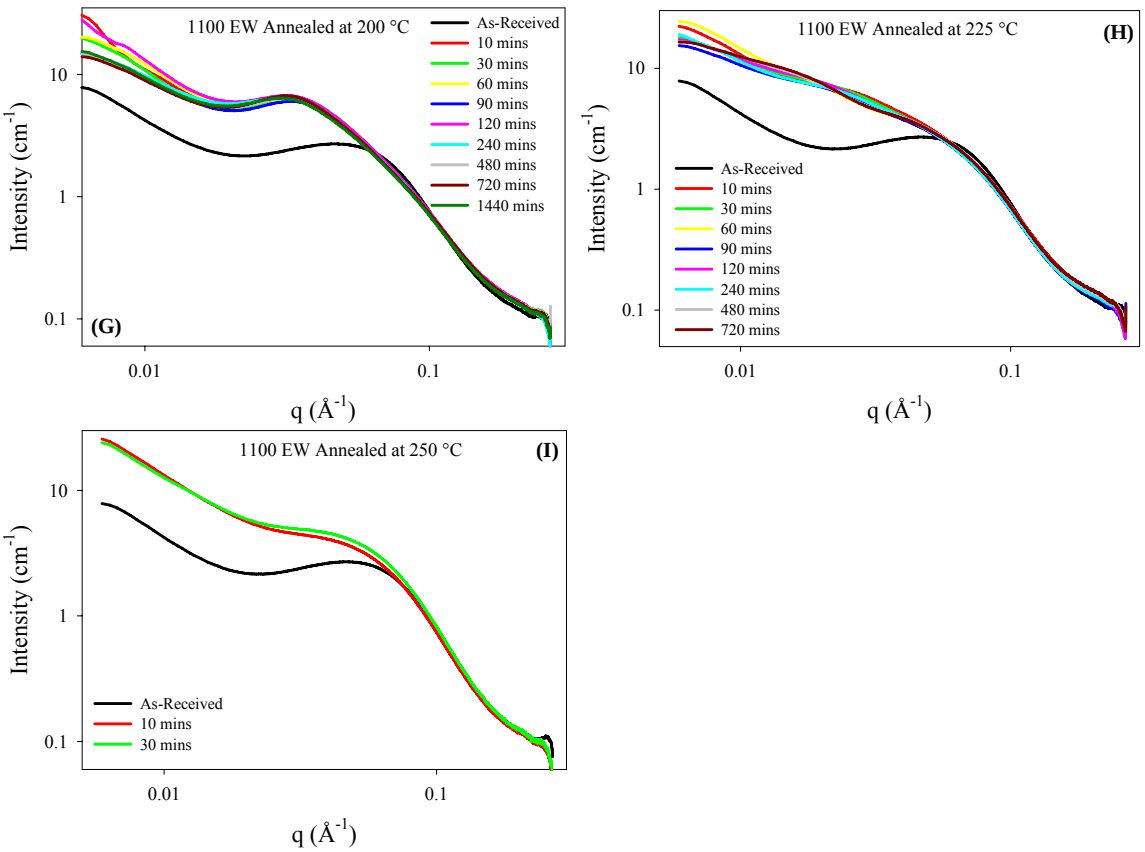

Figure 4.19. SAXS profiles of 1100 equivalent weight, sulfonyl fluoride Nafion® precursor before and after annealing from 10-1440 minutes at **A)** 50 °C, **B)** 75 °C, **C)** 100 °C, **D)** 125 °C, **E)** 150 °C, **F)** 175 °C, **G)** 200 °C, **H)** 225 °C, **I)** 250 °C.

Figures 4.20 A-I display SAXS profiles of the 1200 equivalent weight, sulfonyl fluoride Nafion® precursor before and after annealing for 10-1440 minutes at various temperatures. Similar to the SAXS data of the two previous precursor Nafion® materials, the 1200 EW displays no ionic scattering and the intercrystalline peak is observed at $q \approx 0.05$ Å^{-1}. In agreement with the lower equivalent weight precursor data, the intercrystalline peak shifts to lower q values along with a decrease in the full width at half maximum with increasing annealing temperature. One interesting observation between the three different equivalent weight sample sets is the temperature at which the intercrystalline peak begins to change shape and q position. For example, examine the differences of 1000, 1100, and 1200 equivalent weights annealed at 100 °C for various

times in Figures 4.18C, 4.19C, and 4.20C. It is apparent, based on the SAXS data at 100 °C, that the timescale of morphological manipulation is different depending on the equivalent weight of the ionomer. Since 1200 EW membranes inherently have higher crystalline contents, an increase in the annealing temperature is necessary to observe the same shift in the intercrystalline peak displayed by the lower equivalent weight samples. This observation was also present during the annealing of the membranes as the lower equivalent weight samples began to flow at lower temperatures than the higher equivalent weight membranes.

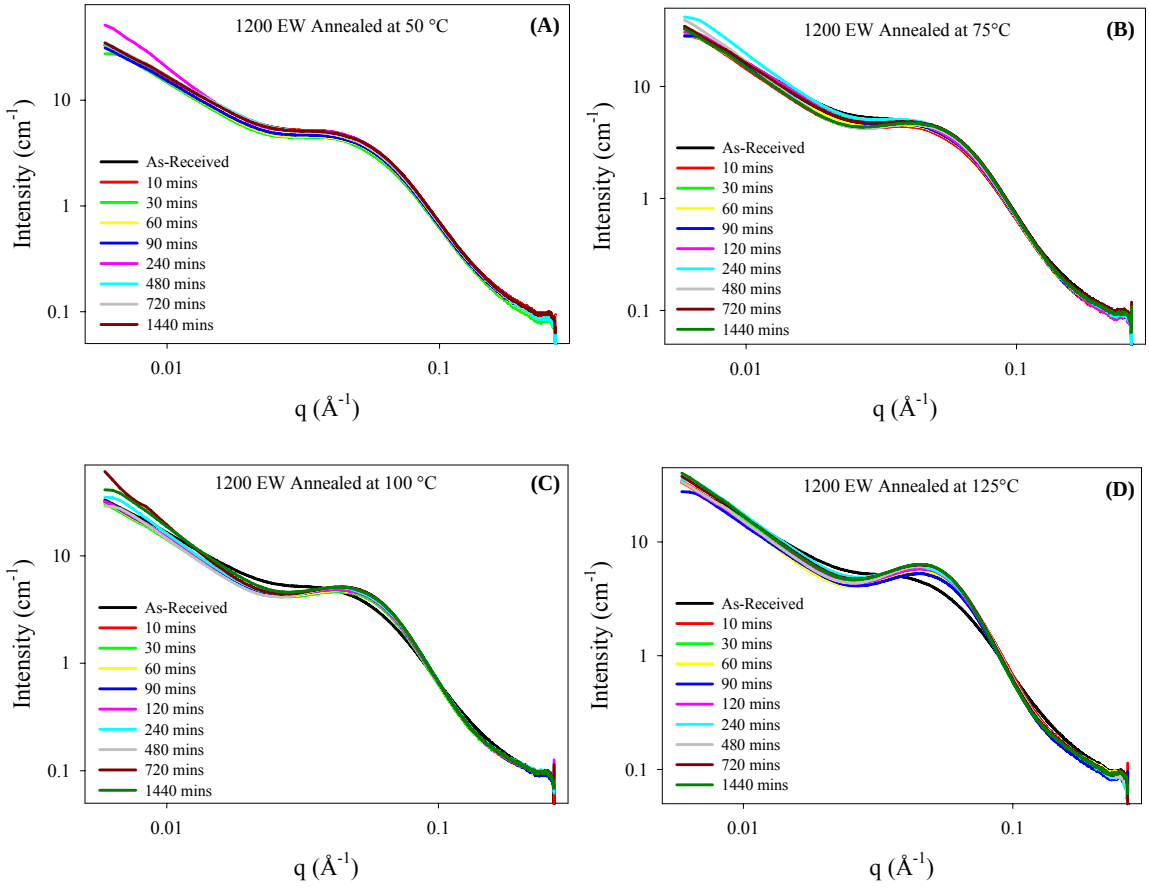

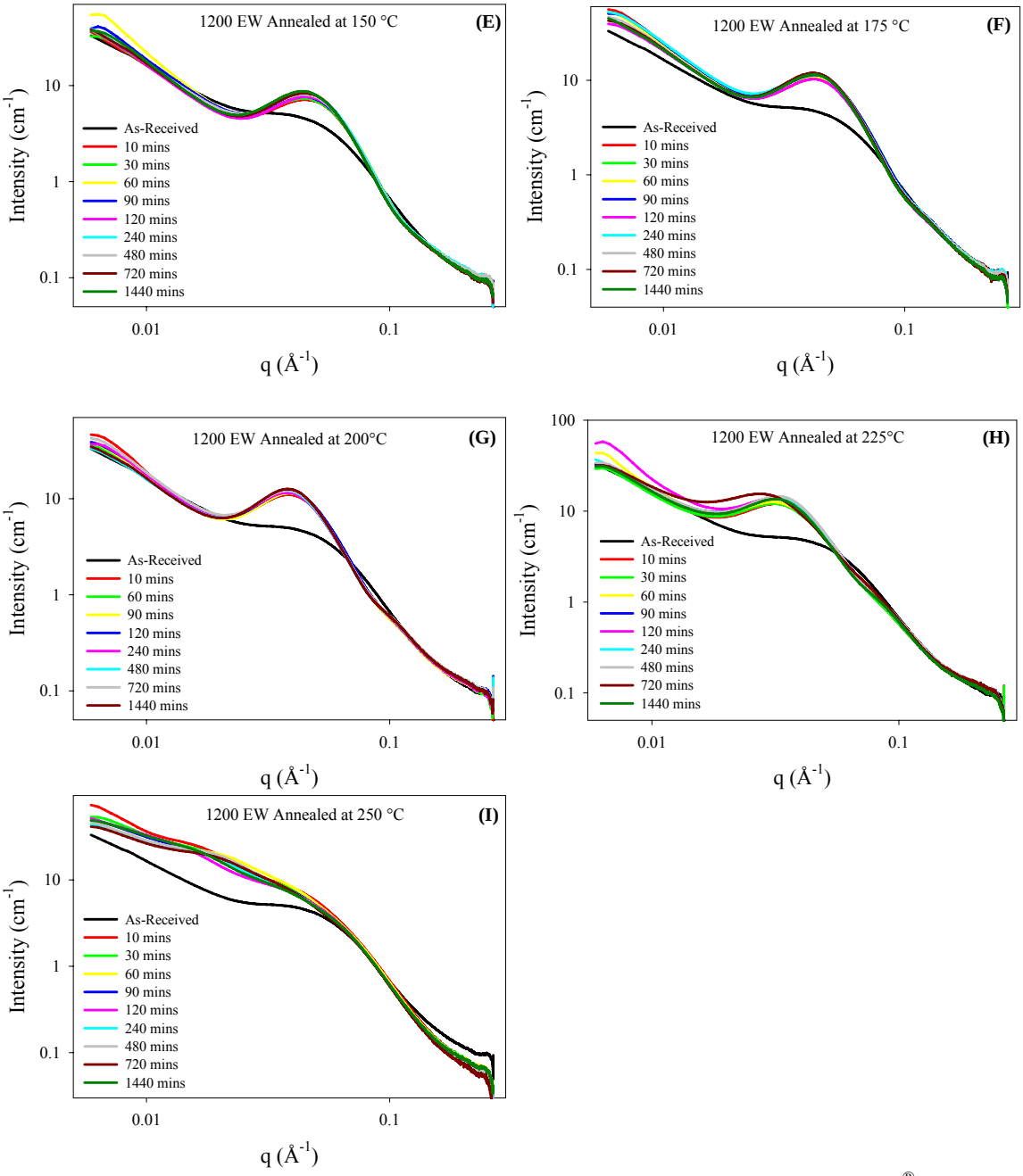

Figure 4.20. SAXS profiles of 1200 equivalent weight, sulfonyl fluoride Nafion® precursor before and after annealing from 10-1440 minutes at **A)** 50 °C, **B)** 75 °C, **C)** 100 °C, **D)** 125 °C, **E)** 150 °C, **F)** 175 °C, **G)** 200 °C, **H)** 225 °C, **I)** 250 °C.

Figures 4.21 A-F display SAXS profiles of H^+-form extruded Nafion® 117CS before and after annealing for 10-1440 minutes at various temperatures. Both the intercrystalline peak ($q \approx 0.05$ Å^{-1}) and ionomer peak ($q \approx 0.2$ Å^{-1}) are present in all SAXS profiles regardless of annealing temperature. Similar to the behavior observed

with the Nafion® precursor membranes, the intercrystalline peak of the H^+-form ionomer shifts to lower q values and the full width at half maximum decreases with increasing annealing temperature from 100 to 175 °C. Above 175 °C, both the intercrystalline and ionomer peaks broaden and decrease in intensity. The changes in the intercrystalline peak are inherent to melting of the crystallites with increasing temperature. The changes to the ionomer peak are less apparent and could be due to a multitude of effects. Since the α-relaxation temperature of H^+-form Nafion® is approximately 110 °C, by annealing at temperatures greater than 100 °C we observe a significant increase in the mobility of the polymer chains.[42] It appears, based on the data in Figure 4.21 D, that annealing H^+-form Nafion® at 175 °C for various times can result in increased resolution of both the intercrystalline and ionomer peaks. An increase in the intercrystalline peak intensity with increasing annealing time is also observed in Figure 4.21 D, indicating that 175 °C may be an excellent temperature to choose for an isothermal crystallization study of H^+-form Nafion®. The broadening and decreasing intensity of the ionomer peak at annealing temperatures above 175 °C could also be attributed to the discoloration observed while annealing H^+-form Nafion® at elevated temperatures. We have already shown that the equivalent weight of the ionomer remains constant up to an annealing temperature of 200 °C (Figure 4.6), but the effects of the discoloration on both the ionomer and crystalline morphology must be examined further.

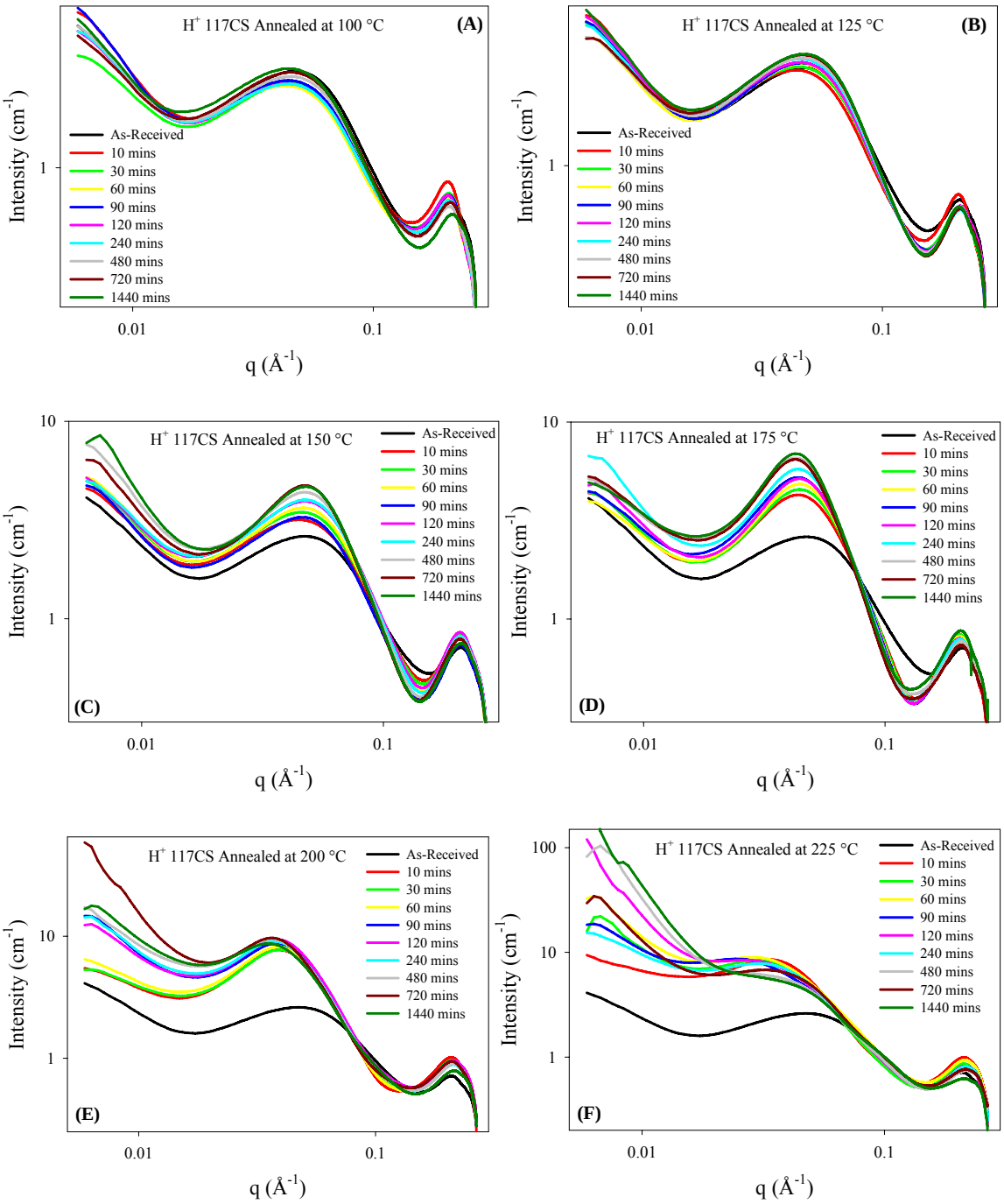

Figure 4.21. SAXS profiles of H^+-form Nafion® 117CS before and after annealing from 10-1440 minutes at **A)** 100 °C, **B)** 125 °C, **C)** 150 °C, **D)** 175 °C, **E)** 200 °C, **F)** 225 °C.

Figures 4.22 A-H display SAXS profiles of Na^+-form extruded Nafion® 117CS before and after annealing for 10-1440 minutes at various temperatures. The intercrystalline peak is present at lower annealing temperatures at $q \approx 0.05$ Å^{-1}, but the

ionomer peak ($q \approx 0.2$ Å^{-1}) is absent in all of the SAXS profiles. Fujimura et al. also observed an absence of the ionomer peak in Na^+-form Nafion® and attributed it to a small electron density difference between the ionic aggregates and the surrounding scattering medium.[34] To prove this theory, Fujimura and coworkers exchanged the membrane back into the H^+-form, where the electron density of the aggregates became lower than that of the surroundings, and the scattering due to the ionomer peak returned. They also exchanged the membrane into the cesium, Cs^+-form, which increased the electron difference, resulting in an increase in the ionomer peak intensity. Without the ionomer peak present in Figures 4.22 A-H, the intercrystalline peak can be examined without any scattering interference. Similar to the thermal annealing studies on dispersion-cast Na^+-form NRE 212CS (Figure 4.14 and Table 4-5) the crystalline domain remains constant at annealing temperatures below 175 °C. By annealing at temperatures greater than 175 °C, the crystallinity begins to decrease and finally disappears due to melting at 275 °C.

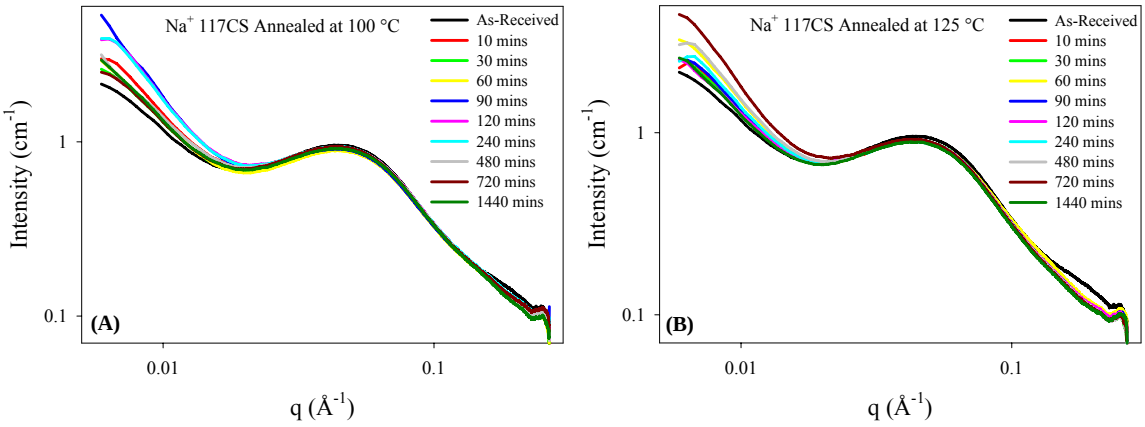

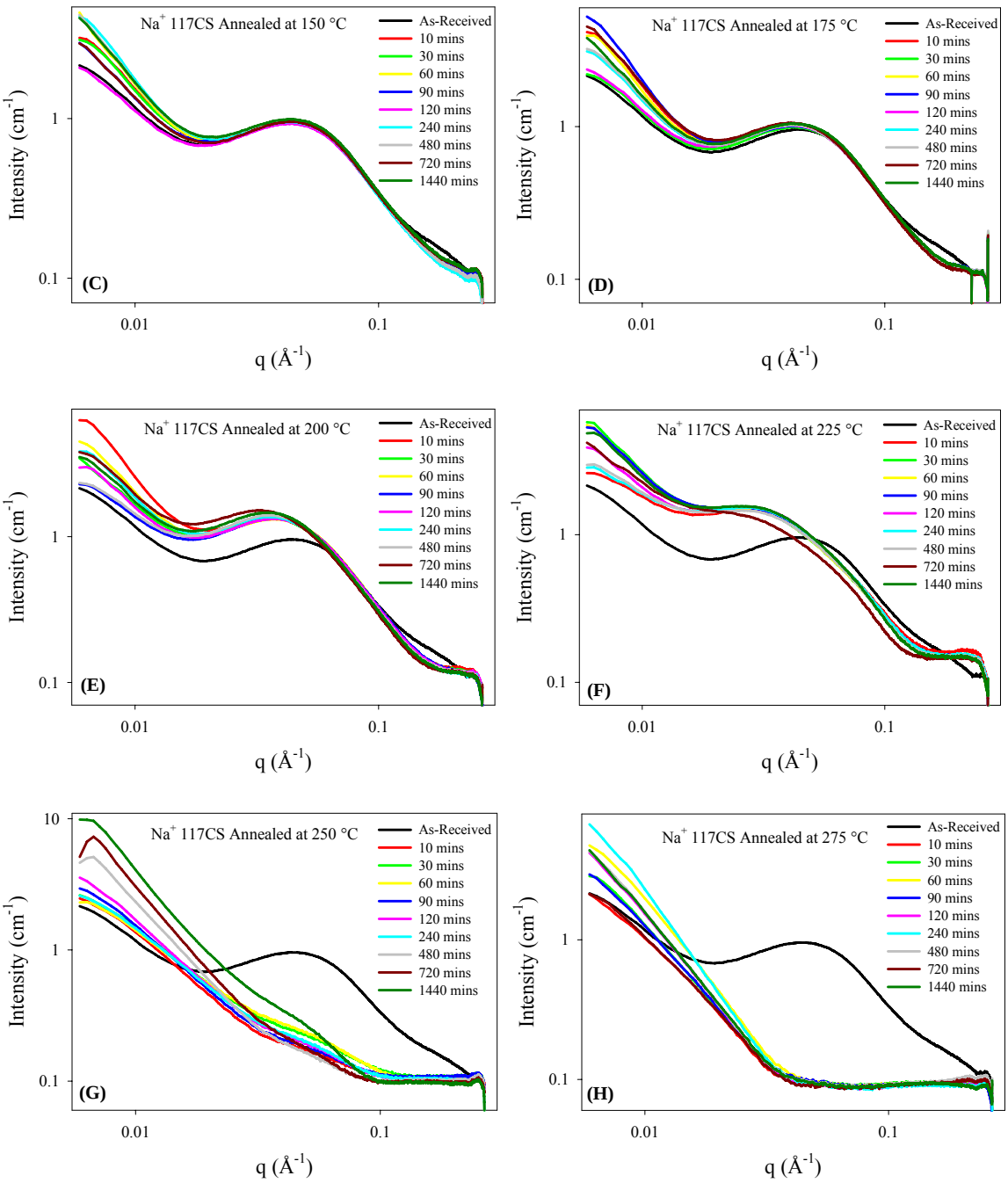

Figure 4.22. SAXS profiles of sodium (Na^+) form Nafion® 117CS before and after annealing from 10-1440 minutes at **A)** 100 °C, **B)** 125 °C, **C)** 150 °C, **D)** 175 °C, **E)** 200 °C, **F)** 225 °C, **G)** 250 °C, **H)** 275 °C.

Figures 4.23 A-H display SAXS profiles of Cs^+-form extruded Nafion® 117CS before and after annealing for 10-1440 minutes at various temperatures. The most distinct portion of the SAXS profiles is the ionomer peak at $q \approx 0.2$ Å^{-1}. Based on the

discussions of Fujimura et al. the cesium counterion allows for an increase in the electron density difference between the ionic domains and the surrounding scattering medium, which causes an increase in the scattering intensity of the ionomer peak. On the other hand, the electron density contrast has also caused a disappearance of the intercrystalline peak ($q \approx 0.05$ Å^{-1}) due to similar scattering electron densities between the ionic and crystalline domains. Because of this phenomenon, we now have the ability to examine both the intercrystalline and ionomer peaks of Nafion® individually without any scattering interference with the aid of either sodium or cesium counterions. From the data shown in Figures 4.23 A-H, we observe that annealing temperature has a profound impact on the ionomer morphology of Cs^+-form Nafion®. As the annealing temperature increases from 100 to 200 °C, the ionomer peak intensity increases and the full width at half maximum decreases. By annealing at temperatures from 200 to 275 °C, the ionomer peak begins to broaden and decrease in intensity. The sharpening of the ionomer peak at lower annealing temperatures may be indicative of a more isotropic ionic aggregate morphology as depicted by Page and coworkers.[55] Another observation from Figures 4.23 A-H is the appearance of the intercrystalline peak at annealing temperatures between 200 and 225 °C. The emergence of a crystalline peak at these temperatures could be attributed to two different mechanisms. First, as the ionomer morphology becomes more uniform between 175 and 225 °C, the electron density contrast between the intercrystalline and ionomer peaks may vary, allowing for the detection of the intercrystalline peak of Cs^+-form Nafion® using SAXS. Second, since we are performing an annealing experiment and not an isothermal crystallization experiment, the appearance of the intercrystalline peak at temperatures above 200 °C could be due to the increased

crystallization kinetics of Cs^+-form Nafion®. Page et al. have demonstrated that by increasing the counterion size, the dipole-dipole interactions of the electrostatic network weaken, thereby facilitating increased chain mobility and rate of crystallization.[42] Due to the increased crystallization kinetics of Cs^+-form Nafion®, the time required to quench the membrane from the annealing temperature to room temperature may be sufficient to induce the formation of Teflon-like crystallites seen in Figures 4.23 E and F.

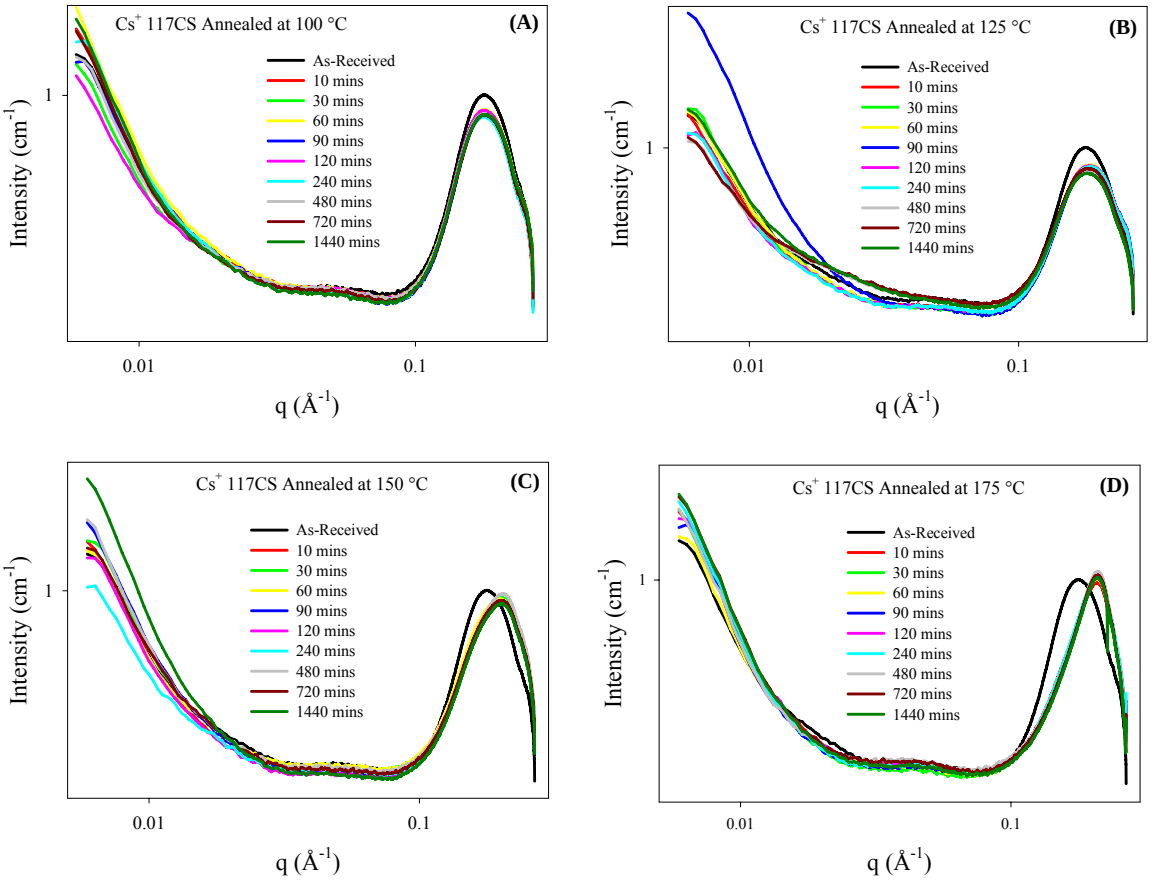

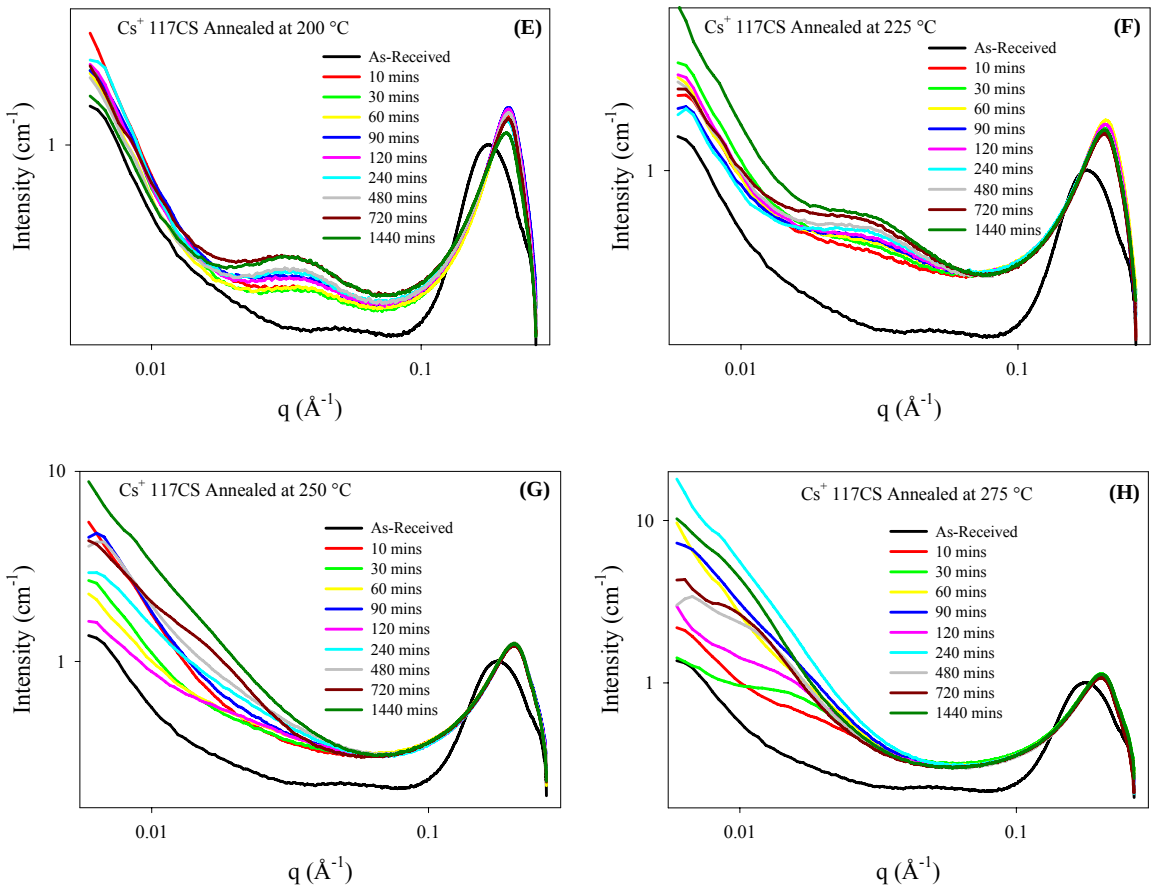

Figure 4.23. SAXS profiles of cesium (Cs^+) form Nafion® 117CS before and after annealing from 10-1440 minutes at **A)** 100 °C, **B)** 125 °C, **C)** 150 °C, **D)** 175 °C, **E)** 200 °C, **F)** 225 °C, **G)** 250 °C, **H)** 275 °C.

Figures 4.24 A-H display SAXS profiles of tetramethylammonium or TMA^+-form extruded Nafion® 117CS before and after annealing for 10-1440 minutes at various temperatures. Both the intercrystalline peak ($q \approx 0.05$ $Å^{-1}$) and ionomer peak ($q \approx 0.2$ $Å^{-1}$) are present in the SAXS profiles before and after annealing up to 250 °C. At annealing temperatures beyond 250 °C, the intercrystalline peak disappears due to melting of the Teflon-like crystallites. Similar to the SAXS data on previous counterion forms of extruded Nafion®, the intercrystalline peak sharpens and shifts to smaller q values with increasing annealing temperature until disappearing due to melting of the crystallites at approximately 275 °C. The morphological changes with annealing temperature of the TMA^+-form ionomer peak are similar to the changes observed while

using the cesium counterion. The ionomer peak gradually sharpens and increases in intensity until approximately 200 or 225 °C, upon which the peak broadens and slightly decreases in intensity up to an annealing temperature of 275 °C. In agreement with Page and coworkers' discussion on the morphological changes of the Cs^+-form SAXS ionomer peak as a function of annealing temperature, we agree that the sharpening of the TMA^+-form ionomer peak between annealing at 200 and 250 °C may be indicative of a more isotropic ionic aggregate morphology.[55] Finally, coinciding with the trend of the other counterion forms, annealing time had minimal effect on the overall change in ionomer or crystalline morphology. Maximum morphological manipulation was achieved after annealing no longer than thirty minutes at each annealing temperature.

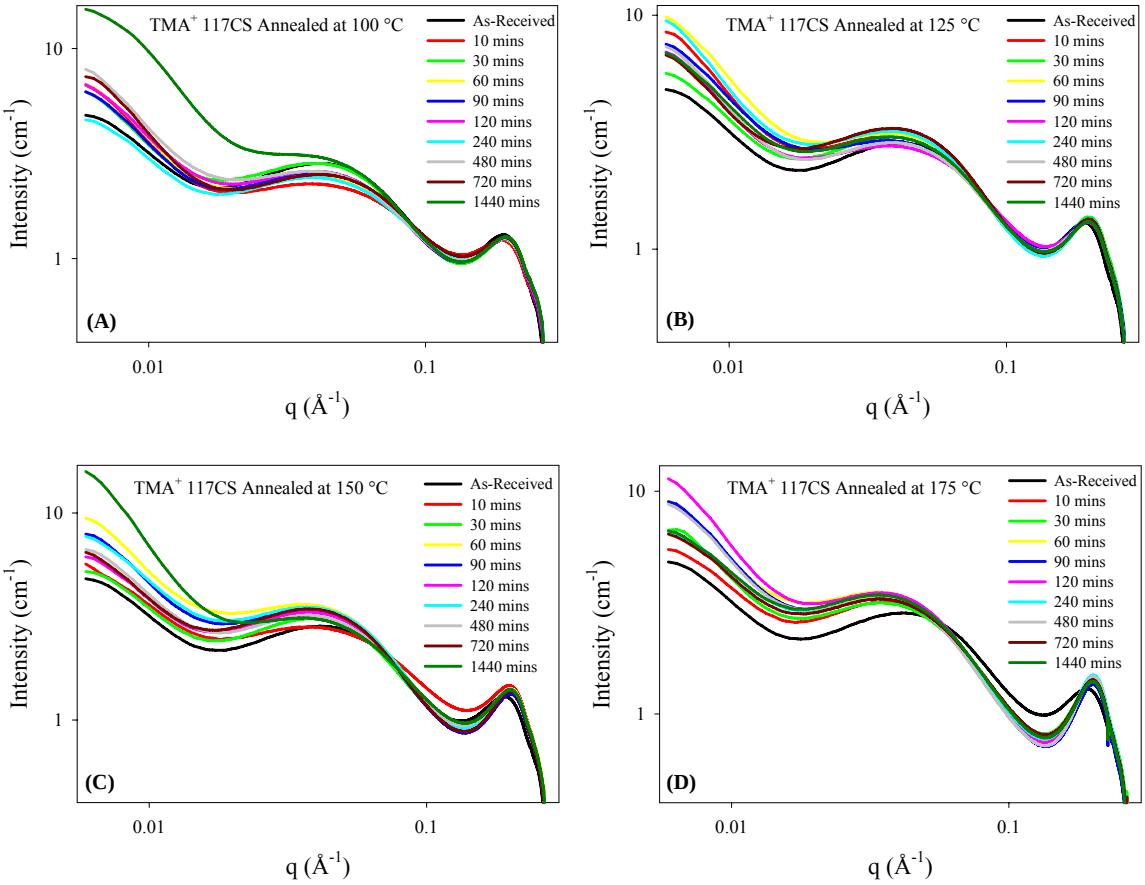

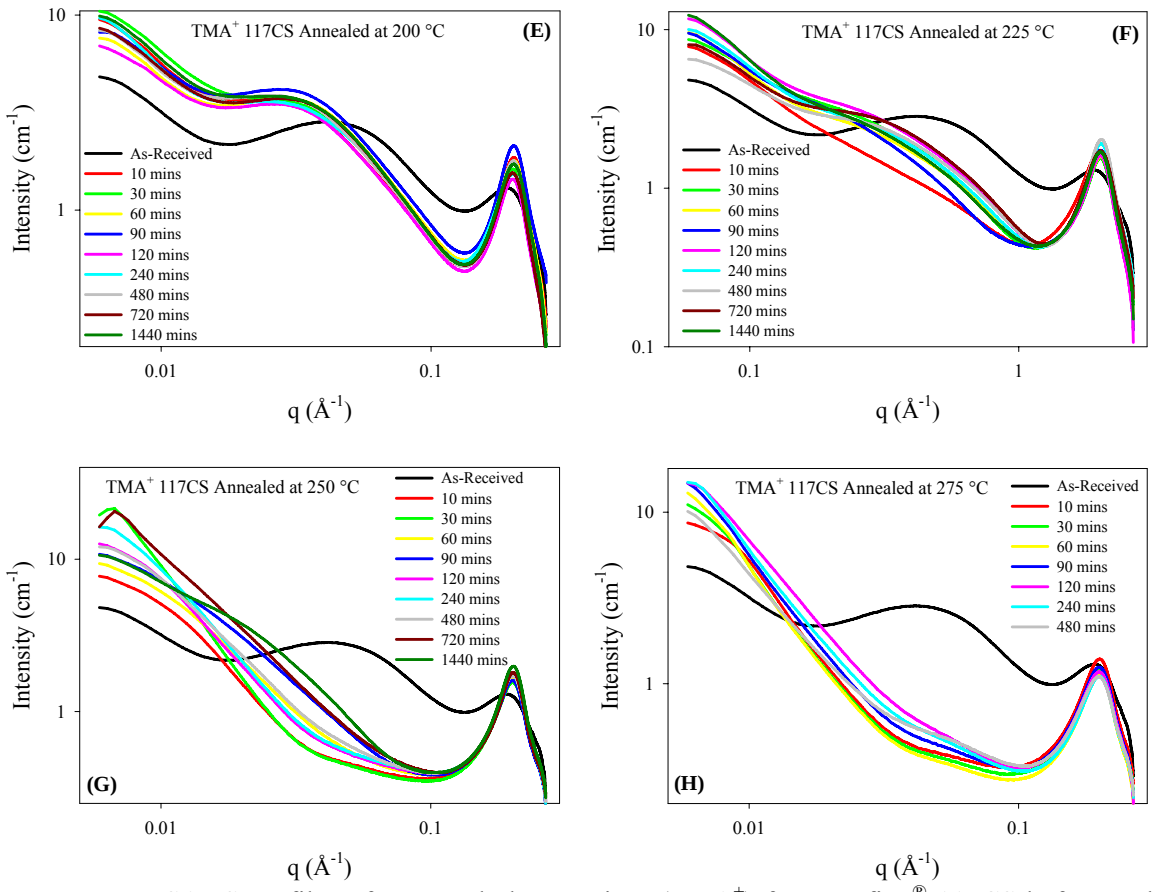

Figure 4.24. SAXS profiles of tetramethylammonium (TMA^+) form Nafion® 117CS before and after annealing from 10-1440 minutes at **A)** 100 °C, **B)** 125 °C, **C)** 150 °C, **D)** 175 °C, **E)** 200 °C, **F)** 225 °C, **G)** 250 °C, **H)** 275 °C.

Figures 4.25 A-H display SAXS profiles of tetrabutylammonium or TBA^+-form extruded Nafion® 117CS before and after annealing for 10-1440 minutes at various temperatures. Both the intercrystalline peak ($q \approx 0.05$ $Å^{-1}$) and ionomer peak ($q \approx 0.2$ $Å^{-1}$) are present in all SAXS profiles regardless of annealing temperature. The ionomer peak of TBA^+-form Nafion® undergoes morphological changes similar to that of the TMA^+ counterion shown in Figure 4.24. The TBA^+-form ionomer peak full width at half maximum decreases and the intensity increases by annealing from 100 to 175 °C. Between 175 and 275 °C the ionomer peak begins to broaden and the full width at half maximum increases as a function of annealing temperature. In contrast to the SAXS data of the TMA^+-form ionomer peak, the TBA^+-form ionomer peak reaches a maximum peak

resolution after annealing at 175 °C for at least thirty minutes. The difference in the maximum resolution temperatures between the TBA^+ and TMA^+ counterions is associated with the counterion sizes and their abilities to strengthen or weaken the electrostatic network. Page et al. have shown using variable temperature SAXS that the temperature at which Nafion's® *static* electrostatic network becomes *dynamic*, through ion-hopping, depends on the size of the counterion.[42] Due to the stronger dipole-dipole forces of the TMA^+-counterion, it requires a higher annealing temperature before morphological manipulation occurs. On the other hand, since the TBA^+ counterion is so large and bulky, it effectively plasticizes the electrostatic network and hence a lower annealing temperature is necessary to induce ion-hopping or significant manipulation of the ionomer morphology.

The most striking feature of the TBA^+-form SAXS profiles shown in Figures 4.25 A-H is the persistence of the intercrystalline peak with annealing temperature. Unlike the previous counterion forms of Nafion®, the q position of intercrystalline peak of the TBA^+-form remains relatively constant through annealing from 100-275 °C. Similar to H^+-form, the intercrystalline peak of TBA^+-form displays a maximum in peak intensity and a minimum full width at half maximum after annealing at 175 °C. The morphological changes witnessed at 175 °C for both the H^+ and TBA^+ counterion forms coincide well with the dynamic mechanical α-relaxation temperatures of both counterions being relatively the same, 110 °C and 125 °C, respectively. Due to the excessive discoloration and thermal degradation of H^+-form Nafion® at annealing temperatures greater than 225 °C, we were unable to directly correlate changes in the intercrystalline peak of both H^+ and TBA^+ form Nafion®. It is interesting to note that the intercrystalline

peak of TBA^+-form Nafion® persists beyond the crystalline melting temperature of 275 °C shown in Figure 4.25 H. We predict that the crystallization behavior of the TBA^+-couterion form is in agreement with that of the cesium counterion, in that the time required to quench the membrane from the annealing temperature to room temperature may be sufficient to induce the formation of Teflon-like crystallites.

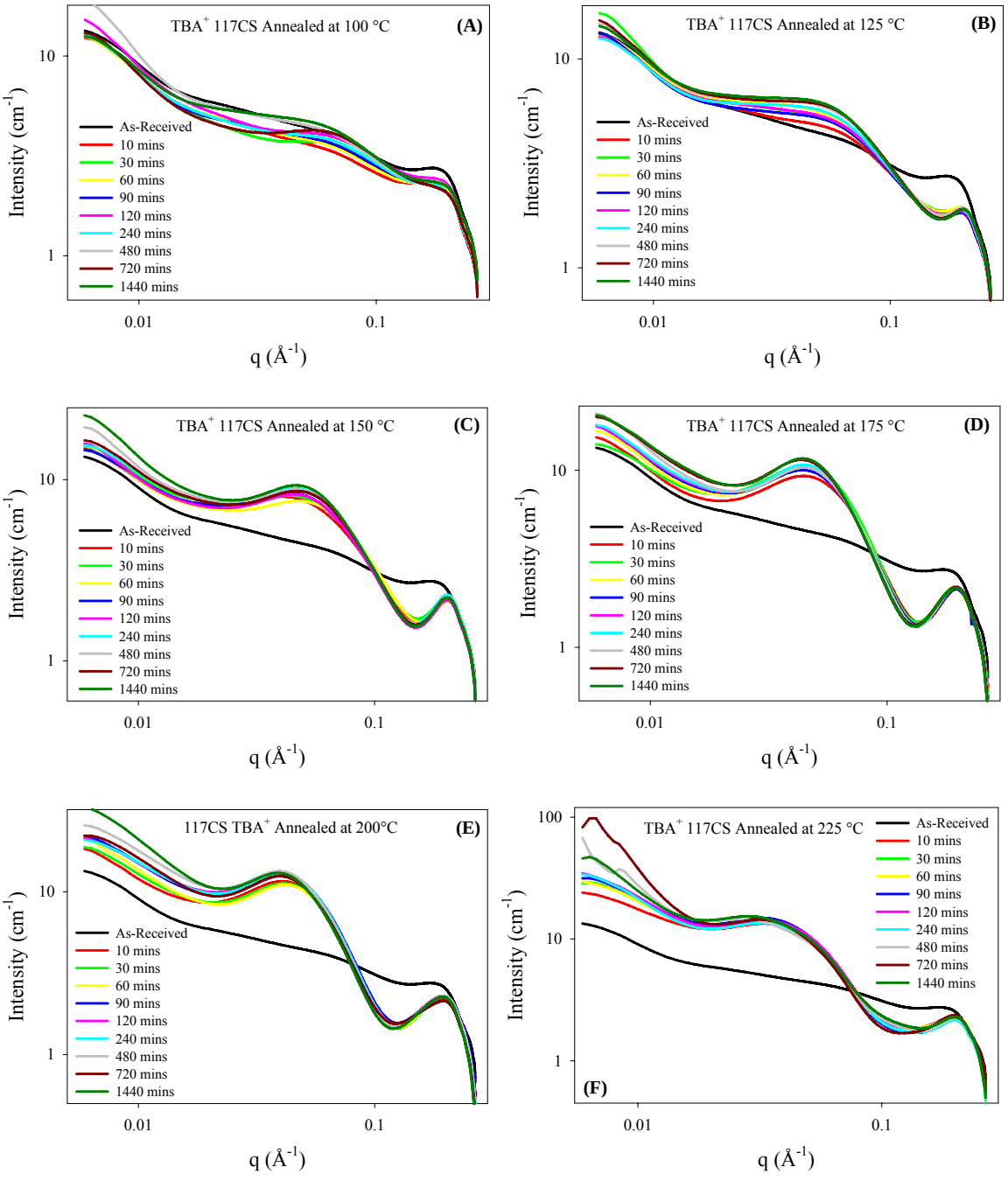

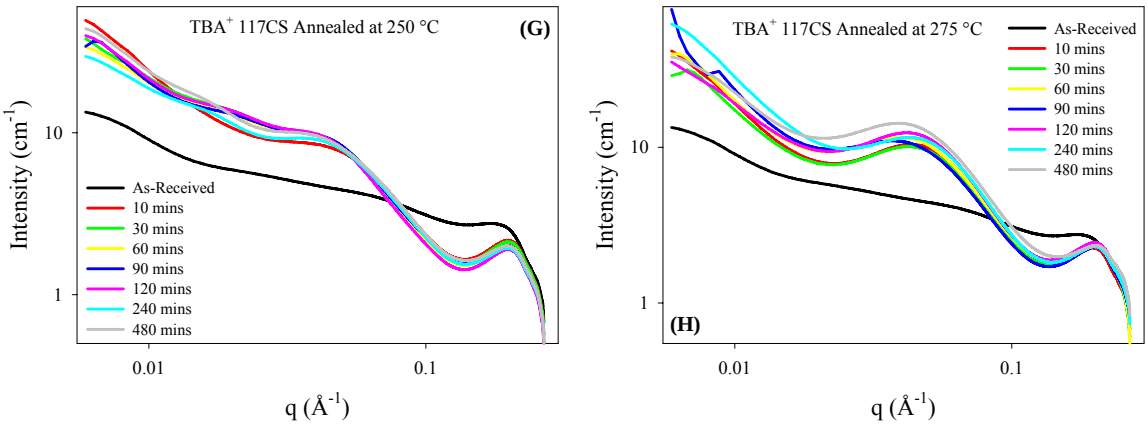

Figure 4.25. SAXS profiles of tetrabutylammonium (TBA^+) form Nafion® 117CS before and after annealing from 10-1440 minutes at **A)** 100 °C, **B)** 125 °C, **C)** 150 °C, **D)** 175 °C, **E)** 200 °C, **F)** 225 °C, **G)** 250 °C, **H)** 275 °C.

References

(1) Connolly, D. J.; Gresham, W. F. *Fluorocarbon Vinyl Ether Polymers*. Patent US3282875, 1966.

(2) Grot, W. *Chemie Ingenieur Technik* **1978,** 50, 299-301.

(3) Mauritz, K. A.; Moore, R. B. *Chemical Reviews* **2004,** 104, (10), 4535-4585.

(4) Hsu, W. Y.; Gierke, T. D. *Journal of Membrane Science* **1983,** 13, 307-326.

(5) Doyle, M.; Rajendran, G., Perfluorinated membranes. In *Handbook of Fuel Cells - Fundamentals, Technology and Applications*, Wolf Vielstich, A. L., and Hubert A. Gasteiger, Ed. John Wiley & Sons, Ltd, Chichester: 2003; Vol. 3 Part 3, pp 351-395.

(6) Borup, R.; Meyers, J.; Pivovar, B.; Kim, Y. S.; Mukundan, R.; Garland, N.; Myers, D.; Wilson, M.; Garzon, F.; Wood, D.; Zelenay, P.; More, K.; Stroh, K.; Zawodzinski, T.; Boncella, J.; McGrath, J. E.; Inaba, M.; Miyatake, K.; Hori, M.; Ota, K.; Ogumi, Z.; Miyata, S.; Nishikata, A.; Siroma, Z.; Uchimoto, Y.; Yasuda, K.; Kimijima, K.; Iwashita, N. *Chemical Reviews* **2007,** 107, 3904-3951.

(7) EG & G Technical Services, Inc. *Fuel Cell Handbook (Seventh Edition)*; U.S. Department of Energy: Morgantown, WV, 2004.

(8) Grubb, Willard T. *Fuel Cell*. Patent US2913511, 1959.

(9) Heinzel, A.; Barragan, V. M. *Journal of Power Sources* **1999,** 84, 70-74.

(10) Majsztrik, P. W.; Bocarsly, A. B.; Benziger, J. B. *Review of Scientific Instruments* **2007,** 78, (10), 103904 1-7.

(11) Huang, X. Y.; Solasi, R.; Zou, Y.; Feshler, M.; Reifsnider, K.; Condit, D.; Burlatsky, S.; Madden, T. *Journal of Polymer Science Part B-Polymer Physics* **2006,** 44, (16), 2346-2357.

(12) E. I. Dupont De Nemours & Co Inc. *DuPont™ Nafion® PFSA Membranes NRE-211 and NRE-212*. http://www.fuelcellmarkets.com/content/images/articles/nae201.pdf (January 3, 2009).

(13) E. I. Dupont De Nemours & Co Inc. *DuPont™ Nafion® PFSA Membranes N-115, N-117, NE-1110*.

http://www.fuelcellmarkets.com/content/images/articles/nae101.pdf (January 3, 2009).
(14) Curtin, D. E.; Lousenberg, R. D.; Henry, T. J.; Tangeman, P. C.; Tisack, M. E. *Journal of Power Sources* **2004,** 131, (1-2), 41-48.
(15) Grot, W. G. *Production of a liquid composition containing a perfluorinated ion exchange polymer*. Patent EP0066369, 1982.
(16) Martin, Charles R.; Rhoades, Teresa A.; Ferguson, James A. *Analytical Chemistry* **1982,** 54, (9), 1639-1641.
(17) Yeo, R. S. *Polymer* **1980,** 21, (4), 432-435.
(18) Moore, Robert B.; Martin, Charles R. *Analytical Chemistry* **1986,** 58, 2569-2570.
(19) Moore, Robert. B.; Martin, Charles R. *Macromolecules* **1988,** 88, (21), 1334-1339.
(20) Martin, C. R.; Moore, R. B. *Method for the Preparation of Ionomer Films*. Patent US4731263, 1988.
(21) Gebel, G.; Aldebert, P.; Pineri, M. *Macromolecules* **1987,** 20, 1425-1428.
(22) Moore, Robert B.; Martin, Charles B. *Macromolecules* **1989,** 22, 3594-3599.
(23) Laporta, M.; Pegoraro, M.; Zanderighi, L. *Macromolecular Materials and Engineering* **2000,** 282, 22-29.
(24) Siroma, Z.; Ioroi, T.; Fujiwara, N.; Yasuda, K. *Electrochemistry Communications* **2002,** 4, (2), 143-145.
(25) Sanders, E. H.; McGrady, K. A.; Wnek, G. E.; Edmondson, C. A.; Mueller, J. M.; Fontanella, J. J.; Suarez, S.; Greenbaum, S. G. *Journal of Power Sources* **2004,** 129, (1), 55-61.
(26) Lee, K.; Ishihara, A.; Mitsushima, S.; Kamiya, N.; Ota, K. *Journal Of The Electrochemical Society* **2004,** 151, (4), A639-A645.
(27) Silva, R. F.; De Francesco, M.; Pozio, A. *Electrochimica Acta* **2004,** 49, (19), 3211-3219.
(28) Parra, S.; Henao, L.; Mielczarski, E.; Mielczarski, J.; Albers, P.; Suvorova, E.; Guindet, J.; Kiwi, J. *Langmuir* **2004,** 20, (13), 5621-5629.
(29) Tian, H.; Savadogo, O. *Fuel Cells* **2005,** 5, (3), 375-382.
(30) Lin, H. L.; Yu, T. L.; Huang, C. H.; Lin, T. L. *Journal of Polymer Science Part B-Polymer Physics* **2005,** 43, (21), 3044-3057.
(31) Sacca, A.; Carbone, A.; Pedicini, R.; Portale, G.; D'Ilario, L.; Longo, A.; Martorana, A.; Passalacqua, E. *Journal of Membrane Science* **2006,** 278, (1-2), 105-113.
(32) Zook, L. A.; Leddy, J. *Analytical Chemistry* **1996,** 68, (21), 3793-3796.
(33) Gierke, T.D.; Munn, G.E.; Wilson, F.C. *Journal of Polymer Science: Polymer Physics Edition* **1981,** 19, 1687-1704.
(34) Fujimura, M.; Hashimoto, T.; Kawai, H. *Macromolecules* **1981,** 14, (5), 1309-1315.
(35) Roche, E. J.; Pineri, M.; Duplessix, R.; Levelut, A. M. *Journal of Polymer Science: Polymer Physics Edition* **1981,** 19, 1-11.
(36) Roche, E. J.; Pineri, M.; Duplessix, R. *Journal of Polymer Science: Polymer Physics Edition* **1982,** 20, 107-116.
(37) Thomas, T. J.; Ponnusamy, K. E.; Chang, N. M.; Galmore, K.; Minteer, S. D. *Journal of Membrane Science* **2003,** 213, 55-66.

(38) Zawodzinski, Thomas; Springer, Thomas E.; Uribe, Francisco; Gottesfeld, Shimshon. *Solid State Ionics* **1993,** 60, 199-211.
(39) Xie, J.; Garzon, F.; Zawodzinski, T.; Smith, W. *Journal of the Electrochemical Society* **2004,** 151, (7), A1084-A1093.
(40) Sone, Y.; Ekdunge, P.; Simonsson, D. *Journal of the Electrochemical Society* **1996,** 143, (4), 1254-1259.
(41) Rollet, A. L.; Gebel, G.; Simonin, J. P.; Turq, P. *Journal of Polymer Science Part B-Polymer Physics* **2001,** 39, (5), 548-558.
(42) Page, K. A.; Cable, K. M.; Moore, R. B. *Macromolecules* **2005,** 38, (15), 6472-6484.
(43) DeLuca, N. W.; Elabd, Y. A. *Journal of Membrane Science* **2006,** 282, (1-2), 217-224.
(44) Jung, H. Y.; Cho, K. Y.; Lee, Y. M.; Park, J. K.; Choi, J. H.; Sung, Y. E. *Journal of Power Sources* **2007,** 163, 952-956.
(45) Alberti, G.; Narducci, R.; Sganappa, M. *Journal of Power Sources* **2008,** 178, 575-583.
(46) Hensley, J. E.; Way, J. D.; Dec, S. F.; Abney, K. D. *Journal of Membrane Science* **2007,** 298, 190-201.
(47) Almeida, S.H.; Kawano, Y. *Journal of Thermal Analysis and Calorimetry* **1999,** 58, 569-577.
(48) Evans, C. E.; Noble, R. D.; Nazeri-Thompson, S.; Nazeri, B.; Koval, C. A. *Journal of Membrane Science* **2006,** 279, (1-2), 521-528.
(49) Hinatsu, J. T.; Mizuhata, M.; Takenaka, H. *Journal of the Electrochemical Society* **1994,** 141, (6), 1493-1498.
(50) Satterfield, M. B.; Majsztrik, P. W.; Ota, H.; Benziger, J. B.; Bocarsly, A. B. *Journal of Polymer Science Part B-Polymer Physics* **2006,** 44, (16), 2327-2345.
(51) Shah, R. K.; Hunter, D. L.; Paul, D. R. *Polymer* **2005,** 46, 2646-2662.
(52) Gilbert, M.; Haworth, B.; Myers, D. J. B. *Polymer Engineering And Science* **2004,** 44, (2), 272-282.
(53) van der Heijden, P. C.; Rubatat, L.; Diat, O. *Macromolecules* **2004,** 37, (14), 5327-5336.
(54) Gebel, Gerard; Lambard, Jacques. *Macromolecules* **1997,** 30, 7914-7920.
(55) Page, K. A.; Landis, F. A.; Phillips, A. K.; Moore, R. B. *Macromolecules* **2006,** 39, (11), 3939-3946.
(56) Starkweather, H. W. *Macromolecules* **1982,** 15, (2), 320-323.
(57) Moore, Robert B.; Cable, K. M.; Croley, T. L. *Journal of Membrane Science* **1992,** 75, (1), 7-14.
(58) Phillips, A. K.; Moore, R. B. *Journal of Polymer Science Part B-Polymer Physics* **2006,** 44, (16), 2267-2277.
(59) Page, K.; Jarrett, W.; Moore, R. B. *Journal of Polymer Science Part B: Polymer Physics* **2007,** 45, 2177-2186.
(60) Luan, Y.; Zhang, Y.; Zhang, H.; Li, L.; Li, H.; Liu, Y. *Journal of Applied Polymer Science* **2008,** 107, 396-402.

CHAPTER 5

INVESTIGATION OF THE STRUCTURE, MORPHOLOGY, AND MECHANICAL PROPERTIES OF DISPERSION-CAST NAFION® AFTER CHEMICAL DEGRADATION VIA RADICAL ATTACK FROM FENTON'S REAGENT

Introduction

The Department of Energy has currently set proton exchange membrane fuel cell (PEMFC) durability targets of 5,000 hours for transportation applications and 40,000 hours for stationary power applications.[1] It has been shown that one of the weakest components in achieving extended fuel cell lifetimes is the proton exchange membrane.[2] Although Nafion® is currently the benchmark material for use in PEMFCs, chemical and mechanical degradation continue to be the main causes of premature failure during operation.[1, 3] Nafion® is currently available commercially from E.I. du Pont de Nemours and Company and consist of a polytetrafluoroethylene (PTFE) backbone with perfluorovinylether side chains that terminate with a sulfonic acid functionality, as shown in Figure 5.1.[4]

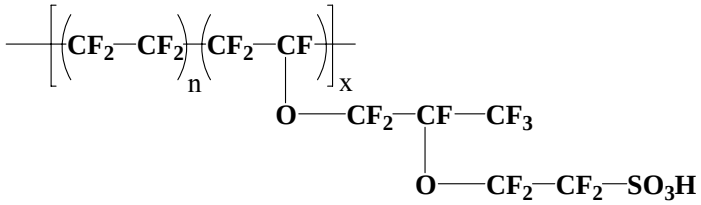

Figure 5.1. Chemical structure of Nafion®.

Nafion®, with a thickness of 180 μm, was used by Stucki et al. to demonstrate that a fuel cell stack can last approximately 15,000 hours at 80 °C under continuous operating conditions.[5] Alternatively, Curtin et al. showed that 25 μm thick Nafion® lasts

approximately 2,500 hours in a hydrogen/air fuel cell under a continuous load of 0.8 A/cm^2 at 65 °C, 100% RH, and ambient pressure.[6] Curtin et al. showed that although fuel cell life expectancy decreases with thinner proton exchange membranes, a higher performance efficiency along with a decrease in material cost are driving the use of thinner proton exchange membranes in fuel cells.[6, 7]

The two main causes for membrane failure during fuel cell operation are chemical and physical degradation.[7] LaConti et al. proposed a chemical degradation mechanism within a hydrogen/oxygen fuel cell where molecular oxygen permeates through the membrane from the cathode and reduces to hydrogen peroxide by reacting with the Pt catalyst at the anode.[3, 8] A schematic of this mechanism is shown in equations 5-1 through 5-3.

$$H_2 + Pt \rightarrow Pt\text{-}H \quad \text{(at anode)} \qquad \textbf{Eq. 5-1}$$

$$Pt\text{-}H + O_2 \rightarrow \bullet OOH \qquad \textbf{Eq. 5-2}$$

$$\bullet OOH + Pt\text{-}H \rightarrow H_2O_2 \qquad \textbf{Eq. 5-3}$$

Various authors have also documented the production of hydrogen peroxide at the cathode due to oxygen reduction on Platinum/Carbon catalysts.[9-12] The oxygen reduction reaction at the cathode is considered a multielectron reaction that proceeds via several elementary steps. Oxygen can go through a "direct", four electron reduction to water (Eq. 5-4), or a series of two electron reactions with a hydrogen peroxide intermediate (Eq. 5-5).[12]

$$O_2 + 4H^+ + 4e^- \rightarrow 2H_2O \qquad \textbf{Eq. 5-4}$$

$$O_2 + 2H^+ + 2e^- \rightarrow H_2O_2 + 2H^+ + 2e^- \rightarrow 2H_2O \qquad \textbf{Eq. 5-5}$$

Paulus and coworkers verified the presence of hydrogen peroxide by using a rotating ring-disk electrode (RRDE) where the oxygen reduction reaction takes place on the central disk electrode and H_2O_2 is produced on the concentric ring electrode, depending on the potential difference between the two electrodes.[10] By operating with potentials greater than 0.6 V, a relevant fuel cell cathode potential, Paulus et al. demonstrated that oxygen reduces exclusively to H_2O via a complete four-electron process as shown in equation 5-4.[10] On the other hand, by operating at potentials lower than 0.3 V (anodic potentials), up to 80% of the oxygen molecules were transformed to H_2O_2 when in contact with the Platinum/Carbon catalysts.[10, 11] Although the absolute concentration of H_2O_2 remains questionable, various authors have confirmed the presence of H_2O_2 in the exhaust, drain water, and membrane of a PEMFC during operation.[13-15]

Due to the relatively long fuel cell operational times and low degradation rates, accelerated chemical degradation experiments were developed to examine proton exchange membranes without waiting for membrane failure to occur during fuel cell operation.[1, 16, 17] Four common *in-situ* accelerated fuel cell life tests include testing; 1) elevated temperatures[18], 2) reduced humidity[19], 3) cycling of humidity, temperature, or cell potential[20], and 4) open circuit voltage (OCV).[21] Changes in both gas crossover and fluoride-ion emission rate are monitored in order to accurately determine membrane degradation during accelerated in-situ testing.[7]

As opposed to the various *in-situ* accelerated fuel cell life tests, various authors have chosen to examine the chemical degradation of proton exchange membranes via an *ex-situ* method, most commonly referred to as the Fenton's Test.[6, 8, 22-36] The Fenton's Test focuses mainly on the fact that the presence of H_2/O_2 in the fuel cell exhaust has

been verified using direct gas mass spectroscopy.[13] By introducing Fe^{2+} or Cu^{2+} catalysts to aqueous H_2/O_2 (3-30%) at fuel cell operating temperatures, •OH and •OOH radicals are created, which in turn can attack various organic species used as proton exchange membranes.[1] The main reaction mechanisms for the creation of both •OH and •OOH radicals during the Fenton's Test are shown below in Equations. 5-6 and 5-7.[7]

$$H_2O_2 + Fe^{2+} \rightarrow Fe^{3+} + \bullet OH + OH^- \qquad \textbf{Eq. 5-6}$$

$$\bullet OH + H_2O_2 \rightarrow H_2O + \bullet OOH \qquad \textbf{Eq. 5-7}$$

Even though the Fenton's Test is an ex-situ chemical degradation method, it is based on the idea that various catalytic counterions are present during fuel cell operation either by contaminated feed streams or hardware degradation. Pozio et al. have shown that using SS316L stainless steel as a material for bipolar plates within a fuel cell can cause membrane degradation and contamination based on residual iron, chromium, and nickel counterions leaching into both the hydrogen and oxygen feed and exhaust streams.[22] The authors examined both membrane degradation as well as fuel cell performance degradation based on the use of either stainless steel or aluminum bipolar plates. By comparing fuel cell voltage versus time, Pozio and coworkers noted a continual decrease in the fuel cell voltage when using stainless steel bipolar plates as opposed to minimal performance degradation with the aluminum bipolar plates. Coincidently, the average fluoride concentration in both the anode and cathode exhaust was significantly higher when stainless steel was used as opposed to aluminum. Upon removal of the stainless steel material, the contamination decreased by approximately 20%. With the aide of atomic absorption spectroscopy, Pozio et al. verified that the cathode exhaust contained trace amounts of chromium and nickel and a significant

amount of iron, which was attributed to the decrease in fuel cell performance and increase in fluoride release or chemical degradation of the polymer membrane.

Based on the formation of hydroxyl and hydroperoxyl radicals via in-situ or ex-situ fuel cell degradation, Curtin et al. have recently proposed a chemical degradation mechanism for Nafion® involving abstraction of a hydrogen atom from residual carboxylic acid found on the ends of the polytetrafluoroethylene backbone.[6] Curtin's degradation scheme is explained in three parts using Equations 5-8 through 5-10.

$$R_f{-}CF_2COOH + \bullet OH \rightarrow R_f{-}CF_2\bullet + CO_2 + H_2O \qquad \textbf{Eq. 5-8}$$

$$R_f{-}CF_2\bullet + \bullet OH \rightarrow R_f{-}CF_2OH \rightarrow R_f{-}COF + HF \qquad \textbf{Eq. 5-9}$$

$$R_f{-}COF + H_2O \rightarrow R_f{-}COOH + HF \qquad \textbf{Eq. 5-10}$$

As shown in Eq. 5-8, the hydrogen abstraction initiates a systematic chain oxidation to carbon dioxide and water. The perfluorocarbon radical then reacts with the hydroxyl radical forming an intermediate that rearranges to an acyl fluoride and one equivalent of hydrogen fluoride (Eq. 5-9). The acyl fluoride then goes through hydrolysis to generate a second equivalent of hydrogen fluoride as well as regeneration of the carboxylic acid endgroup (Eq. 5-10), causing an unzipping degradation mechanism continuing through the backbone of the proton exchange membrane.

The formation of various highly reactive radical species due to the decomposition of hydrogen peroxide has been examined by numerous authors.[37-41] Bosnjakovic et al. examined the presence of various free radical species present during the Fenton's Test using electron spin resonance (ESR).[38] For this particular study, Bosnjakovic and coworkers first neutralized Nafion® into the Titanium cation form and proceeded to measure the ESR signal at various temperatures as a function of membrane exposure time

to 30% w/v H_2O_2. Ti^{3+} was chosen as the Nafion® counterion due to its ability to act as a catalyst during the Fenton's Test as well as being easily detected using ESR. After approximately 20 minutes of exposure to 30% w/v H_2O_2 at 200 K, an ESR signal appeared near g = 2, which was attributed to the •OOH. The signal intensity and resolution increased with peroxide exposure time and the isometric g value was determined to be g_{iso} = 2.0127. Although the published g values of •OOH and •OH are relatively similar (2.0117 and 2.0102 respectively), Bosnjakovic and coworkers assume they observed the •OOH radical species during their ESR tests based on the calculated g value (2.0127) and the fact that •OH radicals can only be detected at temperatures below 77 K or by spin trapping.[38] Another reason for assuming a high quantity of •OOH radicals is due to the reaction in Equation 5-7, which shows that in the presence of excess H_2O_2, the •OOH will be the dominant species. By keeping the Ti^+-form Nafion® submersed in 30% w/v H_2O_2 and increasing the temperature from 250 to 320 K, the authors noticed the disappearance of the •OOH radical signal along with the appearance of an ESR peak with a g_{iso} value of 2.0122, which was attributed to the TiOO• radical. The formation of the TiOO• radical along with a superoxide radical were believed to occur through the mechanisms shown in Equations 5-11 and 5-12.

$$HOO\bullet + H_2O \leftrightarrow O_2^- + H_3O^+ \qquad \textbf{Eq. 5-11}$$

$$O_2^- + Ti^{4+} \rightarrow TiOO\bullet \qquad \textbf{Eq. 5-12}$$

Upon dehydration, or removal of the H_2O_2, Bosnjakovic et al. observed an ESR peak present between 160 and 360 K with a g_{iso} value of 2.0106 and was assigned to the O_2^- superoxide species. Finally, the authors examined the ESR signal of Ti^+-form Nafion® treated with 30% w/v H_2O_2 as a function of storage time from 0-92 days at ambient

conditions. A signal at approximately g_{iso} = 2.0023 emerged and broadened over time to a line width of approximately 84 G. The authors concluded that the signal represented fluorinated alkyl radicals, which were formed by the attack of the TiOO• species on the polymer.

Continuing their previous work, Kadirov, Bosnjakovic, and Schlick used ESR to examine various chemical degradation species in both Nafion® and Hyflon Ion® perfluorosulfonate ionomers during the Fenton's Test as well as UV degradation.[39] In contrast to their previous study, the authors chose to neutralize the perfluorosulfonate ionomers with Cu(II), Fe(II), and Fe(III) counterions as opposed to titanium due to the increased catalytic activity of both the copper and iron species. Kadirov et al. first examined the effect of neutralization on the UV degradation of an Fe(II)/Nafion® system. After 60 minutes of UV irradiation at 77 K (in the absence of H_2O_2), Kadirov et al. noticed a signal intensity maximum for membranes with 10% neutralization. They also noticed a linear increase in the ESR signal intensity of 10% neutralized Fe^{2+}-form Nafion® as a function of UV irradiation time from 0-60 minutes. With the addition of H_2O_2, prior to UV irradiation, the signal increased exponentially, mainly due to the homolytic cleavage of H_2O_2 into two •OH species. As a function of time, Kadirov et al. noticed an increase of the ESR signal at g_{iso} = 2.0023 and a decrease in the ESR signal at g_{iso} = 4.31. The first signal was attributed to the emergence of the chain-end perfluorinated radical $ROCF_2CF_2$•, which was determined based on its similar magnetic parameters to the propogating chain-end radical in polytetrafluoroethylene. The second signal was assumed to be the disappearance of the Fe(III) species as the chemical degradation proceeded as a function of time. The authors concluded, based on the quintet

ESR signal, that the formation of the $ROCF_2CF_2$• species was due to the attack of the carbon backbone atom linked to the pendant side chain, accompanied by the loss of a fluorine atom.

Based on the confirmation of various radical species present during the Fenton's Test, several authors have used the ex-situ degradation technique to quantify membrane stability based on percent weight loss, fluoride loss, and membrane dissolution[6, 8, 25-27, 29-36] Curtin et al. were the first to publish chemical degradation results via Fenton's Reagent for the new generation, chemically stable (CS), dispersion-cast NRE Nafion® membranes from DuPont.[6] DuPont has recently switched from extrusion to solution-casting Nafion® based on increased production rates, improved thickness control, and the ability to obtain thinner membranes. Along with switching the processing technique, DuPont has also decreased the number of carboxylic acid endgroups present in the solution-cast membrane by 61% via pre-treating the polymer with elemental fluorine, hence increasing the chemical stability. Curtin et al. subjected both chemically stable and non-chemically stable Nafion® to Fenton's Reagent for 55 hours and noticed a 56% decrease in the fluoride ion release rate between the two polymers, verifying the dramatic increase in chemical stability for the new generation Nafion®. This result confirmed that the carboxylic acid endgroups were the primary source for chemical degradation via hydroxyl and hydroperoxyl radical attack.

A later study by Escobedo et al. showed that even when the reactive endgroups are reduced close to zero, Nafion® fluoride loss is still present.[42] A secondary degradation mechanism was deemed essential to explain the additional loss of fluoride without the presence of carboxylic acid endgroups. Based on the data presented by

Escobedo et al., Zhou and coworkers performed the Fenton's Test on Nafion® as well as several model compounds that mimic Nafion®'s backbone and sidechain in order to determine a secondary route for chemical radical attack.[23, 24, 31] The structures of Nafion® and the various model compounds examined by Zhou et al. are shown in Figure 5.2.

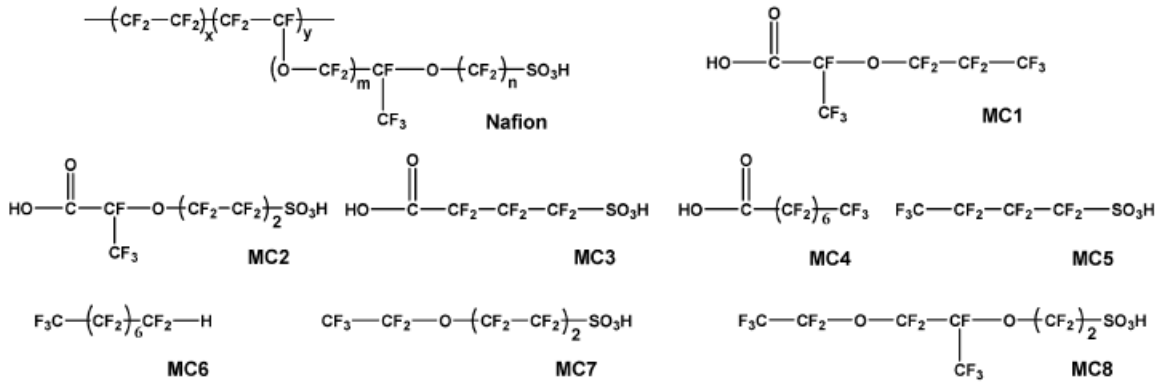

Figure 5.2. Structures of Nafion® and various model compounds. (Reprinted with permission from ref[31] *Macromolecules*, **40**, 8695 (2007). Copyright 2007, American Chemical Society.)

In order to conduct the Fenton's Test on the model compounds, Zhou et al. added a known concentration of Fe(II), H_2O_2, and model compound to ensure reproducibility between the various samples. The Fenton's Test on Nafion® was accomplished by exchanging the polymer into the Fe^{2+}-form prior to subjection to the H_2O_2. The evaluation of fluoride loss was calculated for each model compound based on the atomic percentage ratio, which was the total fluoride released divided by the total fluorine atoms possible for each model compound. There was a significant increase in the fluoride loss between the model compounds with carboxylic acid endgroups and those without such functionality. Of the compounds without any carboxylic acid endgroups, the fluoride loss decreased in the following order; MC5 > MC7 > MC8 > MC6. Zhou et al. believe that MC5 had the highest fluoride loss ratio due to having the shortest chain or fewest fluorine atoms, which would increase the percentage of fluoride release. On the other hand, MC6 had the lowest fluoride loss mainly due to its insolubility in the aqueous media. Zhou et

al. also note that although the fluoride loss was approximately an order of magnitude higher for the model compounds containing carboxylic acid groups, the remaining compounds still displayed a loss of fluoride in the Fenton's Reagent, indicating that there must be a secondary degradation pathway. By performing liquid chromatography-mass spectroscopy (LC-MS) on the degradation product of MC4, Zhou et al. were able to clearly show the evolution of the perfluorinated eight carbon acid into various seven through three carbon analogues, giving further proof for the primary unzipping degradation mechanism. For a more direct comparison to Nafion®, LC-MS was performed on the degradation product of MC8. Based on the LC-MS results, MC8 appeared to degrade into four various perfluorinated species, primarily dominated by a fluorinated carboxylic acid compound similar to MC2. Zhou et al. clearly state that all of the major degradation products of MC8 involved the cleavage of the ether linkage, which would mimic the loss of the sidechain in Nafion®. The authors also mention that there was no evidence of sulfonic acid loss in any of the degraded compounds.

As a corresponding publication to Zhou et al., Healy and coworkers incorporated ^{19}F NMR as well as mass spectroscopy to interpret both in-situ and ex-situ chemical degradation products of Nafion® membranes.[25] The authors' overall goal was to determine if the degradation products could be identified as well as confirm the degradation mechanism of Curtin et al. and thereby determine the similarity between in-situ and ex-situ degradation products. By allowing severely degraded fuel cell membrane electrode assemblies to soak in water for six days, Healy et al. were able to presumably extract any low molecular weight degradation species and compare them to the Fenton's degradation solution using ^{19}F NMR. From the ^{19}F NMR analysis, Healy et al. observed

numerous peaks that coincided between the two degradation solutions. The peaks were believed to be associated with a single fluorinated organic compound based on the consistent intensity ratio observed between the different samples. With the aid of mass spectroscopy, Healy et al. determined that the principal degradation product was fluoro(3-oxapentane)-1-sulfonic-4-carboxylic diacid, which is very similar to the MC2 compound examined earlier by Zhou et al.[31] Because the degraded compounds were so similar to the sidechain of Nafion®, Healy et al. assumed that their analytical results confirm the backbone unzipping degradation mechanism proposed by Curtin et al., upon which the sidechain is released during the process.

In a separate ex-situ Fenton's Test study, Kinumoto et al. used ion chromatography as well as ^{19}F NMR to examine the resulting degradation solution of Nafion® in various counterion forms.[26] Two main peaks were observed in the ion chromatographs of degraded Fe^{2+}-form Nafion® after 12 hours at 80 °C and were assigned to the F^- ions as well as the SO_4^{2-} ions. The authors note that the fluoride ions are the result of both the backbone and sidechain degradation, while the SO_4^{2-} ions are due to degradation of the sulfonate moieties, which directly contrast the previously mentioned chemical degradation study of Zhou et al. Decomposition ratios of both ions were calculated as a function of time and counterion type. The authors determined that alkali and alkaline metal counterions had minimal effect on the chemical degradation, while both Fe^{2+} and Cu^{2+} had the largest influence on the release of the fluoride and SO_4^{2-} ions. The weight loss of the Fe^{2+}-form Nafion® membrane after five days of chemical degradation via Fenton's Reagent was approximately 40%, which significantly decreased the membranes' mechanical properties as well as the proton conductivity. Kinumoto et al.

also examined Fe^{2+}-form Nafion® after chemical degradation using Fourier Transform Infrared Spectroscopy (FTIR). Because the normalized absorbances of the backbone and sidechain peaks did not change after severe chemical degradation, the authors concluded that the hydroxyl and hydroperoxyl radicals attacked both the sidechain and backbone. On the other hand, the authors suspect that Nafion®'s sidechain degrades slightly faster than the backbone based on the larger integrated peak area for the backbone fluorine atoms measured using ^{19}F NMR.

In another accelerated chemical degradation study, Liu et al. examined an in-situ Fenton's Test versus the conventional, ex-situ batch test.[3, 8] The in-situ Fenton's Test involved constructing a flow cell similar to a regular fuel cell where 10 wt% H_2O_2 flows to one side while the opposite side is purged with nitrogen gas. The H_2O_2 residence time was approximately three minutes and effluent water from both sides of the cell was used to measure fluoride loss. To examine the Fenton's degradation mechanism, the Nafion® membrane was doped with 10% Fe^{3+} ions and run in direct contact with the H_2O_2 solution at 90 °C for 48 hours. After completion of the in-situ Fenton's Test, the iron-doped membrane had a fluoride release rate similar to the chemical degradation observed using a regular hydrogen/oxygen fuel cell. The batch-wise or ex-situ Fenton's Test was conducted by again doping a Nafion® membrane with 10% Fe^{3+} ions and submersing it in 10wt% H_2O_2 at 68 °C for 24 hours. The fluoride release rate for the ex-situ Fenton's Test was approximately two orders of magnitude lower than the in-situ test. Liu et al. explain the discrepancy in the degradation results based on the constant supply of free radical generation during the in-situ test when compared to the batch-wise test, where the H_2O_2 concentration decreased over time and could be relatively ineffective after a few hours.

In conclusion, Liu et al. recommend the in-situ Fenton's Test due to its similarity to actual fuel cell operation.

Tang and coworkers implemented the use of FTIR, ^{13}C NMR, and Scanning Electron Microscopy (SEM) to examine the chemical degradation of Nafion® NRE 111 membranes after 48, 72, and 96 hours in Fenton's Reagent.[29] All membranes were submersed in 30 wt% H_2O_2 at 80 °C with the addition of 12.3 ppm Fe, 6.1 ppm Cr, and 5.4 ppm Ni ions, which represented the combination of contaminants after subjecting stainless steel to a 0.5 M nitric acid solution. Based on the FTIR spectra of the polymer fragments collected from the Fenton's solution, Tang et al. observed the appearance of the C=O stretching band at 1700 cm^{-1} and the S=O stretching band at 930 cm^{-1}. Both of these bands were documented as being indicative of the loss of sulfonate moieties as well as carboxylic acid groups. After performing ^{13}C NMR analysis on the 96 hour Fenton's solution, Tang et al. identified four peaks which were C=O at 168 ppm, CF at 68.5 ppm, CF_2 at 63 ppm, and CF_3 at 61.5 ppm. The existence of the last three bands was not surprising since they make up both the backbone and sidechain of Nafion®. The appearance of the C=O band, coinciding with the FTIR data, helped confirm the presence of carboxylic acids in the degraded Nafion® fragments. SEM images of Nafion® subjected to the Fenton's Reagent for 48 hours showed severe physical degradation in the formation of bubbles and cracks on both the surface and throughout the cross section of the membranes. The authors comment on how the formation of the bubbles can lead to pinholes in the membrane which then increases the likelihood of gas crossover and ultimate membrane failure within a fuel cell. Overall, Tang and coworkers were in agreement with the primary degradation mechanism proposed by Curtin et al. involving

the unzipping of the Nafion® backbone via radical attack of the carboxylic acid endgroups.

A more recent study by Merlo and coworkers focused on examining the ex-situ Fenton's Test degradation of the Hyflon Ion® produced by Solvey Solexis.[33] The Fenton's Test conditions were 36 ppm Fe^{2+} in a solution of 30 wt% H_2O_2 with 1 g of polymer at 55 °C for thirty hours, while replenishing the Fenton's solution every six hours. The total fluoride emission for the Hyflon Ion® was approximately the same when compared to both extruded Nafion® 112 and dispersion-cast Nafion® NR 112. A significant decrease in fluoride emission was noticed for an extruded, stabilized Hyflon Ion® membrane which is characteristic for membranes that have been pretreated with fluorine gas to help reduce the number of reactive carboxylic endgroups present in the polymer. As part of a continuing study, Merlo et al. chemically degraded both standard Hyflon Ion® and stabilized Hyflon Ion® for thirty hours, but instead of simply replacing the Fenton's solution every six hours, the authors removed the membrane, purified it with acid, followed by a washing treatment, and reinserted the membrane into fresh Fenton's solution. By measuring the amount of fluoride released during each six hour cycle, Merlo et al. were able to display a linear trend of increasing fluoride release for both stabilized and unstablized Hyflon Ion®. The authors also point out that there is no change in the rate of degradation throughout the thirty hour Fenton's Test. Due to the consistency of the degradation rate, Merlo and coworkers suggests that the number of chain sites which were attacked by the peroxide radicals remained constant, which was consistent with the unzipping mechanism proposed by Curtin et al.

Kundu et al. recently focused on the differences between performing a Fenton's Test on Nafion® using the solution method or exchange method.[34] The solution method involved subjecting a Nafion® membrane to a solution of both hydrogen peroxide and metal ions, while the exchange method involved first ion exchanging the membrane into the desired metal ion form followed by submersion in a hydrogen peroxide/water mixture. For this study, the solution method consisted of a 40 mL solution of 30 wt% H_2O_2 mixed with 16 mg/L of $FeCl_2 \cdot 4H_2O$ in a closed vessel with a 7.5 cm x 2.5 cm sample of Nafion® 112. The solution was kept at 72 °C and replenished every twelve hours to ensure a constant supply of free radicals. For the exchange method, a 7.5 cm x 2.5 cm sample of Nafion® 112 was first submersed in a solution of $FeCl_2 \cdot 4H_2O$ for 24 hours to fully exchange the membrane into the Fe^{2+}-form. The sample was then rinsed and placed into vials with 40 mL of 30 wt% H_2O_2 at 72 °C with the hydrogen peroxide being replenished every 24 hours. The overall goal of the study was to examine the differences between both methods as well as accurately interpreting which method closely mimics in-situ chemical degradation during fuel cell operation. The first analytical method used to compare the two degradation procedures was percent weight loss of polymer after chemical degradation between 0 and 120 hours. The first observation that Kundu et al. reported is that both methods succeeded in significantly degrading the membranes to the point where approximately 20% of the original weight was lost after approximately 80 hours. The authors thought this conclusion was surprising since both the solution replenishing times and total amount of iron were different between the solution and exchange methods. Their explanation for this phenomenon was that the majority of the radicals in the solution method were more than likely to terminate before ever reacting

with any polymer fragment. On the other hand, with the exchange method, the concentration of iron present within the polymer membrane may be so small that the chemical degradation within the polymer may equal that of the solution method. In contrast to the percent weight loss results, Kundu et al. noticed a significantly higher cumulative fluoride loss for the solution method as opposed to the exchange method after 120 hours of chemical degradation. The authors explain this result based on the solution method's ability to continue degrading polymer fragments that break off of the polymer film and dissolve in the Fenton's media. Both ion exchange capacity and electron dispersive spectroscopy were performed on the chemically degraded membranes to determine if the ratio of backbone to sidechain groups had changed. The results showed no significant change in the ion exchange capacity or the atomic ratio of oxygen to fluorine or sulfur to fluorine over the exposure time for both the solution and exchange methods. The FTIR results were in agreement with the ion exchange capacity and electron dispersive spectroscopic results in that no significant changes in the sidechain to backbone ratio was observed between the two degradation techniques. Despite the similarities in the degradation results of the solution method and exchange method, Kundu et al. noticed a significant visual difference between the two methods using SEM. SEM images of Nafion® degraded using the solution method were similar to images shown by Tang and coworkers where the presence of large bubbles and voids covered the exterior as well as the cross sections of the membrane.[29] The bubble density seemed to increase with degradation time and the diameters were reported on the order of hundreds of microns. In contrast, the membranes degraded using the exchange method displayed fewer defects and the bubbles or voids were much smaller in comparison to the solution

method. The cross section of the membrane degraded using the exchange method was drastically different than the cross section of the film degraded using the solution method. The cross section images of Nafion® degraded using the exchange method appeared to be foam-like on the surface but relatively untouched or homogenous in the center. The authors attribute the differences in the degraded morphology of the membranes to how well the reactive species can diffuse into the membrane during either degradation method.

Rather than characterize perfluorosulfonate ionomer degradation via the Fenton's Test, Hommura et al. chose to devise a method for accelerating and assessing the membrane degradation, while clarifying the chemical degradation mechanism during fuel cell operation.[35] A gas-phase H_2O_2 exposure method was devised, where 30 wt% H_2O_2 was maintained at 73 °C while nitrogen was used to purge the system and blow the heated peroxide to a chamber containing a Fe^{2+}-form Flemion® membrane at 120 °C and 14% relative humidity. The gaseous decomposed products were then trapped in a potassium hydroxide solution and new H_2O_2 was added every three days to maintain a constant 30 wt% throughout the experiment. The authors point out that the gas-phase H_2O_2 degradation method has the following advantages; uniform degradation, no membrane contamination, no effects from mechanical degradation, and independent evaluation of temperature, relative humidity, and H_2O_2 concentration throughout the experiment. Verification of the degradation method was observed by an increase in both the percent weight loss and fluoride release rate during exposure to gaseous H_2O_2 over a period of 700 hours. The degradation rate accelerated with time, indicating a change in the carboxylic acid endgroup concentration during the degradation test. The authors suggest that if the number of carboxylic acid endgroups is constant as in the degradation

mechanism proposed by Curtin et al. then the degradation rate would remain constant throughout the chemical degradation timeframe. In contrast, since the chemical degradation rate increases with time, a secondary radical attack position must exist upon which more carboxyl groups are created to increase the rate of chemical degradation. Using FTIR, Hommura et al. observed an increased in the number of carboxyl groups present in the membrane as a function of degradation time from 0-700 hours, which had a direct correlation to the increase in the fluoride release rate over the same time period. Size exclusion chromatography (SEC) was also performed to examine changes in the molecular weight of Flemion® as a function of degradation time during exposure to aqueous H_2O_2. The SEC analysis showed an approximate 10% decrease in the number average molecular weight of Flemion® after 700 hours of chemical degradation. Hommura et al. attribute both a decrease in the molecular weight and increase in the number of carboxyl groups to chain scission of the polymer backbone in Flemion®. Based on the SEC results, Hommura et al. suggest that the change in molecular weight is too large to be explained by the endgroup unzipping degradation mechanism alone. The authors finally conclude that PFSI membrane degradation proceeds via both the unzipping reaction at unstable polymer endgroups as well as by scission of the main chain to form reactive carboxyl groups at the severed locations.

Even with the wealth of information provided from the previous authors on chemical degradation techniques, along with primary and secondary peroxide radical attack mechanisms, the true chemical degradation behavior of Nafion® is still unknown. The purpose of this investigation is to obtain a fundamental understanding on how chemical degradation via a Fenton's Test affects Nafion®'s structure, morphology, and

mechanical properties. Following thorough characterization of degraded, dispersion-cast Nafion®, we will attempt to comprehend the effects of morphological manipulation of the crystalline domain on the fluoride loss of the polymer during peroxide radical attack via Fenton's Reagent.

Experimental

Materials. Dispersion-cast H^+-form Nafion® (1100 g/equiv) NRE 212 and NRE 212CS were obtained from E.I. DuPont de Nemours & Co. Methanol and 30 wt% hydrogen peroxide in water were purchased from Fisher Scientific and used without further purification. A.C.S. reagent grade Iron(II) sulfate heptahydrate was purchased from Aldrich Chemical Co. and used without further purification. Sodium hydroxide was also obtained from Aldrich Chemical Co. and dissolved in deionized water to form a 1M solution used for counterion exchange.

Ex-situ Chemical Degradation via Fenton's Test. The Fenton's Test protocol was supplied from DuPont as a Fuel Cells Technical Procedure. As-received, dispersion-cast membranes were first cut into strips approximately 155 x 20 mm and dried under vacuum at 70 °C for 12 hours to obtain an accurate dry weight. Each sample was then lowered into a 25 x 200 mm test tube and a 5 x 200 mm glass rod was placed at the midpoint of the sample to act as a weight during degradation and to maintain the symmetry of the folded sample within the test tube. The sample and test tube were then placed on an in-house manufactured test tube rack which allowed the sample to be suspended above an 80 °C water bath. The Fenton's Reagent, consisting of 50 mL of 30 wt% H_2O_2 and 0.005g of ferrous sulfate heptahydrate per gram of dry polymer, was added to each test tube with the sample completely submerged within the Fenton's Reagent. The test tube

was covered with a watch glass and slowly lowered into the 80 °C water bath over a period of one hour. After 15 hours in the water bath, the sample was raised, and the Fenton's solution was collected in a 400 mL beaker. The test tube and sample were then rinsed twice with deionized water, followed by collection of both the rinse water and initial Fenton's solution. Two drops of phenolphthalein were added to the rinse water and Fenton's solution, and neutralization performed using a 0.1M NaOH solution. After neutralization, 10 mL was pipetted into a 25 mL volumetric flask along with 10 mL of a buffer solution and 5 mL of deionized water. The buffer solution consisted of 292.2 g of NaCl, 34 g of sodium acetate trihydrate, and 15.8 mL of glacial acetic acid mixed into a 1 L volumetric flask and the remaining volume filled with deionized water. A Mettler Toledo SevenMulti pH/ion meter with an ion selective electrode was used to measure the fluoride content (ppm) of the Fenton's solution within the 25 mL volumetric flask. The test tube with the partially degraded sample was then placed back onto the rack above the water bath and a fresh batch of Fenton's Reagent was added to initiate another 15 hour cycle. This process was repeated every 15 hours until a final degradation time was reached, between 45 and 75 total hours.

Scanning Electron Microscopy (SEM). SEM images of dispersion-cast Nafion® before and after chemical degradation were obtained using an FEI Quanta 200. Before imaging, samples were sputter coated with ten nanometers of gold to avoid sample deterioration during imaging. Images were obtained in high vacuum mode at 15 kV, spot size of six, one torr of pressure, and various magnifications.

Tensile Analysis of Dispersion-Cast Nafion® NRE 212 Membranes. Tensile tests were conducted on dispersion-cast Nafion® NRE 212 in the as-received state and after

chemical degradation via the Fenton's Test for 3, 6, 9, 12, 15, 18, 21, 24, 27, 30, 33, 36, 39, 42, and 45 hours. Prior to testing, both as-received and degraded membranes were dried under vacuum at 70 °C for 12 hours. In order to reduce experimental error, six strips (75 mm by 5.5 mm) were cut from each degraded membrane. All samples were tested on an MTS Alliance RT/10 with a crosshead speed of 25.4 mm/min and a gauge length of 25 mm.

Thermal Gravimetric Analysis (TGA). Thermal gravimetric analysis was performed on dispersion-cast Nafion® NRE 212 membranes before and after chemical degradation for 3, 6, 9, 12, 15, 18, 21, 24, 27, 30, 33, 36, 39, 42, and 45 hours using a TA Instruments TGA Q50. All samples were first dried under vacuum at 70 °C for 12 hours to remove any residual bulk water from the membranes prior to testing. The membranes were analyzed from 25-600 °C with a heating ramp of 20 °C/min while under a nitrogen flow of 40 mL/min.

Dynamic Mechanical Analysis (DMA). Dynamic mechanical analysis of dispersion-cast Nafion® NRE 212 membranes before and after chemical degradation for 3, 6, 9, 12, 15, 18, 21, 24, 27, 30, 33, 36, 39, 42, and 45 hours was performed on a TA Instruments DMA Q800 Analyzer in tensile mode using clamps for thin film samples. All samples were cut from dried membranes (70 °C vacuum, overnight) with a width of 5.3 mm and gauge length of approximately 10 mm. The membranes were analyzed at a frequency of 1 Hz from -120 °C to 200 °C with a heating ramp of 2 °C/min. The temperature range was chosen in order to span all three thermo-mechanical relaxations (α, β, and γ).

Water and Methanol Uptake Analysis. As-received, dispersion-cast membranes were dried under vacuum at 70 °C for 12 hours to obtain a dry weight (m_d). To remove

any residual iron counterions, the membranes subjected to a 45 hour Fenton's Test were cleaned in refluxing 2M HCl for two hours, rinsed three times with deionized water, and boiled in deionized water for an additional hour. The degraded membranes were then dried under vacuum at 70 °C for 12 hours to obtain a dry weight (m_d). For water uptake analysis, both as-received and degraded membranes were submersed in boiling water for one hour, patted dry, and weighed to obtain the hydrated membrane weight (m_h). Equation 5-13 was used to calculate the water uptake (λ_w) values of dispersion-cast Nafion® before and after chemical degradation. The molecular weight of water (18 g/mol) and the equivalent weight of Nafion® (1100 g/equiv) were used in calculating the λ_w values as moles of water per moles of sulfonate groups.

$$\lambda_w = \frac{\left(m_h - m_d\right)/18}{\left(m_d/1100\right)} \qquad \textbf{Eq. 5-13}$$

Due to the dissolution of dispersion-cast membranes in boiling methanol, the methanol uptake values were determined by soaking, rather than boiling, both the as-received and degraded membranes in methanol for one hour, to obtain the hydrated membrane weight (m_h). Equation 5-14, shown below, was used to calculate the methanol uptake (λ_m) values of dispersion-cast Nafion® before and after chemical degradation. The molecular weight of methanol (32 g/mol) and the equivalent weight of Nafion® (1100 g/equiv) were used in calculating the λ_m values as moles of methanol per moles of sulfonate groups.

$$\lambda_m = \frac{\left(m_h - m_d\right)/32}{\left(m_d/1100\right)} \qquad \textbf{Eq. 5-14}$$

The water and methanol uptake values are representative of calculated averages based on three samples before and after the 45 hour Fenton's Test.

^{19}F Solid-State Nuclear Magnetic Resonance (SS-NMR) Spectroscopy. ^{19}F SS-NMR was performed on a Varian® UNITY-INOVA 400 MHz spectrometer using the ^{1}H channel of a Chemagnetics H-X-Y 4mm triple resonance probe. The probe circuit was tuned to 376 MHz for ^{19}F detection. Dispersion-cast Nafion® NRE 212CS membranes were examined both before and after chemical degradation via a 45 hour Fenton's Test. The as-received membranes were cleaned in refluxing 8M HNO_3 for two hours, rinsed three times with deionized water, boiled in deionized water for an additional hour, and dried overnight under vacuum at 70 °C. Degraded NRE 212CS membranes were first cleaned in refluxing 2M HCl to remove any residual iron, rinsed three times with deionized water, boiled in deionized water for an additional hour, and finally dried overnight under vacuum at 70 °C. Both as-received and degraded NRE 212CS membranes were then converted into the TBA^+ counterion form by stirring in a solution of TBAOH in deionized water for 12 hours. The use of TBA^+-form Nafion® as well as performing the ^{19}F SS-NMR experiments at elevated temperatures (225 °C) allowed for a decrease in the side band intensity as the dipolar coupling between ^{19}F resonances was averaged-out more effectively.[43] Samples in the TBA^+-form were then loaded into zirconia cylinder rotors sealed with Torlon® drive tips and Teflon® caps and spun at 11 kHz with data acquisition occurring at 225 °C. The DEPTH pulse sequence was used to remove ^{19}F background contributions from the cap and probe body. The acquisition parameters were as follows: the ^{19}F 90° pulse width was 3.1 μs, the acquisition time was 32 ms, the recycle delay ranged from 5 to 6 seconds, and the number of scans acquired for each data set was 32. The spectral width was set to 500 kHz, and peak positions were referenced externally to 30% C_6F_6 in dimethylsulfoxide. In the ^{19}F NMR spectrum, the

peaks at approximately -80 ppm and -120 ppm are attributed to the $–OCF_2$ and $–CF_3$ nuclei in the sidechain and the $–CF_2$'s in the backbone, respectively.

Thermal Treatment of H^+ and Na^+-form NRE 212CS Membranes. All membranes were sandwiched between Kapton® films and annealed between stainless steel plates with 0.10 mm shims to avoid unnecessary pressure during the thermal treatment. After thermal annealing, membranes were quenched to room temperature by removing the Nafion® and Kapton® films from the heated plates. The H^+-form membranes were annealed for one hour at the following temperatures; 100, 125, 150, 175, and 200 °C. Na^+-form membranes were annealed for one hour at the following temperatures: 100, 125, 150, 175, 200, 225, 250, 275, and 300 °C. H^+ and Na^+-form samples were also annealed at 175 °C and 275 °C, respectively, for 1, 2, 5, 10, 15, and 20 minutes.

Wide Angle X-ray Diffraction (WAXD) of NRE 212CS Membranes. WAXD was performed at the University of Southern Mississippi using a Rigaku Ultima III x-ray diffractometer in reflection mode. A Copper K_α radiation source was used with a beam wavelength of 1.54 Å. The one-dimensional diffraction images were recorded using a computer controlled scintillation counter. Diffraction data was collected every 0.05°, 2θ between 4-25°, 2θ at a scan rate of 0.1°, 2θ per minute. The scattering profiles are displayed as relative intensity as a function of the scattering angle, 2θ. PeakFit® analysis software was used to deconvolute the crystalline peak from the amorphous halo and aid in determining the percent crystallinity present in the film. A linear, two-point baseline subtraction was applied to the WAXD profiles, and the data were fit with three gaussian/lorentzian peaks. The three peaks represented a broad amorphous scattering

peak, a distinct amorphous halo, and a crystalline reflection. The three artificial peaks were then numerically fit to the experimental data to obtain the best r^2 value relative to the experimental data. Finally the percent crystallinity was determined from the ratio of the integrated crystalline peak area versus the entire integrated area under the curve.

Results and Discussion

Chemical Degradation of Dispersion-cast Nafion®. In additon to performing a true Fenton's Test, various dispersion-cast Nafion® samples were subjected to a modified version of the Fenton's Test where iron and hydrogen peroxide were examined separately. Based on the fluoride concentration data shown in Table 5-1, both iron and hydrogen peroxide must be present to initiate chemical degradation of Nafion®.

Sample	15hr F^- (ppm)	30hr F^- (ppm)	45hr F^- (ppm)
	Iron Only		
NR 112	0.080	0.012	0.015
NRE 212	0.038	0.013	0.015
NRE 212CS	0.043	0.011	0.011
	H_2O_2 Only		
NR 112	1.822	1.436	1.691
NRE 212	1.017	1.625	1.614
NRE 212CS	0.464	0.681	0.386
	Iron and H_2O_2		
NR 112	17.52	23.95	25.66
NRE 212	15.91	23.64	24.12
NRE 212CS	2.82	6.64	8.07

Table 5-1. Fluoride concentration as a function of time for dispersion-cast Nafion® subjected to the modified Fenton's Test (iron or hydrogen peroxide only) and the true Fenton's Test (iron and hydrogen peroxide together).

The fluoride concentration of dispersion-cast membranes subjected to ferrous sulfate in deionized water was essentially zero due to the experimental error of the ion selective probe. This led us to believe that the presence of iron(II) by itself was not enough to induce chemical degradation of dispersion-cast Nafion®. On the other hand, a slight

increase in the fluoride content of the Fenton's solution was observed when the membranes were subjected to hydrogen peroxide in the absence of the iron catalyst. We believe the minute amount of fluoride present in the Fenton's solution was due to the homolytic cleavage of the hydrogen peroxide in the presence of ultraviolet light.[39] Throughout the 45 hour test, the test tubes were covered with watch glasses, which allowed light to penetrate through the top of the test tube, ultimately reaching the sample submersed in the 30% hydrogen peroxide.

By submersing the samples in solutions containing both iron and hydrogen peroxide, we observed a significant amount of fluoride released into the Fenton's media, indicating that chemical attack via hydroxyl and hydroperoxyl radicals was occurring. The fluoride concentration of the NR 112 and NRE 212 membranes was approximately 21.8 ppm on average after 45 hours in the Fenton's Reagent. On the contrary, the chemically stabilized NRE 212CS membrane had an average of 5.8 ppm fluoride present in the Fenton's media after 45 hours. By reducing the number of carboxylic acid endgroups on the polymer backbone, DuPont has effectively increased the chemical resistance of NRE 212CS to 3.8 times that of either NR 112 or NRE 212.

Scanning Electron Microscopy (SEM) of Chemically Degraded Dispersion-cast Nafion®. Membranes subjected to the Fenton's media for more than 30 hours experienced the formation of large voids and bubbles that initiated severe surface cracks as shown in Figure 5.3 A-F.

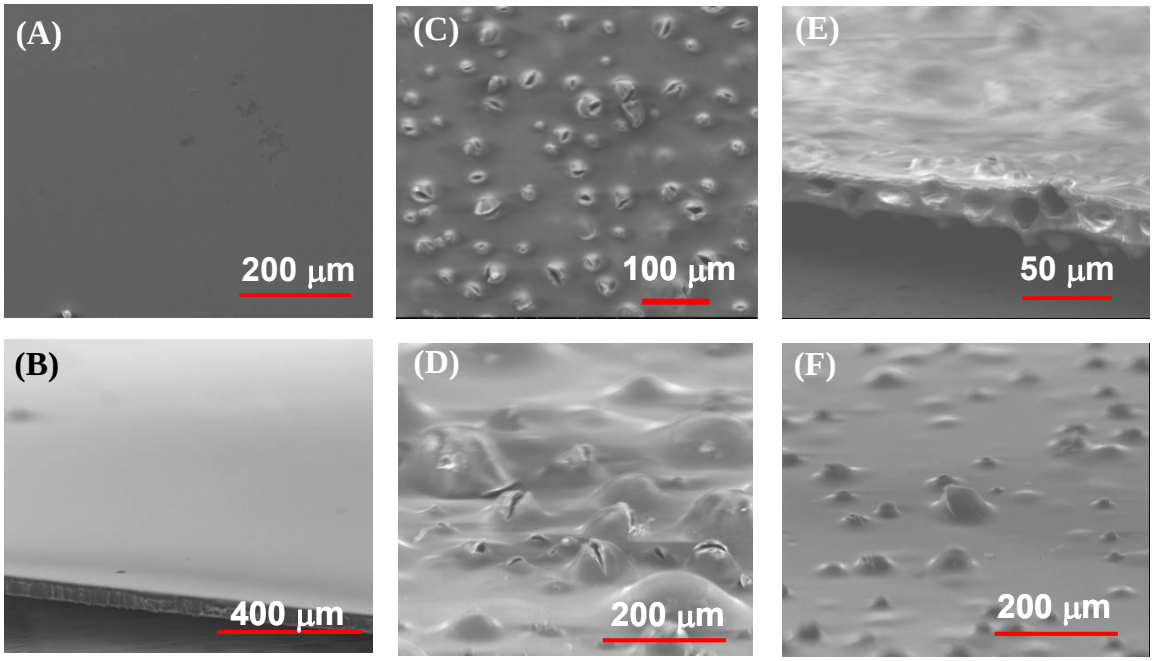

Figure 5.3. Scanning electron micrographs of **A)** top view and **B)** cross-section of as-received, dispersion-cast NRE 211, **C)** top view and **D)** side view of dispersion-cast NRE 211 after exposure to Fenton's Reagent for 45 hours, and **E)** cross-section and **F)** side view of dispersion-cast NRE 212CS after exposure to Fenton's Reagent for 45 hours.

Figures 5.3 A and B represent SEM images of dispersion-cast NRE 211 in the as-received state, before exposure to the Fenton's media. Both the top view, Figure 5.3A, and the cross-section, Figure 5.3B, display a clean, smooth, featureless surface at relatively high magnification. On the other hand, after 45 hours in the Fenton's Reagent, large bubbles are formed throughout the NRE 211 membranes as shown in Figures 5.3 C and D. The appearance of bubbles or voids in non-chemically stable Nafion® is in agreement with the study by Tang and coworkers where NRE 111 was degraded for 48 hours in Fenton's Reagent.[29] Based on Figures 5.3 C and D, the bubbles on the membrane surface appear to rupture at their apex, yielding surface cracks on the order of several microns in width. In the cross-section, interior lateral cracks are formed as the bubbles coalesce. In general bubble formation is somewhat less pronounced in the chemically-stabilized membranes as shown in Figures 5.3 E and F. However, it is

important to note that chemical stabilization does not completely prevent bubble formation. Non-uniform bubble formation in the NRE 212CS membranes during the accelerated ex-situ, chemical degradation test may suggest chemical and/or physical heterogeneity throughout the membrane. One main concern of the accelerated Fenton's chemical degradation test is the relevance of the formation of bubbles and voids compared to the cracks and pinholes observed after long term fuel cell operation. In an attempt to understand the creation and evolution of the voids or bubbles, we have conducted a time-dependent study of degradation effects on bubble formation and changes in the physical properties of various dispersion-cast Nafion® films.

Fenton's Test as a Function of Time. To examine the chemical degradation of dispersion-cast Nafion® NRE 212 as a function of time, samples were removed from the Fenton's Reagent every three hours until the maximum 45 hour threshold was reached. Plots of fluoride concentration in the resulting Fenton's media as well as percent weight loss as a function of degradation time are shown in Figures 5.4 A and B.

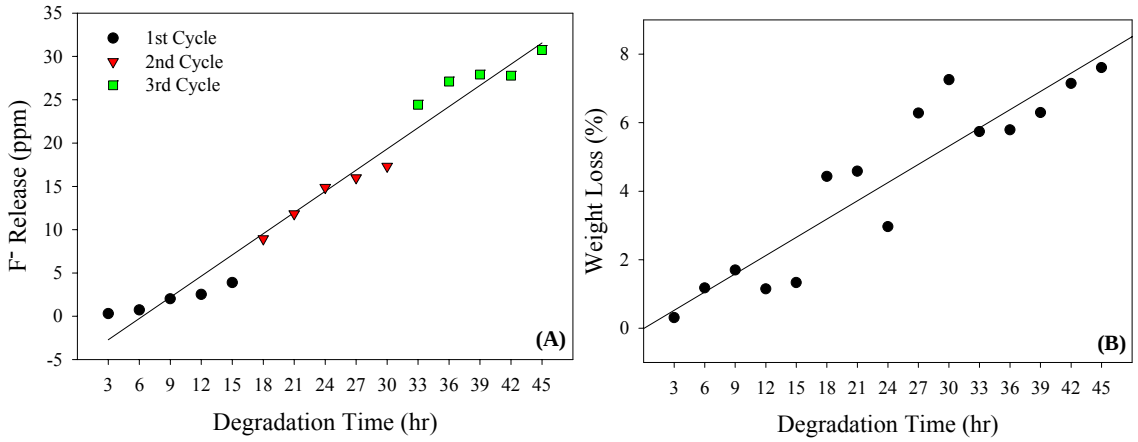

Figure 5.4. A) Fluoride concentration and **B)** percent weight loss of dispersion-cast NRE 212 as a function of exposure time to Fenton's Reagent.

From Figure 5.4A, we notice a significant increase in the amount of fluoride released throughout the duration of the 45 hour Fenton's Test. The concentration of fluoride

increased from 0.3 to 31 ppm between 3 and 45 hours of membrane exposure to the Fenton's Reagent. The different colored symbols seen in Figure 5.4A represent the fluoride concentration as a function of Fenton's Test cycle. Due to replenishing of the Fenton's Reagent every 15 hours, sudden increases in the fluoride concentration were observed for samples degraded for 18 and 33 hours. The dramatic increase in fluoride concentration in the Fenton's media is based on the increased concentration of hydroxyl and hydroperoxyl radicals due to the introduction of new Fenton's solution every 15 hours. A similar trend is observed with the weight loss of NRE 212 as a function of degradation time, as shown in Figure 5.4B. Dispersion-cast NRE 212 lost approximately 0.3-7.6 wt% after exposure to the Fenton's media for 3-45 hours. Similar to the increase in fluoride concentration at the beginning of each 15 hour cycle, the weight percent also fluctuated significantly with the addition of a fresh batch of Fenton's Reagent. It is also important to note that the formation of bubbles or voids was only observed during the final 15 hours of chemical degradation, but unfortunately, a uniform nucleation and growth process was not observed throughout the time-dependant study. The behavior was more of a catastrophic appearance of bubbles during the final hours of exposure to the third cycle of Fenton's Reagent. Future work is necessary to isolate the complex experimental variables that control the bubble formation and growth observed during the chemical degradation of dispersion-cast Nafion®.

The tensile properties of dispersion-cast NRE 212 were also examined as a function of degradation time in the Fenton's Reagent. Figures 5.5 A-D, shown below, display stress versus strain, strain at break, modulus, and yield stress as a function of degradation time.

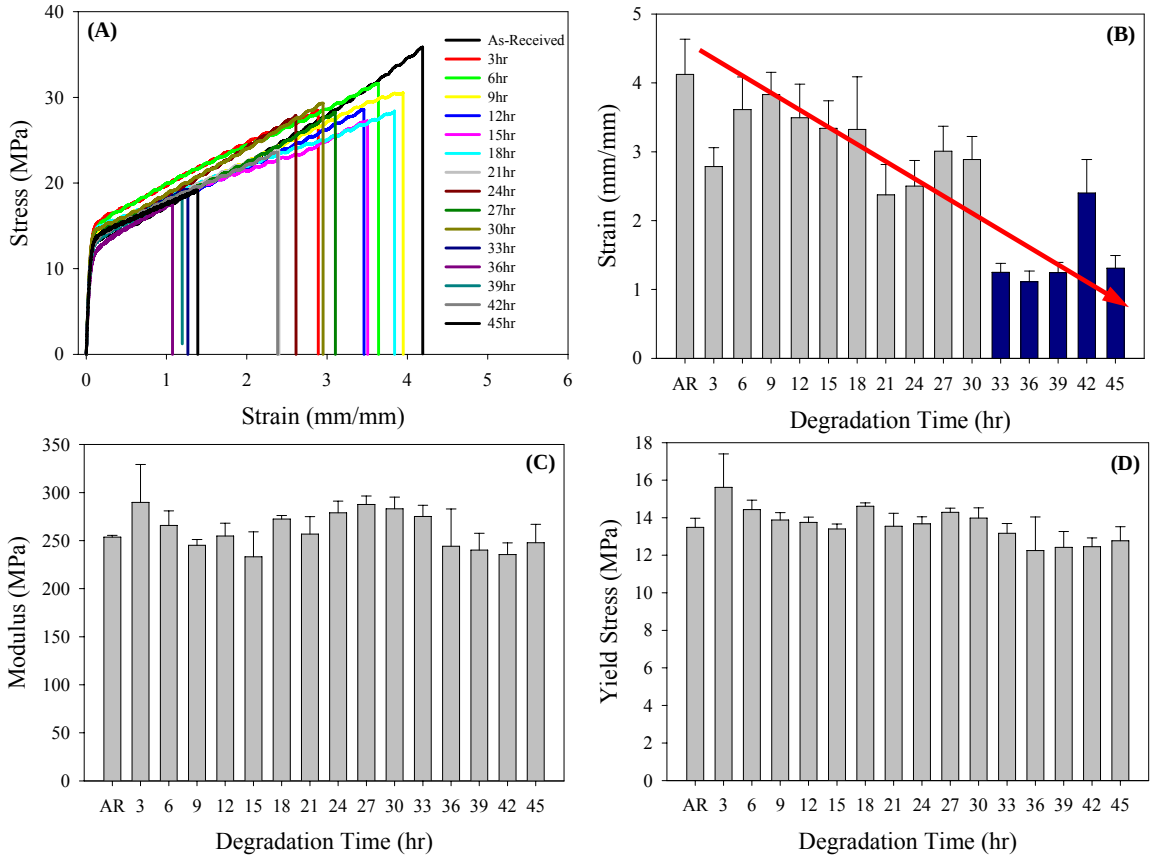

Figure 5.5. H^+-form NRE 212 before and after exposure to Fenton's Reagent for 3-45 hours. **A)** Stress versus strain **B)** Strain at break versus degradation time **C)** Modulus versus degradation time **D)** Yield stress versus degradation time.

The stress versus strain data shown in Figure 5.5A displays a dramatic decrease in the strain at break as a function of degradation time. A direct correlation of this phenomenon is shown in Figure 5.5B where the membranes subjected to the Fenton's Test for 33-45 hours are shaded in dark blue. A significant drop in elongation is witnessed for the samples exposed to Fenton's Reagent for longer than 33 hours. Due to replenishing of the Fenton's Reagent every 15 hours, we believe that both the increased concentration of hydroxyl radicals and the appearance of bubbles and voids within the membrane caused the significant drop in the strain at break of the membranes. Over the entire exposure time of 45 hours, both the tensile modulus and yield stress remain relatively constant as shown in Figures 5.5 C and D.

The membranes subjected to variable time exposures to the Fenton's Reagent were also characterized using thermogravimetric analysis as shown in Figures 5.6 and 5.7.

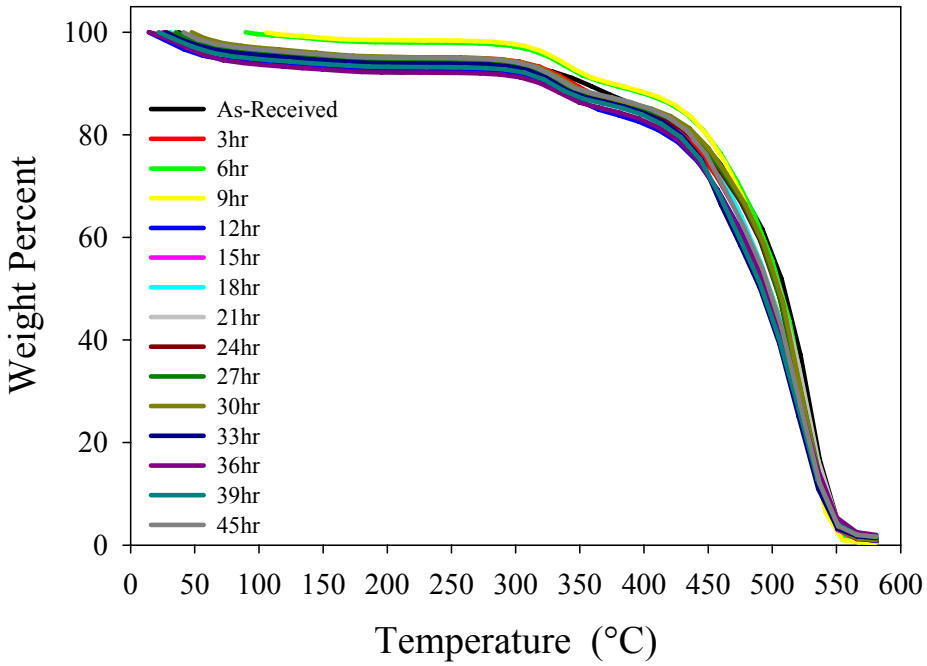

Figure 5.6. Weight percent versus temperature of H^+-form NRE 212 before and after exposure to Fenton's Reagent for 3-45 hours.

For all of the samples, the thermal degradation profiles shown in Figure 5.6 were quite comparable and are representative of three repetitions. However, further analysis of the extremes (as-received NRE 212 versus 45 hour degraded NRE 212) shown in Figure 5.7, show that there is a slight shift in the thermal stability of the degraded membranes.

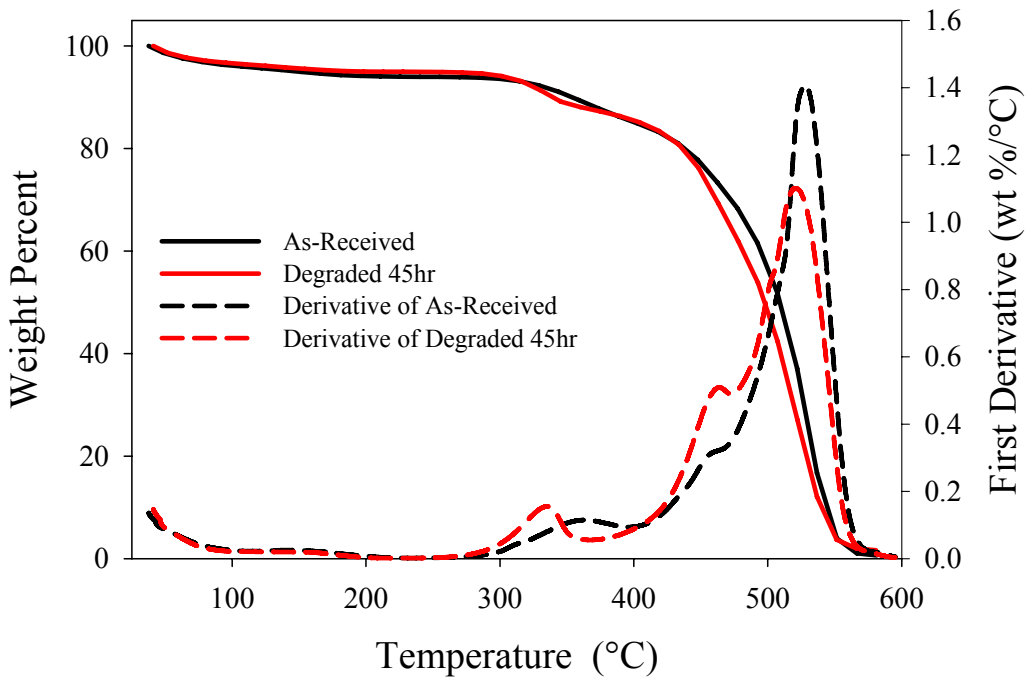

Figure 5.7. Weight percent and first derivative of weight percent versus temperature of H^+-form NRE 212 before and after exposure to Fenton's Reagent for 3-45 hours.

The small peak observed in the derivative profiles at 320-350 °C has been determined to be attributed to the loss of sulfonate functionality within the ionomer.[44] After degrading NRE 212 for 45 hours, this peak shifts to lower temperatures, possibly indicating a slight weakening of the matrix mobility surrounding the ionic aggregates. While this is somewhat interesting, it is much more important to note that the relative mass fractions of sulfonate groups lost in both the as-received and degraded membranes is essentially identical. This indicates that the chemical degradation of Nafion® is not specifically selective towards the functional side chains, but is in fact much more homogenous in nature. The chemical degradation of Nafion® via peroxide radical attack appears to be uniform based on the data presented in Figure 5.7, which coincides with the proposed degradation mechanism by Curtin et al.[6]

Dynamic mechanical analysis was also conducted on dispersion-cast NRE 212 membranes between 3 and 45 hours of exposure to the Fenton's Reagent. The DMA

studies revealed that with increased degradation time, the α-relaxation temperature of Nafion® increases with degradation time, as shown in Figure 5.8A.

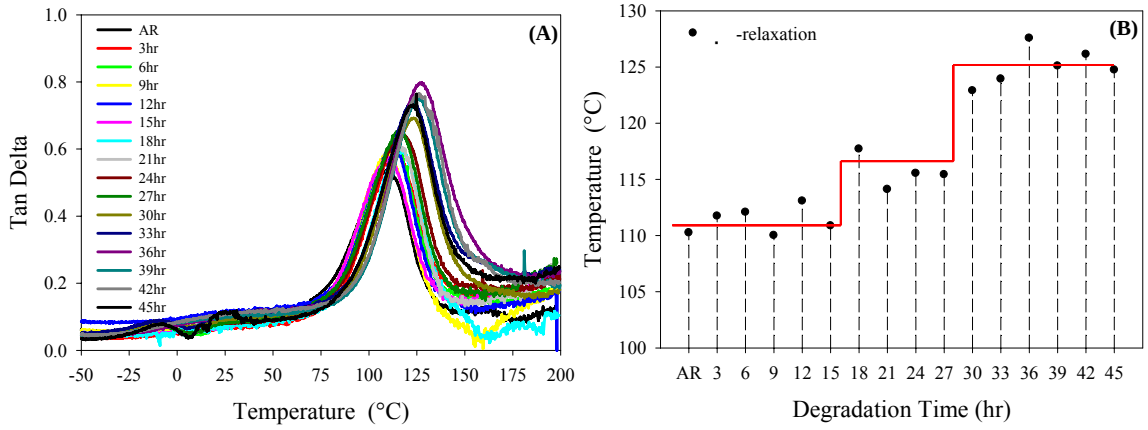

Figure 5.8. A) Tan delta versus temperature of H^+-form NRE 212CS before and after exposure to Fenton's Reagent for 3-45 hours. **B)** Alpha-relaxation temperature of H^+-form NRE 212CS 212CS before and after exposure to Fenton's Reagent for 3-45 hours.

A clearer representation of the increasing α-relaxation temperature with increasing degradation time is shown in Figure 5.8B. The α-relaxation temperature of as-received Nafion® is well documented in the literature and is observed at 110 °C, which coincides well with our initial results. The α-relaxation temperature then increases, reaching a maximum value of approximately 125 °C after 45 hours of exposure to the Fenton's Reagent. Based on the data shown in Figure 5.8A, our first instinct was that the α-relaxation temperature was increasing linearly as a function of degradation time. However, by plotting the actual α-relaxation temperature as a function of degradation time (Figure 5.8B), we observed a step-wise increase in the α-relaxation temperature as opposed to our initial assumption of a uniform linear progression. Upon further contemplation, we determined that the step-wise increase in the α-relaxation temperature was due to the additional iron counterions introduced into the system during the replenishing of the Fenton's Reagent every 15 hours. Further confirmation of this theory is shown below in Figure 5.9.

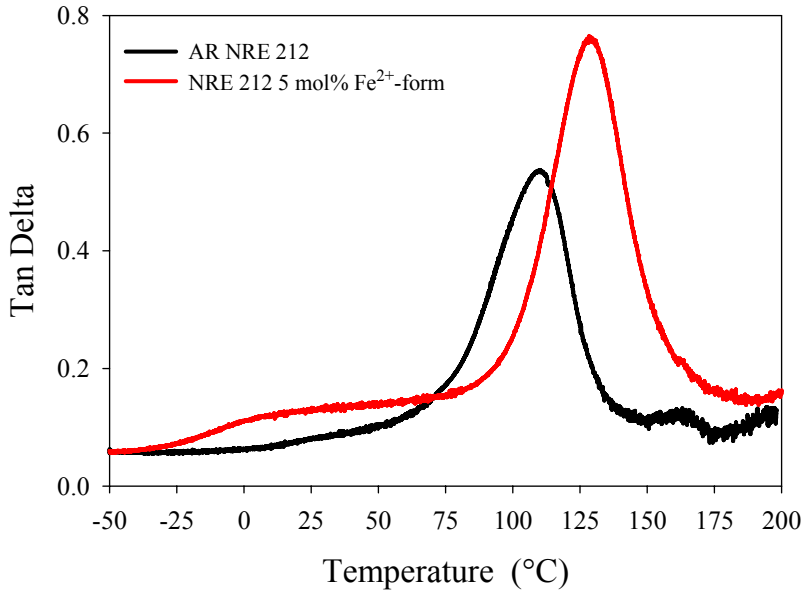

Figure 5.9. Tan delta versus temperature of dispersion-cast NRE 212 in H+ and 5 mol% Fe^{2+} forms.

Figure 5.9 displays the effect of partially neutralizing as-received NRE 212 with 5 mol% of Iron(II) sulfate heptahydrate on the dynamic mechanical properties of the ionomer. Neutralization of 5 mol% was chosen based on the amount of catalyst added during the three additions of Fenton's Reagent along with assuming that every divalent iron cation is associated with two sulfonate moieties within the membrane. From the data shown in Figure 5.9, we observe a similar increase in the α-relaxation temperature of dispersion-cast Nafion® NRE 212 from 110 to 128 °C, which is in agreement with the data shown in Figures 5.8 A and B. Because the presence of iron in the membranes had such a profound influence on the dynamic mechanical properties of Nafion®, a cleaning procedure involving refluxing in 2M HCl for 2 hours was introduced to reacidify the ionomer into the H^+-form prior to further studies. Based on the dramatic increase of the α-relaxation temperature being attributed to the introduction of iron counterions within the membrane, we conclude that the dynamic mechanical properties of dispersion-cast

Nafion® are similar before and after 45 hours of chemical degradation via peroxide radical attack.

Solvent Uptake of Nafion® Before and After Chemical Degradation. Preliminary water and methanol uptake values are reported for extruded Nafion® 112, dispersion-cast NRE 212 and NRE 212CS before and after the 45 hour chemical degradation Fenton's Test. Figure 5.10 displays the solvent uptake (mol solvent/mol sulfonate) of each membrane before and after chemical degradation. Based on our previous experience with the dynamic mechanical analysis of Nafion® before and after chemical degradation, we reacidified all membranes prior to performing the solvent uptake study.

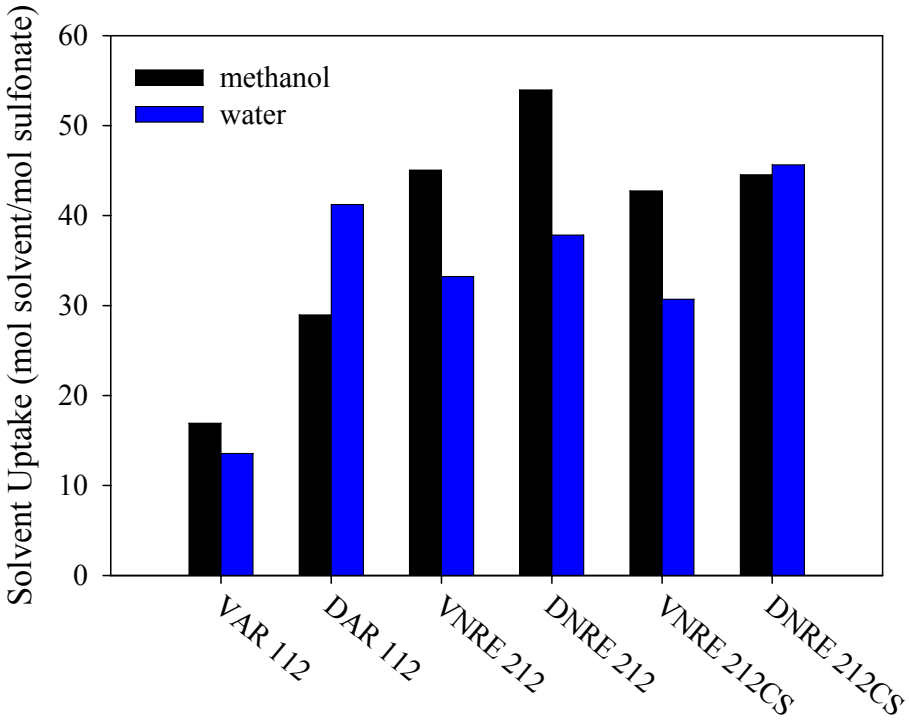

Figure 5.10. Methanol and water uptake of as-received, extruded Nafion® 112, dispersion-cast Nafion® NRE 212, and dispersion-cast Nafion® NRE 212CS before and after a 45 hour Fenton's Test. (V = virgin membrane, D = degraded membrane)

The most striking attribute of the data shown in Figure 5.10 is the dramatic increase in solvent uptake of the as-received, dispersion-cast membranes when compared to the as-received, extruded Nafion® films. In agreement with DuPont's technical product

information, the water uptake of dispersion-cast Nafion® is inherently higher than that of extruded form Nafion®.[45, 46] So far, no explanation for the increased water uptake of dispersion-cast Nafion® has been discussed in the literature, but we assume it involves differences in the way dispersion-cast and extruded Nafion® are processed. Another observation from the data shown in Figure 5.10 is that both the water and methanol uptake increase after 45 hours of chemical degradation in Fenton's Reagent. It is also interesting to point out that all of the as-received membranes display a higher methanol uptake as compared to water uptake. On the other hand, after chemical degradation the trend is reversed for both extruded AR 112 and dispersion-cast NRE 212CS membranes. In the case of NRE 212CS, the water and methanol uptakes are virtually identical after chemical degradation and may be within error of the experiment. Several theories are plausible as to why the solvent uptake of Nafion® dramatically increases with chemical degradation, but due to the onset of large bubbles and voids within the last 15 hours of the Fenton's Test, we believe that the majority of the solvent is becoming trapped in the voids, hence artificially inflating the true solvent uptake values. Future work on devising a method to create a more homogenous membrane surface morphology is underway in order to further mitigate the effects of chemical degradation on both water and methanol uptake of dispersion-cast Nafion®.

^{19}F Solid-State NMR of Nafion® Before and After Chemical Degradation. ^{19}F solid-state NMR was chosen as a spectroscopic technique for observing changes in the chemical structure of dispersion-cast Nafion® before and after chemical degradation via exposure to Fenton's Reagent for 75 hours. By increasing the Fenton's Test from 45 to 75 hours, we were able to introduce two additional batches of Fenton's Reagent and

create more disparity between the as-received and chemically degraded membranes. Figure 5.11, shown below, displays the ^{19}F solid-state NMR spectrum of TBA^+-form NRE 212CS before and after chemical degradation performed in the H^+-form.

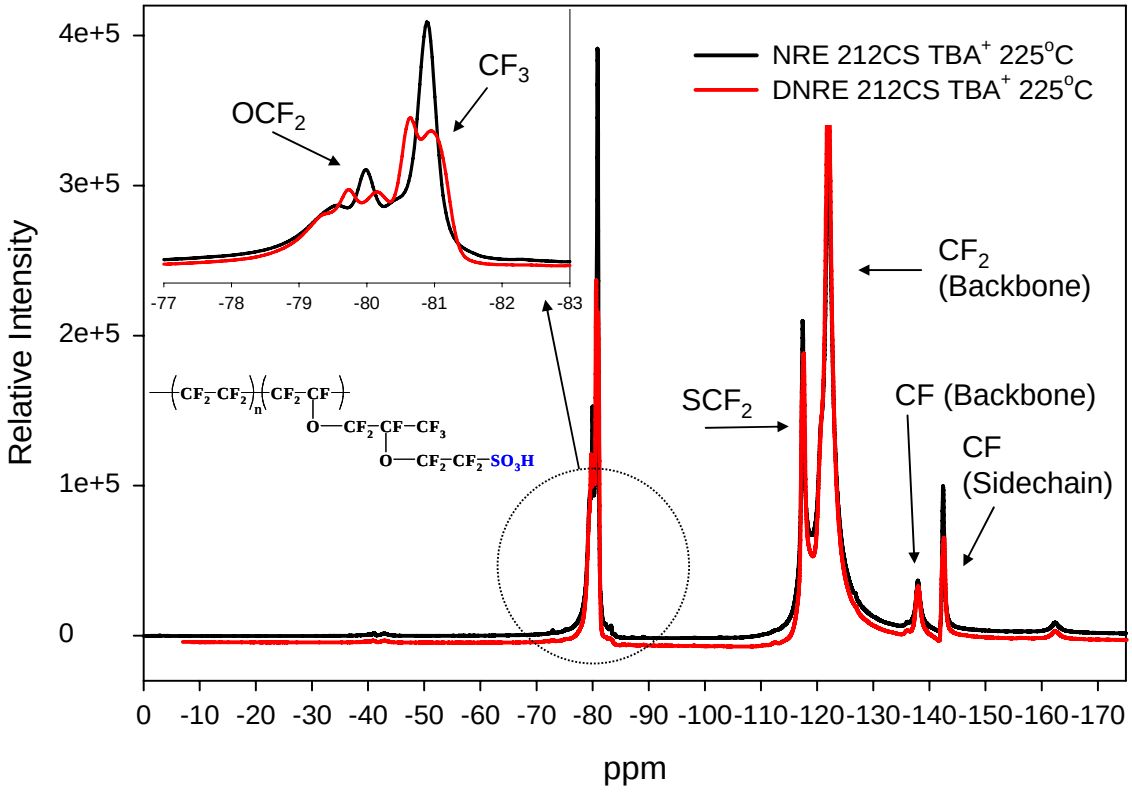

Figure 5.11. ^{19}F solid-state NMR of TBA^+-form dispersion-cast Nafion® NRE 212CS performed at 225 °C before and after chemical degradation in the H^+-form via a 75 hour Fenton's Test.

As mentioned earlier, the dispersion-cast membranes were converted into the TBA^+ counterion form prior to NMR analysis in order to increase chain mobility at elevated temperatures, hence increasing the spectra resolution by decreasing the influence of spinning side bands. The chemical structure assignments, shown in Figure 5.11, of the fluorine atoms present in Nafion® have been verified using various 2D NMR techniques.[47, 48] Based on the appearance of peaks coinciding with both the side chain and backbone of the polymer, we can conclude that the unzipping chemical degradation mechanism proposed by Curtin et al. is plausible.[6] If the peroxide radicals preferentially

attacked either the side chain or backbone we would have observed either a disappearance or significant drop in intensity of their respective ^{19}F peaks. From Figure 5.11, we observe a slight decrease in the relative intensity of the peaks corresponding to fluorine atoms in the side chain of dispersion-cast NRE 212CS located at -80, -81, -118, and -143 ppm. An expanded view of the OCF_2 (-80 ppm) and CF_3 (-81 ppm) peaks is located in the upper left hand corner of Figure 5.11. A dramatic change in both the shape and intensity of the two peaks is observed after chemical degradation for 75 hours in Fenton's Reagent. It is obvious that the environment surrounding the side chain fluorine atoms has changed after exposure to Fenton's Reagent for 75 hours. Due to the significant changes of the OCF_2 and CF_3 peaks observed using ^{19}F solid-state NMR, we conclude that the secondary degradation pathway, proposed by Escobedo et al., may involve peroxide radical attack of the side chain as opposed to the carboxylic endgroups present on the backbone of Nafion®.

Effects of Annealing on the Chemical Degradation of Dispersion-Cast Nafion®. By annealing dispersion-cast Nafion® at elevated temperatures, we were able to manipulate the crystalline morphology of the membrane and determine its effects on chemical degradation by examining the concentration of fluoride ions in the resulting Fenton's Media. Changes to the crystalline morphology of H^+-form NRE 212CS annealed at various temperatures were verified with the aid of Wide Angle X-ray Diffraction (WAXD). Figure 5.12 shows the WAXD pattern of relative intensity versus degrees, 2θ for H^+-form NRE 212CS before and after annealing between 100 and 200 °C for one hour.

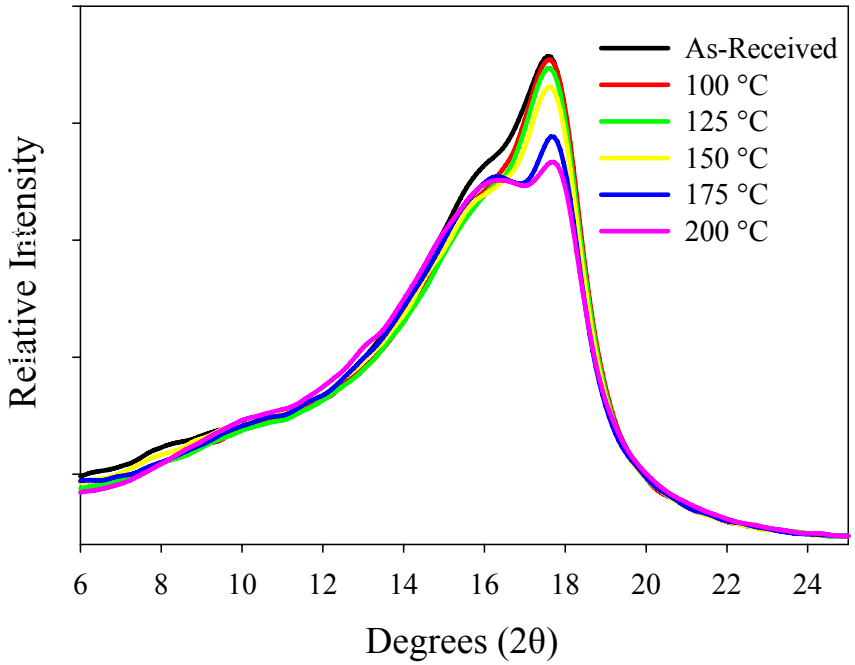

Figure 5.12. WAXD profile of H^+-form NRE 212CS membranes before and after annealing for one hour at 100, 125, 150, 175, and 200 °C.

The WAXD profile of as-received H^+-form NRE 212CS is in agreement with various WAXD patterns of extruded Nafion® that are widely reported in the literature.[49-51] The general Nafion® WAXD profile consists of a broad amorphous halo from 12-22°, 2θ along with a distinct crystalline reflection at 18°, 2θ. A simple deconvolution of the crystalline peak from the amorphous region was done using PeakFit® analysis software (an example is shown in Figure 5.13).

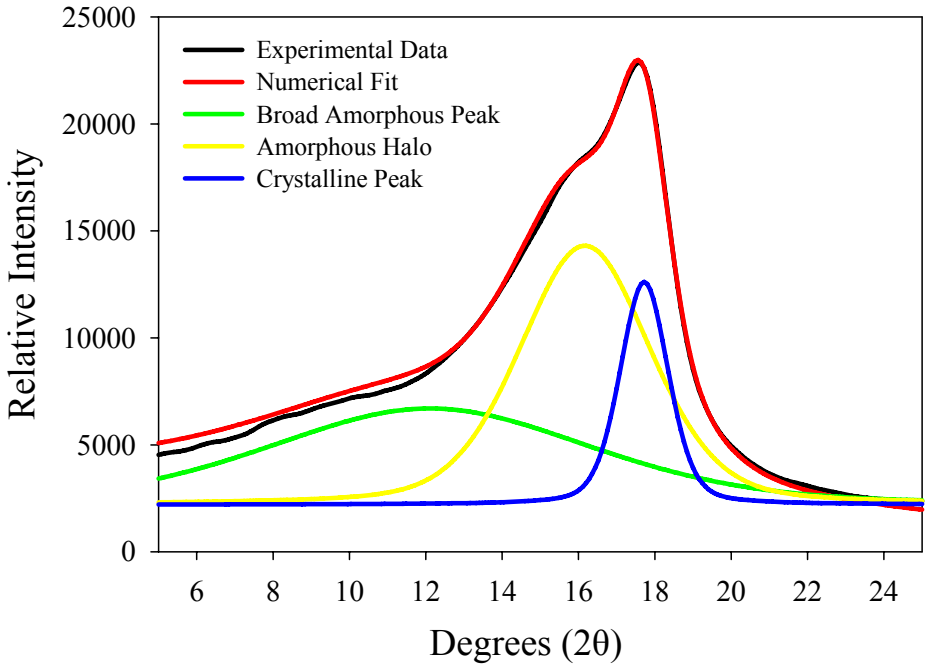

Figure 5.13. WAXD data of as-received, H^+-form NRE 212CS displaying the deconvoluation of the crystalline peak and amorphous peaks using PeakFit® analysis software.

Based on deconvolution analysis of the crystalline peak from the amorphous halo, decreases in percent crystallinity and full width at half maximum (FWHM) were observed after annealing H^+-form NRE 212CS at 100, 125, 150, 175, and 200 °C, as shown in Table 5-2. It is interesting to note that both the percent crystallinity and FHWM remain relatively constant while annealing at temperatures below 175 °C. By annealing at temperatures beyond 175 °C, a significant change in the morphology of the membrane occurs, which also aids in increasing the mechanical stability of NRE 212CS when subjected to boiling methanol, as discussed in our previous study on the mechanical stability of dispersion-cast Nafion®.

T_{Anneal}	H^+-form $\%X_c$	FWHM
AR	14.2	1.5
100 °C	15.2	1.4
125 °C	15.3	1.4
150 °C	13.1	1.4
175 °C	8.7	1.2
200 °C	6.8	1.2

Table 5-2. Percent crystallinity and full width at half maximum (FWHM) of H^+-form NRE 212CS before and after annealing for one hour at 100, 125, 150, 175, and 200 °C.

By annealing at elevated temperatures, the overall crystallinity of H^+-form NRE 212CS decreased due to melting of the smaller, imperfect crystallites. The crystallites with a melting temperature above the annealing temperature consequently became larger and thicker, creating a more uniform crystalline domain.

Dispersion-cast, H^+-form NRE 212CS membranes were also annealed at 100, 125, 150, 175, 200, 225, and 250 °C for one hour, followed by chemical degradation via a 75 hour Fenton's Test. Our goal was to examine the effects of decreasing crystallinity on fluoride loss after peroxide radical attack from Fenton's Reagent. The results of the 75 hour Fenton's Test on dispersion-cast, H^+-form NRE 212CS before and after annealing are shown in Table 5-3.

H^+ 212CS	15hr F- (ppm)	30hr F- (ppm)	45hr F- (ppm)	60hr F- (ppm)	75hr F- (ppm)	Avg F- (ppm) after 75 h	% wt loss
Unannealed	**2.12**	**5.15**	**6.19**	**5.96**	**6.09**	**5.10**	**0.31**
100 °C 1hr	**2.33**	**5.62**	**6.34**	**6.52**	**6.31**	**5.42**	**0.40**
125 °C 1hr	**5.85**	**8.51**	**9.11**	**9.12**	**9.10**	**8.34**	**0.72**
150 °C 1hr	**6.83**	**11.95**	**13.03**	**12.91**	**12.49**	**11.44**	**1.99**
175 °C 1hr	**13.26**	**18.56**	**19.82**	**19.39**	**19.38**	**18.08**	**3.90**
200 °C 1hr	**25.21**	**29.58**	**29.92**	**29.32**	**29.32**	**28.67**	**12.06**
225 °C 1hr	**28.46**	**27.33**	**26.64**	**27.31**			
250 °C 1hr	**22.61**						

Table 5-3. Fluoride release and percent weight loss of chemically degraded H^+-form NRE 212CS before and after annealing at various temperatures for one hour.

The most vivid correlation observed in Table 5-3 is the increase in percent weight loss of the ionomer as a function of annealing temperature. The initial weight loss after 75 hours of chemical degradation for the as-received H^+-form NRE 212CS membrane is approximately 0.3%. By performing the Fenton's Test on H^+-form NRE 212CS annealed at 200 °C for one hour, we observe a total weight loss of approximately 12%, which is 40 times the weight loss documented for the as-received membrane. It must also be noted that the percent weight loss of H^+-form NRE 212CS annealed at 225 and 250 °C could not be calculated due to disintegration of both membranes in the Fenton's Reagent at 60 and 15 hours, respectively. A graphical representation of the data from Table 5-3 is shown below in Figure 5.14.

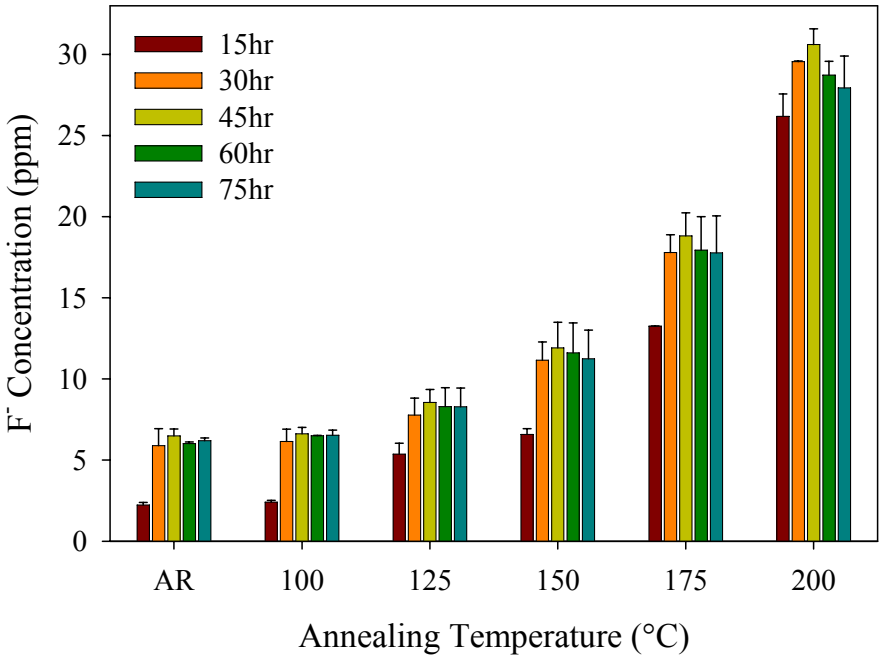

Figure 5.14. Fluoride concentration versus annealing temperature of dispersion-cast H^+-form NRE 212CS recorded after replenishing the Fenton's Reagent every 15 hours of a compiled 75 hour ex-situ chemical degradation Fenton's Test.

From Figure 5.14, we observe the same dramatic increase in fluoride loss as a function of annealing temperature for H^+-form NRE 212CS as mentioned previously. A closer look at the individual 15 hour cycle data shows that the highest fluoride concentration in the

Fenton's Reagent occurs after 45 hours of degradation, regardless of annealing conditions. We currently have no explanation for the maximum fluoride loss occurring after 45 hours of chemical degradation, but it apparently is not affected by changes in crystallinity. What is interesting is the increase of fluoride loss after annealing from 100 to 150 °C. Based on the deconvoluted WAXD data, the crystallinity of dispersion-cast H^+-form Nafion® remains relatively constant until annealed at 175 °C. The Fenton's degradation data indicates that the average 75 hour fluoride loss doubles between annealing at 100 °C and 150 °C for one hour. Since the crystalline morphology between these two membranes is virtually identical, we conclude that an external variable is responsible for the increased fluoride concentrations during the 75 hour Fenton's Test. The most obvious external variable that could have affected our degradation results was the discoloration of H^+-form Nafion® when subjected to elevated temperatures. Figure 5.15 displays the effect of annealing dispersion-cast H^+-form NRE 212CS for one hour at 100, 125, 150, 175, 200, 225, and 250 °C.

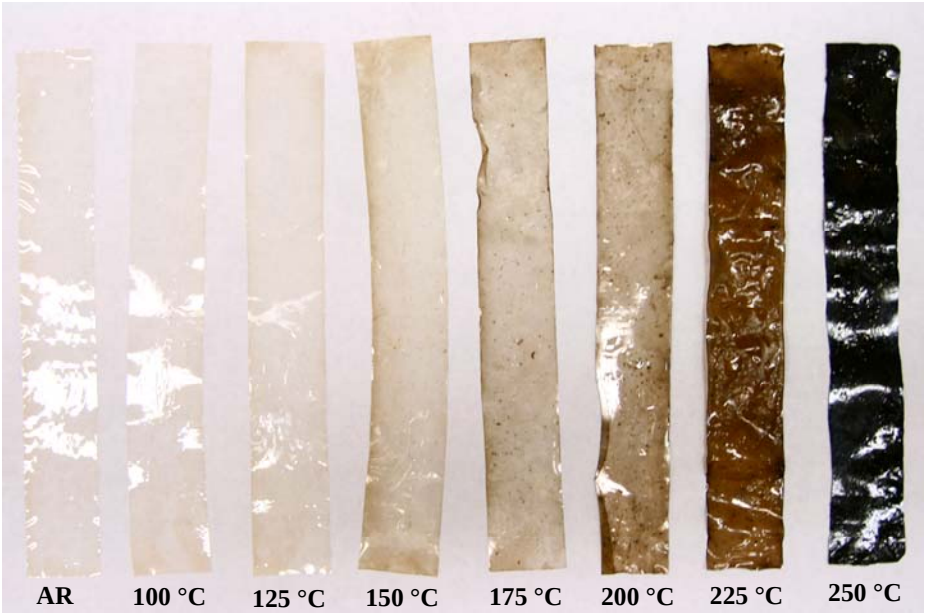

Figure 5.15. Image of H^+-form NRE 212CS before and after annealing for one hour at 100, 125, 150, 175, 200, 225, and 250 °C.

As the annealing temperature increases, the Nafion® membranes begin to turn brown and finally appear black after annealing at 250 °C for one hour. The observation of H^+-form Nafion® discoloration after annealing at elevated temperatures has been previously observed by other scientists, but the source has yet to be determined.[44, 52, 53] Most researchers ignore the discoloration of Nafion® due to the ability to reclaim transparent membranes after treating the films with nitric acid or 3% hydrogen peroxide. It is ironic that hydrogen peroxide is currently being used to clean Nafion® membranes when we observe a significant amount of membrane weight loss after performing a 75 hour Fenton's Test on annealed dispersion-cast Nafion® in the presence of hydrogen peroxide. After approximately 15 hours of exposure to the Fenton's Reagent, which contains 30% H_2O_2, all of the annealed membranes became transparent. We conclude that the thermal degradation or discoloration of Nafion® behaves as a catalyst for the peroxide radical attack, hence increasing the fluoride concentration observed for membranes annealed at elevated temperatures. So, rather than studying the effects of crystallinity on the fluoride release of dispersion-cast Nafion®, we were actually examining the effects of thermal discoloration on the chemical degradation via a 75 hour Fenton's Test.

One way to avoid the discoloration of Nafion® during thermal treatment is to convert the membrane into an alkali metal counterion form (i.e. Na^+) prior to annealing.[44] In order to further mitigate the effects of crystallinity on the chemical degradation of dispersion-cast Nafion®, we chose to anneal various samples of NRE 212CS in the Na^+-form to avoid the dramatic effects thermal discoloration has on the total fluoride loss of the polymer. Figure 5.16 shows the WAXD profile of relative intensity versus degrees, 2θ for Na^+-form NRE 212CS before and after annealing between 100 and 300 °C.

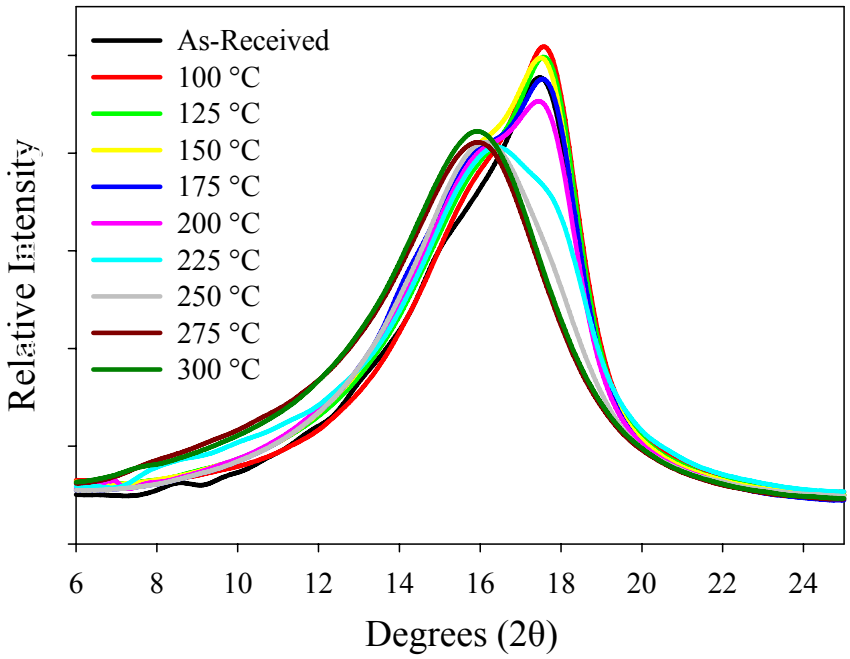

Figure 5.16. WAXD profile of Na^+-form NRE 212CS membranes before and after annealing for one hour at 100, 125, 150, 175, 200, 225, 250, 275, and 300 °C.

The WAXD profiles of Na^+-form NRE 212CS after annealing at elevated temperatures verify the disappearance of crystallinity seen in the SAXS analysis at annealing temperatures above 275 °C. In a similar study, Luan et al. examined the effects of annealing on the resulting crystallinity of cast Nafion® membranes.[54] The sulfonyl fluoride precursor of Nafion® was first synthesized by Luan and coworkers, and then converted directly into the Na^+ counterion form. The Na^+-form Nafion® was then dissolved under high temperature and pressure in dimethylformamide and cast under vacuum at 125 °C over a period of 1.75 hours. The film was then cut into six equal sections, and five of the samples were annealed for 1.5 hours at the following temperatures: 150, 170, 190, 210, 230, and 250 °C. Based on WAXD results, Luan et al. noticed a similar decrease in both the intensity and full width at half maximum of the crystalline reflection at 17.5 °, 2θ as a function of increasing annealing temperature as compared to our results. The change in percent crystallinity was calculated based on the

deconvolution of an amorphous and crystalline peak from the WAXD profiles, resulting in a decrease in crystallinity from 22.0 to 7.4% with increasing annealing temperature from 150 to 230 °C. These results are in agreement with our percent crystallinity deconvolutions of Na^+-form NRE 212CS, shown in Table 5-4. The only difference between our results and Luan's is that we annealed at temperatures high enough to melt all of the crystallites present in Nafion® (275 °C) and Luan et al. only annealed up to 230 °C.

T_{Anneal}	Na^+-form $\%X_c$	FWHM
AR	21.4	1.7
100 °C	17.5	1.5
125 °C	16.3	1.5
150 °C	13.9	1.4
175 °C	15.1	1.5
200 °C	12.8	1.5
225 °C	3.45	1.3
250 °C	2.22	1.6
275 °C	0	0
300 °C	0	0

Table 5-4. Percent crystallinity and full width at half maximum (FWHM) of Na^+-form NRE 212CS before and after annealing for one hour at 100, 125, 150, 175, 200, 225, 250, 275, and 300 °C.

To examine the effects of crystallinity on the chemical degradation of dispersion-cast Nafion®, Na^+-form samples were first annealed between 100 and 350 °C. Samples annealed between 100 and 300 °C were held at their respective annealing temperatures for one hour. Samples annealed at 325 and 350 °C were thermally treated for fifteen minutes due to the onset of discoloration similar to annealing the H^+-form of Nafion®. The results of the 75 hour Fenton's Test on dispersion-cast, H^+-form NRE 212CS before and after annealing at elevated temperatures in the Na^+-form are shown in Table 5-5.

Na+ 212CS	15hr F- (ppm)	30hr F- (ppm)	45hr F- (ppm)	60hr F- (ppm)	F- (ppm)	Avg F- (ppm) after 75 h	% wt loss
Unannealed → H^+	3.21	5.39	6.00	5.96	5.77	5.27	0.028
100 °C 1hr → H^+	4.23	5.96	6.47	6.74	6.23	5.92	-0.057
125 °C 1hr → H^+	3.78	6.32	6.59	6.82	6.57	6.02	0.000
150 °C 1hr → H^+	3.50	5.80	6.46	6.68	6.51	5.79	-0.064
175 °C 1hr → H^+	2.66	5.26	6.08	6.49	6.13	5.32	0.029
200 °C 1hr → H^+	2.96	5.35	6.11	6.32	5.94	5.33	0.085
225 °C 1hr → H^+	5.78	7.65	8.15	8.10	8.07	7.55	0.086
250 °C 1hr → H^+	4.18	7.12	7.93	7.88	8.33	7.09	0.156
275 °C 1hr → H^+	8.29	11.92	12.57	12.36	14.19	11.87	0.806
300 °C 1hr → H^+	18.19	20.75	21.25	21.13	20.79	20.42	4.149
325 °C 15 min → H^+	18.82	22.01	22.41	21.68	21.33	21.25	4.695
350 °C 15 min → H^+	31.22	30.69	30.28	29.89	29.92	28.40	18.080

Table 5-5. Fluoride release and percent weight loss of dispersion-cast NRE 212CS annealed in the Na^+-form at various temperatures for one hour, reacidified, and chemically degraded for 75 hours using Fenton's Reagent.

From Table 5-5, we see that the average fluoride concentration after 75 hours in the Fenton's Reagent remains relatively constant until an annealing temperature of approximately 225 °C. This data corresponds exceedingly well with our WAXD deconvolution data shown in Table 5-4, where a clear decrease in the percent crystallinity of the membranes occurs after annealing at 225 °C for one hour. By increasing the annealing temperature to 275 °C, we observe an increase of the average fluoride concentration from 7.55 to 11.87 ppm. Based on visual inspection of the membrane after annealing at 275 °C for one hour, we conclude that the film was absent of thermal discoloration, and the fluoride release results are based on the absence of crystallinity within the ionomer. The WAXD results from Table 5-4 also indicate that the Na^+-form membranes should be in the amorphous state after annealing at 275 °C for one hour. We thus correlate that crystallinity is a key component in deterring the effects of peroxide radical attack on dispersion-cast Nafion®. We also observed a dramatic increase of the average fluoride concentration beyond annealing at 275 °C, which can be attributed to the

onset of thermal discoloration, which as we saw with the H^+-form membranes, rapidly increases the rate of chemical degradation. The percent weight loss of the membranes is also documented in Table 5-5. Similar to the fluoride concentrations, the weight loss remains minimal until a sudden increase after annealing at 275 °C for one hour. It should be mentioned that further studies will be necessary to determine the error associated with calculating the percent weight loss, due to the observation of some samples actually gaining weight after the Fenton's Test. Overall, the percent weight loss increased dramatically for the samples annealed above 300 °C, which is attributed to the onset of thermal discoloration, which acts as a catalyst during peroxide radical attack. The fluoride concentration data shown in Table 5-5 is also represented graphically in Figure 5.17.

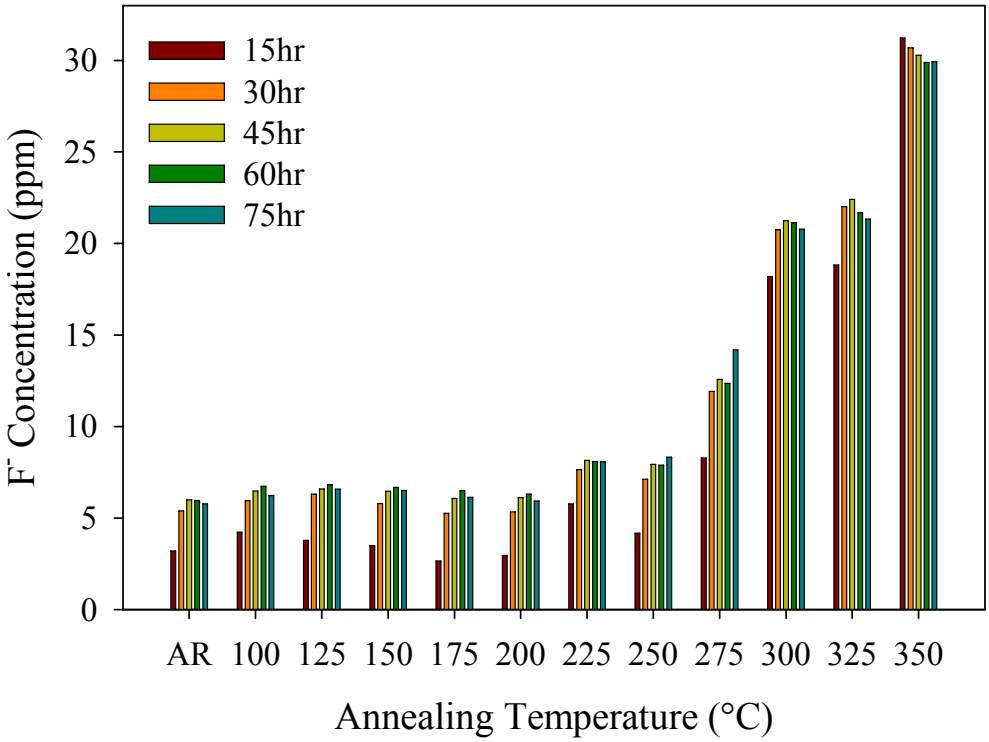

Figure 5.17. Fluoride concentration versus annealing temperature of dispersion-cast NRE 212CS annealed in the Na^+-form at various temperatures for one hour, reacidified, and chemically degraded for 75 hours using Fenton's Reagent. The fluoride concentrations were recorded after replenishing the Fenton's Reagent every 15 hours, until reaching the 75 hour threshold.

Similar to the chemical degradation data of H^+-form Nafion® as a function of annealing temperature, the majority of the Na^+-form annealed membranes exhibited their highest levels of fluoride release during the third Fenton's Reagent cycle (after 45 hours of peroxide radical attack). As mentioned earlier, the samples annealed between 100 and 200 °C had similar fluoride release, as shown in Figure 5.17, but at annealing temperatures beyond 200 °C, a significant increase in the fluoride concentration is observed due to melting of the Teflon-like crystallites as well as the onset of thermal discoloration after annealing at 300 °C or higher. Future work will involve determining an appropriate annealing condition where the crystalline domain is manipulated without the onset of thermal discoloration of Nafion®.

Conclusions

Chemical degradation of dispersion-cast Nafion® via peroxide radical attack from Fenton's Reagent dramatically changes the morphology and mechanical properties of the ionomer. As exposure time of the membrane in Fenton's Reagent increases, bubbles or voids begin to appear within and on the surface of the polymer, consequently decreasing the mechanical properties and affecting Nafion®'s chemical structure. The primary chemical degradation route of Nafion®, proposed by Curtin et al., involves unzipping of the polymer backbone via peroxide radical attack of the residual carboxylic acid endgroups.[6] Based on the appearance of both side chain and backbone related peaks in ^{19}F solid-state NMR data on chemically degraded dispersion-cast Nafion® NRE 212CS, we conclude that the unzipping mechanism proposed by Curtin et al. is plausible. On the other hand, Escobedo et al. suggest a secondary chemical degradation mechanism due to a nonzero intercept of fluoride loss versus carboxylic endgroups present on the polymer

backbone.[42] Further observation of our ^{19}F solid-state NMR data reveals dramatic changes to both the OCF_2 and CF_3 side chain peaks, possibly due to a secondary degradation mechanism.

By annealing dispersion-cast Nafion® in the H^+-form, we examined how changes to the crystalline morphology affected the release of fluoride ions during the Fenton's Test. Unfortunately, due to the severe discoloration of acid form Nafion® while annealing at elevated temperatures (> 150 °C), we were unable to conclude whether the fluoride loss of the membrane was attributed to decreasing crystallinity or increased thermal discoloration. Based on the dramatic change in fluoride loss with increased darkening of the membrane, we concluded that thermal discoloration had a larger influence on the rate of chemical degradation as opposed to changes in the crystalline morphology. To avoid discoloration during thermal treatment, we annealed membranes in the Na^+-form and were able to conclude that crystallinity in Nafion® is an important factor in deterring peroxide radical attack. As the percent crystallinity decreased with annealing temperature, the fluoride concentration in the resulting Fenton's media increased accordingly, indicating that the amorphous regions of the polymer are more susceptible to chemical degradation via peroxide radical attack.

Acknowledgements

We would like to thank E.I. Du Pont De Nemours and Company for supplying the extruded Nafion® 112 and dispersion-cast NRE 212 and NRE 212CS membranes. Funding for this work was provided by DuPont Fuel Cells and DOE Office of Energy Efficiency and Renewable Energy; contract # DE-FC36-03GO13100 and DE-FG36-06GO86065.

We would also like to acknowledge the assistance of the Polymer Science Department at the University of Southern Mississippi for the use of their wide angle x-ray diffractometer and a special thanks to Dr. William Jarrett at the University of Southern Mississippi for his expertise and assistance with performing solid-state ^{19}F NMR experiments.

References

(1) Schiraldi, D. A. *Polymer Reviews* **2006,** 46, (3), 315-327.
(2) Chalk, S. G.; Miller, J. F. *Journal of Power Sources* **2006,** 159, (1), 73-80.
(3) LaConti, A. B.; Liu, H.; Mittelsteadt, C. K.; McDonald, R. C. *ECS Transactions* **2006,** 1, (8), 199-219.
(4) Mauritz, K. A.; Moore, R. B. *Chemical Reviews* **2004,** 104, (10), 4535-4585.
(5) Stucki, S.; Scherer, G. G. *Journal of Applied Electrochemistry* **1998,** 28, (10), 1041-1049.
(6) Curtin, D. E.; Lousenberg, R. D.; Henry, T. J.; Tangeman, P. C.; Tisack, M. E. *Journal of Power Sources* **2004,** 131, (1-2), 41-48.
(7) Borup, R.; Meyers, J.; Pivovar, B.; Kim, Y. S.; Mukundan, R.; Garland, N.; Myers, D.; Wilson, M.; Garzon, F.; Wood, D.; Zelenay, P.; More, K.; Stroh, K.; Zawodzinski, T.; Boncella, J.; McGrath, J. E.; Inaba, M.; Miyatake, K.; Hori, M.; Ota, K.; Ogumi, Z.; Miyata, S.; Nishikata, A.; Siroma, Z.; Uchimoto, Y.; Yasuda, K.; Kimijima, K.; Iwashita, N. *Chemical Reviews* **2007,** 107, 3904-3951.
(8) Liu, H.; Gasteiger, H.; Laconti, A. B.; Zhang, J. *ECS Transactions* **2006,** 1, (8), 283-293.
(9) Antoine, O.; Durand, R. *Journal of Applied Electrochemistry* **2000,** 30, 839-844.
(10) Paulus, U. A.; Schmidt, T. J.; Gasteiger, H. A.; Behm, R. J. *Journal of Electroanalytical Chemistry* **2001,** 495, 134-145.
(11) Inaba, M.; Yamada, H.; Tokunaga, J.; Matsuzawa, K.; Hatanaka, A.; Tasaka, A. *ECS Transactions* **2006,** 1, (8), 315-322.
(12) Shao, M.; Liu, P.; Adzic, R. R. *Journal of the American Chemical Society* **2006,** 128, 7408-7409.
(13) Teranishi, K.; Kawata, K.; Tsushima, S.; Hirai, S. *Electrochemical and Solid State Letters* **2006,** 9, (10), A475-A477.
(14) Inaba, M.; Kinumoto, T.; Kiriake, M.; Umebayashi, R.; Tasaka, A.; Ogumi, Z. *Electrochimica Acta* **2006,** 51, (26), 5746-5753.
(15) Liu, W.; Zuckerbrod, D. *Journal of the Electrochemical Society* **2005,** 152, (6), A1165-A1170.
(16) Knights, S.; Colbow, K.; St Pierre, J.; Wilkinson, D. *Journal of Power Sources* **2004,** 127, 127-134.
(17) Cho, E.; Ko, J.; Ha, H. Y.; Hong, S. A.; Lee, K. Y.; Lim, T. W.; Oh, I. H. *Journal of the Electrochemical Society* **2004,** 151, (5), A661-A665.

(18) Lakshmanan, B.; Huang, W.; Olmeijer, D.; Weidner, J. W. *Electrochemical and Solid State Letters* **2003,** 6, (12), A282-a285.
(19) Yu, J. R.; Matsuura, T.; Yoshikawa, Y.; Islam, M. N.; Hori, M. *Electrochemical and Solid State Letters* **2005,** 8, (3), A156-a158.
(20) Mathias, M. F.; Makharia, R.; Gasteiger, H.; Conley, J. J.; Fuller, T. F.; Gittleman, C. J.; Kocha, S. S.; Miller, D. P.; Mittelsteadt, C. K.; Xie, T.; Yan, S. G.; Yu, P. T. *The Electrochemical Society Interface* **2005,** 14, (3), 24-35.
(21) Ohma, A.; Suga, S.; Yamamoto, S.; Shinohara, K. *Journal of the Electrochemical Society* **2007,** 154, (8), B757-B760.
(22) Pozio, A.; Silva, R. F.; De Francesco, M.; Giorgi, L. *Electrochimica Acta* **2003,** 48, (11), 1543-1549.
(23) Zhou, C.; Zawodzinski, T.; Schiraldi, D. *Polymer Preprints* **2004,** 45, (2), 760-761.
(24) Zhou, C.; Zawodzinski, T.; Schiraldi, D. *Polymer Preprints* **2006,** 47, (2), 485-486.
(25) Healy, J.; Hayden, C.; Xie, T.; Olson, K.; Waldo, R.; Brundage, A.; Gasteiger, H.; Abbott, J. *Fuel Cells* **2005,** 5, (2), 302-308.
(26) Kinumoto, T.; Inaba, M.; Nakayama, Y.; Ogata, K.; Umebayashi, R.; Tasaka, A.; Iriyama, Y.; Abe, T.; Ogumi, Z. *Journal of Power Sources* **2006,** 158, 1222-1228.
(27) Nosaka, A. Y.; Watanabe, S.; Toyoda, I.; Nosaka, Y. *Macromolecules* **2006,** 39, (13), 4425-4427.
(28) Duesterberg, C. K.; Waite, T. D. *Environmental Science & Technology* **2006,** 40, (13), 4189-4195.
(29) Tang, H.; Peikang, S.; Jiang, S. P.; Wang, F.; Pan, M. *Journal of Power Sources* **2007,** 170, 85-92.
(30) Rhoades, D.; Hassan, M.; Osborn, S.; Moore, R. B.; Mauritz, K. *Journal of Power Sources* **2007,** 172, 72-77.
(31) Zhou, C.; Guerra, M.; Qiu, Z. M.; Zawodzinski, T.; Schiraldi, D. *Macromolecules* **2007,** 40, 8695-8707.
(32) Mittal, V. O.; Kunz, H. R.; Fenton, J. M. *Journal of the Electrochemical Society* **2007,** 154, (7), B652-B656.
(33) Merlo, L.; Ghielmi, A.; Cirillo, L.; Gebert, M.; Arcella, V. *Journal of Power Sources* **2007,** 171, 140-147.
(34) Kundu, S.; Simon, L. C.; Fowler, M. *Polymer Degradation and Stability* **2008,** 93, 214-224.
(35) Hommura, S.; Kawahara, K.; Shimohira, T.; Teraoka, Y. *Journal of the Electrochemical Society* **2008,** 155, (1), A29-A33.
(36) Sethuraman, V. A.; Weidner, J. W.; Haug, A. T.; Protsailo, L. V. *Journal of the Electrochemical Society* **2008,** 155, (2), B119-B124.
(37) Panchenko, A.; Dilger, H.; Moller, E.; Sixt, T.; Roduner, E. *Journal of Power Sources* **2004,** 127, 325-330.
(38) Bosnjakovic, A.; Schlick, S. *Journal of Physical Chemistry B* **2004,** 108, (14), 4332-4337.
(39) Kadirov, M. K.; Bosnjakovic, A.; Schlick, S. *Journal of Physical Chemistry B* **2005,** 109, (16), 7664-7670.

(40) Bosnjakovic, A.; Schlick, S. *Journal of Physical Chemistry B* **2006,** 110, 10720-10728.
(41) Schlick, S.; Motyakin, M. *Electron Paramagnetic Resonance* **2007,** 20, 1-28.
(42) Escobedo, G. *Strategies to improve the durability of perfluorosulfonic acid membranes for PEM fuel cells*, KFTCA International Symposium, Washington, DC, December 8-9, 2005.
(43) Page, K.; Jarrett, W.; Moore, R. B. *Journal of Polymer Science Part B: Polymer Physics* **2007,** 45, 2177-2186.
(44) Almeida, S.H.; Kawano, Y. *Journal of Thermal Analysis and Calorimetry* **1999,** 58, 569-577.
(45) E. I. Dupont De Nemours & Co Inc. *DuPont™ Nafion® PFSA Membranes NRE-211 and NRE-212*. http://www.fuelcellmarkets.com/content/images/articles/nae201.pdf (January 3, 2009).
(46) E. I. Dupont De Nemours & Co Inc. *DuPont™ Nafion® PFSA Membranes N-115, N-117, NE-1110*. http://www.fuelcellmarkets.com/content/images/articles/nae101.pdf (January 3, 2009).
(47) Chen, Q.; Schmidt-Rohr, K. *Macromolecules* **2004,** 37, 5995-6003.
(48) Takasaki, M.; Kimura, K.; Kawaguchi, K.; Abe, A.; Katagiri, G. *Macromolecules* **2005,** 38, (14), 6031-6037.
(49) Gierke, T.D.; Munn, G.E.; Wilson, F.C. *Journal of Polymer Science: Polymer Physics Edition* **1981,** 19, 1687-1704.
(50) Fujimura, M.; Hashimoto, T.; Kawai, H. *Macromolecules* **1981,** 14, (5), 1309-1315.
(51) Starkweather, H. W. *Macromolecules* **1982,** 15, (2), 320-323.
(52) Gebel, G.; Aldebert, P.; Pineri, M. *Macromolecules* **1987,** 20, 1425-1428.
(53) Hensley, J. E.; Way, J. D.; Dec, S. F.; Abney, K. D. *Journal of Membrane Science* **2007,** 298, 190-201.
(54) Luan, Y.; Zhang, Y.; Zhang, H.; Li, L.; Li, H.; Liu, Y. *Journal of Applied Polymer Science* **2008,** 107, 396-402.

CHAPTER 6

FUTURE WORK: DYNAMIC LIGHT SCATTERING OF NAFION® IN SOLUTION

Introduction

The perflurosulfonic acid ionomer Nafion® is the current benchmark material for proton exchange membrane fuel cells (PEMFCs) and consists of a polytetrafluoroethylene (PTFE) backbone with perfluorovinylether side chains that terminate with a sulfonic acid functionality.[1] Nafion® is currently available commercially from E.I. du Pont de Nemours and Company and has the following structure:

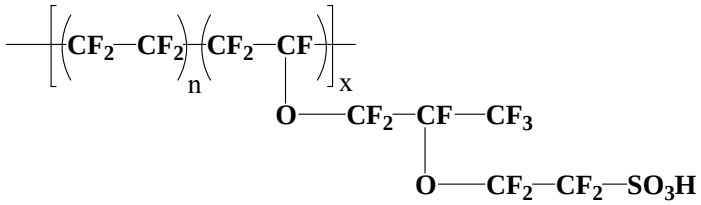

Due to the difference in polarity between the nonpolar fluorocarbon matrix and polar ionic moieties, the ionic groups tend to phase separate and form what is referred to as ionic aggregates.[2] Along with the aggregate structures are the crystalline domains involving runs of polytetrafluoroethylene, which have unit cell dimensions virtually identical to that of pure PTFE.[3, 4] In the interest of accurately describing Nafion's® complex, phase-separated network of both ionic aggregates and crystalline domains, the majority of investigations have focused on characterizing both the morphological[4-9] and thermo-mechanical[1, 10-19] properties of Nafion® in the membrane form.

For the past forty years, the main method for producing Nafion® membranes was through melt extrusion of a sulfonyl fluoride (SO_2F) precursor, followed by hydrolysis into the sulfonate ionomer (SO_3^-) form.[1, 18] Dupont has recently introduced dispersion-

cast membranes which exhibit lower thicknesses and higher water uptake values when compared to their extruded counterparts.[20] The focal point of this research will be to utilize dynamic light scattering to examine extruded and dispersion-cast Nafion® aggregation behavior in 50/50 ethanol/water solutions.

In the early 1980's, publications by Grot[21] and Martin[22] detailed a procedure for dissolving Nafion® membranes in water/alcohol mixtures at elevated temperatures and pressures. Martin et al. developed their Nafion® dissolution procedure based on the solvent swelling studies of extruded Nafion®, conducted by Yeo and coworkers.[23] Yeo et al. concluded from uptake and solubility data of Nafion® in various solvents that the ionomer exhibits a dual solubility parameter with maximum solubilities at 9.5 and 18.1 Hb. The solubility envelope at 9.5 Hb was attributed to swelling of Nafion's® organic phase, while the solubility envelope at 18.1 Hb was attributed to swelling of the ionic aggregate domain. Martin et al. chose to dissolve Nafion® membranes in ethanol/water mixtures due to ethanol's solubility parameter (12.7 Hb) being closer to Nafion®'s organic phase solubility value of 9.5 Hb as opposed to methanol's solubility parameter of (14.5 Hb). Martin et al. also demonstrated that high temperature and pressure were necessary to obtain high degrees of swelling and to melt the polytetrafluoroethylene crystallites present in the membrane during dissolution.[22]

To date, there are considerably more publications discussing the structure and morphology of Nafion® in the membrane form rather than focusing on how the ionomer behaves in solution. Loppinet and Szajdzinska-Pietek were among the first to characterize Nafion® solutions using small angle x-ray scattering and electron spin resonance, respectively.[24, 25] From these studies, Nafion® was believed to exist as rodlike

aggregates in polar solvents such as water, methanol and N,N'-dimethylformamide (DMF). With the aid of dynamic light scattering, various authors have concluded that multimodal particle sizes of Nafion® aggregates are possible in various solvents (methanol/water, ethanol/water, isopropanol/water, and DMF).[26-32] In general, small particle sizes (< 100 nm) correspond to single Nafion® chains, medium particle sizes (100-1000 nm) are related to primary rodlike aggregation due to the hydrophobic interaction of Nafion®'s fluorocarbon backbone, and large particle sizes (> 1000 nm) are attributed to secondary aggregation of the primary aggregates via ionic interactions. The concentration of Nafion® within the solution as well as choice of solvent have been determined to affect the particle sizes and distributions of the resulting Nafion® aggregates. Lee et al. observed a dramatic change in the particle distribution and size of Nafion® aggregates by varying the concentration from 0.2 to 9 mg/mL in a 4/1 weight ratio of methanol to water solution.[28] At a concentration of 0.2 mg/mL, Lee and coworkers noticed one distinct peak near 1000 nm, suggesting the entire solution consisted of primary aggregates, confirming that even at very dilute concentrations, the hydrophobic nature of Nafion®'s backbone structure suggests aggregation. An increase in the concentration to 1 mg/mL resulted in a shift of the peak to approximately 15 microns, indicating a large influence of secondary ionic aggregation of the Nafion® particles. Finally, at concentrations of 7 and 9 mg/mL, a bimodal particle size distribution was observed, where both primary and secondary Nafion® aggregates were present in the 4/1 methanol/water solution. Lee et al. also examined the influence of adding 0.3M NaCl to a 4/1 methanol/water solution containing 3 mg/mL of Nafion®. A shift in the particle size peak to smaller dimensions was observed and attributed to the

dissociation of the secondary ionic aggregates into primary aggregates. The authors concluded that obtaining individual chains of Nafion® in methanol/water solutions was not possible due to the solubility parameters of methanol and water being closer to the solubility parameter of Nafion®'s ionic region as opposed to the hydrophobic organic phase. In a future publication, Lee et al. used dynamic light scattering to examine Nafion® aggregation in isopropanol/water and DMF solutions due to the relatively low solubility parameters of isopropanol and DMF.[29] Lee et al. observed a significant decrease in the primary aggregate sizes with the addition of either isopropanol or DMF. A bimodal aggregate distribution of Nafion® was observed at approximately 100 and 1000 nm in a 4/1 weight ratio of isopropanol and water solution. In contrast, a single peak representing primary aggregation at approximately 125 nm was observed for Nafion® dissolved in DMF. The authors concluded that using a solvent with a solubility parameter closest to that of Nafion®'s organic phase is necessary to obtain particle sizes near the individual ionomer chain domain (< 100 nm).

The focus of this work is to compare the dynamic light scattering properties of both extruded and dispersion-cast H^+-form Nafion® in 50/50 ethanol/water solutions. The resulting particle sizes of the ionomer solutions will also be examined after 30 and 60 minutes of ultrasonication. Future studies involving dynamic light scattering of Nafion® dissolved in high temperature boiling point solvents and performed at variable temperatures will be discussed in the conclusions of this paper. Obtaining a fundamental understanding on Nafion® aggregation in solution is paramount in understanding how to optimize the catalyst layer of a proton exchange membrane fuel cell to provide maximum output with increased longevity.

Experimental

Materials. Extruded Nafion® 117 (1100 g/equivalent, sulfonic acid form, 7 mil or 0.178 mm thick) and dispersion-cast NRE 212CS (1100 g/equivalent, sulfonic acid form, 2 mil or 0.051 mm thick, CS = chemically stable) was provided by E.I. du Pont de Nemours and Company.

Preparation of H^+-form Perfluorosulfonic Ionomer Solutions. To remove impurities, the Nafion® membranes were cleaned in refluxing 8M HNO_3 for two hours, rinsed three times with deionized water, boiled in deionized water for one hour, and dried under vacuum overnight at 70 °C. Solutions of extruded H^+ and dispersion-cast H^+-form Nafion® were prepared using a PARR pressure reactor following the procedure by Martin and coworkers.[22] Seven grams of Nafion® were added to a 200 ml solution of 50:50 deionized water and ethanol, which was then placed into the high pressure reactor and stirred at 250 °C for two hours at approximately 1000 psi. After cooling, each solution was filtered under vacuum through Whatman number four filter paper. The average solution concentration was determined by extracting one milliliter of solution into three separate scintillation vials and obtaining the dry weight of the polymer after evaporating the residual solvent.

Dynamic Light Scattering. Dynamic light scattering studies of extruded H^+-form Nafion® solution (20.42 mg/mL) and dispersion-cast H^+-form Nafion® solution (20.75 mg/mL) were conducted using a Malvern Instruments Zetasizer Nano series instrument equipped with a 22 mW He-Ne laser operating at $\lambda = 632.8$ nm, an avalanche photodiode detector with high quantum efficiency, and an ALV/LSE-5003 multiple tau digital

correlator electronics system. All measurements were performed in triplicate at 25 °C, and the Nafion® particle size distributions were calculated using CONTIN software.

Results and Discussion

Figure 6.1 A and B shows the dynamic light scattering particle size profiles of extruded and dispersion-cast, H^+-form Nafion® in 50/50 ethanol/water solutions before and after ultrasonication.

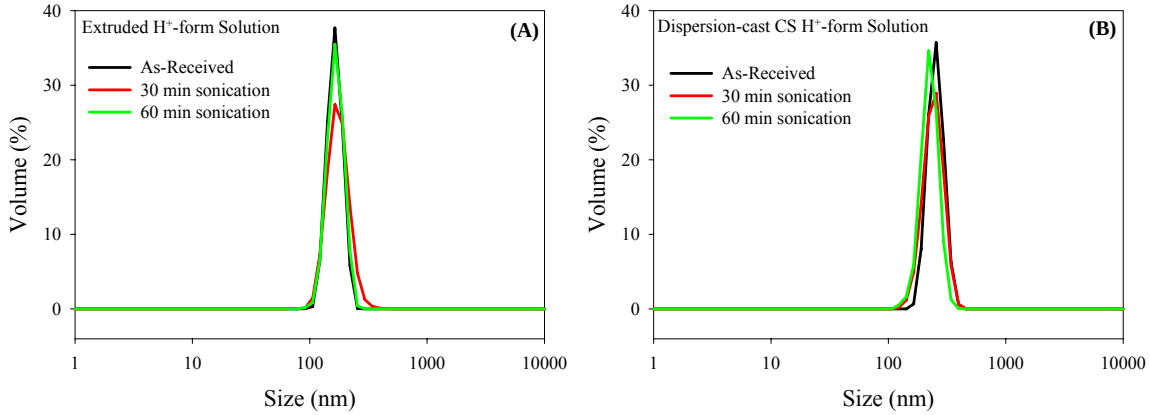

Figure 6.1. Particle size distributions before and after ultrasonication of **A)** 50/50 ethanol/water, extruded H^+-form Nafion® solution (20.42 mg/mL) **B)** 50/50 ethanol/water, dispersion-cast NRE 212CS H^+-form Nafion® solution (20.75 mg/mL).

The data in Figure 6.1 A and B show that extruded and dispersion-cast Nafion® solutions have similar scattering profiles, which exhibit a single primary aggregate peak with particle sizes greater than 100 nm. These results are in direct contrast to the dynamic light scattering results of both Cirkel et al.[26] and Lin et al.[31] who showed that extruded H^+-form Nafion® in ethanol/water solutions displayed bimodal particle sizes with peaks near 1000 and 10000 nm. It should also be noted that the concentrations and ethanol/water ratios were different between all three studies. Lee et al. showed that Nafion® concentration within the solution can have a dramatic effect on the overall particle size distribution.

The effect of ultrasonication time on the primary Nafion® aggregate particle size is also shown in Figure 6.1 A and B. At first glance, it appears that ultrasonication time had minimal influence on the particle size distribution of either extruded or dispersion-cast Nafion® in solution. A more accurate representation of the effects of ultrasonication time on the size of primary Nafion® aggregates is shown in Figure 6.2.

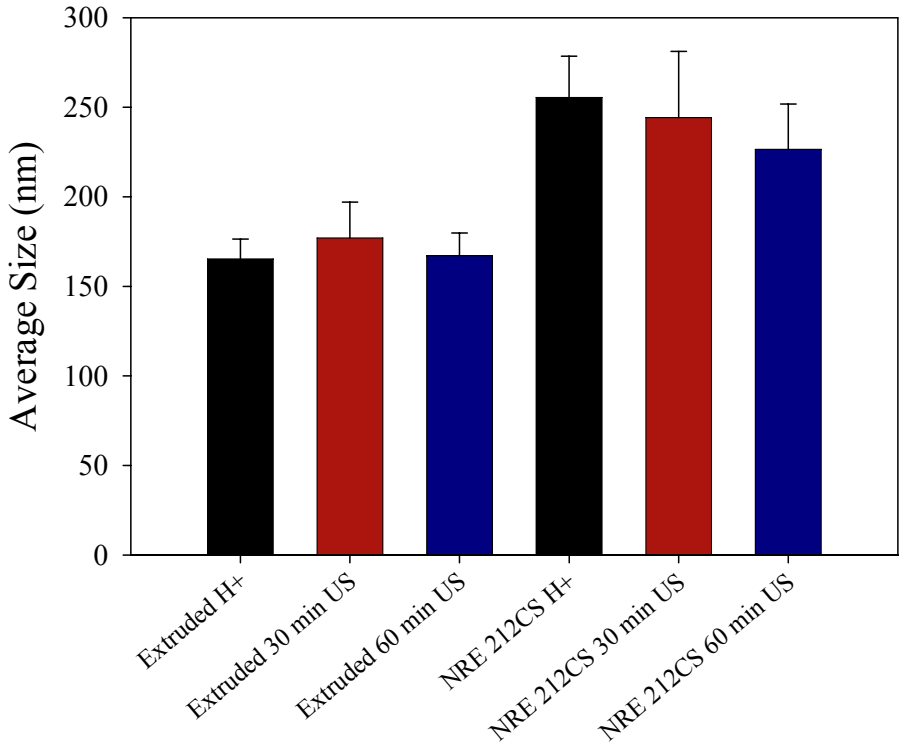

Figure 6.2. Average particle size before and after sonication of 50/50 ethanol/water extruded 117 H^+-form (20.42 mg/mL) and dispersion-cast NRE 212CS H^+-form (20.75 mg/mL).

The initial results shown in Figure 6.2 indicate that ultrasonication time had minimal effect on the average primary aggregate size of extruded H^+-form Nafion® in 50/50 ethanol/water solution. On the other hand, the average size of primary dispersion-cast H^+-form Nafion® aggregates appeared to decrease slightly after ultrasonicating for one hour. Overall, the extruded Nafion® solution exhibited smaller primary aggregate sizes in comparison to dispersion-cast Nafion®, indicating that extruded Nafion® behaves more like single isolated chains in 50/50 ethanol/water solution.

Conclusions

The preliminary research shown in this paper indicates that extruded and dispersion-cast H^+-form Nafion® behave similarly after dissolution in 50/50 ethanol/water mixtures. The dynamic light scattering particle size profiles of both solutions display a single peak between 100 and 500 nm, indicating that both extruded and dispersion-cast Nafion® consist of primary aggregates, which are attributed to the hydrophobic interaction of the polymer's fluorocarbon backbone. Ultrasonicating the solutions for 30 and 60 minutes prior to performing dynamic light scattering appeared to have minimal effect on the aggregate size of H^+-form, extruded Nafion®, while slightly decreasing the aggregate size of H^+-form, dispersion-cast Nafion® after ultrasonicating for one hour.

Numerous studies are still necessary to fundamentally understand the morphology of Nafion® in solution, ultimately leading to optimization of the transport and mechanical properties of the resulting cast membrane. In conjunction with our initial results, it would be interesting to examine the aggregation behavior of H^+-form Nafion® in dimethylsulfoxide (DMSO), which is commonly used in our group to solution-process Nafion® membranes.[4, 33] Variable temperature dynamic light scattering of Nafion® in DMSO would also be beneficial in examining how the aggregates behave as mobility is decreased and before gelation occurs due to loss of solvent. Future work is also necessary in examining the role various counterions play in affecting the aggregation behavior of Nafion® dissolved in DMSO. Two authors have shown that with the addition of Li^+ or Na^+ counterions, Nafion® particle sizes decrease and a higher concentration of single polymer chains are observed.[27, 28] To date no one has examined the influence of

alkylammonium counterions such as tetramethylammonium (TMA^+) or tetrabutylammonium (TBA^+) on the aggregation behavior of Nafion® in DMSO or other solvents. The overall goal of this research would be to obtain a solution of Nafion® consisting completely of individual chains without the presence of primary or secondary aggregation. Being able to isolate Nafion® chains and maintaining the isolation behavior during casting would provide membranes with significantly different transport and mechanical properties.

References

(1) Mauritz, K. A.; Moore, R. B. *Chemical Reviews* **2004,** 104, (10), 4535-4585.
(2) Eisenberg, A.; Hird, B.; Moore, R. B. *Macromolecules* **1990,** 23, 4098-4107.
(3) Starkweather, H. W. *Macromolecules* **1982,** 15, (2), 320-323.
(4) Moore, Robert. B.; Martin, Charles R. *Macromolecules* **1988,** 88, (21), 1334-1339.
(5) Gierke, T.D.; Munn, G.E.; Wilson, F.C. *Journal of Polymer Science: Polymer Physics Edition* **1981,** 19, 1687-1704.
(6) Gebel, Gerard; Lambard, Jacques. *Macromolecules* **1997,** 30, 7914-7920.
(7) Gebel, G. *Polymer* **2000,** 41, (15), 5829-5838.
(8) Fujimura, M.; Hashimoto, T.; Kawai, H. *Macromolecules* **1981,** 14, (5), 1309-1315.
(9) Schmidt-Rohr, K.; Chen, Q. *Nature Materials* **2008,** 7, (1), 75-83.
(10) Page, K. A.; Landis, F. A.; Phillips, A. K.; Moore, R. B. *Macromolecules* **2006,** 39, (11), 3939-3946.
(11) Hodge, I. M.; Eisenberg, A. *Macromolecules* **1978,** 11, (2), 289-293.
(12) Yeo, S.; Eisenberg, A. *Journal of Applied Polymer Science* **1977,** 21, 875-898.
(13) Kyu, T.; Hashiyama, M.; Eisenberg, A. *Canadian Journal of Chemistry* **1983,** 61, 680-687.
(14) Miura, Y.; Yoshida, H. *Thermochimica Acta* **1990,** 163, 161-168.
(15) Moore, Robert B.; Cable, K. M.; Croley, T. L. *Journal of Membrane Science* **1992,** 75, (1), 7-14.
(16) Moore, R. B.; Cable, K. *Polymer Preprints* **1997,** 38, 272-273.
(17) Young, S.; Mauritz, K. *Journal of Polymer Science: Polymer Physics Edition* **2001,** 39, 1282-1295.
(18) Doyle, M.; Rajendran, G., Perfluorinated membranes. In *Handbook of Fuel Cells - Fundamentals, Technology and Applications*, Wolf Vielstich, A. L., and Hubert A. Gasteiger, Ed. John Wiley & Sons, Ltd, Chichester: 2003; Vol. 3 Part 3, pp 351-395.
(19) Page, K. A.; Cable, K. M.; Moore, R. B. *Macromolecules* **2005,** 38, (15), 6472-6484.

(20) Curtin, D. E.; Lousenberg, R. D.; Henry, T. J.; Tangeman, P. C.; Tisack, M. E. *Journal of Power Sources* **2004,** 131, (1-2), 41-48.
(21) Grot, W. G. *Production of a liquid composition containing a perfluorinated ion exchange polymer*. Patent EP0066369, 1982.
(22) Martin, Charles R.; Rhoades, Teresa A.; Ferguson, James A. *Analytical Chemistry* **1982,** 54, (9), 1639-1641.
(23) Yeo, R. S. *Polymer* **1980,** 21, (4), 432-435.
(24) Loppinet, B.; Gebel, G.; Williams, C. E. *Journal of Physical Chemistry B* **1997,** 101, 1884-1892.
(25) Szajdzinska-Pietek, E.; Schlick, S.; Plonka, A. *Langmuir* **1994,** 10, (4), 1101-1109.
(26) Cirkel, P. A.; Okada, T.; Kinugasa, S. *Macromolecules* **1999,** 32, 531-533.
(27) Jiang, S.; Xia, K. Q.; Xu, G. *Macromolecules* **2001,** 34, 7783-7788.
(28) Lee, S. J.; Yu, T. L.; Lin, H. L.; Liu, W. H.; Lai, C. L. *Polymer* **2004,** 45, 2853-2862.
(29) Lin, H. L.; Yu, T. L.; Huang, C. H.; Lin, T. L. *Journal of Polymer Science Part B-Polymer Physics* **2005,** 43, (21), 3044-3057.
(30) Wang, S.; Sun, G.; Wu, Z.; Xin, Q. *Journal of Power Sources* **2007,** 165, 128-133.
(31) Lin, H. L.; Yu, T. L.; Huang, L. N.; Chen, L. C.; Shen, K. S.; Jung, G. B. *Journal of Power Sources* **2005,** 150, 11-19.
(32) Chen, H.; Snyder, J. D.; Elabd, Y. A. *Macromolecules* **2008,** 41, 128-135.
(33) Moore, Robert B.; Martin, Charles R. *Analytical Chemistry* **1986,** 58, 2569-2570.